



UNIVERSITÀ  
POLITECNICA  
DELLE MARCHE

FACULTY OF ENGINEERING

Master degree in Biomedical Engineering

---

**Design and Development of an Augmented  
Reality Application deployed in Microsoft  
HoloLens V2 for Maxillary and Mandibular  
Osteotomy and Repositioning**

Supervisor:

*Prof. Mandolini Marco*

Graduating student:

Andrea Danieli

Co-Supervisors:

*Dr. Brunzini Agnese*

*Prof. Mazzoli Alida*

---

Academic Year 2020-2021



# I. Index

<b>1</b>	<b>Introduction</b>	<b>1</b>
<b>2</b>	<b>Research and Background</b>	<b>4</b>
2.1	Maxillofacial Surgery	4
2.1.1	Osteotomies and Maxillary Repositioning	5
2.1.1	Surgical Guides	7
2.1.2	Resin Dental Splints	8
2.1.3	Fixation Plates and Screws	9
2.1.4	Computed Tomography (CT)	11
2.2	Augmented Reality (AR)	14
2.2.1	History	15
2.2.2	AR Technology	16
2.2.3	AR Tracking	19
2.2.4	AR Registration	27
2.2.5	AR Visualization	27
2.2.6	AR Displays	29
2.2.7	Medical AR State of Art	32
2.2.7.1	AR Advantages and Disadvantages	60
2.2.7.2	Novelty of the Study	63
<b>3</b>	<b>Materials and Methods</b>	<b>64</b>
3.1	Computer Aided Design (CAD) Tools	65
3.1.1	Rhinoceros	67
3.2	AR Application Development	71
3.2.1	Hardware	71
3.2.1.1	Microsoft HoloLens V2	71
3.2.2	Software	75
3.2.2.1	Marker Generation and Vuforia SDK	76
3.2.2.2	Unity	81
3.2.2.3	Visual Studio	83
3.3	3D-Printing	85
3.3.1	Multi Jet Fusion	86
3.3.2	Color Jet Printing (CJP)	88
3.4	AR Application Validation	91
3.4.1	Go!Scan3D	91

3.4.2	CloudCompare	94
<b>3.5</b>	<b>AR Application</b>	<b>97</b>
3.5.1	Virtual Surgical Guides and Contents	101
3.5.2	Markers Generation	103
3.5.3	Application Development	104
3.5.3.1	<i>Packages Import</i>	105
3.5.3.2	<i>Project and Build Settings</i>	109
3.5.3.3	<i>Scene Creation</i>	118
3.5.3.4	<i>Script</i>	144
3.5.3.5	<i>Build, Compilation and Distribution</i>	150
3.5.4	Proposals for Marker M1 Placement	152
<b>4</b>	<b>Case Study</b>	<b>157</b>
<b>4.1</b>	<b>Modelling</b>	<b>159</b>
4.1.1	Skull CAD Model	159
4.1.2	Bites, Marker M2 and Marker M1	162
4.1.3	Osteotomy Lines and Drilled Holes	166
4.1.4	Skull Components Assembly	169
4.1.5	AR Application Settings	171
4.1.5.1	<i>Scene Completion</i>	171
4.1.5.2	<i>Script Inputs Assignment</i>	172
4.1.5.3	<i>Build, Compilation and Distribution</i>	172
<b>4.2</b>	<b>3D-Printing of Skull Phantom</b>	<b>173</b>
<b>4.3</b>	<b>AR Application Outlook</b>	<b>177</b>
<b>4.4</b>	<b>Test</b>	<b>179</b>
<b>4.5</b>	<b>Validation</b>	<b>182</b>
<b>5</b>	<b>Results</b>	<b>189</b>
<b>6</b>	<b>Discussions</b>	<b>199</b>
<b>7</b>	<b>Conclusions and Future Research</b>	<b>204</b>
<b>8</b>	<b>Bibliography</b>	<b>208</b>

## II. Figure's List

Figure 2. 1 Cutting lines for the Mandibular and Maxillary Osteotomies.	6
Figure 2. 2 Moving axes for the maxillary repositioning.	7
Figure 2. 3 Printed surgical guides for mandibular and maxillary osteotomies.	8
Figure 2. 4 Dental splint example of usage.	9
Figure 2. 5 Details of the commercialized screws by the Stryker company.	10
Figure 2. 6 Details of the commercialized plates by Stryker company.	11
Figure 2. 7 Representation and real appearance of the CT gantry structure.	12
Figure 2. 8 Working principle of the CT Imaging.	13
Figure 2. 9 Procedure performed for the creation of the CT images.	13
Figure 2. 10 Attenuation Coefficient distribution for some human structures and tissues.	13
Figure 2. 11 Virtual Reality, Augmented Reality and Mixed Reality definitions.	14
Figure 2. 12 Representation of the reality-virtuality continuum proposed by Milgram.	15
Figure 2. 13 The "Sword of Damocles" device by Sutherland.	15
Figure 2. 14 Image of the KARMA project.	16
Figure 2. 15 Block schemes of Monitor-based and See-Through (Video and Optical) AR systems.	18
Figure 2. 16 AR tracking modalities.	20
Figure 2. 17 Marker examples.	21
Figure 2. 18 Representation of the model of the camera.	23
Figure 2. 19 Tangential and radial distortion trends in horizontal and vertical directions.	26
Figure 2. 20 Head Mounted Devices examples.	29
Figure 2. 21 Optical see-through AR system diagram.	30
Figure 2. 22 Video see-through AR system diagram.	31
Figure 2. 23 Augmented scene in the Jiang et al. study.	33
Figure 2. 24 Marker system and augmented scene in the Tsukada et al. study.	34
Figure 2. 25 Modality selection and augmented scene in the Garcia-Mato et al. study.	35
Figure 2. 26 Marker system and augmented scene in the Kramers et al. study.	35
Figure 2. 27 Marker system and augmented scene in the Ackermann et al. study.	36
Figure 2. 28 Marker system and augmented scene in the Gao et al. study.	37
Figure 3. 1 Workflow of the thesis.	64
Figure 3. 2 Outlook of the data saved in the *.VRML format.	66
Figure 3. 3 Outlook of the data saved in the *.STL format.	66
Figure 3. 4 Outlook of the data saved in the *.OBJ format.	66
Figure 3. 5 Icons of some of the model creation commands of Rhinoceros.	68
Figure 3. 6 Icons of some of the model editing commands in Rhinoceros.	68
Figure 3. 7 Rhinoceros graphical interface outlook.	70
Figure 3. 8 Microsoft HoloLens V2 HMD.	72
Figure 3. 9 Brovision AR Marker Generator outlook.	77
Figure 3. 10 AR.js Marker Training outlook.	78
Figure 3. 11 Piffero QR Generator outlook.	78
Figure 3. 12 Vuforia Model Target Generator settings.	80
Figure 3. 13 Example of a generated license in Vuforia License Manager.	80
Figure 3. 14 Unity graphical interface outlook.	83
Figure 3. 15 Visual Studio graphical interface outlook.	84
Figure 3. 16 Picture of the Hull patent.	85
Figure 3. 17 Phases of the Multi Jet Fusion 3D-printing process.	86
Figure 3. 18 HP Inc Multi Jet Fusion 3D Printer.	87
Figure 3. 19 Color Jet Printing (CJP) process phases.	89
Figure 3. 20 ZPrinter 450 3D-printer machine.	89

Figure 3. 21 Go!Scan3D device and hand-wearing mechanism.	93
Figure 3. 22 CloudCompare graphical interface outlook.	96
Figure 3. 23 Aligned nominal and scanned models.	96
Figure 3. 24 Single arrow dimension and the whole set of arrows.	102
Figure 3. 25 Reference Frame Outlook.	102
Figure 3. 26 Back, bottom, front, left, right and top QR codes for M1.	103
Figure 3. 27 Back, bottom, front, left, right and top QR codes for M2.	103
Figure 3. 28 Unity Hub interface for the project initiation.	104
Figure 3. 29 Mixed Reality Toolkit (MRTK) Foundation package import procedure.	106
Figure 3. 30 Target database import procedure.	107
Figure 3. 31 Vuforia Engine import procedure.	108
Figure 3. 32 Text Mesh Pro (TMP) installation window.	108
Figure 3. 33 Build settings window.	109
Figure 3. 34 Project settings, Player (Resolution and Presentation).	110
Figure 3. 35 Project settings, Player (Publishing Settings-Supported Device Family).	111
Figure 3. 36 Project settings, XR Plug-in Management.	112
Figure 3. 37 Project settings, XR Plug-in Management (Windows Mixed Reality).	112
Figure 3. 38 Project settings, Audio.	113
Figure 3. 39 Mixed Reality Toolkit inspector, Spatial Awareness.	114
Figure 3. 40 Mixed Reality Toolkit inspector, Input.	115
Figure 3. 41 Mixed Reality Toolkit inspector, Diagnostics.	115
Figure 3. 42 Mixed Reality Toolkit inspector, Camera.	116
Figure 3. 43 Main Camera inspector.	116
Figure 3. 44 Vuforia Engine configuration panel.	117
Figure 3. 45 Multi-target creation path.	119
Figure 3. 46 Inspector of the multi-target M1.	119
Figure 3. 47 Inspector of the multi-target M2.	119
Figure 3. 48 Set of 3D-Arrows object.	121
Figure 3. 49 Reference Frame object.	121
Figure 3. 50 Procedure for the creation of a new material.	121
Figure 3. 51 Material to be assigned to osteotomy lines.	122
Figure 3. 52 Material to be assigned to drilled holes.	123
Figure 3. 53 Material to be assigned to 3D-arrows.	124
Figure 3. 54 Material to be assigned to mediolateral axis of the Reference Frame.	125
Figure 3. 55 Material to be assigned to up-down axis of the Reference Frame.	126
Figure 3. 56 Material to be assigned to anteroposterior axis of the Reference Frame.	127
Figure 3. 57 Model settings of the imported *.OBJ file.	128
Figure 3. 58 Rig settings of the imported *.OBJ file.	128
Figure 3. 59 Materials settings of the imported *.OBJ file.	128
Figure 3. 60 Procedure for the cube creation.	129
Figure 3. 61 Transform component of the cube hologram.	129
Figure 3. 62 Green material to be assigned to the cube hologram.	130
Figure 3. 63 Red material to be assigned to cube hologram.	131
Figure 3. 64 Transform component of the bigger quad of the delta dialog panel.	132
Figure 3. 65 Transform component of the smaller quad of the delta dialog panel.	132
Figure 3. 66 Material to be assigned to the smaller quad of the delta dialog panel.	133
Figure 3. 67 Material to be assigned to the bigger quad of the delta dialog panel.	134
Figure 3. 68 Path for the creation of a Text Mesh Pro object.	135
Figure 3. 69 Transform and Text component of the Up/Down label.	135
Figure 3. 70 Transform and Text component of the Right/Left label.	136
Figure 3. 71 Transform and Text component of the Posterior/ Anterior label.	136
Figure 3. 72 Transform component of the Text Mesh pro elements for current y-delta display.	137
Figure 3. 73 Transform component of the Text Mesh pro elements for current x-delta display.	137
Figure 3. 74 Transform component of the Text Mesh pro elements for current z-delta display.	137

Figure 3. 75 Text component of the Text Mesh pro elements for the current delta display.	138
Figure 3. 76 Transform and Text component of the panel title.	138
Figure 3. 77 Final outlook of the delta dialog panel.	139
Figure 3. 78 'Transform' component of the 'OrientationAxes' object child of M2.	139
Figure 3. 79 'Transform' component of the 'OrientationAxes' object child of cube hologram.	139
Figure 3. 80 Icon component for the first, second and third button.	141
Figure 3. 81 Text Mesh Pro component for the text of the first button.	141
Figure 3. 82 Text Mesh Pro component for the text of the second button.	141
Figure 3. 83 Text Mesh Pro component for the text of the third button.	142
Figure 3. 84 On Click component of the first button.	142
Figure 3. 85 On Click component of the second button.	142
Figure 3. 86 On Click component of the third button.	142
Figure 3. 87 'Transform' component of the Near Menu.	143
Figure 3. 88 Final outlook of the Near Menu.	143
Figure 3. 89 Final outlook of the Unity scene.	143
Figure 3. 90 Line of codes of the 'TargetPosition_Creation' script.	145
Figure 3. 91 Lines of codes of the 'Arrows_Manager' private method.	147
Figure 3. 92 Lines of code of the 'Txt_Manager' private method.	147
Figure 3. 93 Lines of code of the 'Color_Manager' private method.	148
Figure 3. 94 Lines of code of the 'Repositioning_Feedback' script.	149
Figure 3. 95 Input assignment in the 'TargetPosition_Creation' script.	150
Figure 3. 96 Input assignment in the 'Repositioning_Feedback' script.	150
Figure 3. 97 Build creation window.	151
Figure 3. 98 Visual Studio settings to perform compilation and distribution.	152
Figure 3. 99 Path for the launch of the compilation and distribution of the solution.	152
Figure 3. 100 Cranial marker Design A.	153
Figure 3. 101 Cranial marker Design B.	154
Figure 3. 102 Cranial marker Design C.	154
Figure 3. 103 Cranial marker Design D.	155
Figure 3. 104 Cranial marker Design E.	156
Figure 4. 1 Steps of the various phases of the thesis workflow.	159
Figure 4. 2 Skull CAD model from the top viewport.	160
Figure 4. 3 Skull CAD model from the right viewport.	160
Figure 4. 4 Skull CAD model from the perspective viewport.	160
Figure 4. 5 Split and shelled upper skull from the right viewport.	161
Figure 4. 6 Split and shelled upper skull from perspective viewport.	161
Figure 4. 7 Assembly mechanism of bridge support and marker M2 from different views.	162
Figure 4. 8 Skull and bites from the top viewport.	163
Figure 4. 9 Skull and bites from the right viewport.	163
Figure 4. 10 Skull and bites from the perspective viewport.	163
Figure 4. 11 Assembly mechanism of bridge support and marker M1 from different views.	164
Figure 4. 12 Skull, bites, and cranial marker from the top viewport.	164
Figure 4. 13 Skull, bites, and cranial marker from the right viewport.	165
Figure 4. 14 Skull, bites, and cranial marker from the perspective viewport.	165
Figure 4. 15 Colored markers (M1, M2 for upper and lower bite) from the perspective viewport.	166
Figure 4. 16 Colored markers (M1, M2 for upper and lower bite) from the perspective viewport.	166
Figure 4. 17 Osteotomy cutting planes.	167
Figure 4. 18 Relimitation Planes.	167
Figure 4. 19 Relimited osteotomy cutting lines.	168
Figure 4. 20 Drilled holes.	168
Figure 4. 21 Mandible-upper skull assembly mechanism.	170

Figure 4. 22 Internal hooks of the bites for the mandible stabilization. _____	170
Figure 4. 23 Exploded view of the phantom from perspective viewport. _____	170
Figure 4. 24 Final outlook of the M1-related Unity scene. _____	171
Figure 4. 25 Final outlook of the M2-related Unity scene. _____	171
Figure 4. 26 Outlook of the NearMenu. _____	172
Figure 4. 27 Input assignment in the 'TargetPosition_Creation' script. _____	172
Figure 4. 28 Dis-assembled 3D-printed skull phantom. _____	173
Figure 4. 29 Assembled 3D-printed skull phantom. _____	174
Figure 4. 30 Assembled 3D-printed skull phantom. _____	174
Figure 4. 31 3D-printed phantom with QR codes attached on markers. _____	175
Figure 4. 32 Dis-assembled model employed during tests and validation. _____	176
Figure 4. 33 Assembled model employed during tests and validation. _____	176
Figure 4. 34 Initial outlook of augmented scene. _____	177
Figure 4. 35 Outlook of the Near Menu in the augmented scene. _____	178
Figure 4. 36 Outlook of augmented scene after clicking 'App Start' button. _____	178
Figure 4. 37 Outlook of augmented scene after clicking 'Osteotomy Mode' button. _____	178
Figure 4. 38 Outlook of augmented scene after clicking 'Repositioning Mode' button. _____	179
Figure 4. 39 Outlook of augmented scene after M2 has been repositioned. _____	179
Figure 4. 40 Osteotomy task, cutting lines performance. _____	180
Figure 4. 41 Osteotomy task, drilled holes performance. _____	180
Figure 4. 42 Osteotomy task. _____	181
Figure 4. 43 Repositioning task. _____	182
Figure 4. 44 Repositioning task. _____	182
Figure 4. 45 Scanned geometry visualized in the dedicated software of Go!Scan3D. _____	183
Figure 4. 46 Scanned geometry opened in Rhinoceros 6. _____	184
Figure 4. 47 Reconstructed experimental cutting lines and drilled holes. _____	184
Figure 4. 48 Nominal cutting lines and drilled holes. _____	185
Figure 4. 49 Imported nominal (yellow) and experimental (yellow) geometries. _____	186
Figure 4. 50 Sampled points on experimental geometry for the alignment. _____	187
Figure 4. 51 Sampled points on nominal geometry for the alignment. _____	187
Figure 4. 52 Aligned experimental and nominal geometries. _____	187
Figure 4. 53 Cutting lines and drilled holes after alignment. _____	187
Figure 5. 1 User 01 mapping of cloud-to-mesh absolute distance and nominal (blue) lines. _____	191
Figure 5. 2 User 01 mapping of cloud-to-mesh absolute distance and nominal (blue) lines. _____	191
Figure 5. 3 User 01 mapping of cloud-to-mesh absolute distance and nominal (blue) lines. _____	192
Figure 5. 4 User 01 cloud-to-mesh absolute distance histogram and Weibull function. _____	192
Figure 5. 5 User 01 cumulative distribution function. _____	192
Figure 5. 6 User 02 mapping of cloud-to-mesh absolute distance and nominal (blue) lines. _____	193
Figure 5. 7 User 02 mapping of cloud-to-mesh absolute distance and nominal (blue) lines. _____	193
Figure 5. 8 User 02 mapping of cloud-to-mesh absolute distance and nominal (blue) lines. _____	193
Figure 5. 9 User 02 cloud-to-mesh absolute distance histogram and Weibull function. _____	194
Figure 5. 10 User 02 cumulative distribution function. _____	194
Figure 5. 11 User 03 mapping of cloud-to-mesh absolute distance and nominal (blue) lines. _____	195
Figure 5. 12 User 03 mapping of cloud-to-mesh absolute distance and nominal (blue) lines. _____	195
Figure 5. 13 User 03 mapping of cloud-to-mesh absolute distance and nominal (blue) lines. _____	195
Figure 5. 14 User 03 cloud-to-mesh absolute distance histogram and Weibull function. _____	196
Figure 5. 15 User 03 cumulative distribution function. _____	196



### III. Table's List

Table 2. 1 Summary of the commercially available resorbable devices for fixation. _____	10
Table 2. 2 Summary of technical details, results, analysis of all the reviewed studies. _____	38
Table 2. 3 Summary of advantages and disadvantages of AR application in the medical field. _____	62
Table 3. 1 Fundamental technical specification of HMD found in literature. _____	72
Table 3. 2 Technical specifications of the Microsoft HoloLens V2 HMD. _____	73
Table 3. 3 Technical specifications of the HP Multi Jet Fusion 3D-printer. _____	87
Table 3. 4 Technical specifications of the ZPrinter 450 3D-printer. _____	90
Table 3. 5 Technical specification of the Go!Scan3D device. _____	94
Table 5. 1 Approximated distances of the drilled holes in the three osteotomy tasks. _____	189
Table 5. 2 Approximated distances of the cutting lines in the three osteotomy tasks. _____	190
Table 5. 3 Values of 75% Percentile for cutting lines in the three osteotomy tasks. _____	197
Table 5. 4 User 01 performances in the three trials of the repositioning task. _____	198
Table 5. 5 User 02 performances in the three trials of the repositioning task. _____	198
Table 5. 6 User 03 performances in the three trials of the repositioning task. _____	198

## IV. Abstract

Traditional approaches in maxillofacial surgery field expect usage of custom-made 3D-printed surgical guides and resin dental splints obtained with a long CAD modelling process and with high costs. To overcome all related drawbacks of traditional solution, advanced assistances of surgical procedures are emerging, such as Augmented Reality (AR) technology, that blend virtual contents with real-world. The aim of this thesis is the development and test in laboratory of a marker-based AR application to be deployed on Microsoft HoloLens V2 that aids surgeons in both maxillary and/or mandibular osteotomies and repositioning. The application is based on a two-marker system, in which a cranial marker allows to stably visualize holograms both throughout osteotomy and repositioning and a dental marker permits to stably visualize holograms uniquely throughout osteotomy and can be tracked to be aware of osteotomized fragment pose. The application consists of two modalities that user can select from the appropriate menu. First modality is the osteotomy mode, where user displays pipes that stands for osteotomy lines to be followed to cut the target anatomy together with cylinders that highlight on the osteotomized fragment a circular area where drilling will be performed to permit at the end the fixation of the realigned and repositioned fragment. Second modality is the repositioning mode, where user visualizes all the element of the designed interactive feedback for the repositioning of the osteotomized fragment. Virtual contents are designed in Rhinoceros 6 and Unity, the last, together with Visual Studio and Vuforia, is also employed for the development of the AR application. To test the AR application a skull phantom is modelled in Rhinoceros 6 and 3D-printed with ZPrinter 450 Color Jet Printing (CJP) technology. Three participants tested the application. They are asked once to trace with a pencil osteotomy lines guided by cutting lines hologram and the points for drilled holes guided by projected cylinders (osteotomy task) and finally to position dental marker guided by repositioning feedback over a graph paper sheet (repositioning task) for three times. Results are extracted using Go!Scan3D technology, Rhinoceros 6, CloudCompare or directly taking measures on the graph paper sheet.

For the osteotomy sessions, mean deviation for drilled holes is 1.17 mm, while the 75% of points of the traced osteotomy cutting lines falls within 1.24 mm from the designed ones. For the repositioning sessions, anteroposterior mean deviation is 0.97 mm, mediolateral mean deviation is 0.54 mm and mean angular deviation on vertical axis is 0.42°. Results are in line with literature even though errors order hampers an immediate clinical application. Technical annotations from participants, also highlight a certain instability of holograms. Hence, the developed AR application represents a potentially attractive package to be further improved to give to the surgeon a complete assistance for maxillofacial surgeries to correct functional and aesthetic defects.

## V. Abstract

Gli approcci tradizionali nel campo della chirurgia maxillo-facciale prevedono l'utilizzo di guide chirurgiche personalizzate stampate in 3D e splint dentali in resina ottenuti con un lungo processo di modellazione CAD e con costi elevati. Per superare tutti gli inconvenienti relativi alle soluzioni tradizionali, stanno emergendo delle modalità avanzate per l'assistenza delle procedure chirurgiche, come la tecnologia della Realtà Aumentata (AR), che fonde contenuti virtuali con il mondo reale. Lo scopo di questa tesi è lo sviluppo e il test in laboratorio di un'applicazione AR basata su markers da lanciare su Microsoft HoloLens V2 e che aiuti i chirurghi nelle osteotomie e nel riposizionamento sia mascellare che mandibolare. L'applicazione si basa su un sistema a due marker, in cui un marker cranico consente di visualizzare stabilmente gli ologrammi sia durante l'osteotomia che durante il riposizionamento e un marker dentale consente di visualizzare in modo stabile gli ologrammi unicamente durante l'osteotomia e può essere tracciato per accedere alla posa del frammento osteotomizzato. L'applicazione si compone di due modalità selezionabili dall'utente nell'apposito menù. La prima modalità è la modalità osteotomia, dove l'utente visualizza i tubi che rappresentano le linee di osteotomia da seguire per tagliare l'anatomia trattata insieme a cilindri che evidenziano sul frammento osteotomizzato un'area circolare dove verrà eseguita la perforazione per consentire alla fine il fissaggio del frammento riallineato e riposizionato. La seconda modalità è la modalità di riposizionamento, in cui l'utente visualizza tutti gli elementi del feedback interattivo progettato per il riposizionamento del frammento osteotomizzato. I contenuti virtuali sono progettati in Rhinoceros 6 e Unity, quest'ultimo, insieme a Visual Studio e Vuforia, è stato utilizzato anche per lo sviluppo dell'applicazione AR. Per testare l'applicazione AR, un modello di teschio viene modellato in Rhinoceros 6 e stampato in 3D con la stampante ZPrinter 450, una tecnologia Color Jet Printing (CJP). Tre partecipanti hanno testato l'applicazione. Ad essi viene chiesto una volta di tracciare con una matita le linee di osteotomia guidate dall'ologramma delle linee di taglio e i punti per i fori di fissaggio guidati dai cilindri proiettati (attività di osteotomia) e infine

di posizionare il marker dentale guidato dal feedback di riposizionamento su un foglio di carta millimetrata (riposizionamento compito) per tre volte. I risultati vengono estratti utilizzando la tecnologia Go!Scan3D, Rhinoceros 6, CloudCompare o rilevando direttamente le misure sul foglio di carta millimetrata. Per le tre sessioni di osteotomia, la distanza media per i fori per il fissaggio è 1.17111 mm e il 75% percentile per le linee di taglio dell'osteotomia è 1.24342 mm. Per le sette sessioni di riposizionamento che non sono considerate outliers, la deviazione media anteroposteriore è 0.97 mm, la deviazione media mediolaterale è 0.54 mm e la deviazione angolare media sull'asse verticale è 0.42°. I risultati sono in linea con la letteratura anche se l'ordine degli errori ostacola un'applicazione clinica immediata e le annotazioni tecniche dei partecipanti, evidenziano una certa instabilità degli ologrammi. L'applicazione AR sviluppata rappresenta quindi un pacchetto potenzialmente interessante da migliorare ulteriormente per fornire al chirurgo un'assistenza completa per il trattamento di casi clinici che necessitano di interventi chirurgici maxillo-facciali per correggere difetti funzionali ed estetici.

# 1 Introduction

Maxillofacial surgery is the medical field that treats defects of the jawbone, maxillary bone, teeth, and upper skull. In this sphere, the orthognathic surgery or corrective jaw surgery encloses all surgical operations to correct jaw conditions, issues related to lower face structures and airways, TMJ disorders and malocclusion problems that primarily are caused by skeletal disharmonies, asymmetries, and mal proportions and improve facial aesthetics. There are different procedures included in the definition of orthognathic surgery, the main ones are osteotomies and repositioning operations. Osteotomies are those operation in which the treated bony structure is cut to correct the defect or to proceed then with the osteotomized fragment realignment and reorientation through the repositioning procedure.

Before these surgical interventions, the patient undergoes medical routine scanning session and the surgeon commonly studies patient scans to prepare the operation. This phase is commonly named as pre-operative plan. Conventional approaches for the osteotomies are based on the usage of custom-made 3D-printed surgical guides while repositioning operations are assisted by resin dental splints, both obtained with long CAD modelling phases, improved costs, and low adaptive capacity to pre-operative plan changes. To overcome all the related drawbacks of traditional solution some advanced methodologies to aid osteotomies and repositioning interventions are emerging. In particular, the Augmented Reality (AR) technology is the most perspective solution. AR technology is potentially attractive in the whole medical field and especially in the image-guided surgery's context. Furthermore, it is widely tested in maxillofacial surgeries such as osteotomies and repositioning.

AR technology literally augment the real world with a virtual world. AR blends virtual contents, such as virtual surgical guides or graphical aids for the user, with the real object of the environment in which the AR experience is performed. This process is called augmentation. The correct projection of holograms in the real-world is

guaranteed by a robust registration process. Registration can be mediated by vision algorithm, in case of marker-less AR systems, or using active/passive markers, in case of marker-based AR systems. AR systems can be sectioned in two main classes: Monitor-based AR systems and See-Through AR systems. Monitor-based AR systems allow the user to see the virtual content superimposed on the real environment over fixed external monitors while see-through AR systems allow the user to visualize the virtual content in the real surrounding environment directly augmenting its view through head mounted devices.

Since maxillofacial surgeries are long and sophisticated procedures, the integration of the AR devices in the real operating room is not yet reached. However, it must be noticed that AR systems are relatively new technologies, as an example the Microsoft HoloLens V2 device is available in Italy since 2020 and it was released in 2019. Hence, AR system sector is under constant development and current results found in literature are promising for a future application in the real clinical routine.

The aim of this thesis is the development, test in laboratory and validation of a marker-based AR application to be deployed on Microsoft HoloLens V2 see-through device and that can be a complete package to aid surgeons in both maxillary and/or mandibular osteotomies and repositioning.

The AR application will be based on a two-marker AR system and it will expect two modalities. First modality is osteotomy mode, where user displays virtual surgical guides for the assistance of the performance of osteotomy cutting lines and drilled holes for the final fixation of the osteotomized fragment. Second modality is repositioning mode, where user visualizes the elements of an interactive feedback for the repositioning of the osteotomized fragment. Virtual contents of the AR application will be developed starting from surgeon opinions, getting inspired from contents already proposed in literature studies and finally embedding some innovative concepts. The AR application will be then tested on an appositely designed and 3D-printed skull phantom and results extracted validate the application precision. Hardware that will be employed in the workflow of this thesis are the ZPrinter 450 for 3D-printing of the model, the Microsoft HoloLens V2 device for the application

deployment and the Go!Scan3D scanner technology for the results extraction. Software that will be used in the AR application development are Rhinoceros 6 CAD modelling software, Unity videogame and application creation software, Vuforia software for the marker database generation and Visual Studio for C# scripting of all the additional functionality of the AR application. Finally, CloudCompare software will be used for the extraction of some statistical results.

In conclusion, nowadays, it must be noticed that only a few numbers of scientific articles have been published regarding the usage of Microsoft HoloLens V2 device in the medical field, hence, this thesis research is one of the first works that develops AR application for maxillofacial surgery with that technology.



# 2 Research and Background

In this section the fields of application that regards this thesis are introduced. In particular, the Maxillofacial Surgery is analyzed focusing over the mandibular and maxillary osteotomies, involving the maxillary repositioning, and stating the current golden standard solutions in these surgical operations. Then, the Computed Tomography (CT) is introduced focusing on its working principles for the reconstruction of three-dimensional anatomical structure images. Finally, the Augmented Reality (AR) is described in terms of systems, technologies, and methodologies and the state of art of the AR medical application is analyzed.

## 2.1 Maxillofacial Surgery

The main fields of AR application are the maxillofacial surgery, orthopedics, spinal, and neurosurgical fields where target bodies or structures are almost stationary, hence they remain almost still throughout the procedure. This is a crucial requirement for an optimal accuracy of the AR application. For the purposes of this work, we focus over AR application in maxillofacial surgery and hence on this surgical branch.

In details, the application presented in this thesis expects the assistance either of mandibular and maxillary osteotomies (Genioplasty, Sagittal Split Osteotomy (SSO) and Mandible Angle Split Osteotomy and Maxillary Osteotomy) either of maxillary repositioning. All these surgeries require a pre-operative surgical plan to be performed before starting the surgery.

Surgical plan or pre-operative planning is the phase in which the medical equip or the surgeon define all the requirements and steps of the intervention to be performed on the specific clinical case. In this phase, the files to be managed are anatomical models of the patients obtained by scanning targeted structures (Computed Tomography (CT), Magnetic Resonance Imaging (MRI), Fluoroscopy, etc.). CT scans are the golden standard tool for most of the maxillofacial surgeries. The 3D model of the Region of Interest (ROI) in the scanned anatomy are the output of this phase.

Nowadays this phase is fully assisted by computer and dedicated software. Multiple different tools and methodologies to plan and guide surgeries exist, as Computer Aided Design (CAD) and Rapid Prototyping (RP), Computer Aided Engineering (CAE), surgical simulation, Virtual Reality (VR) and AR.

CAD is the use of computers (or workstations) to generate, shape and scale, analyze and hence optimize the design of a surgical instrument or object. CAD output is then employed for 3D printing, machining, or several manufacturing operations.

CAE is the use of computer software to simulate, test, evaluate and possibly optimize the performances of the designed model or production processes before manufacturing.

RP includes different techniques used to fast fabricate a scale model of an object starting from 3D CAD data. Fabrication is performed by 3D printing or additive layer manufacturing technologies. Furthermore, RP models of the anatomy to be treated or phantom permit to test and validate functions, applications, and designs onto the patient data before testing them on real patients.

VR and AR are the most innovative tool in the pre-operative planning. These technologies allow to facilitate data manipulations during the surgery to provide guidelines in the meanwhile of the procedures to give an interactive feedback regarding the status of the surgical operation.

### 2.1.1 Osteotomies and Maxillary Repositioning

Orthognathic surgery or Corrective Jaw surgery involves all surgical operations to correct jaw conditions, issues related to lower face structures and airways, TMJ disorders and malocclusion problems that primarily are caused by skeletal disharmonies, asymmetries, and mal proportions [1]. Finally, this surgery is performed to improve facial aesthetics. There are different procedures included in the definition of orthognathic surgery and osteotomy:

- 1) Maxilla Osteotomy [1]: it is performed to correct upper jaw deformities or open bites, as shown in Figure 2. 1; incisions are made below eye sockets allowing to

move the upper jaw, the roof of the mouth and the upper teeth altogether as a single unit).

- 2) Mandible Osteotomy [1]: it is performed to correct receded mandible or open bites, as shown in Figure 2. 1; Incisions are made behind the molars and lengthwise. Included in mandibular osteotomy procedures there are the Sagittal Split Osteotomies (SSO) and the Mandible Angle Split Osteotomy (MASO). SSO corrects mandible retrusion and mandibular prognathism by forward or backward motion of the cut mandible fragment. MASO corrects prominent mandibular angles.
- 3) Genioplasty [1]: it is performed to advance or retract the chin, as shown in Figure 2. 1; the incision is made below the premolars bilaterally and it is vertically extended to detach the chin from the mandible.

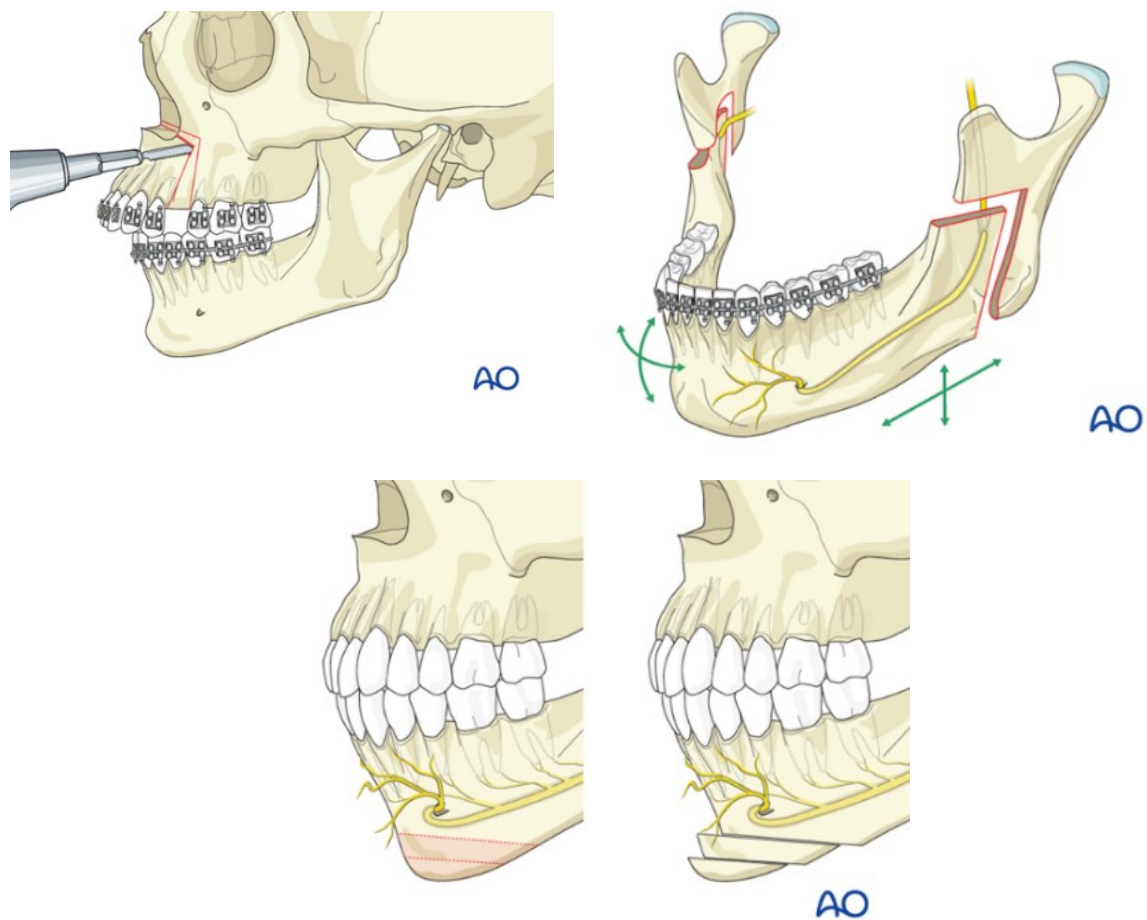


Figure 2. 1 Cutting lines for the Mandibular and Maxillary Osteotomies.

Maxillary repositioning [2] instead is the surgical procedure of orientation and realignment of the cut maxillary fragment to correct the targeted defect by translating and rotating the fragment on the roll-pitch-yaw axes, as shown in Figure 2. 2.

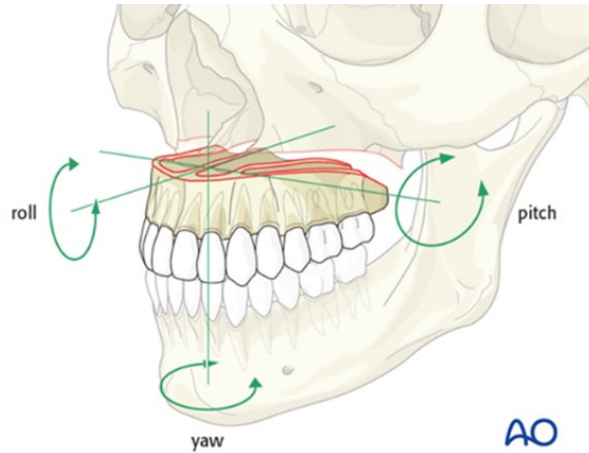


Figure 2. 2 Moving axes for the maxillary repositioning.

Nowadays, the consolidated solution to perform these surgical procedures expects the use of CAD cutting guides and resin dental splints, both custom-made for the specific clinical case.

### 2.1.1 Surgical Guides

The surgical guides for the osteotomies are the lines to be followed by the surgeon during the procedure to correctly cut the bony fragment to be then repositioned and reoriented. These lines are designed on a dedicated software and employed to generate custom-made CAD models of physical objects, shown in Figure 2. 3, that is then 3D-printed and used in the surgical operation [3].

Although CAD cutting guides are an affirmed procedure, supporting osteotomies with them has several drawbacks. First, the time required to design and deliver precludes the use of this technology in emergency situations [4]. Moreover, this technique is highly expensive, and costs are further improved when multiple guides are required to treat the clinical case or to adjust them to inter-operative changes of the surgical plan [4]. Finally, CAD guides-assisted procedures are ideally designed to

attach on bony structures and thus require an extensive dissection of soft tissues around them [4].

With the use of AR application, the perspective is to completely remove and replace the physical cutting guides and directly project the guidance lines on the anatomy. This emerging method requires the usage of CAD software to precisely make the planned osteotomy lines be displayed at the correct position on the anatomy and with the right scale. Moreover, to improve the visualization of these navigation lines they can be realized as surfaces or volumes of few millimeters, they can be colored and meshed to be imported into the dedicated software used to develop the AR application.



*Figure 2. 3 Printed surgical guides for mandibular and maxillary osteotomies.*

### 2.1.2 Resin Dental Splints

Dental splint (Figure 2. 4) is a device, usually made in resin, employed to guide the performance of surgical procedures aimed to correctly reposition the cut part of the jaw [5]. Normally, dental splint is custom-made from bite registrations of the subject. Patient is asked to bite a prefabricated mold realized with a thermoplastic material that easily adapts to patient dental arch [6]. Then the bitten cast is scanned, and the 3D model of its surfaces is obtained and employed in the dedicated CAD software to design the dental splint [6]. The file of the designed dental splint is used to manufacture itself [6]. Intraoperatively, the dental splint is placed on the patient dental

arch and then surgeon shift the cut bony fragment until teeth perfectly fit the splint. In this manner, the surgeon knows when the fragment has been correctly repositioned.

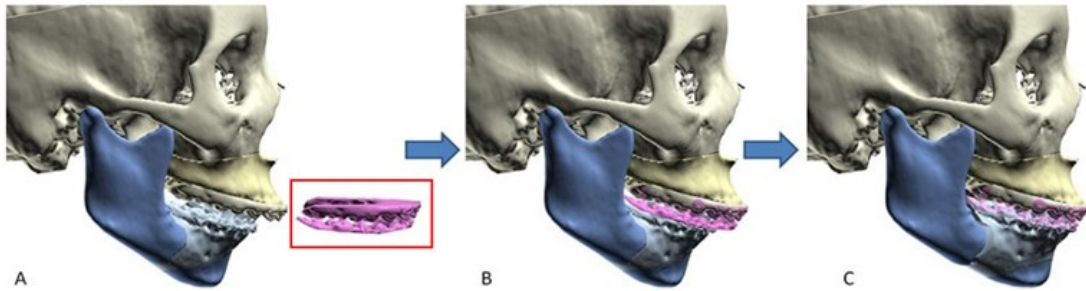


Figure 2. 4 Dental splint example of usage.

### 2.1.3 Fixation Plates and Screws

Orthognathic surgery requires stable fixation for the correct repositioning and healing of osteotomized bony structures. Nowadays, the usage of fixation plates and screws for the bony fragment fixation is a standard.

This fixation modality achieves the appropriate stabilization of the treated structures, allowing a faster bone healing and reducing relapse [7]. Moreover, this solution shortens the intermaxillary fixation period and permits an immediate mouth functionality after the intervention [7].

Titanium plates and screws are normally employed, although the usage of resorbable devices is emerging [8].

The main advantage of the biodegradable or bioresorbable screws and plates is the elimination of the need of a secondary removal operation for the fixation devices [8].

However, the long-term stability and relapse frequency of these solutions are a novel topic of research [8].

Some of the employed resorbable or degradable materials are the Self-reinforced Polyglycolic Acid (SR-PGA), the Polydioxanone (PDS), the Poly-L-Lactic Acid (PLLA), the Poly-D-Lactic Acid (PLDA), the Non-sintered Hydroxyapatite (u-HA) and the Trimethylene-carbonate (TMC) [8]. Table 2. 1 reports some of the commercially available bioresorbable fixation devices solutions.

Table 2. 1 Summary of the commercially available resorbable devices for fixation.

Product	Invention Year	Material	Biodegradation Period
Biofix®	1984	SR-PGA	6 weeks
Orthosorb®	1991	PDS	6 months
FixsorbMX®	1994	PLLA	2 years
Lactosorb®	1996	PLLA/PGA	12-18 months
MacroSorb®	1999	P-L/D-LA	2 years
Resorb®	2001	P-L/D-LA	2 years
Inion CPS®	2001	P-L/D-LA	2 years
BiosorbFX®	2001	P-L/D-LA	2 years
PolyMax®	2003	P-L/D-LA	2 years
Delta System®	2004	P-L/D-LA /GA	2 years
OsteotransMX®	2007	u-HA/PLLA	5.5 years
Inion CPS®	2007	P-L/D-LA/TMC	2 years

Stryker (1998) is one of the world's leading medical technology companies. It spreads in the field of Orthopedics, Neurotechnology and Spine as well as in the Maxillofacial Surgery with innovative products and services. Stryker proposes several valid and advanced alternatives for fixation devices (Figure 2. 5, Figure 2. 6).

Screws could have different lengths, ranging from 3mm to 12mm, and behavior (self-tapping screws, self-drilling screws, locking screws and emergency screws) [9]. Plates could be standard, malleable, Graduated Stability Plates or Locking Plates [9]. They could have different profile heights (0.6 mm, 0.8 mm, or 0.9 mm) and different shapes (L-plates, Z-plates, pre-bent plates, etc.) [9].

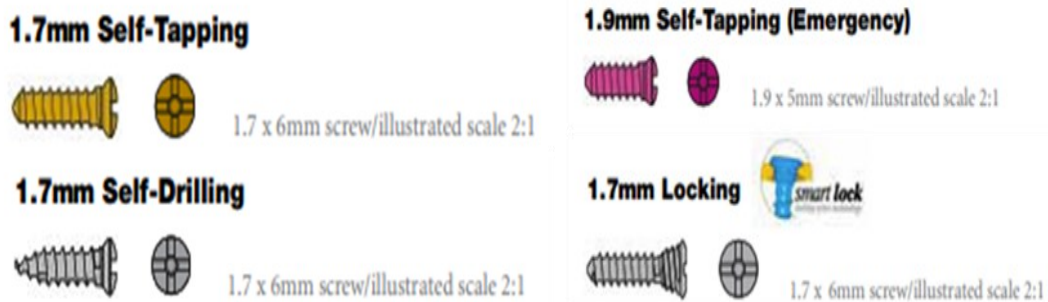


Figure 2. 5 Details of the commercialized screws by the Stryker company.

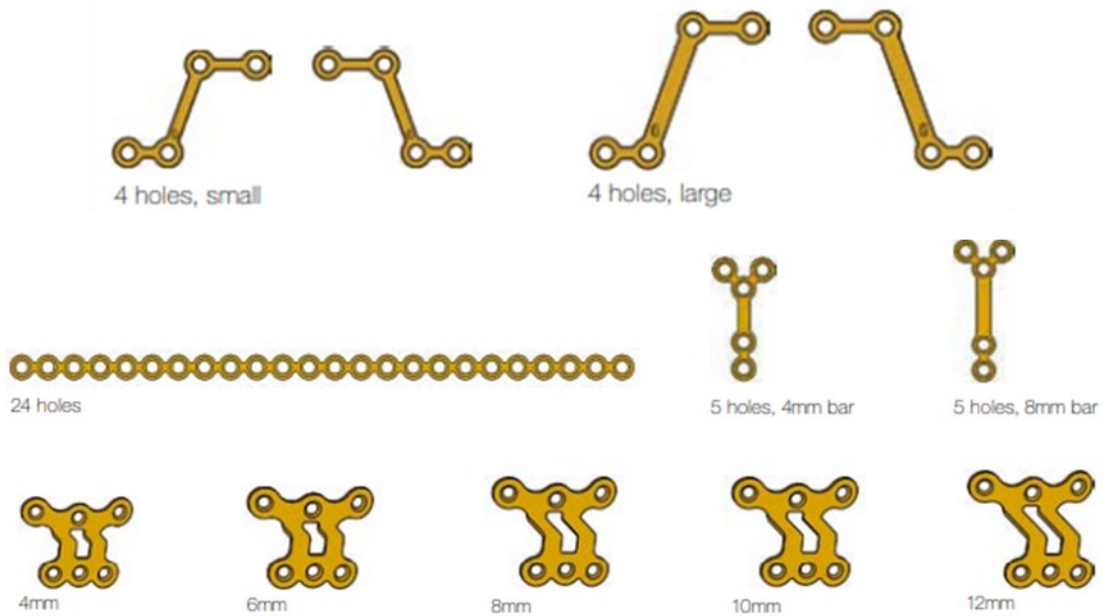


Figure 2. 6 Details of the commercialized plates by Stryker company.

## 2.1.4 Computed Tomography (CT)

In the pre-operative planning phase, commonly, patient undergoes anatomical scanners, such as CT and MRI, to obtain the 3D model of the target anatomy to be treated, such as mandible and maxilla for maxillofacial surgeries. CT is one of the most used scanners in this phase and the 3D model obtained from the scanning session is then employed in the dedicated software to plan the surgical intervention.

CT scan is a medical imaging technique employed in radiology to visualize in a non-invasive manner the internal anatomical structure. CT uses radiation in the form of collimated X-rays (XR) fan beam to slice the object, the result is a series of parallel planar slices to be combined to generate the 3D image of the scanned anatomy.

The main disadvantage of CT imaging is related to the harmful nature due to the usage of ionizing radiation, however novel methodology and technologies employed sufficiently reduced the radiation dose delivered to the patient making CT a clinically safe imaging technique [10]. Moreover, it can be used patients with metallic implants or pacemakers where MRI is contraindicated [10].



CT is composed by an assembly of the XR-tube or source or transmitter and the detector array, named as gantry (Figure 2. 7) [10]. This assembly rotates around the target body at regular angular intervals allowing the scan of the whole target [10].

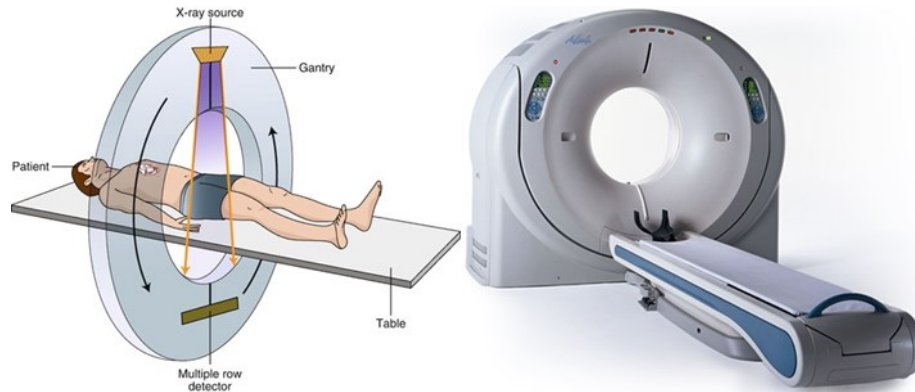


Figure 2. 7 Representation and real appearance of the CT gantry structure.

The XR can penetrate most objects and the absorption of the XR is related to material properties and XR wavelength. Hence detectors, collecting the residual XR beam intensities permits the imaging of the different attenuations induced by the pattern of different densities of the materials in the scanned anatomy [10]. Figure 2. 8 provides a schematic representation of the imaging principle of the CT. The multiple detectors measurements collected from different angles can be rendered in the form of voxels and then further processed with reconstruction algorithms to produce tomographic (cross-sectional) images of scanned anatomy [10]. Hence, tomographic image consists of a square matrix of elements (pixel), each of which represents a voxel of the tissue.

The measurement of the detector permits to assign a value in the grey scale to each pixel proportionally to the correspondent attenuation coefficient in the anatomical voxel [10], as illustrated in Figure 2. 9. The attenuation coefficient, in fact, is a measure of how easily a material can be penetrated by an incident energy beam, such as XR, and it quantifies how XR beam is weakened by the material it is passed through [10][11][12]. Figure 2. 10 present the attenuation coefficient scale for human structures and tissues. It highlights how reproducing through a greyscale the detectors information about the attenuation coefficients permits to easily distinguish targeted structures of the scanned anatomy.

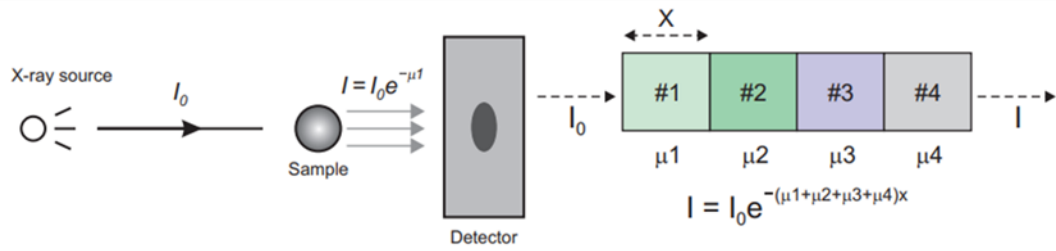


Figure 2. 8 Working principle of the CT Imaging: XR beam pass through a sample object and residual XR beam intensity reaches the detector, based on the sample composition the XR beam pass with multiple different linear attenuation coefficients ( $\mu_1, \mu_2, \mu_3, \mu_4$ ). These measurements are finally employed to recreate the composition of the scanned sample and generate the 2D sliced image to be then composed in the 3D CT image.

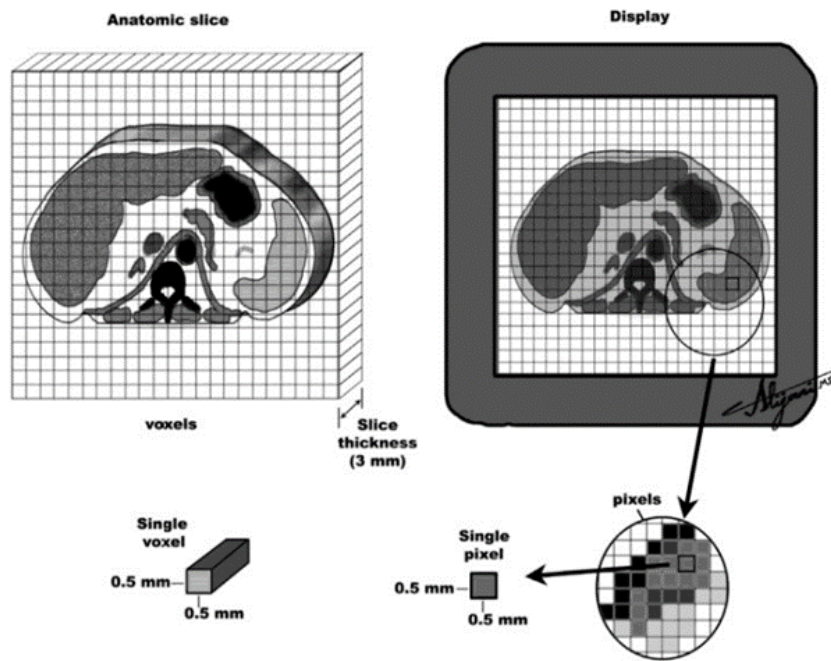


Figure 2. 9 Procedure performed for the creation of the CT images.

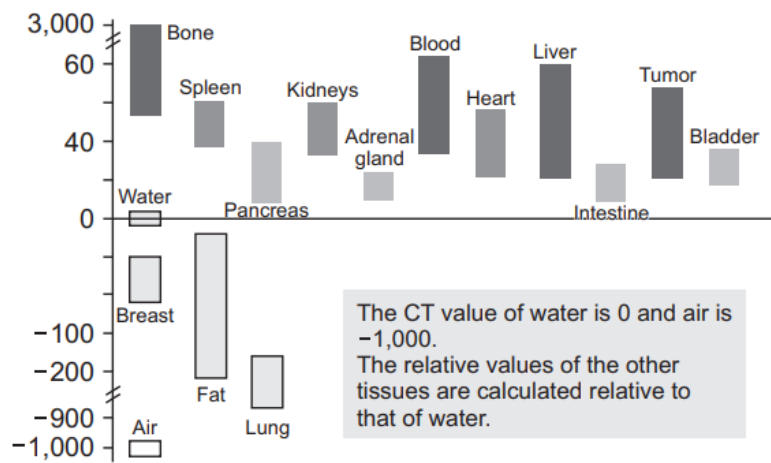


Figure 2. 10 Attenuation Coefficient distribution for some human structures and tissues.

## 2.2 Augmented Reality (AR)

Extended Reality (XR) describes those technologies that improve human vision and perception of the world. The improvement occurs by overlapping, fusion or replacement of real environment and virtual scene. XR is divided in 3 main fields (Figure 2. 11) [13].

First, Virtual Reality (VR), those technologies that completely replace real world creating an artificial virtual world. The user has the visual sensation of complete immersion in the virtual world. VR is mainly employed in entertainment field, as videogames, cinema, film, or sport.

Second, Augmented Reality (AR), those technologies that improve real-world vision by overlapping digital contents expressly digitally designed to the real objects. The user does not lose the real-world perception and vision, but they are improved with additional information that improve or facilitate their experience. AR is not context-specific, and it is widespread employed, hence we found AR in industries and companies as well as in the entertainment field and in many medical applications.

As last, Mixed Reality (MR), those technologies that are in between the VR and AR since here the real and virtual worlds are intertwined and the user can manipulate and interact with digital object overlapping the real world.

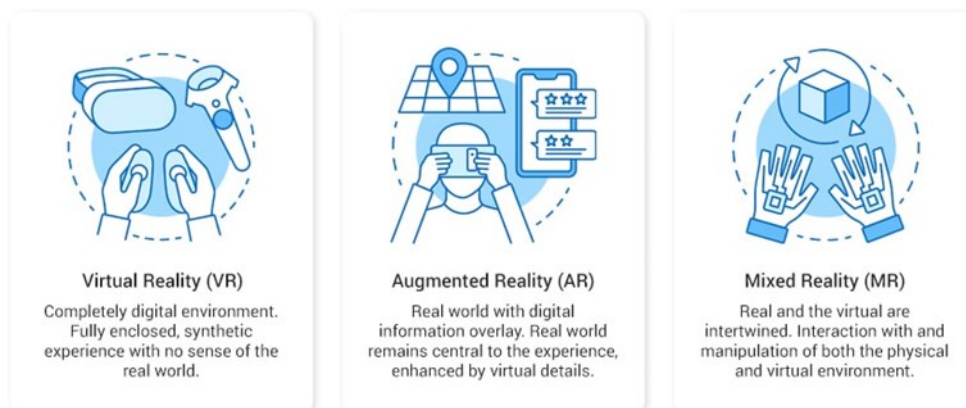


Figure 2. 11 Virtual Reality, Augmented Reality and Mixed Reality definitions.

Milgram (1994) introduced reality-virtuality continuum (Figure 2. 12) that portrays these technologies and their division [14]. Milgram stated that the real world is an

extreme of the continuum and VR is the opposite end. Hence, the AR belongs a place in the continuum that is much closer to real-world extremity than to VR. The closer the technology is to the VR the more real elements reduce and computer-generated content increases. The MR instead touches both the real and virtual environments.

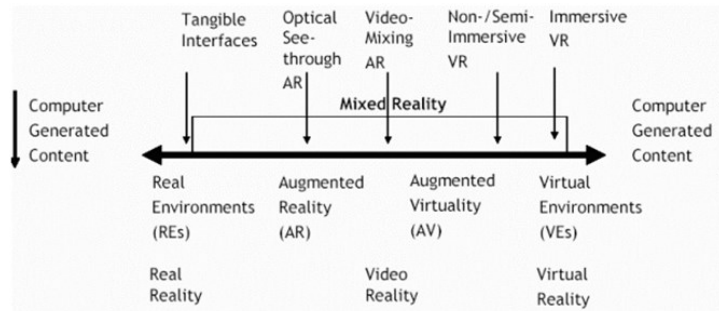


Figure 2. 12 Representation of the reality-virtuality continuum proposed by Milgram.

## 2.2.1 History

In 1968, the first AR technology has been developed by Professor Sutherland at Harvard. He invented “The Sword of Damocles” device (Figure 2. 13). It was a sort of head-mounted display hanging from the ceiling over the user head that permits in this manner the user to experience a virtual content overlayed onto real environment [15].

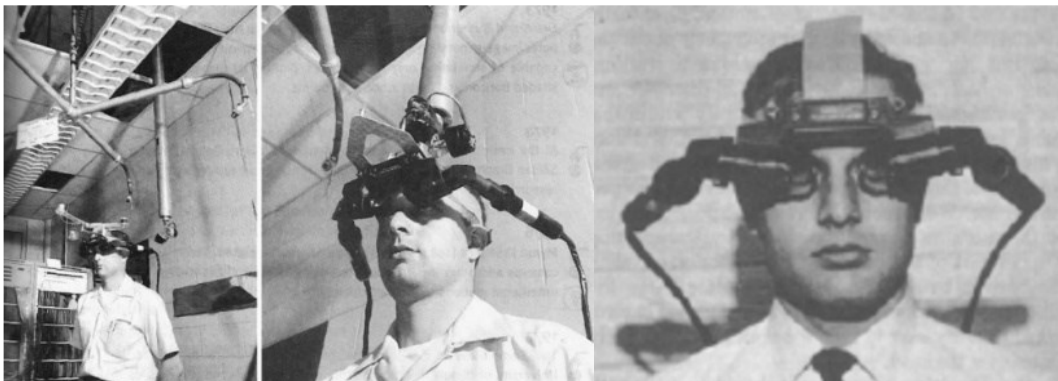


Figure 2. 13 The “Sword of Damocles” device by Sutherland.

In 1983 M. Callahan developed the first optical see-through head-mounted device employing half silvered mirrors and monochrome cathodic-ray tube (CRT) [16]. In 1990, for the first time, T. Caudell employed AR in an industrial application at Boeing

Company. AR was applied to assist military and space applications. In 1993 one of the first major project based on AR, the KARMA (Knowledge-based AR for Maintenance Assistance), has been developed. KARMA project expects the use of a head-mounted device to provide information about the use of a laser printer [17], as shown in Figure 2. 14. In 1999, NASA employed AR technology to improve navigation during flight tests. In 2000, Kato invented the ARToolKit, a software that can capture real actions also allowing the interaction with virtual objects.



*Figure 2. 14 Image of the KARMA project.*

Since then, many improvements have been conducted in the AR sphere. Nowadays, AR is largely employed in a wide variety of fields: advertising, gaming, industry, training and education, medicine, and many other spheres.

## 2.2.2 AR Technology

AR application requires both software and hardware including computing devices as laptop, smart-phone or tablet, a monitor or a display as output device, a camera, one or more markers and a tracking system. Markers, that will be deeply explained in the following sections, are references employed by the AR device to combine real and virtual elements in the proper manner.

Both the mobile and the fixed AR technology forms exist. They differ in the places where the user can use them.

The mobile AR systems are employed with smartphones and tablets while the fixed systems require to be employed in the place where they have been set, and the user

vision is mediated through monitors. The major advantage of the mobile AR technology is the adaptive capacity, they can be employed everywhere without any limitation, however the fixed systems can realize more accurate and advanced augmentations.

A complete AR system requires at least three components: a tracking component, a registration component, and a visualization component.

AR systems could be sectioned in three main classes [14]: Monitor-based AR systems, See-Through AR systems and Spatially AR systems.

The Monitor-based AR systems (Figure 2. 15) allow the user to see the virtual content superimposed on the real environment without the necessity of wearing some special devices or glasses.

This approach is largely preferred when the AR system application or testing is performed in laboratory or whenever low-cost requirements are needed, as an example for demonstrations. Monitor-based AR systems are not hugely complex systems, however, they require the precise positioning in the real world of the object to be augmented, since then on the display it will be frame by frame combined with the virtual content generated by a computer [14].

See-Through AR systems (Figure 2. 15), instead, are more complex systems that adaptively allow the user to visualize the virtual content in the real surrounding environment. Commonly these systems achieve the augmentation on a display by overlapping the computer-generated content onto directly viewed real-world. Displays are an already affirmed technology like the Head-Mounted Displays (HMD), that will be deeply described in the following sections.

Employing See-Through AR systems, the virtual scene is projected in the user view accounting for its head position and direction and as the user moves the virtual content is regenerated with respect to the new position. In this scenario, some critical issues appear. First, there is the need of precisely calibrate and match the viewpoints, then an adequate field of view is necessary and again the visualization must account and prevent, as much as possible, the possibility of occlusion between objects of the virtual and real scenario. Perceptual and technological issues have been partially eliminated

by the usage of video-based, more than optical, HMDs. However, the need of an accurate matching of camera and observer viewpoints remains [14].

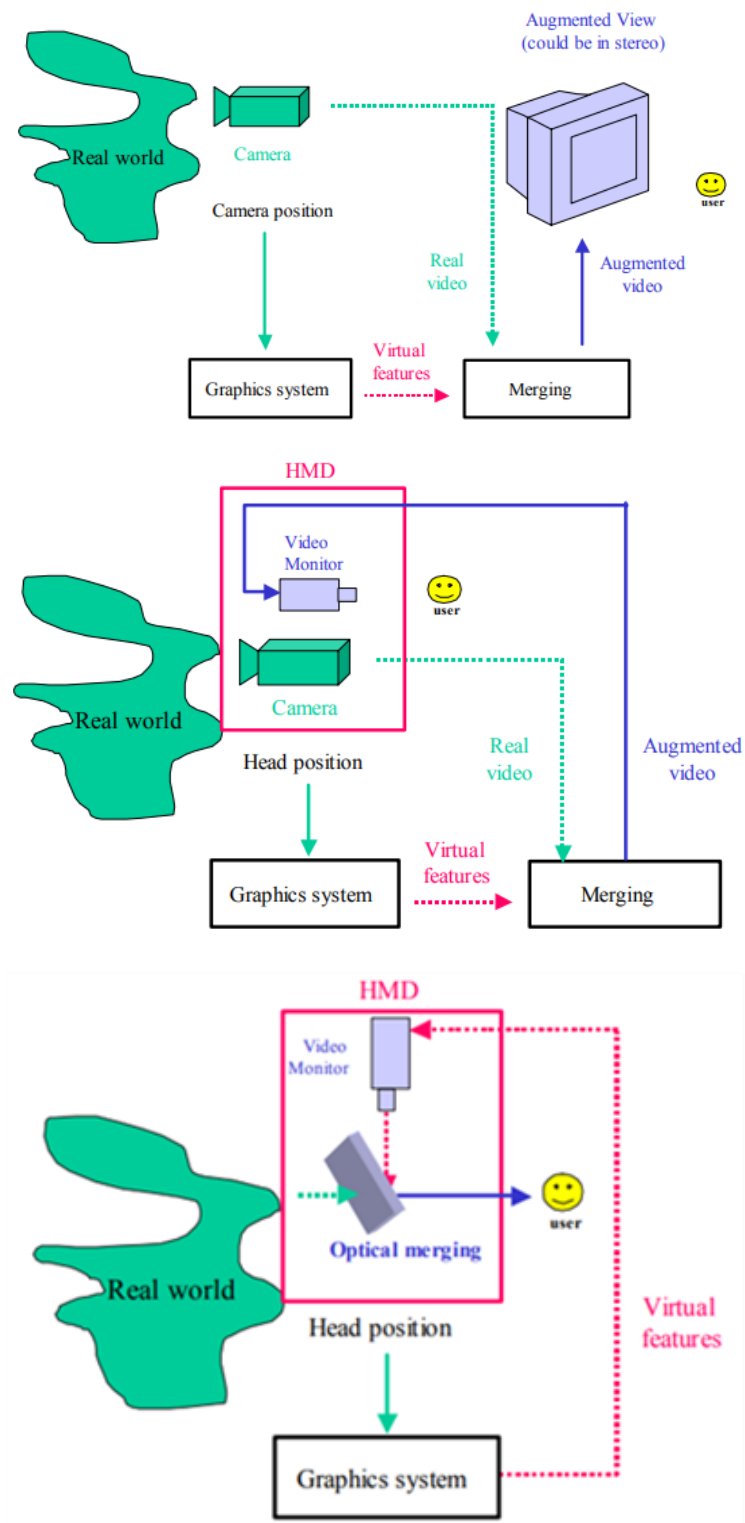


Figure 2. 15 Block schemes of Monitor-based and See-Through (Video and Optical) AR systems.

## 2.2.3 AR Tracking

The tracking system is the technique to be employed to correctly place the reality augmentation in the real scene. It is defined as a dynamic process of scanning and recognition of the HMD's. The tracking system is a strong factor affecting accuracy of the AR application. In this section all the available and different techniques and methods of tracking are explained.

Globally, the tracking problem can be tackled employing two main approaches [14]:

- 1) **Relative Localization:** it consists in the integration of multiple sensor readings to extract the position and orientation, starting from the initial position and continuously iterating that integration.
- 2) **Absolute Localization:** this approach relies on active or passive landmarks, maps matching or satellite-based signals.

As shown in Figure 2. 16 the most common tracking method can be divided into 2 main categories [17]:

- 1) **Outdoor Methods:** they are used when the real scenario is non-constrained, and the user's motions are less predictable. Outdoor techniques are categorized into inertia-based methods and GPS methods:
  - Inertial systems employ gyroscopes and accelerometers to detect mobile device or camera position.
  - GPS methods are systems based on satellites signals capable to track the user position. They employ a database made of multiple viewpoints with images collected during years at different daytimes.
- 2) **Indoor Methods:** they are used when AR application and user's movements are defined within a limited region. Indoor environments mean scenarios that are not dimension-varying and where user's motions are predictable. Indoors-methods are accomplished by two modalities:
  - **Outside-In Method:** the sensor is an external sensor fixed in the environment at a known position. Markers are placed on the user HMD



and the sensor is located outside the user and it senses the user markers. These systems are low obtrusive, but they are affected by occlusion issues.

- Inside-Out Method: markers are placed in the surrounding environment and user carries the sensor that senses marker signals. These methods provide a world-based information.

Indoors-system are categorized into SLAM (Simultaneous Localization and Mapping) and Vision-based techniques.

SLAM method was developed, and it is still commonly applied, in the robotic engineering and industries field [18]. SLAM is a technology which understands the physical world through feature points [18], with this method the device can track itself in the map and simultaneously build a virtual map of the surrounding environment.

Vision-based method uses image processing techniques to solve the tracking problem. Vision-based techniques exploits functionalities of camera vision [19]. They need a computer vision image processing algorithm and are divided into marker-based and marker-less methods [17].

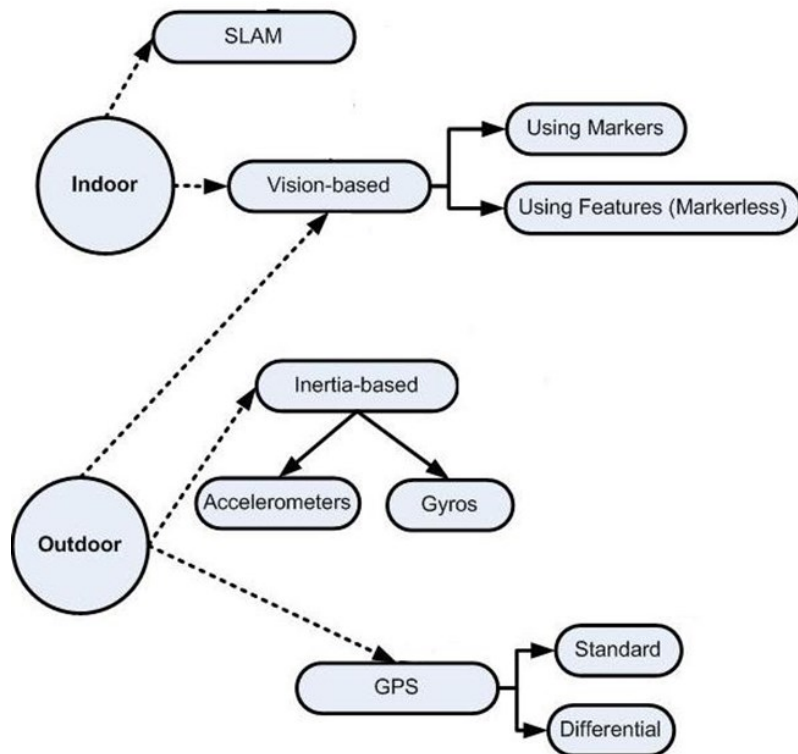


Figure 2. 16 AR tracking modalities.

In Marker-based methods, markers drive computers algorithm in the tracking. This solution reduces the computational costs, but the marker dependency allows the tracking only when they are visible [19]. Hence, marker-less tracking techniques offer solution for the mentioned problems. They are based on the research of real-world elements or features, such as geometrical features, to be registered and employed in the tracking without the need of any marker [19].

Markers are classified into active and passive. Active markers hold an emissive capacity, they generate their own signal that is then collected by sensors. Passive markers do not emit energy but reflect the energy of other sources with a highly featured pattern that define the virtual shape that the AR program or application is looking for in the real scenario. The main requirement to have a good marker deals with sizing of enclosed features and directly with the type of pattern adopted. The higher is the number of features the easier is the detection and recognition of the marker by the vision algorithm. After AR system recognized the target image of the marker, the algorithm calculates the marker/camera relation and permits the virtual object visualization at the correct location. Different websites allow to generate appropriate markers for AR application, with different features, sizes, number of features, colored or non-colored markers, etc. (Figure 1. 7).

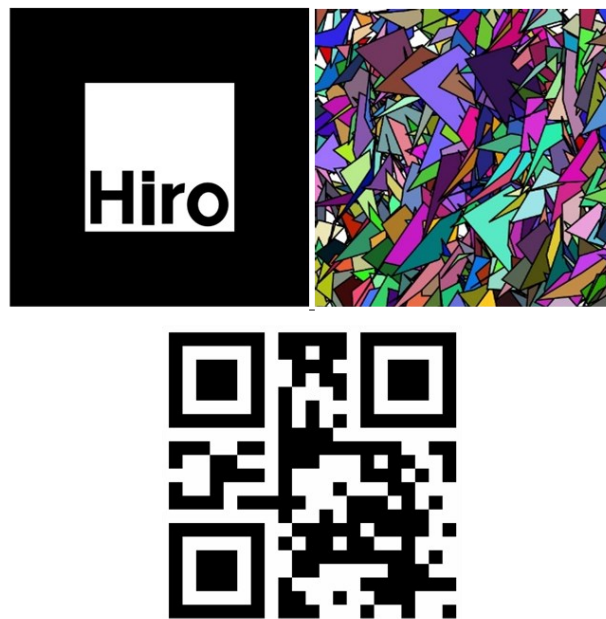


Figure 2. 17 Marker examples.

To correctly show the AR content on the display, the homogeneous transformation matrix (T) is calculated. The T matrix notation is obtained by accounting for the rotation matrix associated to a sequence of ordered rotation, R for which holds  $|R|=1$  and  $R^T R=I$ , and a translation vector t, as illustrated in Equation 1.

Eq.1

$$T = \begin{bmatrix} R & t \\ 0 & 1 \end{bmatrix}$$

Moreover, by employing the Chain Rule is it also possible to compose the coordinate transformation, in detail we can obtain the transformation matrix that allows to pass from coordinate frame A to coordinate frame C by passing through the coordinate system B, through this rule, as explained in Equation 2.

Eq.2

$$T_{C \leftarrow A} = T_{C \leftarrow B} \cdot T_{B \leftarrow A}$$

The T matrix and the Chain Rule are employed to convert from world coordinate system to camera coordinate system, and in turn, to convert from camera coordinate system to retinal coordinate system [20].

The first coordinate conversion occurs by pre-multiplying the homogeneous coordinates expressed in the world frame (W) with the transformation matrix T that allows to pass from world system to camera system, this is a transformation from a three-dimensional point to a three-dimensional point expressed by the Equation 3 [20].

Eq.3

$$\begin{pmatrix} X_c \\ Y_c \\ Z_c \\ 1 \end{pmatrix} = T_{C \leftarrow W} \begin{pmatrix} X_w \\ Y_w \\ Z_w \\ 1 \end{pmatrix} = \begin{bmatrix} R & t \\ 0 & 1 \end{bmatrix} \begin{pmatrix} X_w \\ Y_w \\ Z_w \\ 1 \end{pmatrix}$$

Where R is the rotation matrix and t the three-dimensional translation vector that expresses the relative pose between world and camera coordinate systems.  $[X_c \ Y_c \ Z_c \ 1]^T$  and  $[X_w \ Y_w \ Z_w \ 1]^T$  are the homogeneous coordinates of the same point expressed respectively in the camera and world reference frame [20].

The following step expects the conversion from the camera coordinate system to the retinal coordinate system. This transformation is a transformation from a three-dimensional point to a point displayed in a bi-dimensional plane, hence distortion arises. At this point it could be useful to present the camera model to completely understand the procedure.

Figure 2. 18 illustrate this model. The point O is the camera's center point and corresponds to the center of the camera reference system [20]. The point O<sub>1</sub> indicates the intersection between the z-axis of the camera reference system, termed as principal axis, and the image plane [20]. The retinal reference frame and the pixel reference frame share the same image plane but with different origins [20]. Finally, the distance in between point O and point O<sub>1</sub> (O - O<sub>1</sub>) is named as focal length (f) [20].

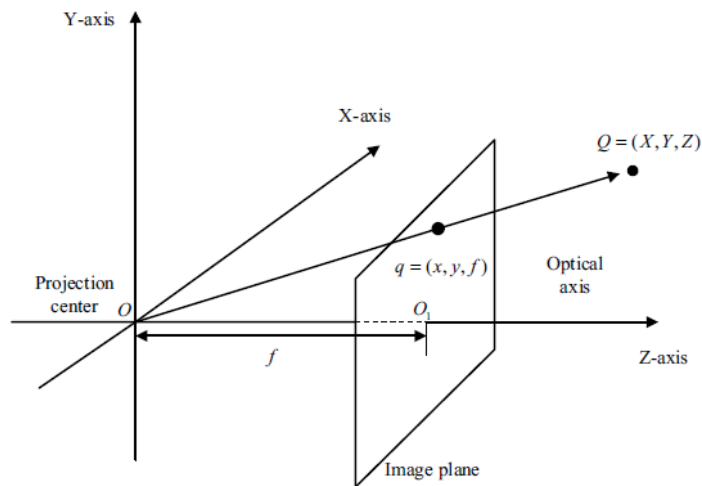


Figure 2. 18 Representation of the model of the camera.

Transformation from camera to retinal frame expressed by Equation 4 [20]:

Eq.4

$$Z_c \begin{pmatrix} x \\ y \\ 1 \end{pmatrix} = \begin{bmatrix} f & 0 & 0 & 0 \\ 0 & f & 0 & 0 \\ 0 & 0 & 1 & 0 \end{bmatrix} \begin{pmatrix} X_c \\ Y_c \\ Z_c \\ 1 \end{pmatrix}$$

Where  $[x \ y \ 1]^T$  are the coordinates of a point in the retinal reference frame,  $[X_c \ Y_c \ Z_c \ 1]^T$  are the homogeneous coordinates of the same point expressed in the camera reference frame [20].

The conversion from retinal coordinate system to pixel reference frame is expressed in the Equation 5 [20].

Eq.5

$$\begin{pmatrix} u \\ v \\ 1 \end{pmatrix} = \begin{bmatrix} \frac{1}{d_y} & 0 & u_0 \\ 0 & \frac{1}{d_y} & v_0 \\ 0 & 0 & 0 \end{bmatrix} \begin{pmatrix} x \\ y \\ 1 \end{pmatrix}$$

Where  $[u \ v \ 1]^T$  are the coordinates of a point in the pixel reference frame,  $[x \ y \ 1]^T$  are the coordinates of the same point expressed in the retinal reference frame,  $(u_0, v_0)$  are the coordinates of the main point of the camera in retinal coordinate system,  $(d_x, d_y)$  are the pixel's physical dimensions about the x-axis and y-axis of the image plane [20].

We now merge the findings of Equation 3, Equation 4 and Equation 5 in a unique expression, Equation 6.

Eq.6

$$Z_c \begin{pmatrix} u \\ v \\ 1 \end{pmatrix} = \begin{bmatrix} \frac{1}{d_y} & 0 & u_0 \\ 0 & \frac{1}{d_y} & v_0 \\ 0 & 0 & 0 \end{bmatrix} \begin{bmatrix} f & 0 & 0 & 0 \\ 0 & f & 0 & 0 \\ 0 & 0 & 1 & 0 \end{bmatrix} T_{c \leftarrow w} \begin{pmatrix} X_w \\ Y_w \\ Z_w \\ 1 \end{pmatrix}$$

The perspective projection matrix (P) could be introduced to simplify the expression of this model and it is defined through the camera internal reference matrix (K) and the already defined external parameter matrix ( $T_{c \leftarrow w}$ ), as depicted in Equation 7, Equation 8 and Equation 9 [20].

Eq.7

$$P = K T_{c \leftarrow w}$$

Eq. 8

$$K = \begin{bmatrix} \frac{f}{d_x} & 0 & u_0 & 0 \\ 0 & \frac{f}{d_y} & v_0 & 0 \\ 0 & 0 & 0 & 0 \end{bmatrix}$$

Eq.9

$$T_{c \leftarrow w} = \begin{bmatrix} R & t \\ 0 & 1 \end{bmatrix}$$

In AR systems exist 4 main static sources of error [21]:

- Optical distortion
- Errors in the tracking system
- Mechanical misalignments
- Incorrect viewing parameters (field of view, tracker-to-eye position, and orientation, interpupillary distance, etc.)

They are termed as static since they affect accuracy when the viewpoint and objects are still.

Distortion is typical of camera-lens systems. It could be subdivided into tangential and radial distortion (Figure 2. 19) [22]. Radial distortion is null at the center of the image plane and then it arises going toward the edges [22]. Tangential distortion occurs since the image plane is non-perfectly parallel to the lens [21]. Distortion, being a systematic error, could be mapped and compensated [21]. This can be a hard challenge since it will add weight to our HMD. An alternative solution is to perform a digital compensation by warping techniques [21]. Images, both graphic and digitized, are pre-distorted in a way that they are displayed undistorted [21].

Errors in tracking system are non-easily eliminable since they are non-systematic error hard to be characterized [21]. Mechanical misalignments are discrepancies between the model or specification of the hardware and the actual physical properties of the real system [21].

Mechanical misalignments can be calibrated but generally their compensation is hard to be achieved [21].

Incorrect viewing parameters belongs in the sphere of alignment errors that can be calibrated [21]. They are wrong specification of those parameters that are employed to convert the reported head or camera locations into viewing matrices used to create graphic images [21].

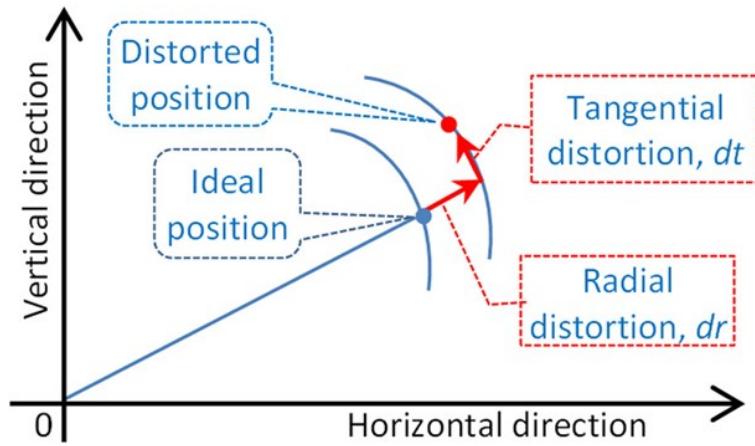


Figure 2.19 Tangential and radial distortion trends in horizontal and vertical directions.

Dynamic errors arise only when viewpoint or objects move in the environment. They are caused by end-to-end system delays or lags [21]. End-to-end system delay corresponds to the time duration from the instant in which the tracking system detected the user's pose to the instant in which the image, corresponding to that pose, is displayed [21]. Delays arise from the fact that AR system components require time to fulfil their role [21]. Delays of 100ms are almost typical, simpler systems can have lower values, but heavier systems can have even longer delays (over 250ms) [21]. To solve this problem, the direct approach is to reduce and theoretically remove system delays hence it becomes crucial to analyze AR system behaviour correlated to tracking speed. At a moderate head rotation rate of 50 degrees per second, system lag should be around 10ms to maintain angular discrepancies below  $0.5^\circ$  [21]. An AR system with 60Hz rate requires 16.67ms. Lower rates than 60Hz can cause object fluttering, while the employment of higher rates that correspond to 10ms lags improve the system expense [21]. Thus, alternative solutions, as matching of temporal streams or prediction of the future viewpoint and object location, are attractive [21].

Moreover, latency problem needs to be accounted. Latency is the difference between camera movement and point movement during time. Due to latency, objects require time to compensate discrepancies with respect to actual position when camera moves [21]. Vice versa, when camera stops the object is corrected. Latency and tracking speed can be faced and solved changing the frame rate and buffering the camera stream [21].

## 2.2.4 AR Registration

The registration is the process through which the physical real world and the virtual contents are aligned to create a coherent augmented environment [23]. Hence, registration permits to correctly display virtual object with respect to the targets.

Practically, registration expects two problem to be faced. First, user's pose in the real world must be accurately determined [14]. Second, the system delay or lag needs to be reduced to tolerance ranges or eliminated to not create harmful location shifts of the virtual objects [14].

The registration in indoor AR systems can be performed using static markers (attached on well-visible parts), small three-dimensional models, a limited number of images or prediction of user path [23].

In outdoor AR systems, registration must rely on markers and the main issue deals with the environmental condition changes [23].

Accuracy in the registration is a crucial requirement in the medical field to make the whole clinical procedure not failing and the registration must be stable with respect to lighting changes and camera rapid motions [23]. To reach the optimal accuracy, information about camera rotation and translation must be collected by sensors [21].

## 2.2.5 AR Visualization

An AR application outlook is made of multiple layers [24]. The main three layers to be identified are real three-dimensional world or scene, augmented or virtual three-dimensional scene and bi-dimensional space of the screen [24].

The real world is the physical environment observable with see-through devices. The augmented or virtual world is the space where the virtual objects are aligned and overlapped to the real physical world. Screen space instead encloses the user-computer interface. It must be noticed the importance of the screen space to make the user that is wearing the HMD understanding and interacting with the virtual content that is projected.

Keil et al. [24] reported different techniques for AR visualization, analyzed below:



- 1) Annotation and labels: by definition, annotations are components that anchor an object and must be registered [24]. They could be of any type of graphical element employable in AR application, vice versa labels are textual information. Annotations and labels are used to add additional contextually useful information in the augmented scene [24]. Nowadays, their usage is widespread.
- 2) Highlights: they consist of the visual highlighting of whole objects or part of them starting from its geometrical model [24]. Highlights could be also animated and commonly they are slightly transparent to avoid occlusion problems. They emphasize elements and drive user selections [24].
- 3) Assisting visual aids: they correspond to all the supplemental visual elements that could be also animated (arrows, pointers, guideline elements or metaphorical indicators) [24]. They could be anchored or indicate specific location of interest of the objects. Aids fulfil a marker function but with an improved information content, due to the communication power that is implicit in their shape and possibly motion [24].
- 4) Additive elements, X-Ray, and AR Explosion: X-Ray visuals uncover hidden and occluded structures [24]. These visualizations represent an enrichment of reality that reveals otherwise non-visible relations [24]. AR explosion diagrams are illustrations employed to present object assemblies, showing relationships, organizing the assembly steps, and describing the layered structure of the parts [24]. They are an enrichment of the reality that creates an additional layer through which the user mental process is stimulated to create a schematic model of a complex object [24].
- 5) Trans-media material: they can be of any form, bi-dimensional or three-dimensional or videos [24]. They are superimposed in the view to enrich the reality simply by improving the user immersion [24].

Between all these solutions for the AR visualization user can customize and select those that result to be the most efficient, adapt and appropriate elements for the development of its AR application.

## 2.2.6 AR Displays

In AR applications, to augment real world with virtual contents displays are necessary. Nowadays, several classes of AR systems can be distinguished [14], but the 2 most general classes, already introduced in previous sections, that can be highlighted are monitor based AR systems and see-through AR systems. We focus on the field of See-Through AR systems (Figure 2. 20). These systems are composed by HMD, tracking system, and scene generator. The tracker measures head position and orientation, with these inputs and with the model the virtual content is generated and then with the scene generator it is appropriately placed in the view as it will be seen from the user head viewpoint. HMDs are defined a set of goggles or a helmet with tiny monitors in front of both eyes that generate the augmented image to be visualized by the wearer [14]. Both AR and VR applications could involve the employment of HMDs. However, in the two fields purposes and procedures are different. The main differences are that in AR systems one or two cameras are embedded on the device, due to the strict dependency to the real world, while on the contrary cameras are not necessary in the VR, where the user is immersed in a completely new virtual world detached from the real world. Hence, the HMD blends virtual content with the real-world scene creating the AR application. See-Through AR systems can be categorized, based on the type of technology employed for the blending, into two main classes [14] that are optical and video see-through displays or HMDs.



*Figure 2. 20 Head Mounted Devices examples.*

Optical see-through displays catch the real-world images through the usage of semi-silvered mirror, termed as optical combiners, in front of the eyes of the user. Optical combiners are partially transmissive hence they permit the real-world direct vision, and partially reflective hence they allow the perception of virtual contents [14] [25]. Theoretically all the light reaching the monitor should be reflected into the eyes and all the real-world light should reach the eyes but, real optical see-through HMDs reduce the amount of light reaching the user by the silver nature of combiners [14]. Silvered mirrors let in only a part of the real-world light, making the user still able to see the real world when the glasses are turned off. Figure 2. 21 shows a scheme of optical see-through AR system [25].

Video see-through AR systems are equipped with head-mounted cameras and for both eyes a correspondent screen. Cameras catch the real scene, the scene generator component generate the graphic images that are then combined with the real scene video, creating the user view in both the eyes' monitors, as a scene in which real physical objects and virtual contents are blended. With these systems, if the HMD is turned off the user becomes blinded, hence, he/she is not able anymore to see both real and virtual scenes [25]. Figure 2. 22 presents the block scheme of a video see-through AR system [25].

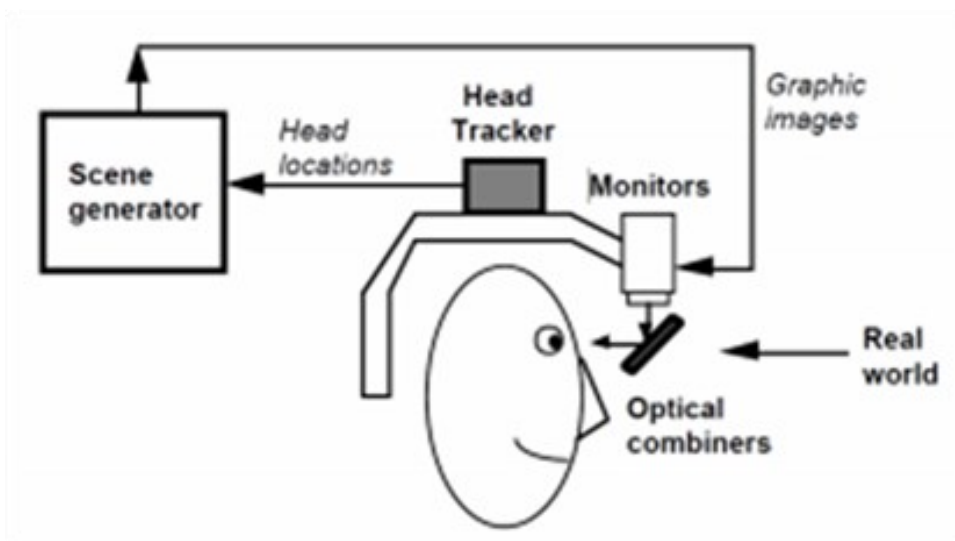


Figure 2. 21 Optical see-through AR system diagram.

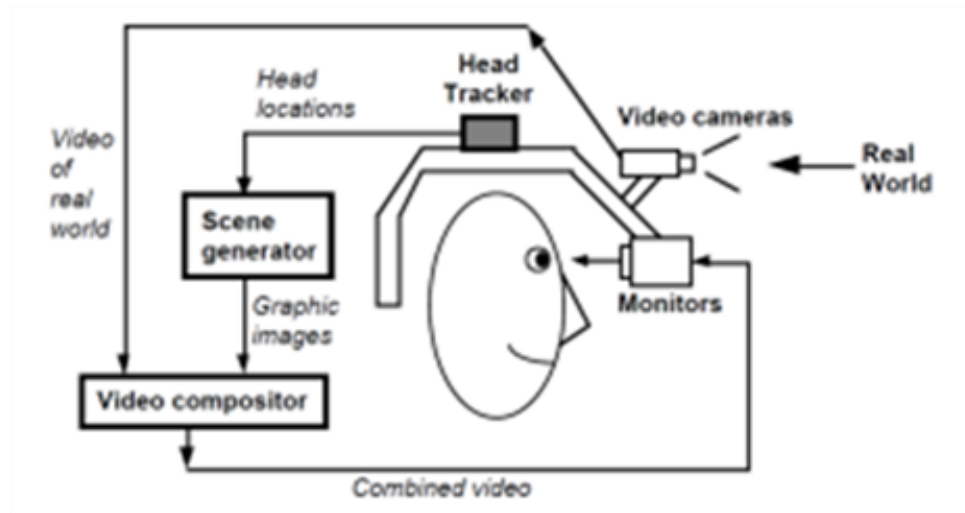


Figure 2. 22 Video see-through AR system diagram.

Video See-Through AR systems offers several advantages despite of the Optical See-Through systems [25]:

- 1) Flexibility in composition strategies. Given the nature of the virtual and real world blending this solution provide a more compelling AR experience, virtual and real scenes are both available in digitized form and can be flexibly merged [25]. Moreover, this situation facilitates the reduction of occlusion problems and ghost-like appearance of virtual contents [25].
- 2) Wide field-of-view. Optical systems are affected by distortion that increases further the visualized object are from the center of view [25]. Manufacturing of wide field-of-view displays with optical mechanism is a hard challenge as well as it is complex to correct distortion with optical systems and they result to be even expensive and physically heavier on the HMD [25]. On the contrary, the digitized nature of the real scene images permits to easily make them undistorted with unwarping image processing techniques [25].
- 3) Real and virtual view delays can be matched. These systems provide the possibility of delaying video of the real world reducing the registration error [25]. In this manner, user always view a lagged version of blended scene [25].

Optical See-Through AR systems offers several advantages despite of the Video See-Through systems [25]:

- 1) **Simplicity.** These systems are simpler approaches than video-based systems. In fact, real world is directly viewed by user and only virtual contents need to be streamed. Although delays could occur, synchronization issues are not present [25]. Optical systems generate a narrow and undistorted field-of-view [25].
- 2) **Optimal Real-World Resolution.** Video systems have a limited resolution that depends on the resolution of the display device. Optical systems only depend on it for virtual contents while the real world is not degraded [25].
- 3) **Absence of eye offset.** Video systems provide a view of real-world that is obtained as if user eyes are placed at cameras locations, creating a spatial lag, termed as offset or displacement from where users see elements to where they can be experienced [25]. Optical systems employing mirrors perfectly mimic the user eyes paths although they make more complex the HMD design [25].

## 2.2.7 Medical AR State of Art

In this section, it is reviewed the usage of AR in medical field analyzing the current state of art. The use of AR in medicine has emerged as training and surgical tool.

AR allows physician to integrate diagnostic and treatment procedures with data visualization for a better surgical experience, improved safety, and optimized costs. AR applications are mainly employed in case of surgeries that involve organs where small movement and deformation occur since mobile organs are hard to be tracked and visualized [26]. For these reasons, more commonly AR applications are focused on the head-brain medical interventions, orthopedic surgery, hepato-biliary system operations, and pancreas treatments [27] [28] [29] [30] [31] [32] [33] [34]. A particular head intervention sphere in which AR found wide application is the Neurosurgical field [27] [28] [29] [30] [31] [32] [33] [34], where it permits a highly accurate localization of lesions and reduced surgical durations. AR applications are improving in their precision and they can be safely employed in endocrine, otorhinolaryngologic, eye,

vascular surgeries, or dental implantology [27] [28] [29] [30] [31] [32] [33] [34]. AR medical applications analyzed in this section are those that were focused on the development of surgical guides to be used during maxillo-facial surgeries or orthopedic surgeries. Literature studies highlighted the powerfulness of AR medical applications in these fields, and they state that AR integrated procedure could achieve comparable performances to traditional surgical methods [27] [28] [29] [30] [31] [32] [33] [34]. However, some limitations still need to be overcome in future developments, as we will see in the following sections.

In Table 2. 2 are listed all the reviewed scientific articles related to the AR application in medical field.

Jiang et al [35] (2018) developed an AR application in the field of dental implant surgery. The application is a marker-less application to guide the correct positioning of the drill to perform the placement of dental implants. Hence, through vision-algorithm, tracking device recognizes drill and dental cast and generates the virtual content that is visualized through a display device over the real scene. Jiang et al. [23] implemented a fast feedback for the user intended as a three-level alarm system capable of changing the color of the planned virtual content (red-yellow-green) based on the optimality of the actual pose of the drill respect to the pose planned in the pre-operative phase, as shown in Figure 2. 23.



Figure 2. 23 Augmented scene in the Jiang et al. study.

Tsukada et al. [36] (2019) proposed a smartphone AR application to assist tibial bone resection. The application is a marker-based procedure (Figure 2. 24). A guide marker is employed to stably visualize holograms that are tibial axes. Holograms are created with a sampling-point process mediated by a pointing marker equipped with fiducial marker (i.e., to generate the hologram of the vertical tibial axis two points of the

vertical axis are sampled with the pointing device, whose marker is tracked, and with them the axis is reproduced). Finally, an oval marker is employed to verify post-operation the accuracy of the operation itself by visualizing the varus/valgus slope, the anterior/posterior slope, and the internal/external rotation angle.

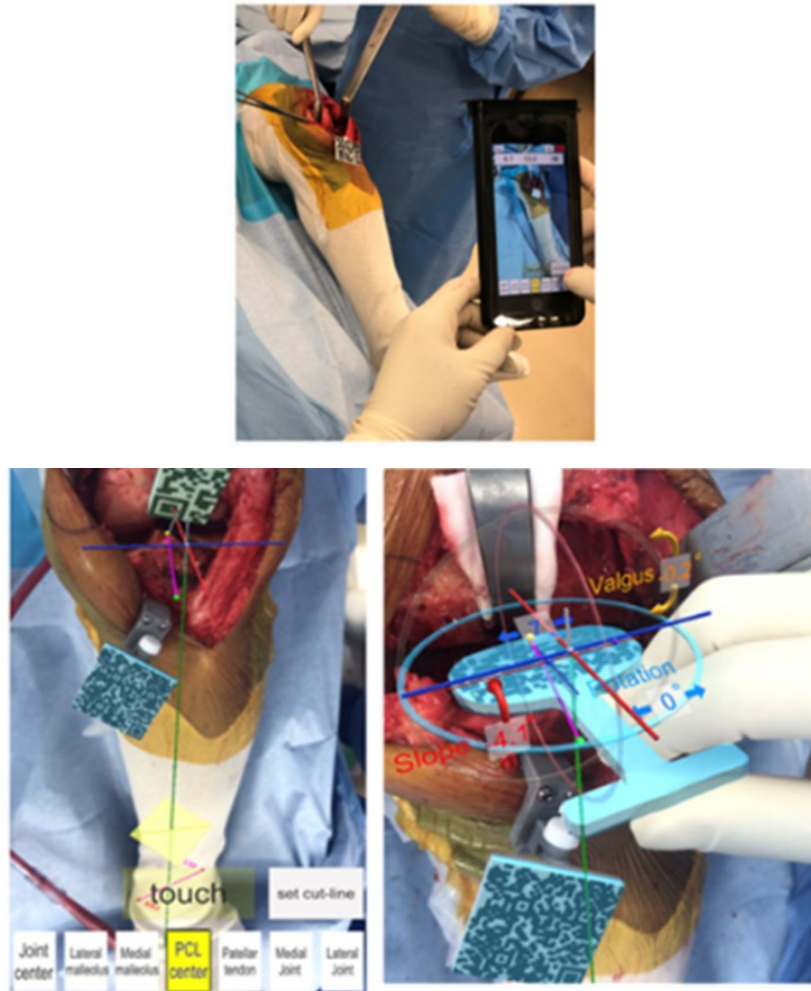


Figure 2. 24 Marker system and augmented scene in the Tsukada et al. study.

Garcia-Mato et al. [37] (2020) developed a smartphone AR application to aid front-orbital advancement procedures. The AR application expects the recognition of fiducial markers placed on the temporal region of the skull phantom by bi-adhesive tape that permits the correct visualization of two different types of holograms for the osteotomy mode (1mm thick osteotomy cutting lines) and for the remodeling mode (cut bone fragment in the target position). Modality can be selected by clicking on the smartphone (Figure 2. 25).

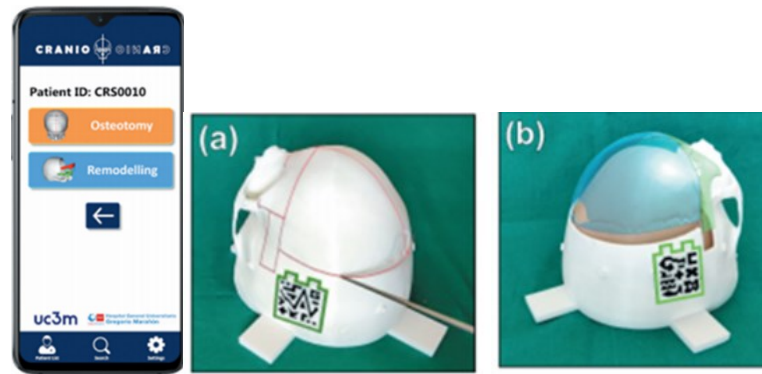


Figure 2. 25 Modality selection and augmented scene in the Garcia-Mato et al. study.

Kramers et al. [38] (2013) developed a smartphone AR application to assist the External Ventricular Drain (EVD) procedure. The application is a marker-based application in which two markers are employed. The first marker is a prismatic marker placed on a pair of safety glasses, hypothesized to be positioned 5mm anteriorly to the nasion and employed to stably visualize the segmented anatomy of the patient's skull with highlighted the ventricles (Figure 2. 26). The second marker is placed on a tool employed as a stylus in the scene, this is a pointing device whose axis is displayed through the equipped marker to improve the depth perception of the user and permit the visualization of the point in which the tool is interacting with the projected anatomy (Figure 2. 26).

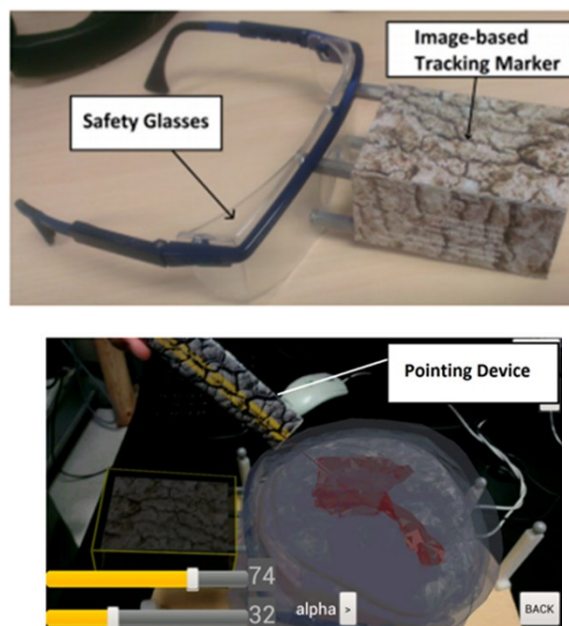


Figure 2. 26 Marker system and augmented scene in the Kramers et al. study.



Ackermann et al. [39] (2021) developed an AR application for Microsoft HoloLens HMD to assist pelvic osteotomy and fragment reorientation. Two custom-made 3D-printed mounts are equipped with markers (black-and-white patterns) and placed through small screws respectively on the pelvis and over the fragment to be reoriented (Figure 2. 27). The pelvic marker is employed to stably visualize the osteotomy cutting planes, as shown in Figure 2. 27, while the marker placed over the fragment is tracked to manage the feedback given to the user. This feedback is composed by two 3D vectors both originating in the center of the femoral head and ending respectively on the center of the actual marker position and on the center of the ideal target position of the marker fixed in the pre-operative planning (Figure 2. 27). Moreover, the angular deviation between these vectors is displayed on a box visualized over the actual marker placed on the fragment to be reoriented (Figure 2. 27).

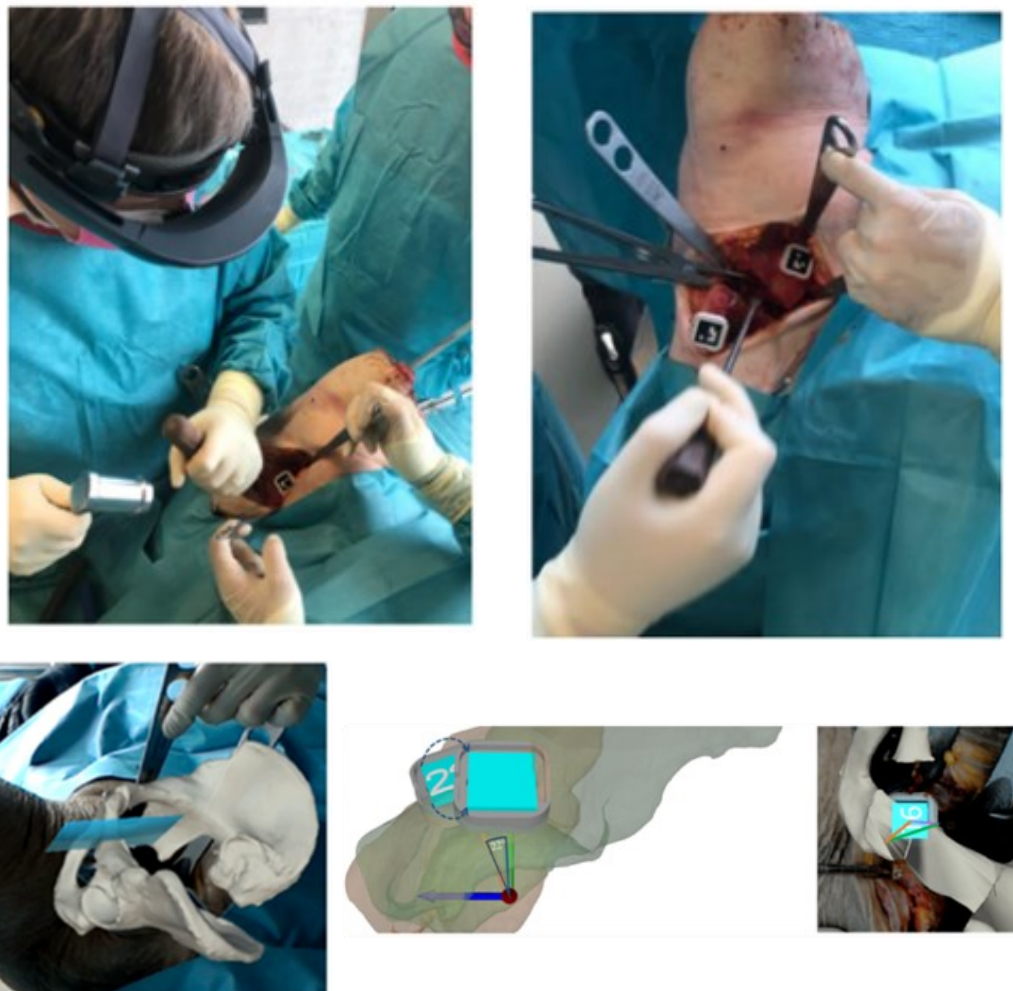


Figure 2. 27 Marker system and augmented scene in the Ackermann et al. study.

Gao et al. [40] (2019) proposed an AR application for the Microsoft HoloLens with the aid of the Unity Software and the Vuforia Toolkit to assist Mandibular Angle Osteotomy Split (MASO) procedures. The application is a marker-based procedure in which two markers (QR-codes) are placed respectively on the splint over the mandible and over the surgical tool employed (Figure 2. 28). The marker plate placed on the mandible through the splint is employed to stably visualize the holograms of the alveolar nerve, mandible, surgical plan (9 navigational points viewed as cylinders), as shown in Figure 2. 28. User can selectively choose which holograms are visualized as transparent holograms and which are hidden, as shown in Figure 2. 28. The marker placed on the surgical tool is continuously tracked and employed to manage the feedback given to the user. The feedback is composed by the angular deviation and the linear deviations on the three axes between the actual pose of the surgical tool, tracked by the equipped marker, and the pose planned in the pre-operative phase for each of the navigational points, as shown in Figure 2. 28. User can select the navigational point whose feedback will be displayed (Figure 2. 28).



Figure 2. 28 Marker system and augmented scene in the Gao et al. study.

Table 2. 2 Summary of technical details, results, analysis of all the reviewed studies.

Study	HMD	Supplementary Devices	Marker	Application	AR Content	Results	Pros	Contros
<b>Lin et al. [41] 2013</b>	Sony HMZ-T1 personal 3D viewer	Charged-coupled Device	Acrylic Resin Marker (60x60x2 mm)	Development of an AR application to assist dental implant placement to either partial (PE) or fully (FE) edentulous patients	Planned implants, adjacent anatomical structures, drill guides and drill stop point, nerve canal and sinus portion	Mean deviation: 0.5±0.33 mm (FE) & 0.46±0.20 mm (PE) Apex: 0.96±0.36 mm (FE) & 1.23±0.42 mm (PE) Angle: 2.70±1.55 ° (FE) & 3.33±1.42 ° (PE) Depth: 0.33±0.27 mm (FE) & 0.48±0.37 mm (PE) Lateral: 0.86±0.34 mm (FE) & 1.1±0.39 mm (PE)	Deviations remain in the clinically safe range, reduced risk of encroaching on sensitive anatomical structures, minimized adverse effects	In vitro study over casts, test performed in ideal conditions hard to be achieved in the reality, uncontrollable human error.
<b>Xu et al. [42] 2015</b>	nVisor ST60	Robot-assisted surgery system (RAS) + Micron Tracker + Micron Tracker cameras	Semi-embedded Marker Complex (MC) fixed with nails	AR Navigation combined with RAS to assist Mandibular Angle Osteotomy (MASO)	Mandible, marker and drill, drilling path and nerves	Position error: 0.95±0.14 mm (experimental group) & 1.64±0.57 mm (control group) Average angle error: 5.34±2.48 ° (experimental group) & 10.46±4.36 ° (control group)	Minimal invasiveness, simplified operation, limited error, RAS improved dexterity and controlled tremor of the surgeon	MC complex design that requires a bridge-support connector module, RAS-related skill requirement for the surgeon

Study	HMD	Supplementary Devices	Marker	Application	AR Content	Results	Pros	Contros
Jiang et al. [43] 2017	nVisor ST60	3D camera	Fiducial marker fixed to mandible by occlusal splint	Development of an AR based Navigation System (NS) to assist Mandibular Angle Split Osteotomy in beagle dogs	Mandible, critical adjacent structures, 5 drilling holes	Time with NS: 208.0±11.9 s Time without NS: 365.7±9.6 s Mean Positional Deviation: 1.29±0.70 mm (entry points) 2.47±0.66 mm (end points) Mean Angular Error: 1.32±1.17°	Decreased operational time, non-invasive placement of the marker, close location of marker to surgical site does not compromise precision, in vivo study	Technical, imaging, registration, tracking and human errors are non-controllable factors
Gibby et al. [44] 2018	Microsoft HoloLens (Novarad OpenSight App)			AR application to place spinal pedicle cannulation guides for pedicle screws placement in lumbar phantom	Trajectory lines (designed angle and depth) and small spheres at the contact point of the phantom with the lines	Placing Time: 200 s Circular Deviation Radius: 2.5 mm	Homogenized performances despite of the skill levels of the user, fast procedure, prevention from fluoroscopy monitoring and radiation delivery	Long preoperative training session, in vitro, non-perfect representation of the phantom to resemble human tissues, manual registration of the holograms
Agten et al. [45] 2017	Microsoft HoloLens		3 Ring Markers attached with adhesive tape	AR-guided lumbar facet joint injections on an agar-embedded phantom	3D model of 2 articulating vertebrae	39/40 perfect needle placements under AR guidance 40/40 perfect needle placements under CT guidance	No potentially harmful placement, no radiation exposure	Manual alignment of the hologram, in vitro, usage of larger needle than routine ones

Study	HMD	Supplementary Devices	Marker	Application	AR Content	Results	Pros	Contros
Tomoki et al. [46] 2017	Microsoft HoloLens (Unity + Vuforia)		Vuforia Markers	Development of an AR method to show stereoscopic view of medical models and surgical instruments	Human models and surgical tools 3D model, additional functions to facilitate the interventions		High quality holograms	
Mitsuno et al. [47] 2018	Microsoft HoloLens	VEC-TRA H1 handheld imaging system		Precise manual alignment of body surface, bone, blood vessels holograms in the surgical field	3D Models of the targeted structures	Alignment time: 45.89 s Mean Error: 2.98 mm	Reduced load to the central processing HMD unit, display stability, easier alignment, sufficient accuracy to conduct navigation tests and intraoperative simulations, objective assistance	Manual alignment
Wang et al. [48] 2016		Panasonic HX A500 (4K Camera) + UI-3370CP-M-GL (monochrome camera) + IntelCore i7-4820K CPU + NVIDIA GeForce GTX Titan Black GPU		Development of an AR system for Oral and Maxillofacial Surgery (OMS) tested on phantom and volunteers	CT-reconstructed model of 6 teeth groups, tooth roots, nerve channels, drilling positions	Overlay Error: 1 mm	Volunteer tests, fast tracking, easy setup, low priced equipment, wide application	Depth perception issues, occlusion problems

Study	HMD	Supplementary Devices	Marker	Application	AR Content	Results	Pros	Contros
Zuo et al. [49] 2020	Microsoft HoloLens	Micron Tracking system		Development of a systematic method to evaluate mixed reality navigation systems during clinical application	3D angiogram of the patient		Qualitative and quantitative evaluation, integration of objective and subjective factors	
Frantz et al. [50] 2018	Microsoft HoloLens (Unity + Vuforia)		RGB Cylindrical Marker	Development of an AR application for Neuro-Navigation on 3D printed skull	Skull model, 2 masses models	Manual registration times: 95 s Mean Holographic Drift: 1.29 mm Mean Surface Point Localization Error: 1.92 mm	Improved hologram stability, continue 360° vision of the marker	In vitro study, manual registration depends on user experience, maintenance of a line of sight is necessary and difficult at arm length distances
Meulstee et al. [51] 2018	Microsoft HoloLens (Unity)	Optical Tracking PS-Tech (PST) Base System with infrared based optical cameras	3D Printed mount to fit one HoloLens site and equipped with reflective markers + reflective 13mm diameter spheres	Development of an AR application for Image-guided Surgery (IGS) on a phantom	Outline of the cube on the measuring board at the planned position	Mean Euclidean Distance: 0.6 ±0.2 mm (Tight-fit Experiment) 0.7±0.4 mm (Loose-fit Experiment)	Uninterrupted view of the surgical site while consulting images, widespread usage, reduced cognitive load, advanced virtual planning	IGS system needs to account for the AR-system generated error that must be estimated

Study	HMD	Supplementary Devices	Marker	Application	AR Content	Results	Pros	Contros
Zhu et al. [52] 2010	Non-Specified (AR Toolkit + 3D Max pose adjustment software)		Marker cemented on the occlusal splint forming Occlusal Splint and Marker Complex (OMS)	Registration strategy for an AR application in Mandibular Angle Oblique Osteotomy	Mandible, OSM complex, cutting planes		Visual information, uninterrupted view of the surgical site, non-invasive marker placement, precise registration method	Synthetic information, occlusal splint does not suit for edentulous patients, markers limited at the lower face
Cecernelli et al. [53] 2020	VOSTARS System	Creo Parametric Software + Simplant Q&O (osteotomy planning)	3 Spherical Markers of 11 mm diameter realized in fluorescent green anchored to occlusal splint	AR application to guide maxillofacial surgical tasks such as Le Fort 1 osteotomy	Osteotomy lines, mandible, nerves, vessels and organs	Trajectory Tracking Accuracy: $\pm 1$ mm Trajectory Length Accuracy: $\pm 0.5$ mm	Simple setup, robust tracking, good ergonomics, possibility of switching from non-augmented and augmented view, appropriate accuracy in guidance of surgical tasks	Need of the integration of some unit in the surgeon equipment to make it freely moving, relatively simple tasks tested, need of an enhanced virtual content involving indicators for repositioning
Schlueter-Brust et al. [54] 2021	Microsoft HoloLens 2			AR application to guide K-wire placement for the glenoid component positioning in reversed shoulder arthroplasty	3D model of the scapula, 2.5mm guidance for k-wire position	Average Entry Point Error: $2.4 \pm 0.7$ mm Average Orientational Error: $3.9 \pm 2.4^\circ$	Comparable accuracy to HoloLens 1 studies	Residual cartilage challenges task and registration, residual soft tissues and blood obscure field of view

Study	HMD	Supplementary Devices	Marker	Application	AR Content	Results	Pros	Contros
Qu et al. [55] 2014	Non-Specified (AR Toolkit + 3D Max pose adjustment software		Marker cemented on the occlusal splint forming Occlusal Splint and Marker Complex (OMS)	AR application for distraction osteogenesis with hemifacial microsomia to define mandibular osteotomy lines and assist intraoral distractor placement	Mandible, critical nerves and tissues, cutting planes, intraoral distractor position		Non-invasive OMS, higher precision in intraoral distractor placement, injuries prevention, better post-operative efficacy	Comfort issues, more user-friendly system is needed
Yavas et al. [56] 2021		Mobile Device Camera (Unity + Vuforia)	Cuboid marker (30x30x30 mm) attached to a triangular prism-shaped support in Polylactic acid and placed on the patient skin	AR marker-based application for neurosurgical navigation in brain tumor visualization	Tumor boundaries at the correct location	Mean Targeting Error: 1.70±1.02 mm Mean Preoperative Preparation Time: 35.7±5.56 s	Clinically feasible technique, low-cost procedure, easy to use navigation technology, prevention from any patient head immobilization	Minimum distance requirement of 10 cm, mobile phone usage limits the duration of the procedure and the capabilities of the application (brain shift detection or deformation due to cerebrospinal fluid), limited battery life



Study	HMD	Supplementary Devices	Marker	Application	AR Content	Results	Pros	Contros
Zhu et al. [57] 2018	Non-Specified (AR Toolkit + 3D Max pose adjustment software)		Marker cemented on the occlusal splint forming Occlusal Splint and Marker Complex (OMS)	Assessment of AR application accuracy in Mandibular Angle Osteotomy (MAO)	Mandible, OSM complex, cutting planes	Post-operative Discrepancies respect to pre-operative plan: 1.18±0.34 mm	Higher accuracy respect to conventional free-hand methods, comparable accuracy respect to individualized templates procedures, more adaptive capacity	Non-suitable for emergency surgery, longer preparation time
Chen et al. [58] 2021		Mobile Computer + Monocular Camera + HuaxiAR1.0 Software	3D printed tooth-borne type visual recognition artificial mark	AR application for the treatment of Unilateral Orbito-Zygomatic Maxillary Fractures	Original fracture appearance, fracture reduction, pre-bending bone plate	Mean Distance between post-operative and virtual surgery plan: 0.431688 mm Average Operation Time: 103.3 min	Strengthened patient-surgeon communication, facilitation of surgical plan revision, shortening of operational time improved safety and accuracy	Limited performances with computer camera, registration is sensible to environmental changes (lights)
Cofano et al. [59] 2021	Epson BT-300, Epson BT-350 nVuzix Vlade, Microsoft HoloLens (Unity)			AR application for the assistance of spinal procedures	CT reconstructions, planned trajectories of screws, sharing of virtual content with non-operative users		Simple and ergonomic modality, shared content, possibility of facing complex hazardous situations rarely faced in the reality (during training)	Accuracy of the simulation and interactions are challenged by the requirements about the acquisition frequency (≥ 500Hz)

Study	HMD	Supplementary Devices	Marker	Application	AR Content	Results	Pros	Contros
Hossain et al. [60] 2021	Non-Specified (EasyAR sense Software Development Kit + Unity + Blender 3D + Audacity)			AR application to aid students as a supplement in anatomy studies	3D model of human structures, animations of the holograms, audio files, User Interface to know about the application, exit or show the details of the scene, labels, gesture interaction with holograms to scale and move them		Quality and promptness and drenching in learning procedure	Audios had some background noise to be removed, heavy application
Han et al. [61] 2018	Non-Specified (AR Toolkit + 3D Max pose adjustment software)		Guiding marker placed on and fixed with an occlusal splint	AR application for the synostotic plagiocephaly surgery	Designed osteotomy lines, segment for the plagiocephaly	Average Absolute change between pre- and post- operative scans :4.9 cm <sup>3</sup>	Permits to perform complex reconstructive surgeries reducing the operating time, allows to foresee the outcome of the operation, reduces the occurrence of complications, occlusal splint is a non-invasive fixation of the marker	

Study	HMD	Supplementary Devices	Marker	Application	AR Content	Results	Pros	Contros
Zhu et al. [62] 2015	Non-Specified (AR Toolkit + 3D Max pose adjustment software)		Marker cemented on the occlusal splint forming Occlusal Splint and Marker Complex (OMS)	Development of an AR application for navigation in craniofacial surgery, in particular in orbital hypertelorism correction	Bone tissue, critical nerves and vessels, globe of each orbital side, medial strip to be removed, cutting lines, OMS complex	Mean preoperative inter-dacryon distance (IOD): 38.29±3.61 mm vs Desired IOD by preoperative design: 23.74±1.79 mm	Registration method based on occlusal splints permits to achieve high precision in a non-invasive manner, surgeon free from any instrument registration, maintenance of the view on the surgical site	Non-suitable for edentulous patients
Zhou et al. [63] 2017	nVisor ST60	Robot system made of AR navigation system (tracking module, operational system module and display) and 7 degree-of-freedom serial arm (support module, position control module, motor module and end-effector module) equipped with a built-in force sensor	Marker cemented on the occlusal splint forming Occlusal Splint and Marker Complex (OMS)	Development of a robot-based AR application to perform Mandibular Angle Split Osteotomy (MASO) on dogs, including a force feedback to better control the drilling procedures	OMS complex, drilling trajectories, osteotomy planes, mandibular nerve, mandible model	Errors at entrance and target points: 1.04±0.19 and 1.22±0.24 mm, respectively Angular error between planned/drilled holes: 6.69±1.05° Drill Time: 21±12 min	Robot usage reduces post-operational complications and resolves problem of hand trembling and fatigue in surgeons, force feedback strengthen the safety of the procedure, it is a valuable system to train and aid inexperienced surgeons	Not appropriate for complicated plastic surgery since the higher number of manipulation modules required will reduce the accuracy, training time required, friendly human-computer interface should be improved, cranial nerve generated heat must be investigated

Study	HMD	Supplementary Devices	Marker	Application	AR Content	Results	Pros	Contros
Zhu et al. [64] 2017	Non-Specified (AR Toolkit + 3D Max pose adjustment software)		Marker cemented on the occlusal splint forming Occlusal Splint and Marker Complex (OMS)	Development of an AR application for maxillofacial surgery in patients with cranial deformities condition (mandibulofacial dysostosis, mandible retrognathism, mandible hypertrophy, etc.)	OSM complex, osteotomy lines/planes, mandibular nerve and mandible model	Position Error: 0.96±0.51 mm	Reduced hand-to-eye modifications, uninterrupted view of the surgical site, non-invasive and accurate registration, acceptable accuracy, non-expensive	Loosening or incorrect placement of occlusal splint could affect the accuracy, non-suitable for edentulous patients
Moreta-Martinez et al. [65] 2020		Smartphone camera (Vuforia + Unity) + Individualized Surgical Guides to anchor the marker at surgical site and mark tumor limits or guides to bone resection	Cubic marker 3D printed in Polylactic Acid	Development of an AR application to be combined with 3D Printing to aid orthopedic oncological surgery	Tumor volume contours, surgical guides and cutting planes  Demo Mode: 3D model without registration  Clinic/Surgery Mode: 3D model in registered position with respect to surgical guide	Overall Surgical Guide Placement Error: 1.75±0.61 mm Augmented Reality Tracking Error or System Error: 2.80±0.98 mm	Automatic image-patient registration with custom-made surgical guides, solution is favorably tested during 2 complete medical workflows of 2 patients	3D virtual models are acquired some days before the intervention and the tumor may have grown in the meanwhile, smartphone must be continuously handled

Study	HMD	Supplementary Devices	Marker	Application	AR Content	Results	Pros	Contros
Schneider et al. [66] 2020	Microsoft HoloLens (Vuforia)		Fiducial marker attached to the forehead	Development of an AR application to assist ventriculostomy	Kocher's point, skin, skull, ventricular system, puncture trajectory	Mean Registration Error of 1.36±1.33 mm (x-axis), 1.45±0.87 mm (y-axis) and 1.19±0.83 mm (z-axis) and 2.71±1.18 mm (overall of the 3 axis) Tracking Accuracy: 0.31±0.38 mm Mean Drift: 1.41±1.08 mm Overall Optical Error: 3.06±2.47 mm	Application that only adds active component to normal setup, compact navigation tool, quick to use, it does not necessitate of rigid head fixation, performances are independent on user experience	Repeated punctures should be tested, haptic feedback of the phantom could be improved to resemble brain tissue at a satisfactory level, slight dizziness and headaches in some participants
Park et al. [67] 2020	Microsoft HoloLens 2 (Unity + Mixed Reality Toolkit + Vuforia)			Development of an AR application for the percutaneous needle-based abdominal interventions	Abdominal phantom model, 11mm targeted lesion, needle planned trajectory, virtual gridlines		Performances are homogeneous regardless of user experience, reduction of needle passes, reduction of radiation dose, reduction of procedure time	Stationary and inanimate phantom are a non-realistic scenario to be improved with high frequency jet ventilation or deformable modelling of the phantom, etc.
Cukovic et al. [68] 2015		Desktop or Smartphone Camera (UbiTrack + Unity)	Square marker	Development of an AR application in the domain of medical visualization of anatomies	Model of bones, foot bones		Less error prone system, replacement of specific hardware drivers and tracking methods	Placing of a marker on all book pages is a non-viable solution that requires extra-space or could annoy users

Study	HMD	Supplementary Devices	Marker	Application	AR Content	Results	Pros	Contros
Rassweiler-Seyfried et al. [69] 2019		Apple iPad Version 2 Camera (Medical Interaction Toolkit MITK)	Colored fiducial marker attached on the skin	Development of an AR application to assist percutaneous access to kidney for the standard puncturing technique for percutaneous nephrolithotomy (PCNL)	Kidney, stone, bowels, bones, renal pelvis, ureter, adjacent organs (liver, spleen, colon, pleura and lungs)	Radiation Exposure with iPad assistance: 380.71 $\mu\text{G m}^2$ Puncturing time with iPad assistance: 6:17 min:s Radiation Exposure with Fluoroscopy / Ultrasound assistance: 66.93 $\mu\text{G m}^2$ Puncturing time with Fluoroscopy / Ultrasound assistance: 2:14 min:s	In patients with anomalies the assistance provides supplementary imaging to ensure complications, CT images are caught in exactly the same position of the procedure and during inspiration and this situation could be replicated by anesthesiologist and short fluoroscopy	For experienced users the golden standard is the fluoroscopy / ultrasound assistance method, static phantom, 2D organs representation on the iPad, lack of real-time imaging
Kim et al. [70] 2019		Smartphone or Tablet Camera (Unity + 3D Max + OpenCV and Dilb Libraries + face recognition deep learning algorithm)		Development of AR application for Botox injections for actual patients, student education, and patient counselling	Facial muscles and bones, needle injection points	Error Measurements Range: from a minimum of 0.0 mm to a maximum of 3.0 mm	Useful educational tool, valuable reference for explanation of Botox therapy to the patients, low costs, good accuracy	Matching with a standardized facial model instead of the actual patient facial model limits the application to training and visualization despite of the application in the clinical practice

Study	HMD	Supplementary Devices	Marker	Application	AR Content	Results	Pros	Contros
Ferraguti et al. [71] 2020	Microsoft HoloLens	KUKA LWR 4+ robot with virtual fixtures in the control scheme to gently assist needle insertion	3 L-shaped Electrocardiogram electrodes or patches used as markers	Development of an AR application for percutaneous nephrolithotomy (PCNL) with robotic assistance	3D Model of the skin, ribs, kidney, calices, stones, ureter, aorta, inferior vena cava and all the neighboring structures and forbidden ones and the correct trajectory to reach the target	Execution Time: 19.56±4.59 s Translation Error with manual procedure: 15.18±12.75 mm Orientation Error with manual procedure: 1.53±0.54°	Possibility of assisting expert as well as novice surgeons improving performances and learning curve, suitability of the application for many other fields of application	Need of improved registration procedure, real time imaging, need of compensation for patient respiratory motion
Long et al. [72] 2020	Microsoft HoloLens	Smartphone Camera	Reference marker 3D printed with metal fiducials embedded at each corner	Development of an AR application to display percutaneous needle insertion trajectories	Virtual needle path, target, entry point, and final virtual position of needle proximal end	Needle Placement Error with iPhone7, HoloLens and CBCT-guidance: 3.98±1.68mm, 5.18±3.84mm, 4.13±2.38mm, respectively Needle Placement Times with iPhone7, HoloLens, and CBCT-guided fluoroscopy: 94.8±28.3s, 68.5±42.6s, and 152.0±118.8s	Accurate placement reducing placement time, improved ergonomics, reduced inter-user variability, potential in reducing learning curve, continuous hand-free AR experience with smart glasses, possibility to have a mixed approach taking the benefit of the 3 modalities	Smartphone usage requires user to shift the view from the surgical site, stationary phantom is employed with homogenous materials that is a non-realistic scenario since not involve respiratory motion and soft tissues properties

Study	HMD	Supplementary Devices	Marker	Application	AR Content	Results	Pros	Contros
<b>Van Gestel et al. [73] 2021</b>	Microsoft HoloLens (Unity)	Calibration Object (CO) for the drain axis and tip estimation	IR retroflective marker spheres in a constellation of 4 spheres attached to needles and to phantom through plexiglass fixture	Development of an AR application for the assistance in the External Ventricular Drain (EVD) placement	Virtual Model of the phantom head (with skin, skull, brain, and Ventricles), bullseye placed at the target (foramen of Monro) and a line protruding from tracked drain down to its long axis is visualized (current trajectory) and bullseye changes of color are based on the entity of trajectory error (red > 4mm, orange, < 4mm, green, < 2mm), system also indicates the distance of drain tip from bullseye	Mean EVD accuracy for Untrained Users and Trained Users with AR assistance: 11.9 mm and 12.2 mm, respectively  Mean EVD accuracy for Untrained Users and Trained Users in freehand procedure: 19.9 mm and 13.5 mm, respectively	Demonstration that AR guidance can improve the accuracy of EDV placement especially in individuals with limited or no training, high accuracy in tracking and low drift with IR markers respect to RGB tracking	Loss of resistance during the puncture is usually used for the feedback in the procedure and it was not replicated
<b>Kanithi et al. [74] 2016</b>	Non-Specified		Fiducial Marker on Ultrasound (US) probe and needle syringe	Development of an AR application for assisting needle positioning during US-guided interventions	Needle trajectory and tip position, US image	Needle Trajectory Deviation: 3.27±2.95 mm	Needle tip position estimation is a valuable tool	Lower error as more orthogonal is camera to marker, resolution light dependency



Study	HMD	Supplementary Devices	Marker	Application	AR Content	Results	Pros	Contros
Gibby et al. [75] 2020	Microsoft HoloLens		Series of adhesive Optical Codes with embedded a visible material to CT and MRI	Development of an AR application to assist percutaneous spine procedures	Model of the CT or MRI treated anatomy, Virtual Needle (VN) trajectory with depth information	Mean Error of Needle Tip to target: 0.998mm (phantom), 1.73±2.20 (clinical practice)	Good precision on phantom and clinical tests, potential to decrease procedural time and radiation exposure, complicated cases are faced in a safer manner, enhanced, and facilitated training	Static images are superimposed to dynamic patient leading to potentially dangerous patient-to-image alignment errors (due to patient motion or breathing)
Van Doormaal et al. [76] 2018	Microsoft HoloLens (InVesalius + MeshLab + Unity + Vuforia + Microsoft Visual Studio)	3D Printed Pointer	Fiducial Marker attached to Pointer to have manual fiducial matching and voice commands to acquire points and end the cloud of points acquisition	Development of an AR application for Holographic Neuro-Navigation (HN) and comparison with Conventional Neuro – Navigation (CN)	Skin, skull, brain, relevant blood vessels and intracranial pathology	Mean HN Fiducial Registration error: 7.2±1.8mm (phantom), 4.4±2.5mm (patients) Mean CN Fiducial Registration error: 1.9±0.45mm (phantom), 3.6±0.5mm (patients)	Availability of anatomies in the surgical site instead of a side-screen	Non-sufficient accuracy for clinical use, matching process should be improved to eliminate holographic drift, need of the implementation of a motion-correction procedure, need of the implementation of a system capable of accounting brain shifts

Study	HMD	Supplementary Devices	Marker	Application	AR Content	Results	Pros	Contros
Liu et al. [77] 2018	Microsoft HoloLens	Robotic Registration System + Depth Camera (Xtion Pro Live) + Algorithm for anchoring of coordinates on femur and coordinate passages	Fiducial Marker-1 on the femur, Fiducial Marker-2 on the base of the Robot (carried out after registration), cubic Fiducial Marker on the drill	Development of an AR application for Hip Resurfacing, for Femoral Preparation	Femur model, virtual arrow divided in the head and shaft (head will be red if the position error of the drill is 3mm far or further from the targeted position or green in the opposite case & shaft will be red if the orientation error of the drill is 2.5° or higher from the targeted orientation)	Mean Time: 2 min (author) and 4 min (other users) Mean 3D Position Error: 1.76mm (author) and 1.91mm (other users) Mean 3D Direction Error: 1.85° (author) and 2.14° (other users)	With a quantitative score accuracy is scored 'acceptable' and close to 'good', simple voice commands and gesture user can interact with HoloLens, absence of manual registration or point collection, potential to reduce intra-operative time, intuitive and non-distracting guidance	Improvement of low-cost robotic assistants are expected, depth perception problems, deviation of HoloLens display for the user (tracking is not happening from the user eyes position), complexity of facing a system with the integration of multiple technologies, difficulty of the type of registration in a realistic scenario
Choi et al. [78] 2015	Non-Specified		Multi-faced Reference cubic Marker rigidly fixed on the patient	Development of an AR application for pelvic tumor resection, tested on pigs	Segmented tumor and Safety Margin for resection displayed as shape of contour	Mean Safety Margin: 12.28 mm (conventional method) and 10.26 mm (AR assistance method)	Portable system, cost effective application, intuitive virtual content, safer surgical operation, uninterrupted view of the surgical site, efficient AR content	Lower accuracy than systems implemented with external optical tracking systems

Study	HMD	Supplementary Devices	Marker	Application	AR Content	Results	Pros	Contros
<b>Badiali et al. [79] 2014</b>	Z800 eMagin	2 USB SXGA cameras (uEye UI-1646LE)	3 Balls with 6 mm-diameter, 6 drilled holes, 7 colored brackets recognized by machine-based vision algorithm	Assessment and validation in vitro of an AR system aiding to LeFort1 maxillary osteotomy and repositioning	Colored asterisks drawn in the designed positions of the maxilla	Mean Error: 1.70±0.51 mm Sagittal Axis Error: 0.89±0.54 mm Frontal Axis Error: 0.60±0.20 mm Craniocaudal Axis Error: 1.06±0.40 mm	Visible light replaces external infrared sources, accuracy is good, the error depends only on the complexity of the plane	In vitro study
<b>Ackermann et al. [39] 2021</b>	Microsoft HoloLens		2 Custom-made 3D Printed mounts equipped with markers attached to the pelvis with small screws	AR application for the guidance of pelvic osteotomies (periacetabular osteotomy of Ganz, PAO) and fragment reorientation in 2 cadavers	Osteotomy: planes for supra- and retro- acetabular cuts Fragment Reorientation: 2 3D vector, one between femoral head center and marker current position and one between femoral head center and target marker position with different colors, their deviation, as a 3D angle, is displayed over the current marker surface	Osteotomy Error: 10.8 mm for osteotomy starting point and 5.4° for osteotomy directions Fragment Reorientation Error: x-axis 6.7°, y-axis 7.0° and z-axis 0.9°	Study conducted over cadavers, radiation-free surgical approach, intuitive guidance and safer execution, no-instrument tracking	HoloLens AR renderings are prone to drift after they have been placed, small number of cadavers were included hampering the results generalization, simplified computation of the fragment orientation without displaying quantitative (rotational and translational) information

Study	HMD	Supplementary Devices	Marker	Application	AR Content	Results	Pros	Contros
<b>Tsukada et al. [36] 2019</b>		Smartphone Camera	Guide marker fixed to bone, camera recognizes the guide marker and then surgeon registers bone landmarks with pointer marker to create tibial coordinate system, oval Marker after the resection to confirm of operation accuracy, all made of acrylonitrile-butadiene-styrene resin	AR application for tibial bone resection and assessment of the accuracy	Tibial axes superimposed on surgical field and for confirmation, in the post-operative phase, the varus/valgus angle, the posterior slope and rotation angle	Absolute Differences between the values displayed on the smartphone screen and the measurement Values: Varus/Valgus Angle: $0.5^\circ \pm 0.2^\circ$ , Posterior Slope Angle: $0.8^\circ \pm 0.9^\circ$ , Internal/External Rotation Angle: $1.8^\circ \pm 1.5^\circ$ . Thickness of resected bone: $0.6 \text{ mm} \pm 0.7 \text{ mm}$	Varus/Valgus, Posterior Slope and Internal/External Rotation angle differences are accurate, absence of preoperative CT-sessions, easy evidence of registration errors	In vitro study without soft tissue presence, the accuracy of the bone resection may depend on the surgeon experience, external device for the visualization of the application (smartphone)
<b>Koyachi et al. [80]</b>	Microsoft HoloLens	3D Printed Device (surgical splint connected to the osteotomy device or to the repositioning device and the registration marker	Registration Marker	Verify the accuracy of preoperative planning in maxilla repositioning surgery, Le Fort I Osteotomy, with HoloLens headset	Holograms of the skull, pre- and post-repositioned maxilla/mandible, arteries, veins and marker	Median Signed Deviation: $-0.03 \text{ mm}$ Median Absolute Deviation: $0.38 \text{ mm}$	Method is capable of reproducing the maxilla position with high accuracy, high details of secondary structures	Lower accuracy in the bone repositioning in the impaction direction and vertical repositioning

Study	HMD	Supplementary Devices	Marker	Application	AR Content	Results	Pros	Contros
Garcia-Mato et al. [37] 2020		Smartphone Camera	Marker made of Poly Lactic Acid (PLA) and attached to cranium with double-sided tape in simulation and with resorbable pins in the surgery	Evaluation of an AR system for the guidance of front-orbital advancement procedures	Osteotomy Mode: virtual model of the osteotomy lines (1mm wide) Remodeling Mode: target positions of remodeled bone fragments (supraorbital bar and frontal bone)	Average Linear Error in Osteotomy Mode: $0.62 \pm 0.51$ mm Average Angular Deviation in Osteotomy Mode: $1.80 \pm 1.88^\circ$ Average Translation Error in Remodeling Mode: $0.70 \pm 0.24$ mm for supraorbital bar and $0.67 \pm 0.33$ mm for frontal bone Average Rotation Error in Remodeling Mode: $0.43 \pm 0.30^\circ$ for supraorbital bar and $0.39 \pm 0.33^\circ$ for frontal bone	Minimal invasiveness, real time feedback, improved hand-eye coordination and reduced cognitive load for the surgeon	Poor lighting condition or occlusions of the markers might interrupt the tracking and cause inaccuracies, depth perception errors, external device for the visualization of the application (smartphone)
Jiang et al. [35] 2018		3D Image Display Device + Tracking Device + 3D Scan Device		Development of a new AR guided workflow for dental implant surgery	Virtual drill, planned pathway, nerve channel holograms, Alarm System: change holograms color according to the deviation of displacement and angle between the tip of the drill and the planning path (red, far, yellow, near, green, close)	Mean Linear Deviation: $< 1.5$ mm Mean Angular Deviation: $< 5.5^\circ$	Reduction of time needed for positioning judgment and enhancement of surgical accuracy, intuitive and convenient AR content, improved eye-hand coordination, and faster execution of surgical procedures	Future applications can have same day CT scans more than few days templates to reduce discrepancies

Study	HMD	Supplementary Devices	Marker	Application	AR Content	Results	Pros	Contros
Kramers et al. [38] 2013		Smartphone Camera (Vuforia)	Rectangular Cuboid Marker (40x60x80 mm) attached on a pair of safety glasses worn by patient, marker attached on a device employed as a stylus or pointing device	Development of a neurosurgical AR system to aid the visualization of ventricles, entry points and trajectories in the External Ventricular Drain (EVD) procedure and analysis of its accuracy	Glasses-attached marker: visualization of segmented patient's anatomy with internal structures (ventricles) and outer skin layer Pointing Device-attached marker: beam toward the patient's head to view entry point trajectories with respect to the projected anatomy	Mean Error (35 Individual known Points): 9.88±5.34 mm (with AR assistance) and 13.03±6.15 mm (without AR assistance)	Application focused on portability and ease of use and costs and efficiency, suitable for intensive care unit and emergency employment, depth perception improvement	Poor user interface to be improved, not focused on user performances evaluation, need of incorporating algorithms to account brain shifts or key anatomy offsetting and variations in patient-mounted tracker position
Gao et al. [40] 2019	Microsoft HoloLens (Vuforia + Unity)		Marker Plate attached to the occlusal splint on the mandible, Surgical Tool Marker Plate	Development of an AR application to simultaneously track model and surgical tools and aid surgeon in mandibular angle split osteotomy and comparison of a deviation-reminder pattern with traditional image guidance one	Mandible, inferior alveolar nerve, cutting plan made of 9 navigational points, Surgical Tool Marker Plate is tracked to manage the Interface (transparency option for holograms, rotation and position error)	Engineers Position Error: 3.26±1.40 mm Orientation Error: 8.11±2.67° Operation Time: 17.32±1.86 min Surgeons Position Error: 2.58±1.06 mm Orientation Error: 5.43±2.60° Operation Time: 13.22±4.45 min	Interactive application and interface, deviation-reminder pattern is a useful extra information, suitability for preoperative design and remote medicine	Difficulty in depth perception, image drift, pupil distance calibration problem, to be employed in clinical practice this method must be tested in vivo to verify stability

Study	HMD	Supplementary Devices	Marker	Application	AR Content	Results	Pros	Contros
<b>Pietruski et al. [4] 2018</b>	Moviero BT-200 Smart Glasses	Navigation Tracking Camera and Display	Dynamic Reference Frame (DRF) with passive optical markers to the mandible and surgical blade	AR application to support mandibular resection and comparison with operation conducted with cutting guides	Mandible, cutting planes, Simple AR or sAR (ribbon with deviations on display or also images of surgical field and saw's blade) Navigated AR or nAR (plan is superimposed on glasses)	sAR Angular Error: 3.55±1.74° (transverse), 3.57±1.96° (sagittal), 7.12±4.15° (frontal) and 5.21±2.72° (transverse) nAR Angular Error 3.94±2.33° (sagittal), 9.92±5.70° (frontal) sAR Control Point Error: 1.79±0.94 mm nAR Control Point Error: 2.41±1.34 mm	Typical drawbacks of CAD guides (time to design, increased costs, limited adaptive capacity during operation) are prevented, good ergonomics, greater safety, shorter duration, facilitation of decision-making process	CAD guides provides the greatest accuracy, invasive fixation of DRF, depth perception problems, nausea or vertigo or headache
<b>Pietruski et al. [81] 2020</b>	Moviero BT-200 Smart Glasses	Navigation Tracking Camera and Display	Dynamic Reference Frame (DRF) with passive optical markers to the mandible and surgical blade	Development of an AR application for assisting Fibula Free Flap (FFF) harvest and comparison with operation conducted with cutting guides	Fibula, cutting planes, Simple AR or sAR (ribbon with deviations on display or also images of surgical field and saw's blade) Navigated AR or nAR (plan is superimposed on glasses)	sAR Angular Error: 5.16±4.18° (sagittal), 5.00±3.05° (frontal) nAR Angular Error: 4.17±0.98° (sagittal), 5.42±3.92° (frontal) sAR Control Point Error: 2.67±1.09 mm nAR Control Point Error: 2.95±1.11 mm	Typical drawbacks of CAD guides (time to design, increased costs, limited adaptive capacity during operation) are prevented, improved eye-hand coordination and uninterrupted view of the surgical site, comparable accuracy with guides	Complexity in integration of multiple technologies, cutting guides were superior in angular deviation parameter, need of reduced input latency, nausea or headache or vertigo problems

Study	HMD	Supplementary Devices	Marker	Application	AR Content	Results	Pros	Contros
Liebmann et al. [82] 2019	Microsoft HoloLens (Unity + AprilTags Library + MixedReality Toolkit)	Pointing Device (PD) for registration process by sampling landmark points of anatomy. Navigation Device (ND) composed by a handle component for the K-wire insertion and sleeve for the drill handling	Fiducial Marker attached on the PD and on the ND	Development of an AR application for surgical navigation in lumbar pedicle screw insertion	Vertebra model, screw entry points, 3D angle between current and target trajectory together with a triangle (screw entry point - current trajectory point - targeted trajectory point) that changes color	Mean Orientation Error: $3.38 \pm 1.73^\circ$ Mean Insertion Point Error: $2.77 \pm 1.46$ mm Mean Procedural Time: 419s	Radiation-free navigation, intuitive navigation, low requirements for computation and hardware, low-costs, sufficient precision for clinical application,	Increased surgery time, evaluation performed on rigid phantoms that do not include soft tissues and do not mimic negative influence on sampling process, in vitro study
Spirig et al. [83] 2020	Microsoft HoloLens	Pointing Device (PD) for registration process by sampling landmark points of anatomy. Navigation Device (ND) composed by a handle component for the K-wire insertion and sleeve for the drill handling	Fiducial Marker attached on the PD and on the ND	Development of an AR application for navigation in pedicle screw placement and comparison with freehand procedure	Vertebra model, screw entry points and trajectories, ND axis, current Euclidean distance of drill tip and planned entry point, degrees of deviation from planned trajectory	Average differences of screw entry points between planning and execution: $4.74 \pm 2.37$ mm (freehand) and $5.99 \pm 3.60$ mm (AR-navigated) Average deviation from planned trajectories: $11.21^\circ \pm 7.64^\circ$ (freehand) and $5.88^\circ \pm 3.69^\circ$ (AR-navigated)	Improved angular precision and comparable precision in entry point selection with respect to freehand, portable, and quick to install and affordable, no operative CT scans	Still high error of entry point positioning, crashes of the software occurred in 2 vertebrae navigation (dangerous in emergency), need to substitute screw with real pedicle screws



### 2.2.7.1 AR Advantages and Disadvantages

In this section, all the advantages and disadvantages of the AR application in the medical field will be presented.

Nowadays, the AR employment in the medical field is developing for the improvement of both educational and surgical aspects. In the surgical field, AR can be used both in the pre-operative and operative environment.

As an operative tool, AR could be based on the collection of three-dimensional datasets of the patient, using non-invasive imaging techniques like Magnetic Resonance Imaging (MRI) or CT or Ultrasound Imaging [21] [26]. These datasets are rendered in the AR application permitting an enriched visualization of the patient during the surgery. Surgeon in fact is capable, through the AR application during the surgery, to have internal and detailed views of the patient. In this manner, the need of larger incisions is constrained [21], surgeons can simultaneously get access to multiple type of images [21] during the surgery and can be accurately guided throughout their tasks [21]. During a surgery, AR permits to perform tailored incisions or to follow pre-designed cutting planes or to visualize the localization of blood vessels, nerves, vital tissues, or any dangerously damageable structure, improving the safety of the whole procedure. During a surgery, AR permits a clear and wide visualization of organs, improving the precision of the whole procedure, above all in case of delicate organs and more efficiently in organs with reduced mobility, such as bones, skull, and brain. AR-induced precision and safety are two aspects that makes the AR application in the medical operative field perfectly suit the purposes of the minimally invasive surgeries, where the traumatic effect on the patient is aimed to be minimized. Moreover, from a more practical point of view, the employment of HMDs during surgery can make more comfortable and faster the data consultation by the surgeon [26]. In the simplest form, an AR application, in fact, permits to have the current visualization during the surgery of all the medical relevant information and values to monitor the status of the patient easily and fast [84] [21]. At the end, AR virtual contents reduces the surgery time. In fact, with AR application, the surgeon does not need to look away from the surgical

site to collect patient information or consult acquired data, hence, breaks of the aseptic protocols are prevented [26].

As a pre-operative tool, AR can be a powerful surgical training or planning instrument. Three-dimensional reconstructions of the patient anatomy experienced with the AR permit to improve the quality and efficiency of the pre-operative planning of the surgery. Hence, AR application optimizes the surgery and surgical plans integration [84].

Moreover, since practice and training help human performances, AR simulations importance in the educational field can be easily understood. In fact, AR simulations offers the possibility to create a safe environment in which the user can experience the surgical procedures and fail in their performances without any dangerous consequence and with a good level of immersion [13]: he/she can iteratively perform the same task, learning from its errors and memorizing the passages of the real surgical procedure that he/she will perform [13]. This is the reasons why AR applications are largely employed as specialized training simulators for medical students, practitioners, or novice surgeons or for well-trained surgeons [13].

Although AR has a perspective future in the medical applications, several limitations exist. First, in the medical field accuracy is the strongest factor for the effectiveness of an AR-induced improvement of the surgical procedure [26]. Secondly, the user inattentive blindness must be cared [26]. The amount of virtual content displayed can distract the surgeon, hence only relevant data should be displayed and a method of accurately display them when necessary should be enclosed in the AR application. Moreover, occlusions problems must be faced [26]. Occlusions consist in the loosening of the hologram due to the hiding of the markers or reference points caused by the superimposition of surgical instruments, members, or their anatomical parts [26]. Another problem arises from the wearing of HMDs [26]. They can be heavy components that generate heat during their performances making uncomfortable their wearing for long-lasting procedures [26]. Moreover, it is needed to remark that AR projections can cause nausea, headache, and sickness symptoms [26], mainly caused by the discrepancies between visual, proprioceptive, and

vestibular systems. From a technical point of view, the main problems regard the life of HMD's batteries [26]. Surgeries can last several hours, and the HMDs must have a compliant battery life duration. Furthermore, even if AR can speed up surgeries, the necessity of AR application preparation is a non-simple and non-short step [26]. Hence, medical AR-applications building-up requires time and the integration of knowledge from both software developers and physicians to create an affordable, feasible and consistent application. At the end, AR applications needs to be tested and validated before being effectively employed real patients. Hence, it could take times to be effectively adoptable in operating medical rooms.

Table 2. 3 summarizes all the advantages and disadvantages for a medical AR application.

*Table 2. 3 Summary of advantages and disadvantages of AR application in the medical field.*

Advantages	Disadvantages
<p>Facilitation of the surgery by means of:</p> <ul style="list-style-type: none"> <li>- Highlights</li> <li>- 3D Images of patient anatomy</li> <li>- Task Guidelines (line, plane, instructions)</li> <li>- Visualization critical structures (nerves, blood vessels, etc.)</li> </ul> <p>Comfortable and fast data consultation for the surgeon during the operation.</p> <p>Improved precision and safety of the procedure.</p> <p>Prevention from large incisions.</p> <p>Optimized integration of the surgery and the surgical planning.</p> <p>Shorter procedure.</p> <p>Safe and immersive training environment for students, novices, and affirmed surgeons to create their own trial and error experience.</p>	<p>Need of high accuracy</p> <p>Occlusion Problems</p> <p>HMD heat production and heavy weight cause discomfort making them non-suitable for long lasting procedures.</p> <p>Selective and adaptive visualization of relevant virtual contents to avoid inattentional blindness.</p> <p>Nausea, headache and unpleasant symptoms.</p> <p>Battery life of HMD.</p> <p>Mixed design team (physician - software developer - clinicians and surgeons).</p> <p>Complex and long application development.</p> <p>Strict requirement of test and validation before being able to have a clinical application on real patients.</p>

### 2.2.7.2 Novelty of the Study

The aim of this thesis is the development of an AR application to aid mandibular and maxillary osteotomies and repositioning.

For the assistance of maxillofacial osteotomies, literature provides many solutions, however, all of them aid surgeon uniquely by displaying cutting planes established in the pre-operative phase. In these situations, surgeons are expected to intuitively and subjectively establish where the cutting plane intersect the anatomical structure to be osteotomized. Hence, surgeon mental load is augmented, and the accuracy of the performances can be reduced by interpretation errors. In this thesis, instead, cutting lines have been directly embedded in the outlook of the developed AR application. This approach can speed up the procedure, it can reduce user cognitive load and it can improve the accuracy of the operation. Moreover, the inclusion of virtual surgical guides for the performance of drilled holes for the final fixation of the osteotomized fragment represents a completely new content with respect to already developed AR application in the maxillofacial field. For the assistance of maxillofacial repositioning operations, literature expects solutions that propose a static assistance of that operation. Commonly, AR applications assist maxillofacial repositioning by displaying anatomical structures at the target position to be reached without any sort of interactive guidance for the user. Hence, over/under-shooting errors in the repositioning frequently occur, damaging the accuracy of the procedure. In this thesis, instead, an interactive, fast, and intuitive feedback has been implemented to guide user in the repositioning of an osteotomized fragment frame by frame. This approach can make user more confident throughout the repositioning procedure and it can reduce under/overshooting errors in the operation. Moreover, it must be noticed that the idea of integrating both osteotomy and repositioning assistance in the same AR application is rarely found in literature and is a completely novel approach in the maxillofacial surgery AR applications. This solution makes the AR application a powerful and attractive package to be employed by surgeons that can employ it to entirely treat a clinical case with the assistance of the AR technology.

# 3 Materials and Methods

The aim of this thesis is the development of an AR application, deployed with Microsoft HoloLens V2, to aid surgeons in maxillofacial surgeries. The application should permit surgeon to conduct osteotomies without the usage of CAD cutting guides, removing all the disadvantages induced by this equipment. Moreover, the application should guide the osteotomized fragment repositioning, giving to the user an interactive, fast, intuitive, and effective feedback. As first, in this section, all hardware, software, technologies, and methodologies employed in this thesis are technically described. Tools include the software for the CAD modelling, the dedicated environments for the development of AR applications and the generation of registration marker database, and the specific software for the statistical results extraction. Instrumentations include the HMD device for the AR application deployment, the registration markers for the correct hologram visualization, the machinery for the 3D-printing of three-dimensional model to be tested, and the device for scanning of the tested phantom. Secondly, the entire AR application development procedure, including marker generation and modelling phase to extract virtual contents and surgical guides, is presented. Figure 3. 1 summarizes all these steps, where 3D-printing, test and validation phases complete the workflow.

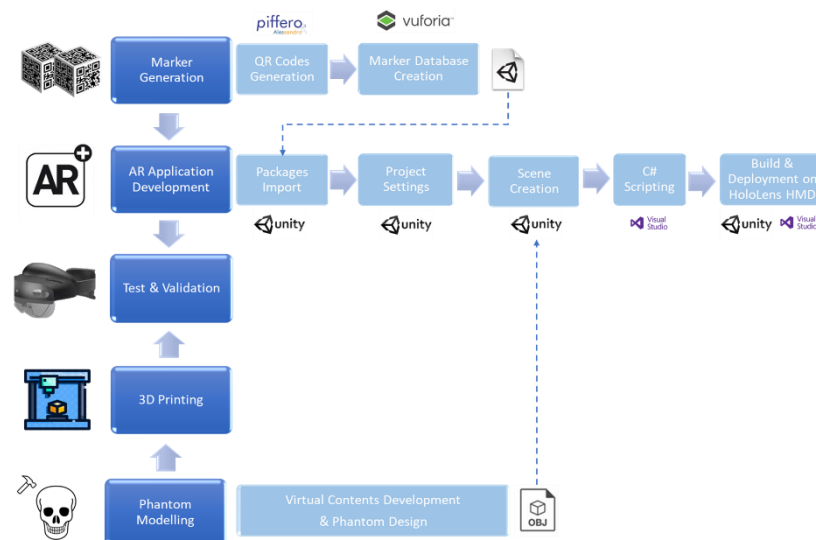


Figure 3. 1 Workflow of the thesis.

### 3.1 Computer Aided Design (CAD) Tools

Computer-Aided Design or CAD tools is a term that describes the usage of computer systems (or workstation) to aid the creation, design, modification, and optimization of a three-dimensional model. CAD tools can be classified based on the sector of application or on the phase in which they can be employed. However, the most important classification of the CAD tools is based on the model that they adopt. They can be 2D CAD, 3D CAD and Hybrid CAD. 2D CAD tools or bidimensional CAD tools are easy to be manage and, being modular they allow to fast scale or modify the mode but, they do not permit simulations. 3D or three-dimensional or solid CAD tools give possibility to conduct simulations. These tools can carry aesthetics and functionality of the model. However, they are non-parametric and more complex to be handled. Hybrid CAD tools finally combine these two modalities. In medical and biomedical field, CAD software allows user to generate the patient model or custom-made surgical guides and pre-operative plans which can be used for 3D-printing of the needed phantoms and in the development of the AR application contents. In detail, CT scanned patient data imported in dedicated software are used to generate the mesh of object to be exported in the adequate format for specific purposes.

Virtual Reality Modeling Language (\*.VRML) format [85] is a standard file format for representing three-dimensional interactive vector graphics. VRML is a file format where vertices and edges for a 3D polygon can be specified along with the surface color, UV-mapped textures, transparency, and so on. A \*.VRML file (Figure 3. 2) has several features such as scene graph (nodes compose the scene graph, they have fields and serve as attributes that define the node persistent state), event processing (nodes messages received from or sent to other nodes), behaviours (user input responses), nodes encapsulation and re-use and extensibility, distributed content (URL are used to connect scene graph to the network), interactivity (sensor nodes) and animation (interpolator nodes to create linear key-framed animations). STereoLithography or Standard Triangulation Language (\*.STL) format [86] is one of the most employed formats. It is used to represent an approximated geometry through a triangular mesh.

The three-dimensional model of the object undergoes a sort of discretization by mean of triangular elements. All these elements are saved using the coordinates of the vertexes and the direction of the facet normal (Figure 3. 3). Object Files (\*.OBJ) format [87] is another widely used format. The \*.OBJ format includes multiple types of data, it contains vertex data, free-form curve/surface attributes, elements, free-form curve/surface body statements, connectivity between free-form surfaces, grouping and display/render attribute information. The most common elements are vertices data represented by 4 vertex lists made of 4 elements representing vertex coordinate, one for each type of vertex coordinates (geometric vertexes (v), texture vertexes (vt), vertex normal (vn) and parameter space vertexes (vp)) as shown in Figure 3. 4.

```
Shape {
  appearance Appearance {
    material Material {
      ambientIntensity 0.5
      diffuseColor 0.1837 0.1837 0.1837
    }
  }
  geometry IndexedFaceSet {
    coord Coordinate {
      point [
        0.94 0.00 -0.33 ,
        -0.47 0.81 -0.33 ,
        -0.47 -0.81 -0.33 ,
        0.00 0.00 1.00 ,
      ]
    }
    coordIndex [
      2, 1, 0, -1,
      3, 2, 0, -1,
      1, 3, 0, -1,
      2, 3, 1, -1,
    ]
    color Color {
      color [
        1.00 0.62 0.00,
        1.00 0.00 0.00,
        0.87 0.00 0.87,
        0.37 0.37 1.00,
      ]
    }
    colorPerVertex FALSE
    colorIndex [ 0 1 2 3 ]
  }
}
```

Figure 3. 2 Outlook of the data saved in the \*.VRML format.

```
facet normal 0.000000e+00 0.000000e+00 1.000000e+00
  outer loop
    vertex 2.029000e+00 1.628000e+00 9.109999e-01
    vertex 2.229000e+00 1.628000e+00 9.109999e-01
    vertex 2.229000e+00 1.672000e+00 9.109999e-01
  endloop
endfacet
```

Figure 3. 3 Outlook of the data saved in the \*.STL format.

```
v -5.000000 5.000000 0.000000
v -5.000000 -5.000000 0.000000
v 5.000000 -5.000000 0.000000
v 5.000000 5.000000 0.000000
vt -5.000000 5.000000 0.000000
vt -5.000000 -5.000000 0.000000
vt 5.000000 -5.000000 0.000000
vt 5.000000 5.000000 0.000000
vn 0.000000 0.000000 1.000000
vn 0.000000 0.000000 1.000000
vn 0.000000 0.000000 1.000000
vp 0.210000 3.590000
vp 0.000000 0.000000
vp 1.000000 0.000000
vp 0.500000 0.500000
```

Figure 3. 4 Outlook of the data saved in the \*.OBJ format.

### 3.1.1 Rhinoceros

This section describes the Rhinoceros CAD tool as illustrated on its user's guide [88] [89]. Rhinoceros is a commercial applicative software for free-form three-dimensional surfaces modelling created by Robert McNeel & Associates Company (Seattle, Washington, USA). Its growing popularity is based on its multidisciplinary functionality, low learning curve, relatively low cost, and the ability to export files in over 30 different formats. With Rhinoceros, modeling takes place with the precision required in designs and prototyping. The models created are compatible with many other design, technical drawing, CAM, analysis, rendering, animation and illustration programs. Rhinoceros has a very simple and understandable user interface and does not require any specific hardware to have efficient performances. Rhinoceros allows you to create, edit, analyze, document, render, animate and translate curves, surfaces, solids, point clouds and polygon meshes. In Rhinoceros, all geometric entities are represented using Non-Uniform Rational B-Splines (NURBS). NURBS is a mathematical representation by which 2D and 3D geometries such as lines, arcs and free-form surfaces can be accurately defined.

Here some of the most employed function available in Rhinoceros for the model creation are listed (Figure 3. 5):

- Points: points, point clouds, point grid, extract from objects, etc.
- Curves: line, polyline, free-form curve, circle, arc, ellipse, rectangle, polygon, helix, spiral, conic, interpolation of points, control points, etc.
- Curves from other objects: through points, through polyline, continuous curve, fillet, chamfer, offset, blend fillet, intermediate curve, sections from profiles, extraction of iso-parametric curves, projection, fill, etc.
- Surfaces: from 3 or 4 points, from 3 or 4 curves, from planar curves, from a network of curves, rectangle, deformable plane, extrusion, ribbon, ruled surface, loft with tangency correspondence, sweep along the path with edge correspondence, sweep along two track curves with edge continuity, blend fillets, revolution, intermediate surfaces, patches, stitch grids, fillets, offsets,



- chamfers, plane by points, etc.
- Solids: box, sphere, cylinder, tube, tubular shape, cone, truncated cone, pyramid, truncated pyramid, ellipsoid, torus, extrude planar curve, extrude surface, close flat holes, join surfaces, regions, non-manifold castings, etc.
- Mesh: from NURBS surfaces, from closed polylines, mesh faces, plane, parallelepiped, cylinder, cone, and sphere, etc.

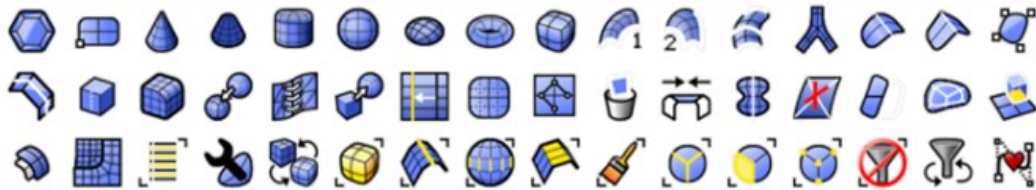


Figure 3. 5 Icons of some of the model creation commands of Rhinoceros.

Here some of most used editing tools in Rhinoceros are listed (Figure 3. 6):

- General: Delete, merge, trim, untrim, split, explode, extend, etc.
- Transformation: Cut, Copy, Paste, Move, Rotate, Mirror, Scale, Array, etc.
- Points and curves: control points, addition/removal of nodes, polylines, or line segments, etc.
- Surfaces: control points, addition/removal of nodes, extension, merging, Boolean operations (union, difference, and intersection), etc.
- Solids: fillet, shell, Boolean operations, etc.
- Mesh: explode, join, etc.

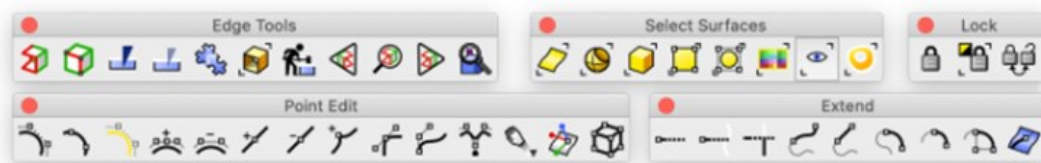


Figure 3. 6 Icons of some of the model editing commands in Rhinoceros.

In Figure 3. 7 is represented the Rhinoceros interface with highlighted the main windows and bars. It is possible to distinguish:

- 1) Title Bar: where currently opened file's name and size are displayed.

- 2) Menu Bar: contains the Rhinoceros commands grouped by function.
- 3) Command History Window: it shows previous command and prompts.
- 4) Command Prompt: it shows prompts for command actions and permits to type command names preventing from research in the Menu.
- 5) Toolbar Group: contains collections of toolbars.
- 6) Toolbar: it includes the graphic icons for starting the commands enclosed in the opened collection of toolbars and it is custom-made on user's preferences.
- 7) Toolbar Menu Button: it permits to customize, hide, and show the toolbar.
- 8) Side Bar: it includes all the graphic icons for starting the commands grouped by their functionalities.
- 9) Viewports: corresponds to Rhinoceros' working environment, including the views' title, the object's visualization, the backgrounds, construction plane's grid and world axis's icon. Moreover, it is possible to subdivide model components into layers differently named to have an organized model.
- 10) Viewport Title: by double left mouse button clicking on these sections the viewport is activated and imposed as the unique principal view.
- 11) Viewport Tabs: it controls the arrangements of the viewports.
- 12) Osnap Control: these toggles constrain the marker to an exact location on a specified object, such as the end of a line, or the center of a circle, etc.
- 13) Status Bar: displays current coordinate system location of the marker, the unit of employed template, the layer pane with the selected layer and its color, the Grid Snap Pane, the Ortho Pane, the Planar Pane, the Osnap Pane, the SmartTrack Pane, the Gumball Pane, the Record History Pane, the Filter Pane, and the Info pane.
- 14) Panel: provides some quick access to some global options, document properties and command dialogs.
- 15) Panel Tabs: tabs that allows to bring the specific panel to the front.
- 16) Panel Menu Button: it permits to control the appearance and the visibility of the panels.
- 17) Page Icons: click to display different pages in the opened panel.

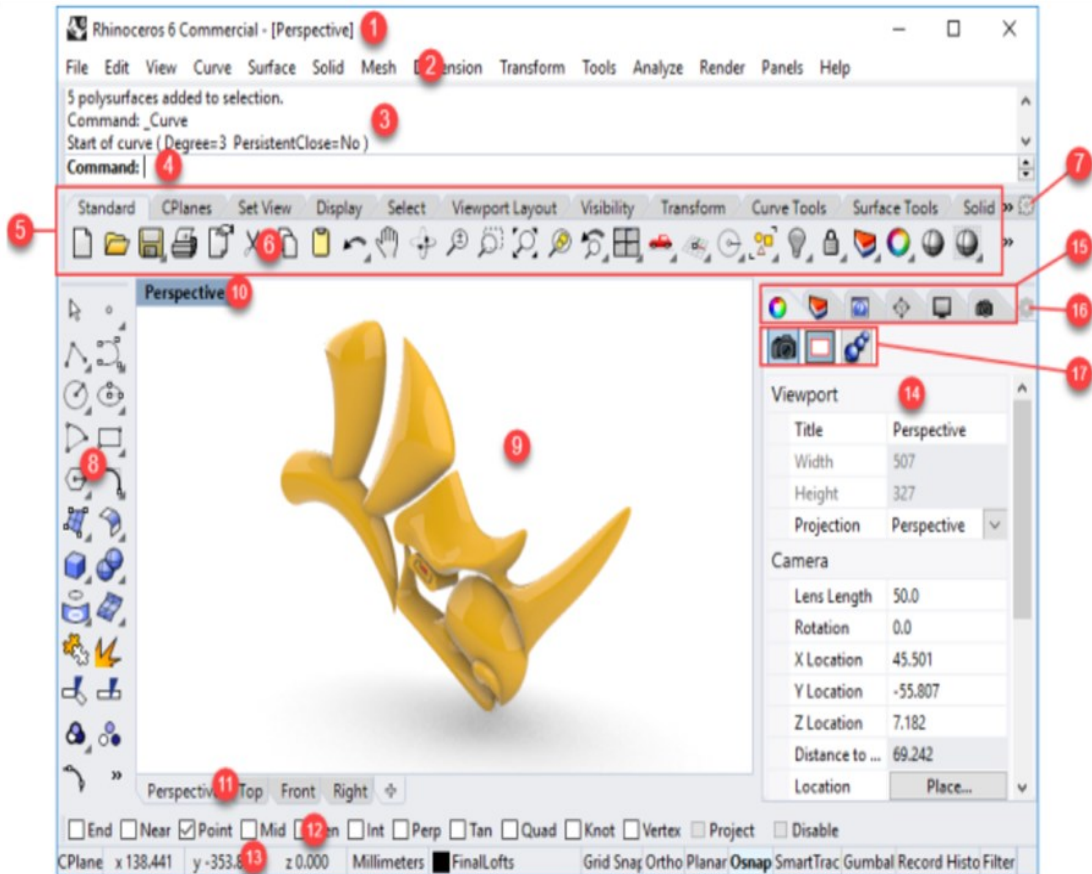


Figure 3. 7 Rhinoceros graphical interface outlook.

Rhinoceros viewports can be parallel or perspective. In Parallel or Orthogonal views, all the grid lines are parallel to each other. In Perspective view, grid lines converge to a vanishing point generating the illusion of depth in the viewport.

Navigation in the viewports is mediated by some toolbar commands and mouse functions. The simplest way to navigate the view is to drag the mouse with right button held down, this action pans or shifts the view in parallel views and rotates the view in perspective view. Moreover, by scrolling the mouse wheel the zoom in and zoom out of the view can be performed and the zoom extends command permits to adapt the zoom on the displayed objects. Icons in the Toolbar permits to run these commands and even more advanced actions, such as undoing view shifts, naked zoom, orient camera to surface, perspective match with one of the parallel viewports, synchronization of the views, show or hide the visibility of the viewport camera, rotate the camera, etc.

## 3.2 AR Application Development

As already anticipated, the 3D CAD tools, such as Rhinoceros, can be used to generate the surgical guides and the virtual content that will be enclosed in the AR application. To develop the AR application, then, few steps are required:

- Choice of the target
- Definition of the registration algorithm to align real and augmented world
- Creation of the virtual content of the application
- Implementation of the script to control the application functionalities
- Compilation and distribution on the device (HMD)

The following sections describe the target selection, the software employed for the creation of the virtual content and for the generation of the application scripts, and the HMD on which this application is deployed.






### 3.2.1 Hardware

Different modalities of AR application share the need of a display in which the virtual world and the real world are blended. Several types of hardware devices are used to fulfil this function, such as display monitors or mobile phones or HMD. HMD, already described in previous sections, are one of the most used solution for the augmentation of the real world.

#### 3.2.1.1 Microsoft HoloLens V2

Nowadays, there are several HMDs available on the market, produced by Sony, NVIS, eMagin, Microsoft and Google. In medical applications, literature suggest that the most used commercialized devices are the Microsoft's HoloLens [39] [40] [44] [45] [46] [47] [49] [50] [51] [52] [54] [66] [67] [71] [72] [73] [75] [76] [77] [80] [82] [83]. However, as it can be seen from Table 3. 2, many other solutions are employed, such as the nVisorST [42] [43] [63] and Z80003DVisor [79], Sony's HMZ [41] and novel proposal like VOSTARS system [53]. Table 3. 1 shows their technical specifications.

Table 3. 1 Fundamental technical specification of HMD found in literature.

HMD	Display Technology	Resolution	Field of View	Vision	Device
HoloLens V1	Holographic lenses	2.3 M total light points	34°	Binocular	
nVisorST	FLCoS	SXGA 1280x1024	60°	Binocular	
Z8003DVisor	OLED	SVGA 800x600	360° horizontal	Binocular	
VOSTARS	SXGA OLED	1280x1024	30°	Binocular	
HMZ-T1	OLED	1280x720	45°	Binocular	

Microsoft HoloLens V2 is an optical-see through HMD (Figure 3. 8). Microsoft HoloLens V2 is a pair of smart glasses designed and manufactured by Microsoft company as an updated version of their first product released in 2019.

As HMD, Microsoft HoloLens V2 are used to project computer-generated virtual contents over the real scene with all the advantages of the optical see-through HMDs illustrated in the previous sections.



Figure 3. 8 Microsoft HoloLens V2 HMD.

Microsoft HoloLens V2 HMD augments the real scene only on the user view, externally none of the participants can see the virtual contents blended in the real world. Being an optical see-through HMD, the user, wearing the device is still viewing the real scene and combiners mediate the augmentation.

Microsoft HoloLens V2 HMD can track the user’s movements letting him to use hand gestures and gaze gesture to interact with the holograms.

This HMD is composed by a visor which contains the sensors and the displays, the headband used to wear the device (it permits by tuning a wheel to regulate the fitting of the band on the user head and reach the best suitability), the brightness and volume buttons. Microsoft HoloLens V2 can be charged using an USB-C cable that can be used also to connect the device to external device. The charger power is 18 W, suppling 9V at 2A. Table 3. 2 present the technical specification for this version of the HMD extracted from the Microsoft website.

*Table 3. 2 Technical specifications of the Microsoft HoloLens V2 HMD.*

<b>Microsoft HoloLens V2 Technical Specifications</b>		
<b>Display</b>	<b>Optics</b>	See-through holographic lenses (waveguides)
	<b>Resolution</b>	2k 3:2 light engines
	<b>Holographic</b>	> 2k radiants (light points per radian)
	<b>Density</b>	
	<b>Eye-based</b>	Display optimization for 3D eye position
	<b>Rendering</b>	
<b>Sensors</b>	<b>Head</b>	4 visible light cameras
	<b>Tracking</b>	
	<b>Eye</b>	2 IR cameras
	<b>Tracking</b>	
	<b>Depth</b>	1-MP time-of-flight (ToF) depth sensor
	<b>IMU</b>	Accelerometer, gyroscope, magnetometer
	<b>Camera</b>	8-MP stills, 1080p30 video
<b>Audio and Speech</b>	<b>Microphone</b>	5 channels
	<b>Array</b>	
	<b>Speakers</b>	Built-in spatial sound

<b>Human Understanding</b>	<b>Hand Tracking</b> Two handed fully articulated model, direct manipulation <b>Eye Tracking</b> Real-time tracking <b>Voice</b> Command and control on-device; natural language with internet connectivity <b>Windows Hello</b> Enterprise-grade security with iris recognition
<b>Environment Understanding</b>	<b>6Dof Tracking</b> World-scale positional tracking <b>Spatial Mapping</b> Real-time environment mesh <b>Mixed Reality Capture</b> Mixed hologram and physical environment photos and video
<b>Compute and Connectivity</b>	<b>SoC</b> Qualcomm Snapdragon 850 Compute Platform <b>HPU</b> Second generation custom-built holographic processing unit <b>Memory</b> 4-GB LPDDR4x system DRAM <b>Storage</b> 64-BB USF 2.1 <b>Wi-Fi</b> Wi-Fi: Wi-Fi 5 (802.11ac 2x2) <b>Bluetooth</b> 5 <b>USB</b> USB Type-C
<b>Fit</b>	<b>Single Size</b> Yes <b>Fits Over Glasses</b> Yes <b>Weight</b> 566 g
<b>Software</b>	<b>Windows Holographic Operating System</b> <b>Microsoft Edge</b> <b>Dynamic 365 Remote Assist</b> <b>Dynamic 365 Guides</b> <b>3D Viewer</b>
<b>Power</b>	<b>Battery Life</b> 2-3 hours of active use <b>Charging</b> USB PD for fast charging <b>Cooling</b> Passive (no fans) <b>Contains lithium batteries</b>

Respect to the older version this HMD results to be lighter, more comfortable, more balanced, it is capable to recognize voice commands through an embedded depth sensor combined with an integrated artificial intelligence with semantic comprehension, it can recognize fingers gestures and eyes motions with an eye-tracking technology. From the technical point of view, the field of view has been doubled keeping the resolution at 47 pixels by degree of vision. The simplest version of the Microsoft HoloLens V2 HMD costs 3,500 \$. However, more expensive solutions are currently available on the market such as the Industrial Edition (4,950 \$), tested to be employed in regulated environments, and the Trimble XR10 version (5,199 \$), equipped with the protective helmet.

### 3.2.2 Software

For the development of an AR application the usage of multiple different types of software and environments, used in the correct sequence and integrated, is an essential requirement.

A Software Development Kit (SDK) and Application Programming Interface (API) are the first requirements. The SDK is a software in which the target image or object can be uploaded in a particular database on which the target will be present and from where it could be picked to be employed in the specific AR application development. Vuforia SDK is one of the most used SDK.

Then a cross platform engine is needed. The main objective of an AR application is the correct visualization of virtual contents in the real world, thus, to register holograms in the precise position in the real scene the user must be able to manage in a dedicated software the relative positions of holograms and targets. This is the functionality of a cross-platform engine and one of the most used, in the AR field, is Unity.

Finally, to to deploy the application on the HMD an Integrated Development Environment (IDE) is required. IDE is the software in which the application can be compiled and distributed, hence, it lets deliver the application to the smart glasses to be then launched. Visual Studio is a widely employed IDE.



### 3.2.2.1 Marker Generation and Vuforia SDK

The target is a crucial element in the development of an AR application. In fact, the HMD recognize it and use it as a sort of reference anchor to project holograms with the right alignment and positioning with respect to the real environment. In few words, targets are reference points for the correct and precise blending of the real and augmented worlds.

The target can be an image or a 3D object. Globally, both image and object targets must fulfil some requirements. Targets must be rich in details or features, they must have the appropriate high contrast, they must not exhibit repetitive patterns, and, in case of image targets they could be in JPG or PNG format. In case of object target the attributes are the rigidity and stability of the target. Images or objects, selected to be targets, must be uploaded in the SDK to create the database to be then exported in the appropriate format. Generally, SDK gives a feedback about the quality of selected target through a grading system that reflects how much the selected target image or object respect the previous cited requirements. With this system, it can be understood the suitability of the selected marker and its effectiveness in AR application.

Image targets can have different forms, they could be flat images or cylindrically shaped images or multitarget images (collection of multiple squared images combined into the facets of a cube). The object targets instead can be originated through physical object scanning or CAD model or 3D scan models. Moreover, it should be noticed that multiple ulterior types of target have been proposed in literature, such as optical markers detected by dedicated cameras, or fluorescent markers used during laparoscopic procedures allowing a good visibility and remaining in the body also after surgery, electromagnetic systems. However, literature also indicates these alternatives as the non-optimal solutions since their adaptive capacity is limited by several drawbacks [14]. As an example, electromagnetic markers exhibit distortion problems induced by the presence of metal tools in during the procedure [14].

The simplest used targets are image targets. They can be fast, easily, and freely generated in some dedicated websites, such as Brovision, AR.js Marker Training, QR-code generators (as Piffero-QR Generator). Here, iteratively, image targets rich of

features and respecting the previously criteria can be generated with a simple click through fast algorithms.

Brovision (Figure 3. 9) is a website that generates 2D image rich in features and characterized by triangular, squared, and linear elements. It gives to the user the capacity of managing the features density (high-medium-low) and the possibility to select black-and-white or colored patterns. The file can be easily downloaded by right clicking the image and saving it in the PNG format. AR.js Marker Training (Figure 3. 10) creates the image target as a black squared box or frame within which an image, that the user is asked to upload, will be visualized. User can also choose the pattern ratio, how big is the image respect to the frame, and the image size in pixels. AR.js Marker Training allows to download a PDF file containing multiple copies of the generated image target or to export the image in the PNG format. Another type of image target is the QR code. QR codes are images rich in features since they are generated by creating singular and non-repetitive patterns of tiny black and white squares. Several QR code generator, such as Piffero QR Generator (Figure 3. 11) are freely available on internet. They permit to refer the generated QR code to URL or website, text, contact, PDF file, image, and multiple other contents and then export it.



Figure 3. 9 Brovision AR Marker Generator outlook.

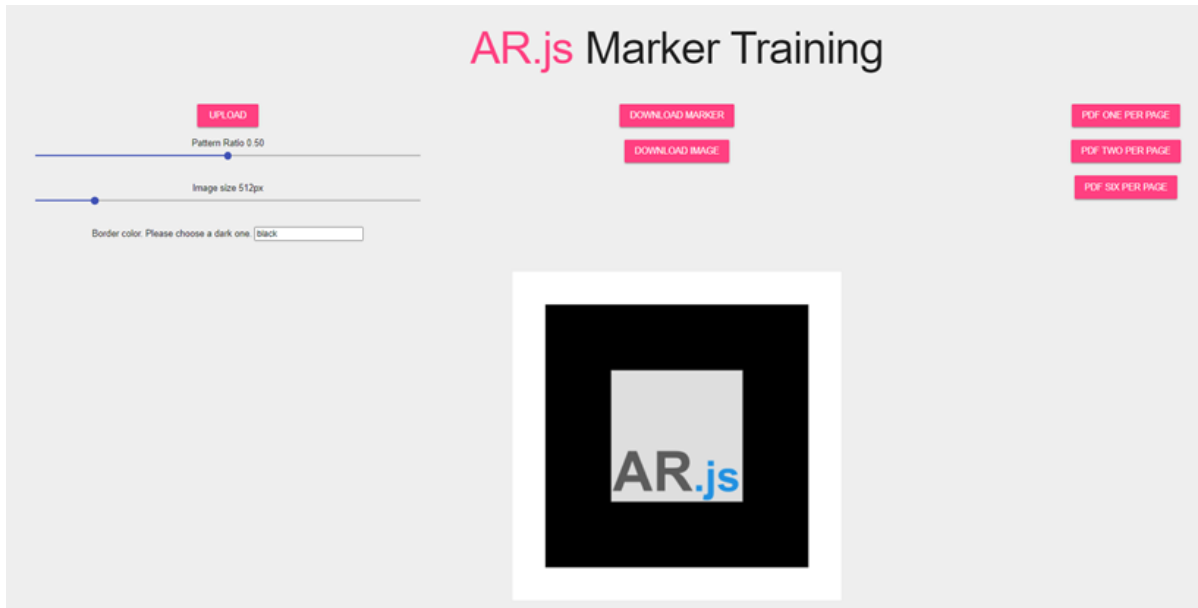


Figure 3. 10 AR.js Marker Training outlook.



Figure 3. 11 Piffero QR Generator outlook.

The generated target images are then uploaded in the SDK. SDK generically refers to a set of tools for software development and documentation. All the SDKs share some basic tools:

- A compiler, to translate the source code into an executable.
- Standard libraries with public interfaces or Application Programming Interface (API) that permits software programs to interact by each other.
- Documentation on programming language for which SDK was developed and about the tools available in the SDK itself.
- Information on licenses to be used to distribute created programs.

Various SDKs are available, such as the Vuforia Engine and the GoogleARCore. In this section will be deepened the Vuforia Engine SDK [90] [91].

Vuforia Engine is an AR SDK designed by Qualcomm for mobile devices and globally useful for the development of AR applications.

Vuforia employs computer vision technology to recognize and track planar images or three-dimensional objects. This tracking permits then to the user to correctly place the virtual contents on the real scene, hence, through this functionality, Vuforia permits the development of target tracking-based AR applications that rely on image or object targets.

Vuforia can recognize different types of targets that can be single images, or multi target, or cylinder or three-dimensional objects. Figure 3. 12 shows an example of target developed in Vuforia.

In the Vuforia 'Model Target Generator' databases of targets can be created, in which any target object or image can be equipped with the uploaded images and can be accurately dimensioned. Finally, the customized database can be easily exported in the appropriate format for the AR application development software.

As an example, the target database to be managed in the Unity software, that will be described in the following sections, must be exported in the \*.unitypackage format.

Another option present in Vuforia is the 'License Manager, which provides the tools and information that the user needs to create and manage the licenses. Each license

key is usable just in a single application, and its usage in the AR application development software will enable the target database. Figure 3. 13 shows an example of license key developed in Vuforia.

Figure 3. 12 Vuforia Model Target Generator settings.

License Key
Usage

Please copy the license key below into your app

```
Aao2Xiv/////AAABmYNYEdUr+EIvomzyFt1+oxNdph6XahtvNfXni/1y3IraoG1eQhg/YHx/pUIy83DcNTm9ZSKYdjeNAqQLtxQ+pw3
DgJRq0YBd512KyKEHm7/w+YxJXz5N1ZJXM7dT0kPMg+j1/xq5g4AheDu/36585D+g9Mcet+Oqd48vHY2e7H8V4SvzntOB/vj uLbNpAU
WD1ZCwYIYR8qeNYkj5OhkzXBCC1bJjRYyXJTIQfaYUH/991F8KZQkR0oi+s1K+Ya/bdCvyh2XuIh0EDhLRnDC4m02qd5ajEH2uU6GZAR
H7E//buYszM1oqVhv0p0rxxsSzzkTCd5wq921B56zYiA0WbKLeVjFKxFO0oPWHMyUHAU8VI
```

**Plan Type:** Develop  
**Status:** Active  
**Created:** Sep 28, 2021 19:47  
**License UUID:** 1cd93dc3d9484a25ba4189b0ac4c32aa

**Permissions:**

- Advanced Camera
- External Camera
- Model Targets
- Watermark

**History:**  
 License Created - Today 19:47

Figure 3. 13 Example of a generated license in Vuforia License Manager.

### 3.2.2.2 Unity

This section describes Unity software starting from online user's guides [92] [93] [94] [95]. Unity is a cross-platform engine developed by Unity Technologies that allows video games development of and other interactive content, such as architectural visualizations, or 3D real time animations, or VR applications, or AR applications.

Unity environment runs on both Microsoft Windows and macOS and Linux, and the generated products can be launched on Microsoft Windows, macOS, Linux, Xbox 360, PlayStation 3, PlayStation Vita, Wii, iPad, iPhone, Android, Windows Mobile, PlayStation 4, Xbox One, Wii U and Nintendo Switch.

One of the first step for the development of a specific application in Unity is the definition of the target platform for the development. Hence, user must specify among the above cited platforms (PC, MAC, Linux, Android, Universal Windows Platform, iOS, Xbox One, Play Station, etc.) which will be the target one.

The following step is the integration in the Unity development environment of all those instruments that will be essential for the application purposes. For the AR application development in the Unity environment, it is crucial to import specific packages. First, to make the application capable of recognizing the target databases developed in Vuforia, the Vuforia package must be imported in the project. Then, as already anticipated in previous sections, it must be imported the target package in the \*.unitypackage format that will import the created target dataset in the Unity scene allowing to manage the holograms registration with respect to all the targets enclosed in the imported database. Last step is the import of packages that includes animation or spatial interactions or interactive functionalities. Multiple packages fulfil this functionality, one of the commonly used is Mixed Reality Toolkit (MRTK), a cross-platform toolkit necessary to build applications or experiences that belong in the field of VR and/or AR.

Unity scene contains 2D or 3D objects, those that will augment the real world and those that will be used as references. Both target and holograms will be organized in a hierarchal structure or Hierarchy. Cameras and light sources complete the set of available objects in the unity scene. In the Hierarchy, parent and child objects can be

distinguished. Parent objects are objects that contain other objects that instead are termed as child objects. Child objects inherit properties of the parent ones and whose behavior will depend on parent behavior throughout the launched application. As an example, child objects of a target will be visualized uniquely when the target will be in the scene. For this reason, when dealing with AR applications, mainly Vuforia targets are employed as parent objects of the other scene objects, the holograms.

Moreover, Unity permits to enclose functionality in the developed application by creating scripts in the C# language, using compatible API such as Visual Studio, and assigning them to scene objects. Script inputs then can be manually assigned by the user by drag and drop objects from the Hierarchy to the dedicated spaces on the script.

Furthermore, Unity provides an Asset Store in which user has the possibility of search and download free or paid packages with animations, scripts, functionalities, tools, or pre-designed object models.

At the end it should be noticed that Unity also offers the possibility of testing the developed application in the meanwhile of its building through the Play Mode option. Play Mode option permits to visualize the virtual scenes just created through the camera object placed in the Hierarchy or alternatively, whenever that camera is replaced by Mixed Reality Toolkit camera, to visualize real-world images with device camera and possibly augment them when targets of scene will be visualized. The Unity graphical interface (Figure 3. 14) is composed by different windows:

- 1) Menu: it contains Unity command grouped based on their functions.
- 2) Toolbar: it is divided into 7 editor sections (motion options, coordinates options, play mode, collaborations and accounts, layers, and layout).
- 3) Hierarchy Window: it is used to manage Game Objects in the scene.
- 4) Scene View: it is the visual representation of current created scene bi- or three-dimensionally visualized, can be rotated, shifted, and zoomed.
- 5) Inspector Window: it is used to inspect and edit the properties and components of the selected Game Object or to modify the options of an asset.
- 6) Project Window: contains all the available assets, models, materials, textures, scripts, and imported packages to be used in the project.

- 7) Console Window: it permits to visualize all the errors or warnings generated during application development or display messages when it is launched.

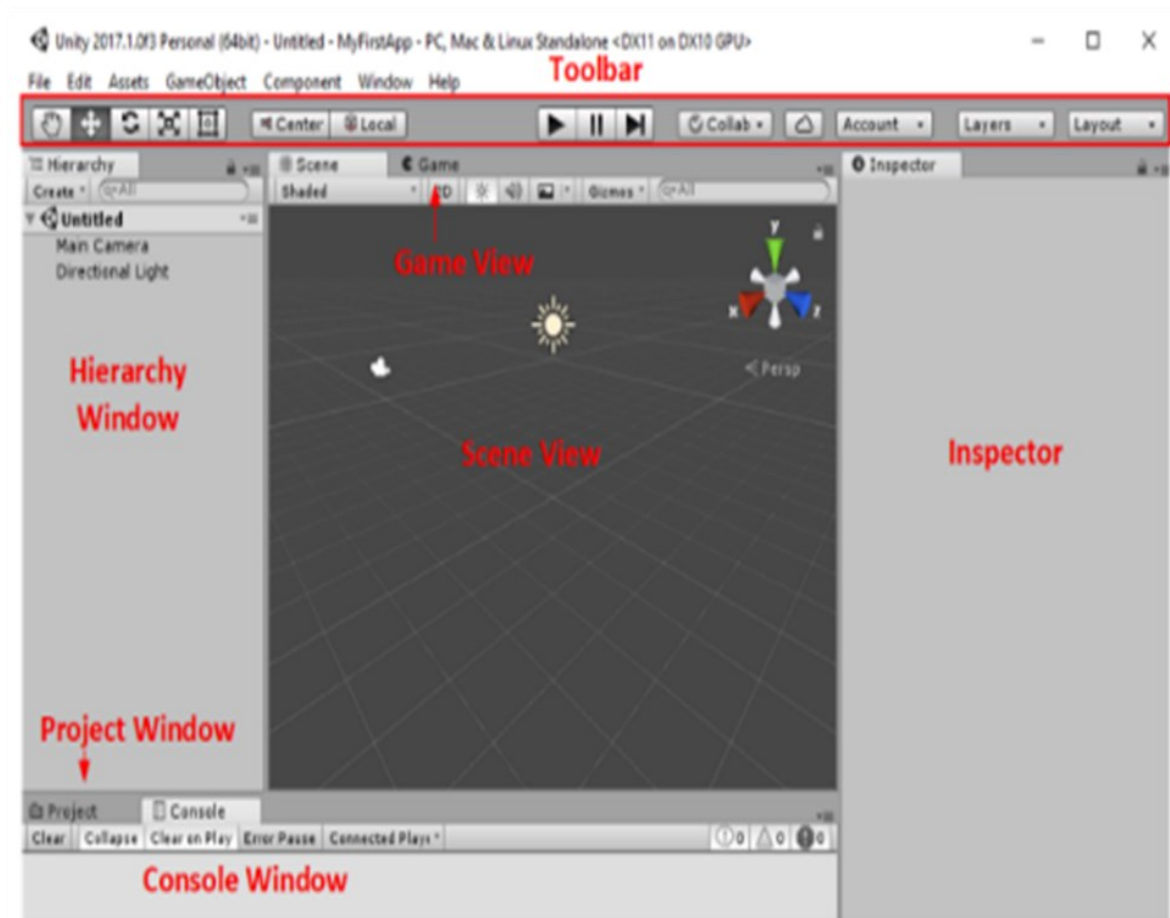


Figure 3. 14 Unity graphical interface outlook.

### 3.2.2.3 Visual Studio

This section describes the Visual Studio environment as it is presented in online user's guides [95] [96]. Visual Studio is an IDE developed by Microsoft and used to develop videogames or applications for multiple platforms. The first version was released in 1997 while its last update is dated in April 2019. It permits to deploy application solution on the specific device and contains a multi-language code editor that supports 36 different coding languages including C#, Visual Basic .Net and C++.

The code editor of Visual Studio can be used to implement scripts that mediate specific functionalities of the AR application. To be compatible with Unity software,



the language to be employed in script editing is the C#. Then, the developed script can be assigned to the Game Objects of the Unity scene and all the inputs can be manually set, as described in the previous section.

As already anticipated, Visual Studio can be also used to deploy the developed application on the targeted device. To perform this task, the solution file of the application should be built in the Unity software and then opened with Visual Studio to be compiled and distributed.

Visual Studio interface is composed by 4 main windows (Figure 3. 15):

- 1) Code Editor: window in which the script code can be written.
- 2) Solution Explorer: it shows the files on which the user is currently working.
- 3) Properties Panel: here user can retrieve information and context about the current project.
- 4) Output Window: window in which are displayed debugs, compiler warnings and error messages.

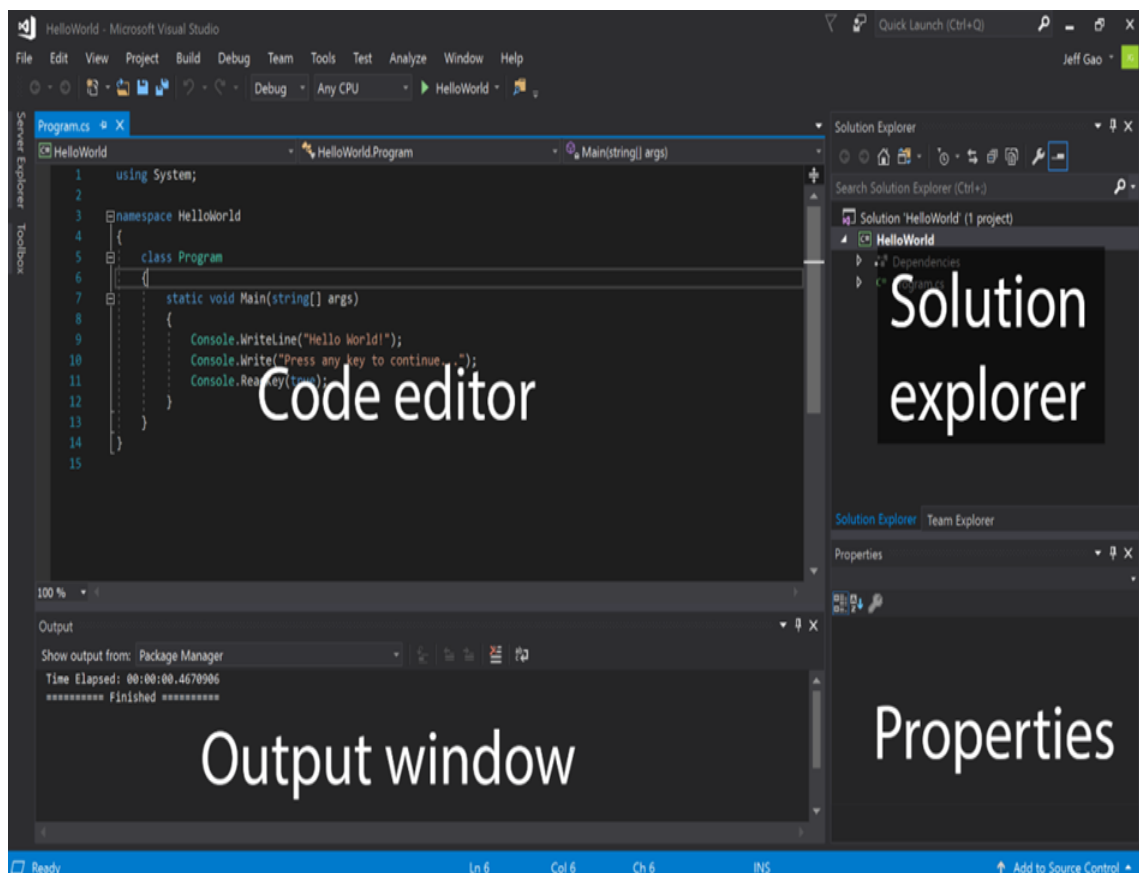


Figure 3. 15 Visual Studio graphical interface outlook.

### 3.3 3D-Printing

3D-printing means the creation of three-dimensional objects through additive manufacturing, starting from a digital 3D model generated and processed in the dedicated software. 3D printing was born in 1986, with the Chuck Hull publication of the patent (Figure 3. 16) which established the invention of Stereolithography [97] [98].

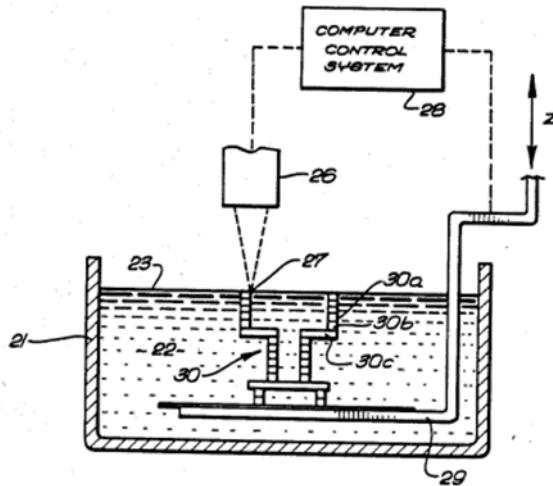


Figure 3. 16 Picture of the Hull patent.

Since 1986, 3D printing has evolved and differentiated in multiple novel printing methodologies and using several different materials or material combinations. Nowadays, 3D Printing it is widely affirmed in various sectors, ranging from industry to medical and domestic fields, even though it still exhibits a perspective potential.

Generally, 3D printers respect some criteria. They must be faster, more reliable, and easier to use than other subtractive manufacturing technologies, they offer the possibility to print and assemble parts realized with different materials in a single construction process.

3D printing, also called Rapid Prototyping (RP), is an additive technology through which the object is layer by layer generated starting from its three-dimensional CAD model. There are multiple technologies for 3D printing that differ from the modality by which layers are printed. As an example, some technologies employ materials that melt, sinter, or soften with heat to produce the layers, such as Selective Laser Sintering

(SLS) and Fused Deposition Modeling (FDM), while others lay liquid materials that are hardened with different technologies. All these technologies show advantages and drawbacks that make them suit specific applications. Generally, the main factors accounted for the technology selections are the printing velocity, allowed materials, costs of the printed prototype and coloring possibility.

The following section will describe in a deeper manner the Multi Jet Fusion 3D-printing technology that represents the most perspective solution to improve technical aspects and performances of the AR application and its test phase. However, the Color Jet Printing (CJP) 3D-printing technology will be employed in this thesis, thus, also this technology has been faced in this section.

### 3.3.1 Multi Jet Fusion

Multi Jet Fusion is a powder-based 3D printing technology that does not employ lasers. The 3D-printing process is always starting from the CAD model that is given as input of the machinery. The powder bed is deposited and uniformly heated evenly. A fusing agent is then selectively jetted over those points where it is necessary that melting occurs. Then, a finishing agent is added around the contours to improve the resolution of model components. Lamps pass over the powder bed and the jetted material captures the heat and uniformly distributes it. This procedure is iterated layer by layer. At the end, dust is removed, and the object is finished. Figure 3. 17 shows the phases of the Multi Jet Fusion process.



Figure 3. 17 Phases of the Multi Jet Fusion 3D-printing process.

Hewlett-Packard (HP) Inc is a US IT multinational and one of the world's largest manufacturers active in the hardware market, from personal computers to printers and 3D printers. HP website provides a description of the advantages and the details of their Multi Jet Fusion technology (Figure 3. 18).



Figure 3. 18 HP Inc Multi Jet Fusion 3D Printer.

Technical specifications of this technology are reported in Table 3. 3. The materials suggested to be employed with Multi Jet Fusion are the Polyamide-12 (PA12) and the Ultrasint TPU 90A-01. PA12 is a high density and low porosity polyamide that can reach maximum part dimensions of 256 x 340 x 360 mm. Ultrasint TPU 90A-01 is a flexible and wear resistant thermoplastic polyurethane that can reach maximum part dimensions of 274 x 370 x 380 mm. The first advantage of the Multi Jet Fusion is that this technology, employing fine-grained materials, permits to realize ultra-thin (80 micron) layers. In addition, generated surfaces are highly smooth and therefore the finishing post-printing procedures are minimized. Both these situations make faster the whole procedure.

Table 3. 3 Technical specifications of the HP Multi Jet Fusion 3D-printer.

HP Multi jet Fusion 3D-Printer Technical Specifications	
Standard Precision	PA12: $\pm 0.3\%$ , lower limit of $\pm 0.3$ mm Ultrasint TPU 90A-01: $\pm 0.9\%$ (XY) until $\pm 1.8\%$ (Z), lower limit from $\pm 1$ mm (XY) to $\pm 1.5$ mm (Z)

<b>Layer Thickness</b>	0.08 mm
<b>Minimum Wall Thickness</b>	1 mm (possibility to realize integrated joint of 0.5 mm)
<b>Maximum Part Dimensions</b>	PA12: 256 x 340 x 360 mm Ultrasint TPU 90A-01: 274 x 370 x 380 mm
<b>Surface Structure</b>	Non-finished part shows a smooth surface grey-colored, then they can be subject to sand blasting and colored

### 3.3.2 Color Jet Printing (CJP)

CJP is an additive manufacturing technology which involves two major components -core and binder. The core is the material that is iteratively disposed and spread layer by layer on the building platform through a roller system. Then an inkjet printing head selectively jet the binder over the spread layer that selectively solidify the powder and the model grows up layer by layer. In fact, the build platform lowers, and the following layer is spread and printed. After printing process is ended, the model is still soft and fragile. Hence, it must be finely cleaned from exceeding powder and finished through the infiltration of an acrylic compound (commonly known as 'super glue') that strengthen the whole model. Figure 3. 19 shows the CJP machinery and the phases that compose the CJP 3D-printing process. The standard material for CJP is plaster powder, a gypsum-based material, or referred to as full-color sandstone. CJP advantages are represented by the full-color printing capability, the cost efficiency, and the fact that 3D-printing process does not require supports. On the contrary, disadvantages are the brittleness and low mechanic strength of final products and the water-permeability.

CJP technology was developed at Massachusetts Institute Technology (MIT) in the early 1990s and later licensed to multiple companies. Chief among them was Z-Corporation (abbreviated Z-Corp, Burlington, USA), which continued to develop the

technology and created the first commercially available machines. Z-Corp is a company that produces 3D printers capable of printing multicolored parts, rapid prototyping machines that build plastic prototypes and 3D scanners. Nowadays, Z-Corp has been acquired by 3D-Systems Company. 3D Systems (South Carolina, USA) is a company specialized in the production of 3D printers, printable materials, professional customizable parts services, and 3D graphics software founded by Chuck Hull, the inventor of stereolithography.

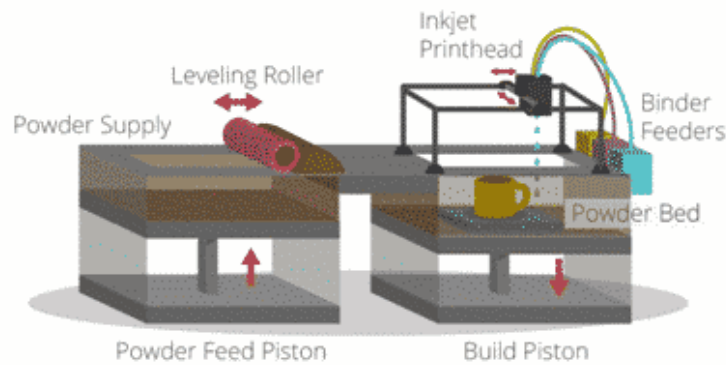


Figure 3. 19 Color Jet Printing (CJP) process phases.

The ZPrinter 450 (Figure 3. 20) is a widespread CJP 3D-printer commercialized by 3D-Systems company. ZPrinter 450 incorporates many features that automate and streamline the 3D printing process. The easy-to-use, quiet, office-friendly design, combined with high-performances, make the ZPrinter 450 one of the most cost-effective 3D printer available on the current market.



Figure 3. 20 ZPrinter 450 3D-printer machine.

The ZPrinter 450 expects a 300 x 450 DPI Resolution yielding excellent surface finish and resolution, a full-color capability, an automated powder loading, recycling and gross de-powdering, and an integrated fine de-powdering. It has a lighter weight, and it is easy to move, its maintenance is reduced, and its usage is office-friendly (office-safe build materials, active dust-control, zero liquid waste). Table 3. 4 reports all the technical specifications of the ZPrinter 450.

Table 3. 4 Technical specifications of the ZPrinter 450 3D-printer.

<b>3D-Systems ZPrinter 4500 Selective Laser Sintering 3D-Printer Technical Specifications</b>	
<b>Printer Dimensions and Type</b>	122 wide x 79 deep x 140/183 high cm (top cover closed/open) Integrated vacuum system and fine powder removal chamber Full color capability with color shell thickness 0.025"
<b>Resolution</b>	300 x 450 dpi
<b>Build Volume and Speed &amp; Layer Thickness</b>	203 x 254 x 203 mm and 2-4 layers per minute 0.089 - 0.102 mm
<b>Operating Environment</b>	Maximum Temperature Range 10-29°C); Recommended Temperature Range (12.7-26.6°C); Maximum Relative Humidity (15-70%); Recommended Relative Humidity Range (20-60%)
<b>Network Connectivity</b>	TCP/IP 100/10 Base T
<b>Noise Levels</b>	57dB (during printing) 66dB (emptying) 86dB (vacuuming - cover open) 80dB (fine powder removal)
<b>Materials - High Performance Composite -</b>	zp <sup>®</sup> 150 Powder with zb <sup>®</sup> 63 Binder,
<b>Power Requirements</b>	Type 1 and 2: 100V, 15A, 50Hz - 115V 15A, 60Hz - 230V, 7A, 50Hz Type 3 100-120V, 7A, 50-60Hz 230V, 4A, 50-60Hz

## 3.4 AR Application Validation

After the 3D model has been printed, and tests have been performed over it, to verify the validity of the performances it can be necessary to scan the tested model. The scanner acquisition of the model over which the test has been performed can be then compared with the designed situation to extract deviations and errors. In this section will be deepened the 3D scanning technology, in detail the Go!Scan3D device by CreaForm3D, and the dedicated point cloud software for the three-dimensional model creation from the performed scans, CloudCompare.

### 3.4.1 Go!Scan3D

3D Scanning is the process of analyzing real-world target objects with the objective of catching their shape and possibly appearance data. This data can be then employed in the dedicated software to reconstruct the 3D CAD model of the scanned object. Hence, 3D Scanners mediate this point collection process. They can be based on multiple technologies with their advantages, drawbacks, and costs.

Globally, 3D scanners can be classified into two main categories:

- 1) Tactile Contact Scanners: scans that need to be in contact with the target object (Coordinate Measuring Machines, Robotic Arms, etc.).
- 2) Non-Contact Scanners: they could explore different properties to scan the object, such as laser triangulation or time of flight (optical scanners) or either acoustic or magnetic properties (non-optical scanners), without contact with it.

Contact scanners exhibit great accuracy and the capacity to catch information even in deep cavities and holes, they are not subjected to external noise, the data density is automatically adjusted by the shape of the scanned object and they do not require any surface treatment before the scanning session. However, they show a low acquisition speed, they are commonly fixed and non-portable, they are not capable of catching appearance information and they are non-compatible with soft materials. Non-contact scanners can be employed with a wide range of materials, they show a good accuracy also giving the possibility to collect color information, they exhibit a fast acquisition



speed and are often portable systems. However, they can require pre-scanning spray treatments of the scanned surface, they are strongly affected by external noise and thus their acquisitions need to be appropriately filtered and processed. Another 3D-scanners classification, based on working principle, divides scanners in 5 classes:

- 1) Laser Triangulation Systems: they employ a single laser or a laser line to scan the object, the initial trajectory of the laser is reflected by the object and after this modification is detected by a sensor that through a triangulation exploits received signal properties, such as the deviation angle, to achieve information about the distance between the object and the laser source; iteratively collecting this distance information, three-dimensional model of the object is generated.
- 2) Structured Light Systems: they employ a projector as a source of a predefined pattern of light projected to the object, it deforms the pattern, and the distorted pattern is collected by a camera that exploits the distortion to extract information about the distance between the object and the projector; iteratively collecting this information, three-dimensional model of the object is generated.
- 3) Photogrammetric Systems: photographic images are collected from multiple orientation by cameras and then fused to reconstruct the three-dimensional model of the object; it should be noticed that, for a correct reconstruction, images must overlap for at least their 60%.
- 4) Contact Systems: they employ a probe that automatically or semiautomatically
- 5) moves over the object to be scanned, the probe motion is ensured on the object surface through a small pressure, the probe follows the contours of the object surface and at any deflection a point is collected; at the end of the probe motion the three-dimensional model of the object is generated.
- 6) Time of Flight or Laser Pulse Systems: they employ a laser emitter that generate a laser pulse toward the object, the laser hit the object and it is detected by receiver that exploits the time of flight, or the duration between the signal emission and reception, to extract the information of the distance between the object and the emitter; iteratively performing this process for each pulse the three-dimensional model of the object is generated.

Several companies produce different types of 3D scanner based on the above-described physical principles, as Javelin (Artec 3D scanners, both in desktop and handheld modes), Mantis Vision, Creaform3D, and V-GER. This section deepens one of the solutions commercialized by Creaform3D, the Go!Scan3D, analyzing its technical specification and details.

The Go!Scan3D (Figure 3. 21) is one of the most recent commercialized scanners on the market. It was released by the CreaForm3D company (Canada) in 2019. Go!Scan3D is a structured light based and handheld scanner that allows user to easily, fast and accurately scan the object and also registers texture information. It consists of 3 cameras, 1 white light projector (99 light stripes) and 1 color camera. To improve scanning procedure the scanner equipment includes 2 packages of marker to be placed on reference plane in which the object is positioned and that mediate calibration. Laterally, it is placed 2 lights that permits to user to understand actual goodness of the scanner placement with respect to reference plane, some multifunctional buttons to start/end the procedure or zoom in/out the scanning and a flexible wrist strap to hand-wear the scanner (Figure 3. 21). The scanner works with a dedicated software named "VXelements" where it is possible to manage and process the scans and export them in different format (.dae, .fbx, .ma, .obj, .ply, .stl, .txt, .wrl, .x3d, .x3dz, .zpr, .3mf). All the technical specification of the Go!Scan3D, listed on the CreaForm3D website, are reported in Table 3. 5.



Figure 3. 21 Go!Scan3D device and hand-wearing mechanism.

Table 3. 5 Technical specification of the Go!Scan3D device.

<b>Go!Scan3D Technical Specifications</b>	
<b>Accuracy</b>	Until 0.05 mm
<b>Volumetric Precision</b>	0.05 mm + 0.15 mm/m
<b>Measurement Resolution</b>	0.100 mm
<b>Meshes Resolution</b>	0.200 mm
<b>Measurement Frequency</b>	1500000 measurements/s
<b>Light Source</b>	White Light
<b>Positioning Method</b>	Geometry and/or color and/or target
<b>Scan Area</b>	390 x 390 mm (250 x 250 mm : 700 x 700 mm)
<b>Working Distance</b>	400 mm
<b>Depth of Field</b>	450 mm
<b>Texture Resolution</b>	50 : 200 DPI
<b>Texture Color Depth</b>	24 bits

### 3.4.2 CloudCompare

This section describes the CloudCompare software starting from online user's guides [99] [100]. CloudCompare was originally created from a collaboration between Telecom ParisTech and the Research & Development division of the EDF company. Nowadays, CloudCompare is an independent open-source project and a free software. CloudCompare is a generic three-dimensional point cloud and triangular meshes processing software that provides tools for editing and rendering and that includes

even more advanced processing algorithms for registration, resampling, color/normal/scalar fields handling, statistical computations, sensors management, interactive or automatic segmentation, etc. CloudCompare is available on Windows, Linux and Mac OS X platforms.

Here it is reported a quick overview of the main windows of the user interface on CloudCompare (Figure 3. 22):

1) Menus:

- File (open, save, quit, etc.)
- Edit (edit selected entities features - colors, normal, scalar fields, etc.)
- Tools (segmentation, registration, projection, etc.)
- Display (display-related options)
- Plugins (loaded plugins)
- 3D Views (3D views management) Help (about, help, etc.)

2) Main toolbar (quick access to main editing and processing tools: open/save, point picking, clone, etc.)

3) Scalar fields toolbar (quick access to scalar fields related tools)

4) Plugin toolbar (quick access to currently loaded plugins - standard and OpenGL shaders)

5) View toolbar (quick access to display-related tools)

6) Database tree (for selection and activation of entities and their features)

7) Property view (information on selected entity)

8) Default 3D view Another 3D view (created with 3D Views > New)

9) Console

CloudCompare permits translate and/or rotate single or multiple entities, pick up group of points but also to open multiple models, align and compare them.

Generally, the comparison operation will be performed between the reference geometries (nominal models) and the geometries obtained after performing the test and scanning the tested object (scanned models). In fact, as soon as the nominal and scanned models are aligned is it possible to extract deviations and errors between the

nominal or reference model and the actual performance resulting from the test. Figure 3. 23 shows an example of comparison between nominal model or geometry and the scanned model or geometry.

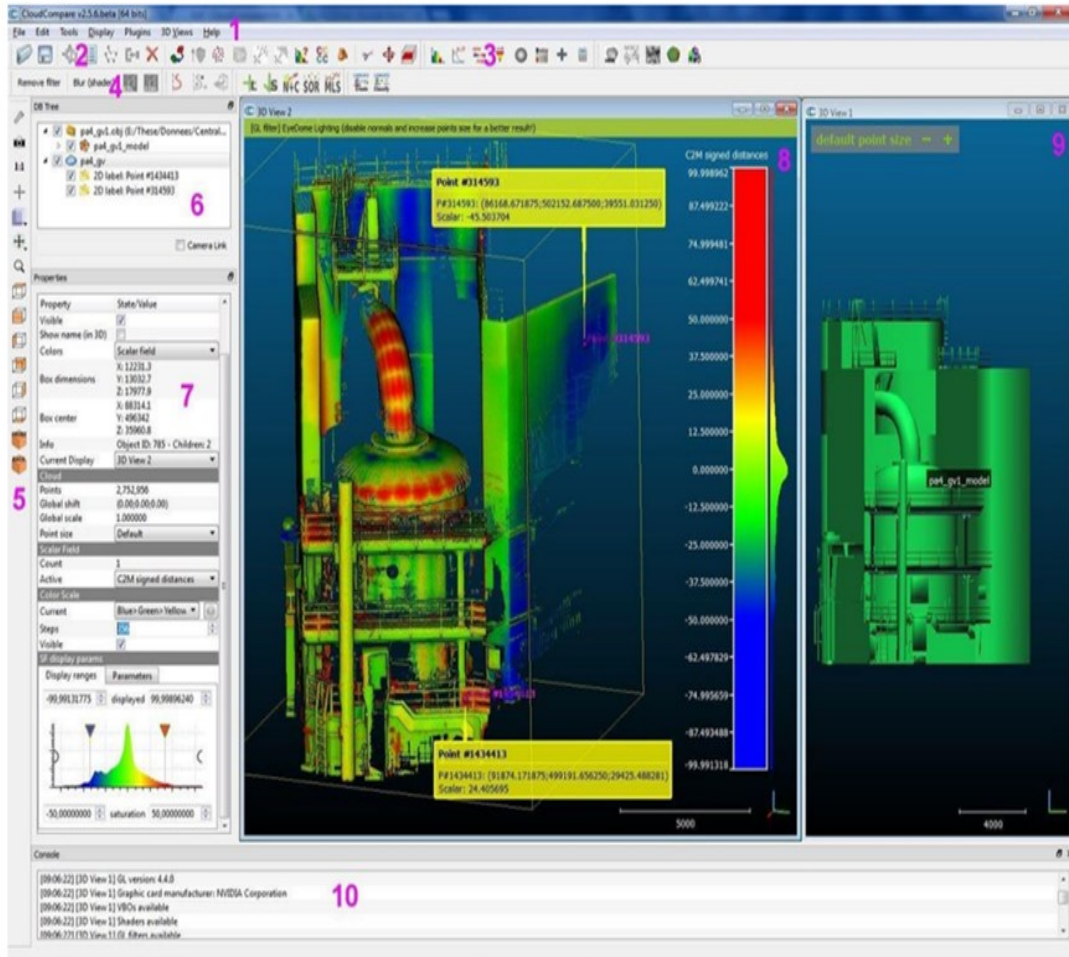


Figure 3. 22 CloudCompare graphical interface outlook.

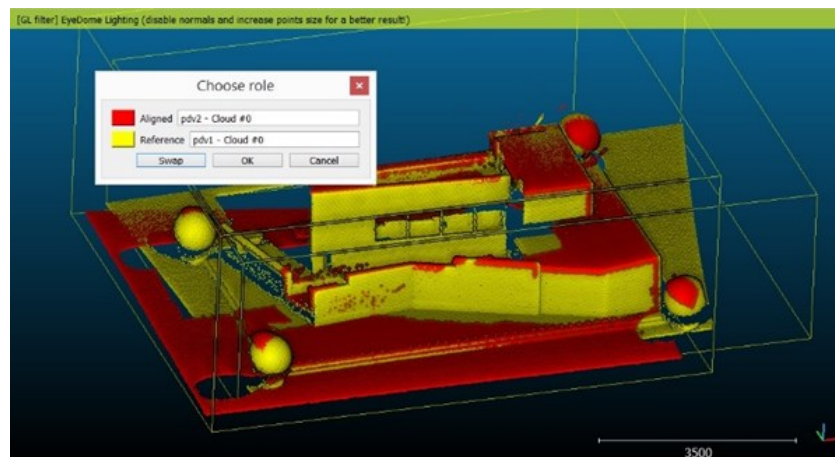


Figure 3. 23 Aligned nominal and scanned models.

## 3.5 AR Application

The objective of this thesis is the development and test of an AR application that allows the assistance of both osteotomy and repositioning operations. In this section, the developed AR application will be described including the marker generation phase and the modelling phase to extract all the expected virtual contents and surgical guides. Moreover, the minimal requirements of a skull phantom, to be used for testing the application, are presented.

First, since markers are crucial in the development of AR application, it is essential to define the requirements imposed on markers in this thesis. Passive markers or feature-rich images, in detail the QR codes, will be used. The main requirements for a well-designed marker are the richness in feature, the high contrast and the elevate definition. QR codes can be generated using online sites and the generated images fulfill these requirements. Moreover, it must be necessary to correctly select the marker dimensions. Marker dimensions must suit both practical constraints (they must not hamper the surgical procedure) and technical constraints of the HMD (they must be recognizable and trackable). Trial and error procedures help in the definition of the optimal dimension and features quantity from both the points of view.

Then, from a general point of view, the AR application must at the meantime permit the visualization of static holograms (cutting lines, drilled holes, and target position to be reached) and keep tracking of the structures that are moving (osteotomized fragment). Hence, the osteotomy task can be easily accomplished with the usage of a single marker solidly attached on the patient, while in case of the repositioning task at least two markers are necessary, the first will permit the stable visualization of holograms such as the target position to be reached while the second will be continuously tracked keeping information about the current position of the osteotomized fragment and using this information to return the feedback to the user. For the development of the AR application proposed in this thesis, a 2-marker system has been employed. The first marker, named M1, is hypothesized to be fixed on patient anatomy that is stable throughout both osteotomy and repositioning tasks. M1 permits

to visualize those holograms that are necessary to aid repositioning task, such as the target position to be reached. The second marker, named M2, instead, is hypothesized to be solidly placed on the osteotomized fragment and it will be stably fixed during the osteotomy task, but it will become a mobile marker as soon as the bony fragment on which it is attached is osteotomized. Hence, M2 will permit the stable visualization of holograms uniquely throughout the osteotomy while the associated holograms will solidly move during repositioning. Indeed, M2 is used to stably visualize cutting lines and drilled holes, for the final fixation of the osteotomized fragment, and then it permits to visualize all the feedback elements that can be useful to be displayed, during repositioning, close to the structure that we are moving. It must be remarked that markers can be tracked by the HMD, hence M2, solidly placed on the osteotomized structure, permits to keep track of the actual position of the osteotomized structure and then to manage the feedback returned to the user during the repositioning task. One of the requirements of the developed AR application is the clearance of the application outlook. For this purpose, virtual contents must be well organized and must not confuse and distract user. Hence, the AR application will expect the presence of buttons within the scene that will permit user to select the virtual contents to be hidden and those to be shown simply by selecting the needed modality between the two available:

- 1) Osteotomy Mode: only cutting lines and drilled holes are displayed.
- 2) Repositioning Mode: only elements of repositioning feedback are visualized.

Then, the application must be consistent with the way in which, normally, the surgical procedure, that it is aiding, is performed. Its outlook must be simple, effective, and intuitive in all the virtual surgical guides proposed to be easily understood by non-AR expertise and at the meantime to be able to assist surgeons, practitioners, and other users. For these reasons, the Osteotomy Mode simply expects the visualization of the cutting lines (as colored prisms, cylinders, etc.) that the user must follow to perform the cut and the display of the drilled holes (as points, cylinders, etc.) to perform the drilling, while the Repositioning Mode expects the visualization of a cube

hologram, exactly dimensioned as M2, positioned at the target position to be reached and oriented as established by the pre-operative plan (3 translations and 3 rotations around Z-X-Y axes in that order), a set of 3D-arrows selectively activated to indicate the direction (positive or negative) that user must follow on principal axes to reach target position, a Reference Frame over cube hologram to understand cube hologram target orientation and over M2 to understand its current orientation. Furthermore, in this modality, to improve the intuitiveness of the feedback retrieved to the user and make faster the user comprehension, an alarm system has been implemented to change the color of the cube positioned at the target position and highlight, in this manner, that achievement. Moreover, to be consistent with the modality of performance of the repositioning tasks in the surgical routine (i.e., surgeons are guided by calipers and continuously check and visualize millimeters values to monitor the procedure), it has been added a panel to display the distances in millimeters between the actual position of the osteotomized fragment and the one to be reached.

Then, to test the developed AR application, a custom-made physical phantom is required. Globally, the first requirement that the phantom must respect is that its three-dimensional model must be consistent with the one on which surgical guides are developed. Hence, surgical guides must be developed on the same three-dimensional model used to 3D-print the phantom. Then, the phantom must expect directly the 2-marker system (M1 and M2) or the possibility to assemble them over the anatomy. M1 can be attached to the skull anatomy outside of the osteotomized fragment. For its fixation screws represents the suggested solution but for practical laboratory usage this marker can be also directly embedded in the skull anatomy. On the contrary, M2 must be attached or solidly placed on the osteotomized fragment. Its fixation can be mediated by screws, directly embedding the marker on the fragment but the most reliable solution is represented by the usage of dental bites on which M2 can be directly attached or assembled. Then, the skull phantom can be a mono-use or multifunctional phantom according to the actual end of use. In all the cases, the skull phantom must allow both osteotomy and repositioning operations, thus, an assembly/dis-assembly mechanism should be embedded. Mono-use phantoms exclusively permits the test of



the developed AR application on the mandible or on the maxilla while multi-functional phantoms permit to test the application on both the bony structures. Moreover, in case of multi-functional phantoms, user should have the possibility to easily select the treated anatomy, for example by assembling M2 on the correspondent bite structure (i.e., upper bite to treat the maxilla and lower bite to treat the mandible).

From a technical point of view, the AR application development is conducted using Unity software and Visual Studio platform. The development starts with the import of all those packages that will be used for the AR nature of the application (Vuforia package, MRTK package, marker database package). The following step is the tuning of all the build and project settings and possibly the configuration of some of the imported packages, to suit the requirements of an AR application to be deployed. Then the scene is created, adding markers created in Vuforia, associating to them the game objects or the exported \*.OBJ files of the surgical guides (osteotomy lines and drilled holes). Furthermore, the scene is completed with all the feedback elements that can be both \*.OBJ files designed and exported from Rhinoceros 6 (3D-arrows and Reference Frame) or composed game objects (panel for the visualization of the distances in millimeters) or pre-designed objects enclosed in the imported packages (menu with buttons to select the view modality). Finally, C# scripts have been developed in Visual Studio, assigned to the Unity objects and their inputs can be manually selected from Unity interface. C# scripts implements all the functionalities of designed AR application, that are cube hologram positioning at the target position and orientation to be reached by the osteotomized fragment, accounting for the pre-operative plan expressed as a vector of 3 translations and a vector of 3 rotations around Z-X-Y axes in that order, management of the 3D-arrows visualization based on deltas between current M2 position and target position to be reached, management of the alarm system to change the cube hologram color based on the same deltas, management of the visualization of delta values over the dedicated panel. The application then is built in Unity, compiled, and distributed in Visual Studio to be deployed on the Microsoft HoloLens V2 HMD. At the end, the application is available on the HMD and ready to be launched.

### 3.5.1 Virtual Surgical Guides and Contents

Rhinoceros 6 has been employed to develop the surgical guides and contents expected in the AR application.

First, the cutting lines to be followed to perform the various osteotomies are custom-made on the patient skull. Osteotomy lines can be realized using multiple geometrical entities in the Rhinoceros 6 environment. They can be colored cylinders, prisms or lines obtained by processing the three-dimensional model of the phantom to be 3D-printed and over which the application will be tested. Cutting lines can be developed by following a standardized procedure that expects:

- 1) Cutting planes creation.
- 2) Extraction of the intersection curves between the phantom anatomy and the cutting planes.
- 3) Reconstruction of the intersection curves.
- 4) Extrusion to generate the cutting volumes.
- 5) Relimitation of the extrusions to obtain the external guides for the osteotomy.
- 6) Meshing of the relimited volumes.

However, this standardized procedure must be personalized on the surgeon requirements and over the clinical case to be treated.

Secondarily, the drilled holes are designed. These virtual guides suggest the area on the patient skull in which the drilled holes must be created to permit, at the end of the surgery, the fixation of the repositioned maxillary fragment by mean of plates and screws. To realize drilled holes simple geometries, such as cylinders or prisms can be created, meshed, and positioned in the appropriate manner on the anatomy. The dimensions of the drilled holes must match the requirements established by the type of the fixation devices employed by the surgeon and must clearly highlight an area over the treated anatomy.

Moreover, for the AR application user interface, some graphical elements, in detail a set of 3D-arrows and a Reference Frame, have been created to compose the feedback that characterize the repositioning mode.

3D-arrows pointing in the positive and negative direction of any of the principal axes have been created in Rhinoceros 6. The 'Box' command has been used to create the tail of the arrow and the combination of the 'Polyline' and 'Extrude Closed Planar Curve' commands has been employed for the realization of the head of the arrow. Head and tail have been joined with the 'Join' command and the arrow is obtained. At the end, 'Copy', 'Paste' and 'Rotate' commands have been used to generate all the required arrows. All the arrows have been meshed with 'Mesh' command. Figure 3. 24 shows dimension of a single arrow and the entire set of arrows. Reference Frame is used to understand the target orientation to be reached according to the pre-operative plan and the current orientation of M2. A set of three axes of 2cm length has been downloaded from the Grabcad online library, it has been opened in Rhinoceros 6 and axes have been modelled using the 'Scale3D' and 'Rotate' commands. Figure 3. 25 shows the outlook of the Reference Frame. All virtual contents employed for augmentation of real-world in the developed AR application have been exported in \*.OBJ format to suit the compatibility requirements of Unity software. 3D-arrows and Reference Frame have been separately exported while osteotomy lines and drilled holes have been exported as unique entities.

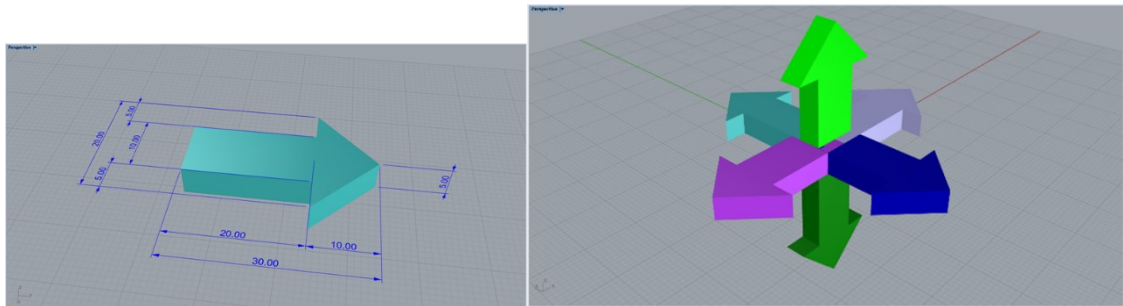


Figure 3. 24 Single arrow dimension and the whole set of arrows.

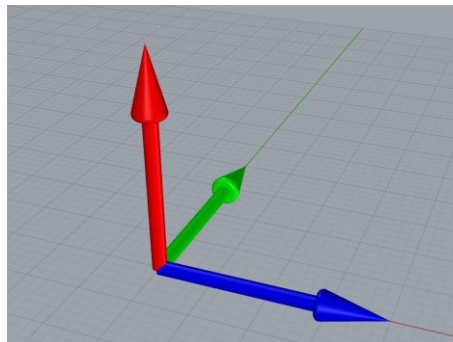


Figure 3. 25 Reference Frame Outlook.

### 3.5.2 Markers Generation

To fulfil the requirements for a well-designed marker, QR codes are selected, in detail, cubic markers to ensure a stable holograms registration by changing viewpoints and reducing line-of-sight problems. The AR application requires 2 markers. Hence, 12 QR codes are generated and grouped as illustrated in Figure 3. 26 and Figure 3. 27.



Figure 3. 26 Back, bottom, front, left, right and top QR codes for M1.



Figure 3. 27 Back, bottom, front, left, right and top QR codes for M2.

QR codes have been generated online on Piffero QR Generator website and they have been imported in Vuforia developer portal to create a database. The database is made of 2 cuboid markers with dimensions 3 x 3 x 3 cm, named M1 and M2. The QR codes shown in Figure 3. 26 have been assigned to back, bottom, top, front left right

and top faces of M1 while QR codes shown in Figure 3. 27 have been assigned to the faces of M2. The database is exported in the \*.unitypackage format to be then imported and used in development of the AR application in Unity. Moreover, a license key is generated in Vuforia developer portal to be associated to the AR application.

### 3.5.3 Application Development

The software used for the development of the AR application are Unity and Visual Studio. The steps to be performed consist of packages import, project settings, scene creation, script writing, build generation, compilation, and distribution of the application on the device, Microsoft HoloLens V2. All the steps, except for step 4, step 6, and step 7, have performed in Unity. The remaining 3 steps has been performed in Visual Studio. To develop an application in Unity as first passage a project must be initiated. To create a project the Unity Hub is employed, here a 3D Project is selected, named, and located in the specific path. Figure 3. 28 shows the Unity Hub interface for initiate a project and the selection of the project type, name, and location. Finally, the 'Create' button has been used to generate the project. Through this procedure, all the project settings, imported assets or packages, created, or downloaded prefabs and generated scripts will be automatically located in the specified path within a folder named as the project name.

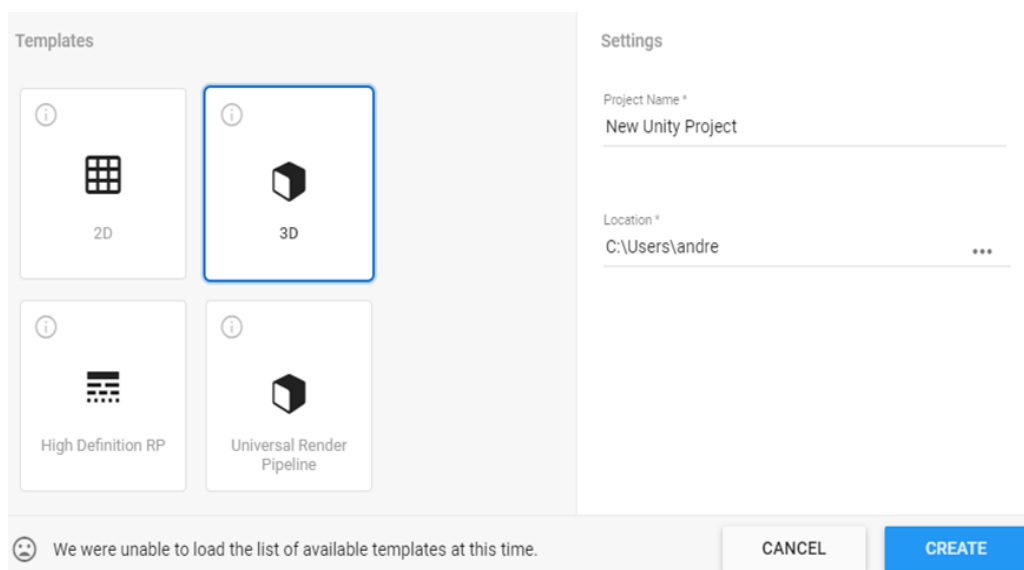


Figure 3. 28 Unity Hub interface for the project initiation.

### 3.5.3.1 Packages Import

First step, as already specified is the packages import. Packages must be appropriately downloaded or created in the dedicated websites such as Vuforia SDK and Microsoft GitHub. In this section, the steps followed to embed all the necessary packages will be described.

The packages, appropriately exported in the \*.unitypackage format as described in the previous sections, that must be imported correspond to Vuforia Engine package, targets database package and MRTK package.

MRTK offers 5 different main items to be downloaded and added to the Unity project (Foundation, Extensions, Tools, Test Utilities and Examples). Among them, just the Foundation item is strictly needed to develop a functioning AR application in Unity. For what concern the MRTK package import, the Mixed Reality Feature Tool - Beta version has been downloaded and the execution file has been launched. The project path has been specified, the foundation item on the Mixed Reality Toolkit field has been selected, validated on the project, and imported following the path illustrated in Figure 3. 29.

The targets database package has been appropriately downloaded from the Vuforia developer portal, it permits to use the targets, in detail the 2 cuboid markers (M1 and M2), enclosed in the imported database in the AR application scene and manage the scene objects with respect to them. Targets database package have been imported in the project following the path illustrated in Figure 3. 30.

Finally, the Vuforia Engine package permits to actively recognize and use targets. Vuforia Engine package has been downloaded and then imported from the Package Manager window of Unity with the 'Add Package from Disk' option, adding the .json file contained in the downloaded folder (Figure 3. 31).

At the end, to be able to manage and use prefabs that are available in the MRTK foundation package ('Packages → Mixed Reality Toolkit Foundation → SDK → Features → UX → Prefabs') the Text Mesh Pro (TMP) Essentials and Examples & Extra has been installed (Figure 3. 32). In detail, TMP allows to use menus available in MRTK that are structured to hold buttons that can be used by user in the scene.

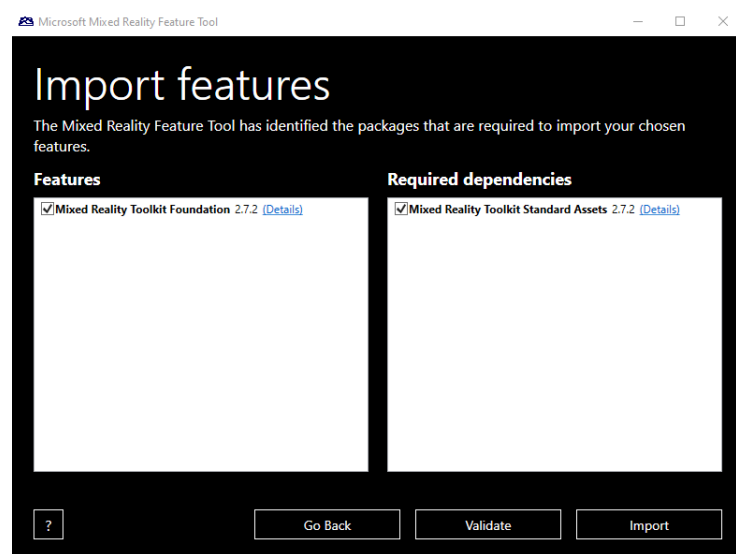
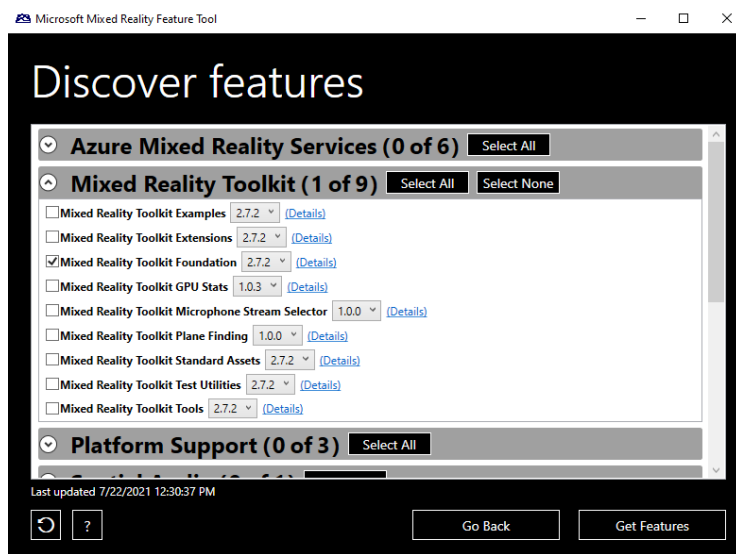
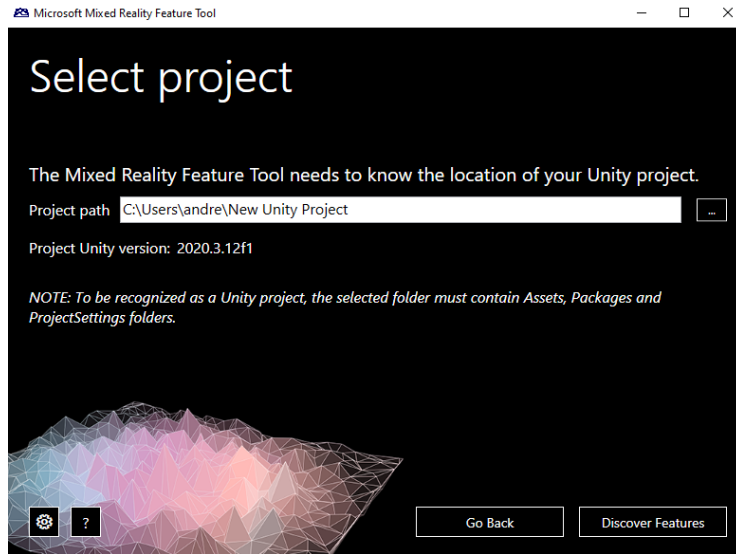


Figure 3. 29 Mixed Reality Toolkit (MRTK) Foundation package import procedure.

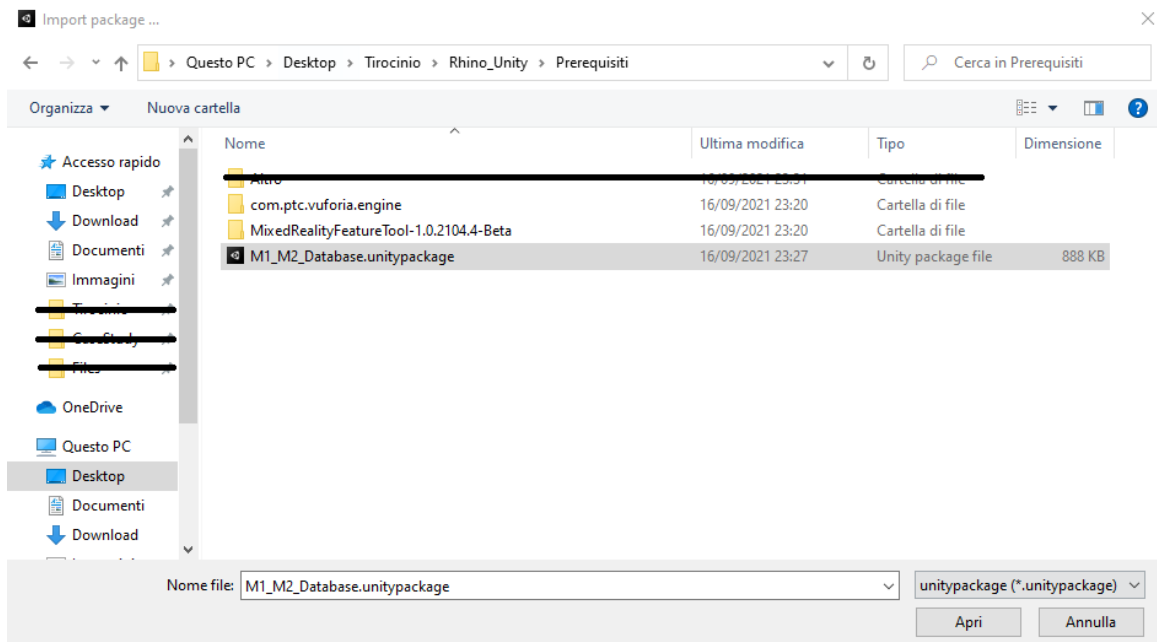
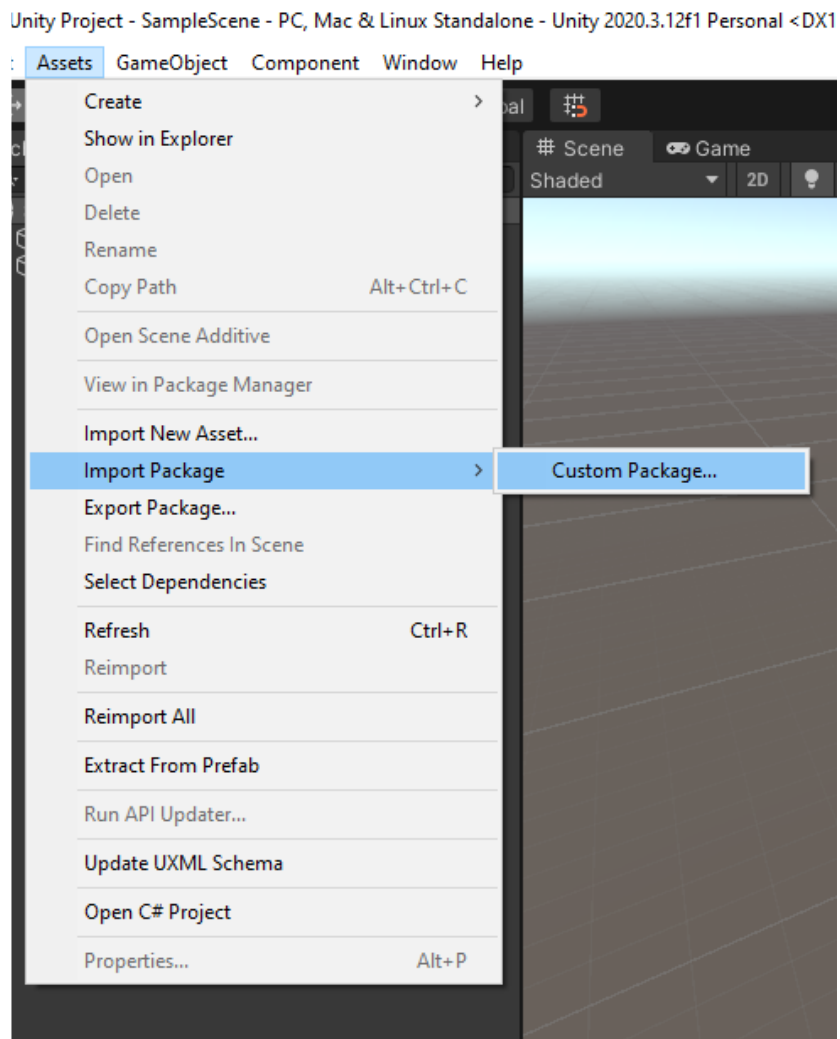


Figure 3. 30 Target database import procedure.



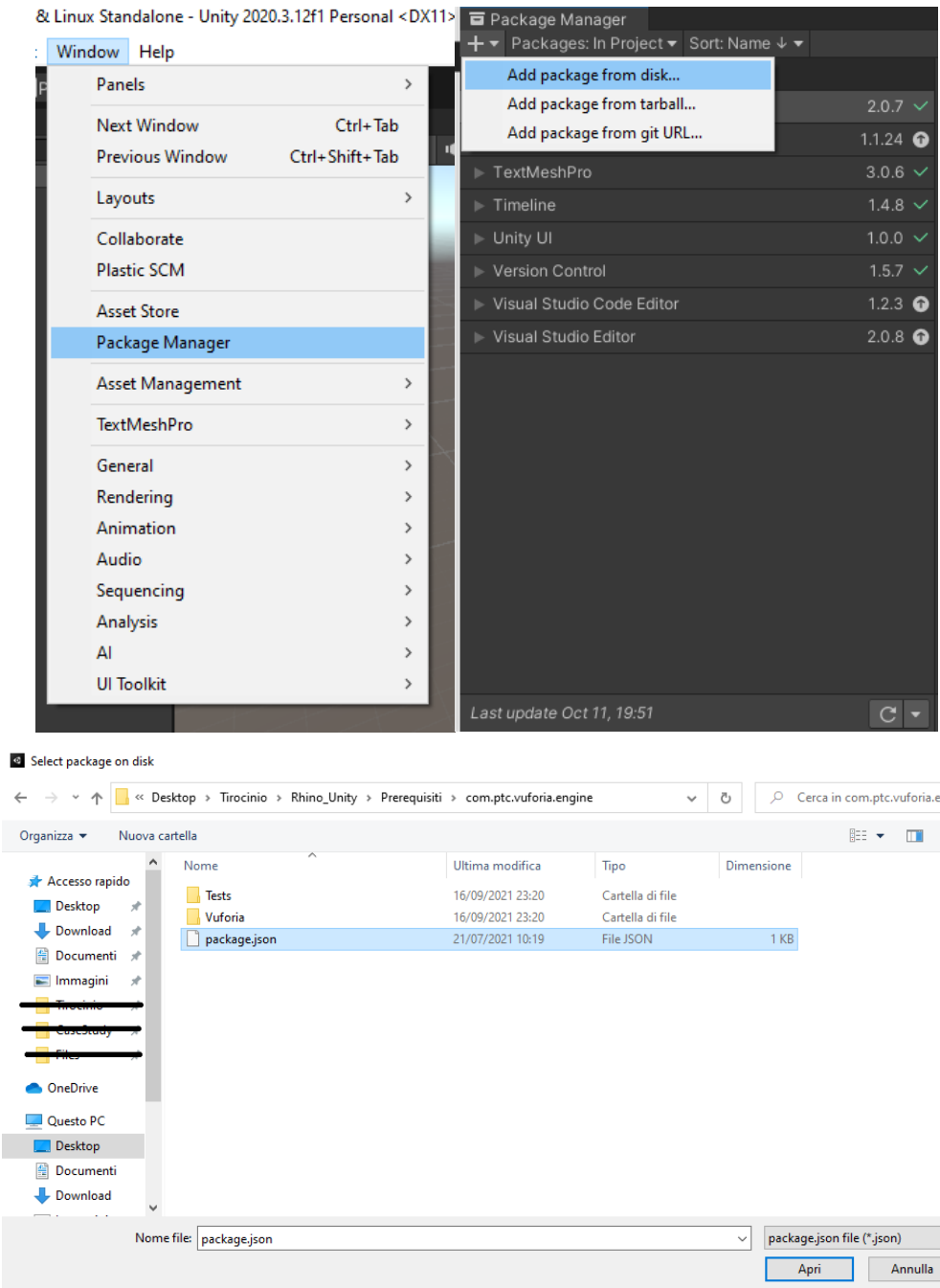


Figure 3. 31 Vuforia Engine import procedure.

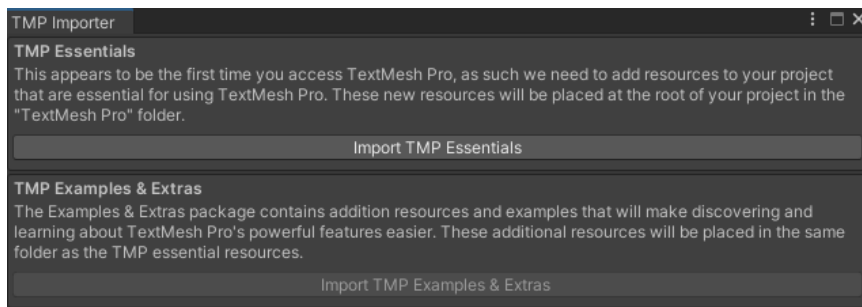


Figure 3. 32 Text Mesh Pro (TMP) installation window.

### 3.5.3.2 Project and Build Settings

The second step is the tuning of all the project settings.

As first passage, the target platform needs to be specified by following the path 'File → Build settings → Switch Platform', specifying the Universal windows Platform (Figure 3. 33).

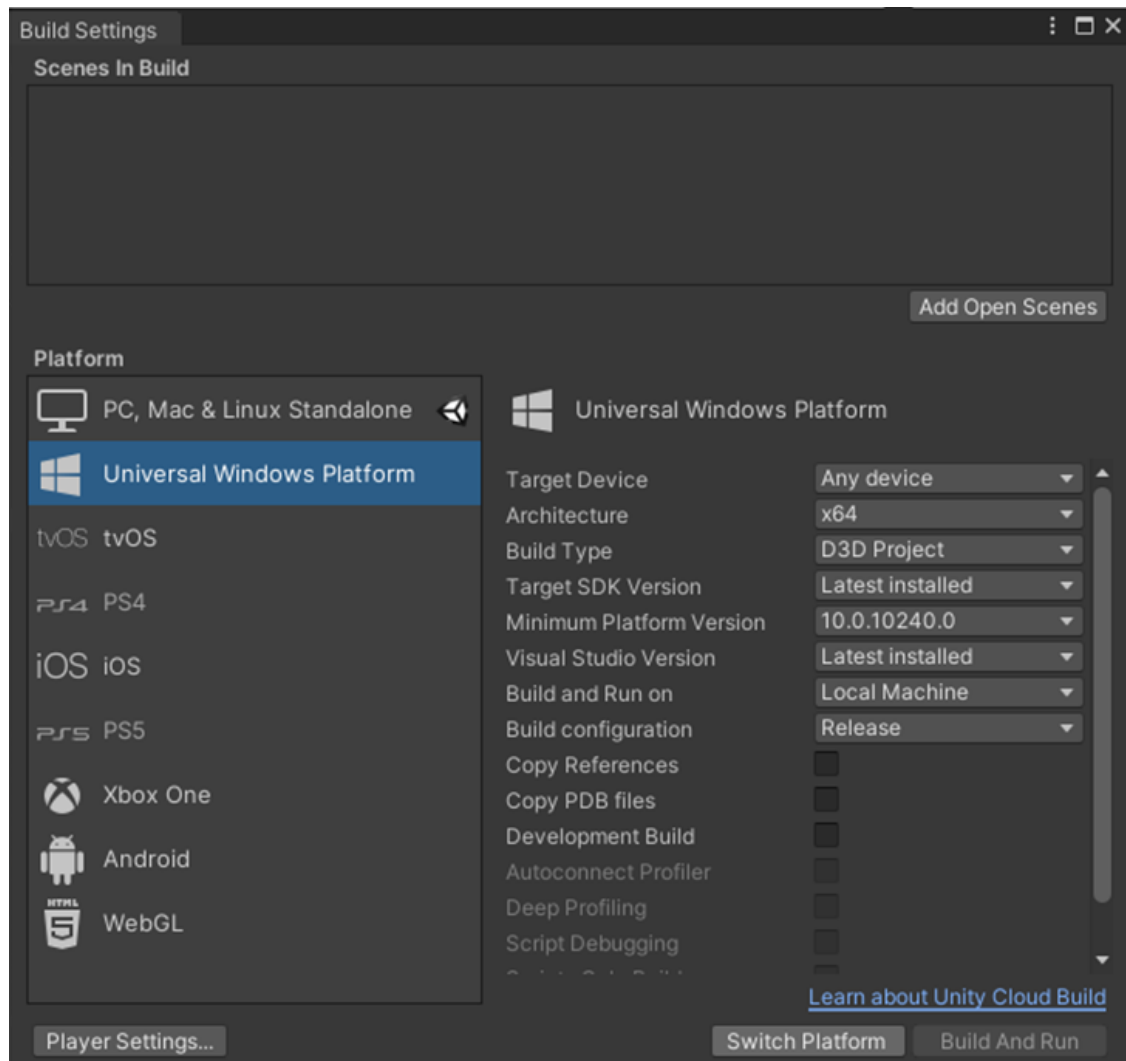


Figure 3. 33 Build settings window.

Then, some parameters of the project settings must be tuned to suit the requirements of an application to be deployed. By following the path 'Edit → Project Settings → Player → Resolution and Presentation' the 'Run in Background' option has been removed and the 'Default Orientation' has been set to 'Landscape Left' (Figure 3.

34). By following the path 'Edit → Project Settings → Player → Publishing Settings' some options have been activated: 'Internet Client', 'Webcam', 'Microphone' and 'Spatial Perception' under the 'Capabilities' field (Figure 3. 35) and 'Holographic' under the 'Supported Device Family' (Figure 3. 35).

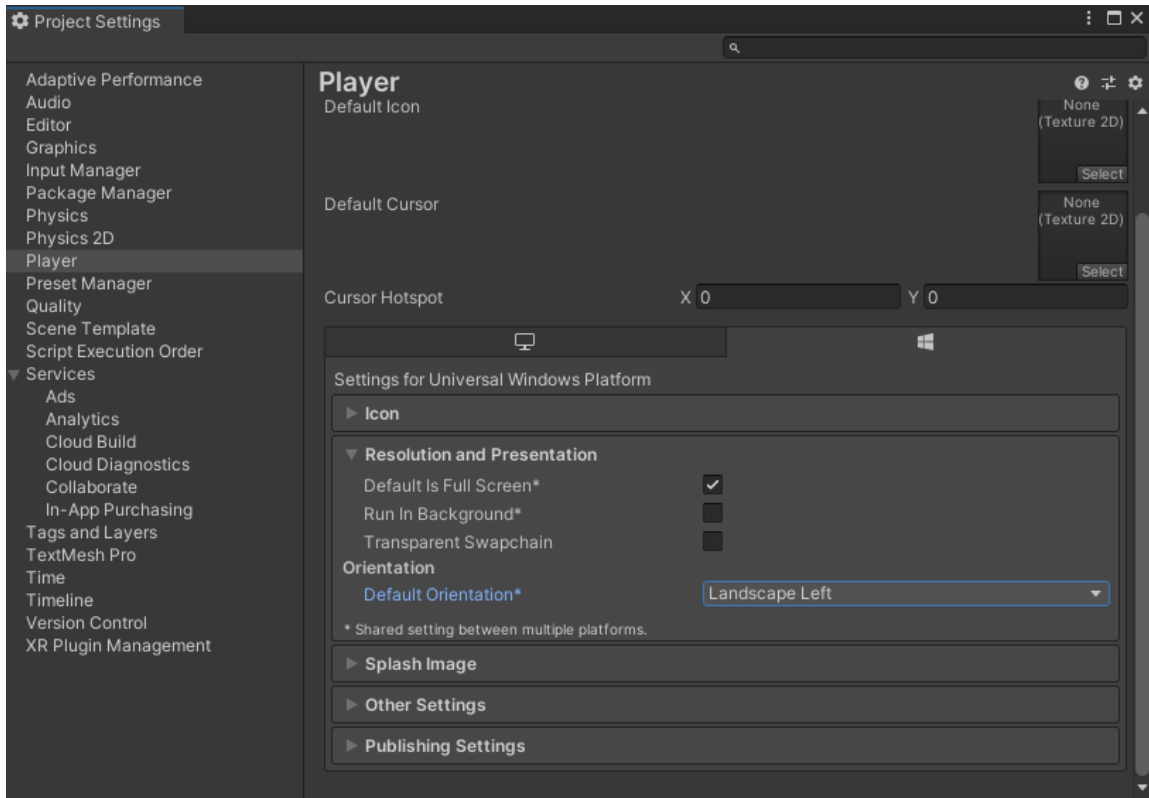
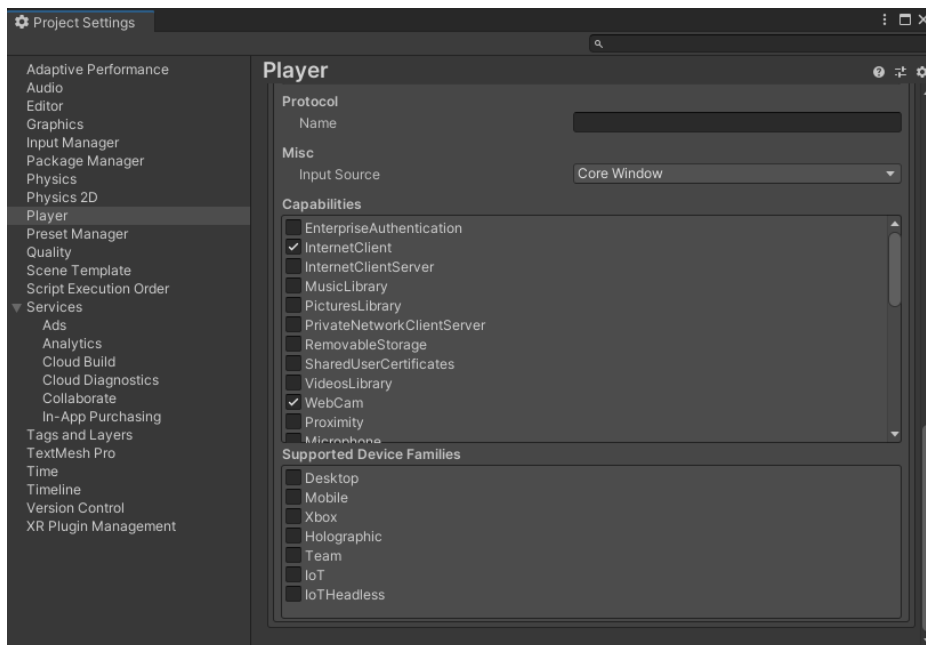


Figure 3. 34 Project settings, Player (Resolution and Presentation).



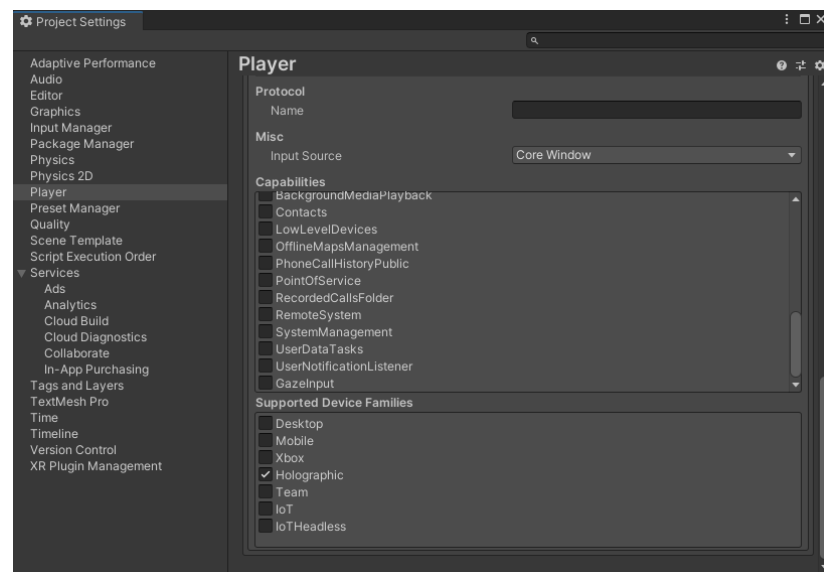
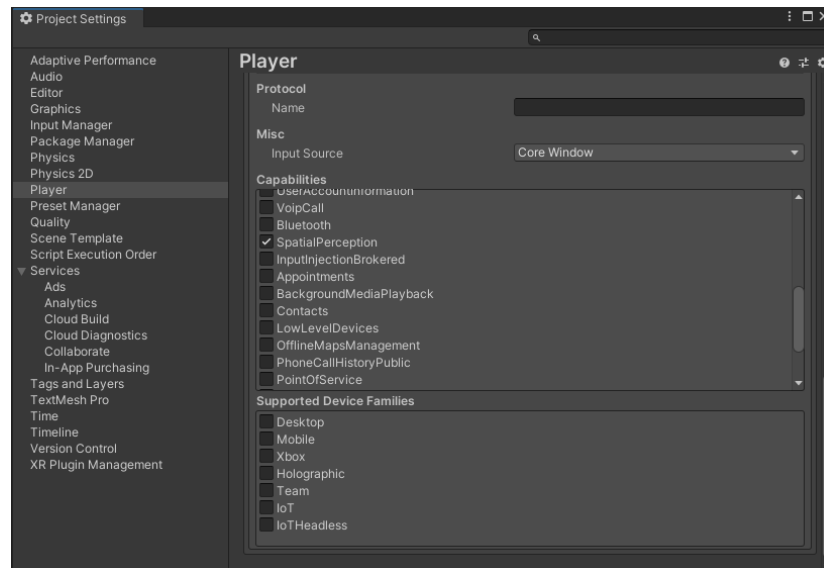
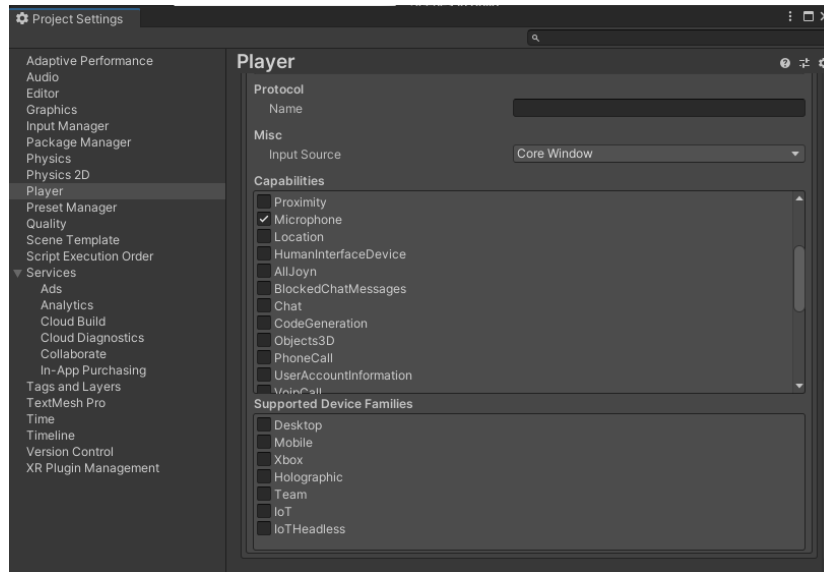


Figure 3. 35 Project settings, Player (Publishing Settings-Supported Device Family).

By following the path 'Edit → Project Settings → XR Plug-in Management' the XR plug-in management has been installed and then the 'Plug-in Providers' has been set to 'Windows Mixed Reality' (Figure 3. 36). Following the path 'Edit → Project Settings → XR Plug-in Management → Windows Mixed Reality', 'Depth Buffer Format' is set to 'Depth Buffer 16-bits' and 'Shared Depth Buffer' is enabled (Figure 3. 37).

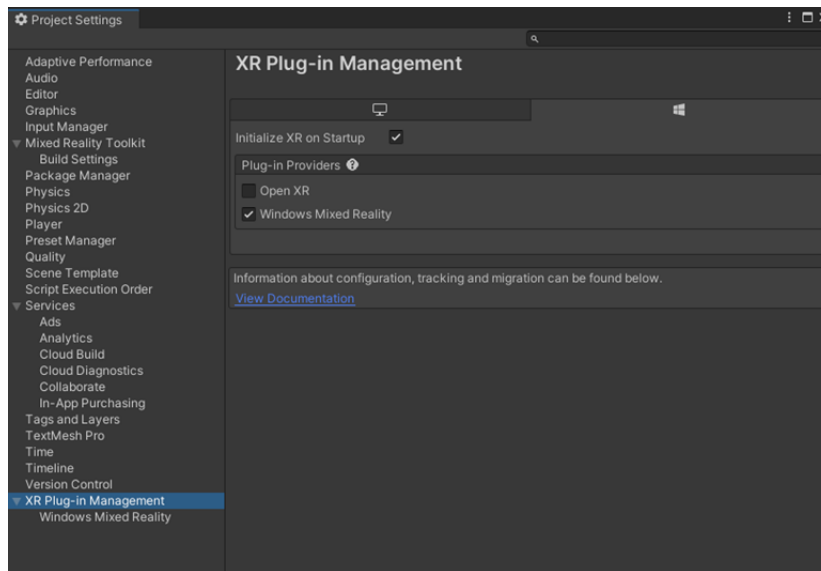


Figure 3. 36 Project settings, XR Plug-in Management.

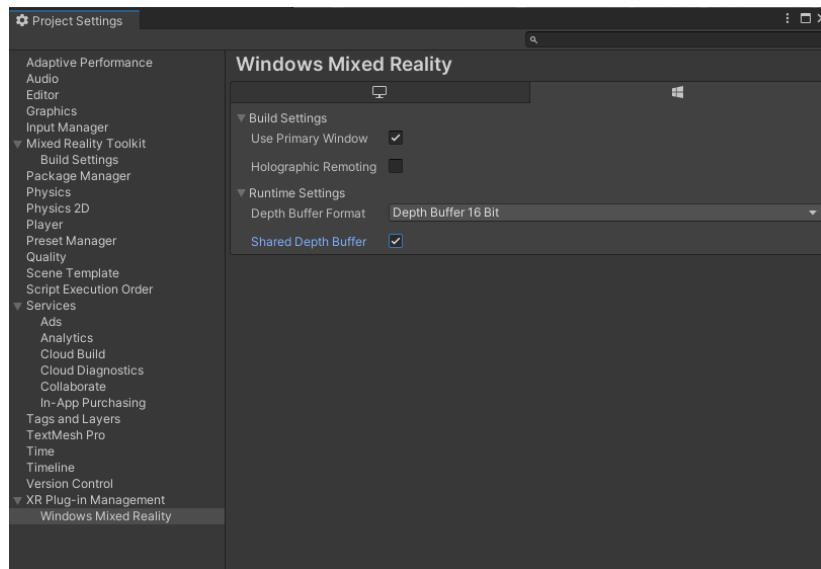


Figure 3. 37 Project settings, XR Plug-in Management (Windows Mixed Reality).

Finally, following the path 'Edit → Project Settings → Audio' the 'Spatializer Plugin' option has been set to 'MS HRTF Spatializer' (Figure 3. 38).

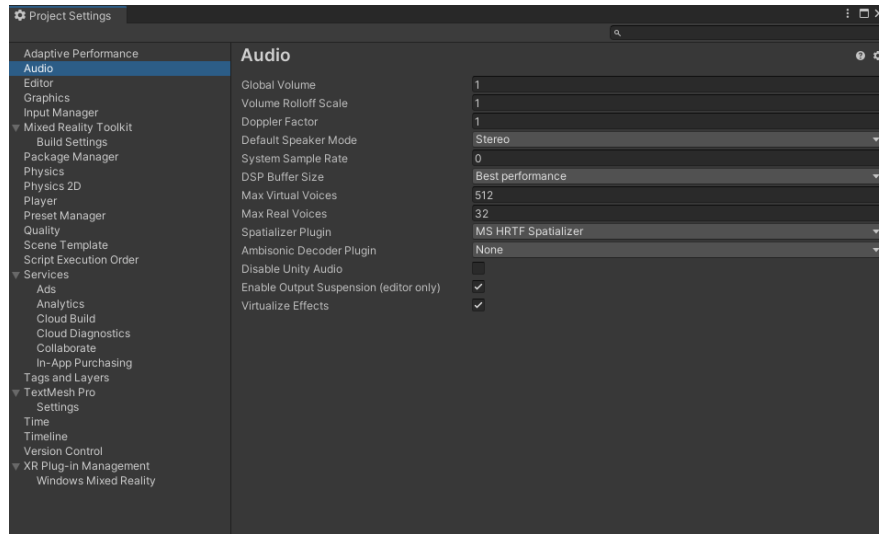


Figure 3. 38 Project settings, Audio.

The following passage is MRTK configuration. A way to configure MRTK is through profiles available in foundation package (Camera, Input, Boundary, Teleport, Spatial Awareness, Diagnostic, Scene System, Extensions and Editor). The toolkit provides a set of default profiles covering most platforms and scenarios although they are non-optimized for specific usages, so, when advanced settings are needed profiles must be cloned and modified. It must be noticed that all the following steps has been made cloning default profiles and modifying new ones. As first, the default main camera has been removed from the scene and the MRTK has been added to the scene and configured by following the path 'Mixed Reality → Add to Scene and Configure'. In this manner, 'Mixed Reality Toolkit' and 'Mixed Reality Playspace', with 'Main Camera' as child, are added in the Hierarchy. Then the settings have been customized for the specific case by managing the options in the inspector of the 'Mixed Reality Toolkit' object just created in the Hierarchy. By default, the application will provide a collection of meshes representing environment geometries or hands in the scene. This option can annoy user and confuse its view in the operating room during the operations. Hence, these meshes must be hidden. 'Spatial Awareness' field is the first to be configured to hide environment geometry meshes. After setting the 'Type' of the Spatial Observer to be added to 'Mixed Reality Toolkit Spatial Object Mesh Observer → Spatial Object Mesh Observer', the 'Display Option' has been set to 'None' (Figure

3. 39). Then, 'Input' field is the second field to be configured, to hide hand meshes. Here, under the 'Articulated Hand Tracking' option the 'Hand Mesh Visualization Modes' and the 'Hand Joint Visualization Modes' are both set to 'Nothing' (Figure 3. 40). As third, in the 'Diagnostic' field, the 'Show Profiler' option has been unchecked (Figure 3. 41). Finally, the 'Camera' field has been managed. In the 'Display Settings' field, as first, under the 'Transparent' option the 'Quality Setting' has been set to 'Ultra', then the 'Near Clip' have been set to '0.3' under both the 'Opaque' and 'Transparent' option, to match the optimality range suggested for the Microsoft HoloLens V2 (Figure 3. 42). Then the main camera, a child of the 'Mixed Reality Playspace', is configured to recognize Vuforia target database imported. The inspector of the 'Main Camera' object must be opened and modified. As first, the 'Clipping Plane → Near' option has been set to '0.3' (Figure 3. 43).

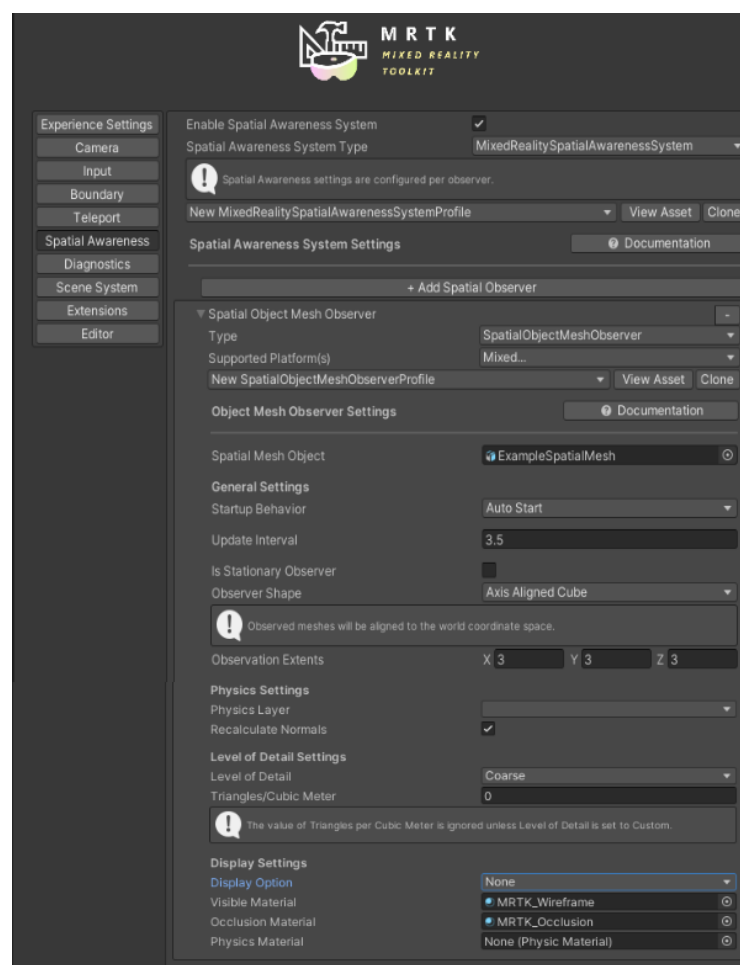


Figure 3. 39 Mixed Reality Toolkit inspector, Spatial Awareness.

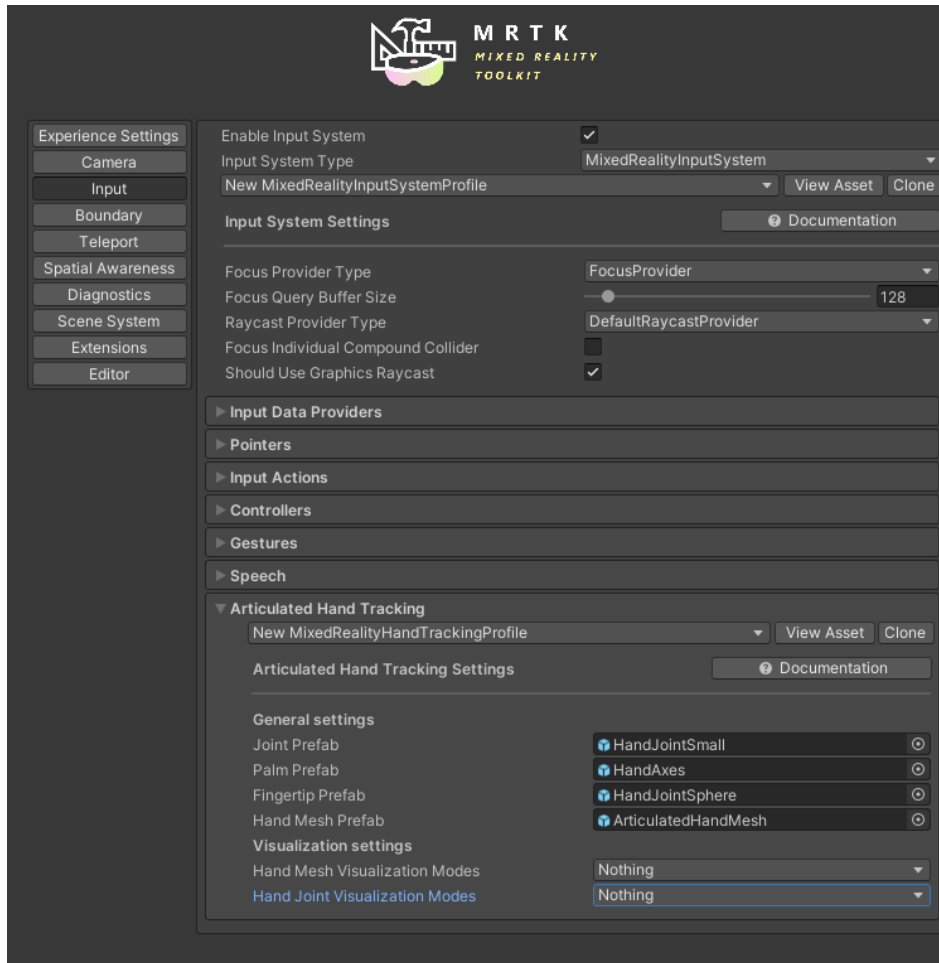


Figure 3. 40 Mixed Reality Toolkit inspector, Input.

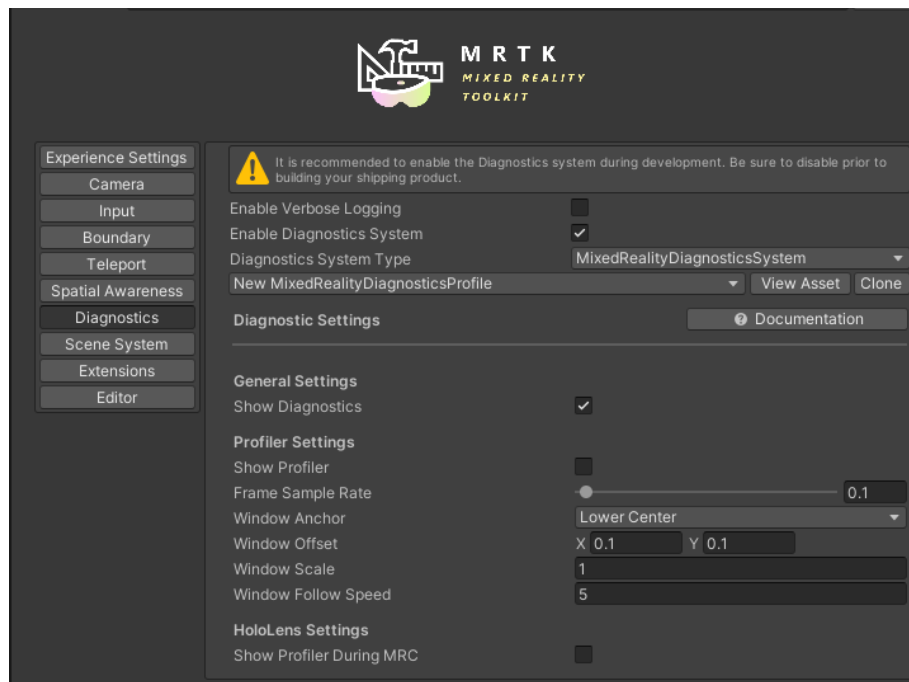


Figure 3. 41 Mixed Reality Toolkit inspector, Diagnostics.



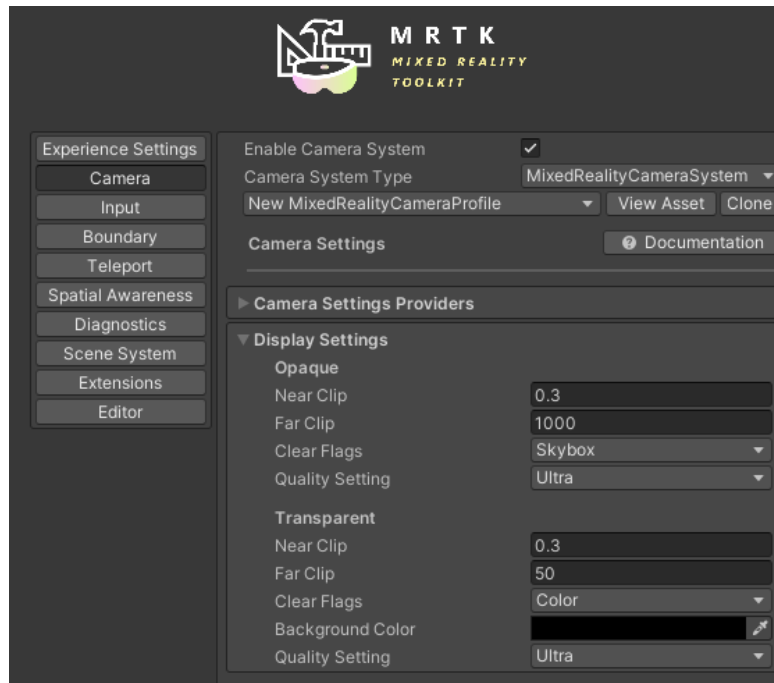


Figure 3. 42 Mixed Reality Toolkit inspector, Camera.

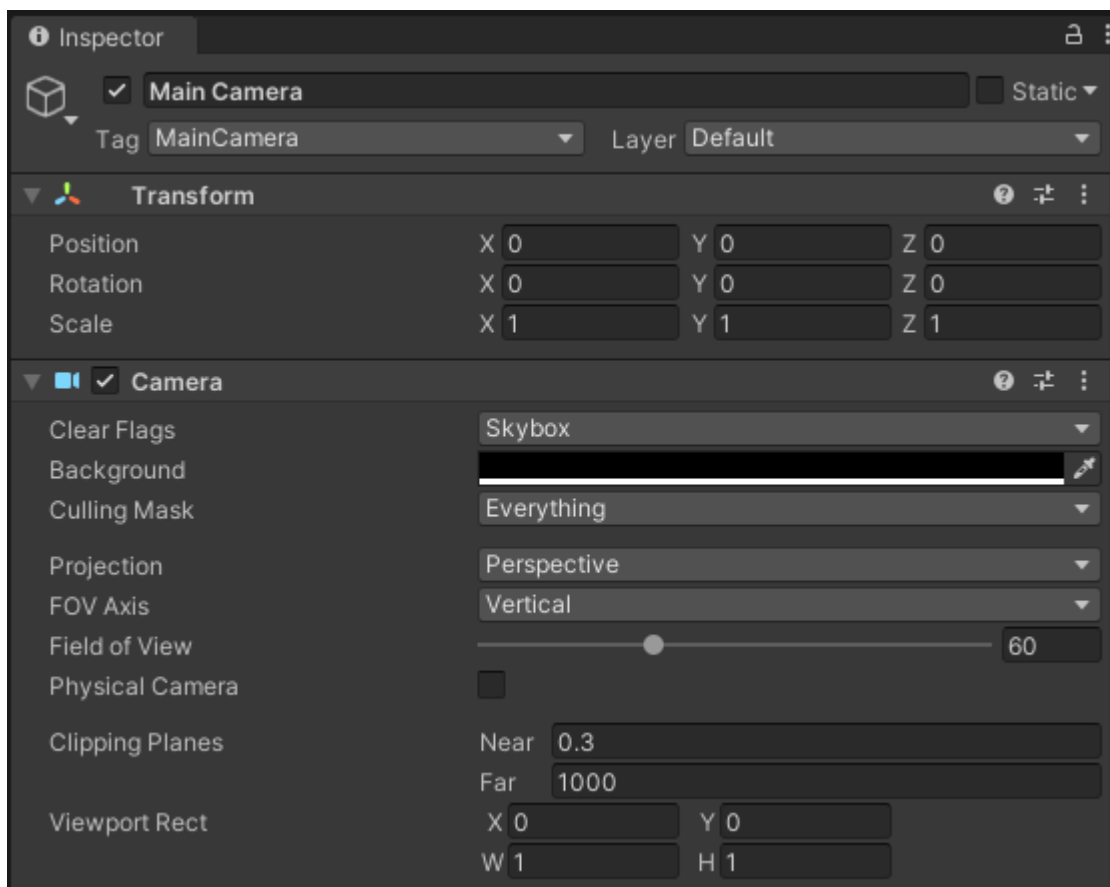


Figure 3. 43 Main Camera inspector.

Moreover, the 'Vuforia Behaviour' component is added, and the Vuforia Engine Configuration is opened. In this panel, some settings must be tuned. As first, the license key, generated in the Vuforia developer portal as described in the previous section, must be copied in the 'App License Key' field (Figure 3. 44). Then the 'Max Simultaneous Tracked Images' must be set to 12, that is the total number of marker cube faces in the developed application (6 for each of the marker cube, M1 and M2), and the 'Max Simultaneous Tracked Objects' must be set to 2 (Figure 3. 44).

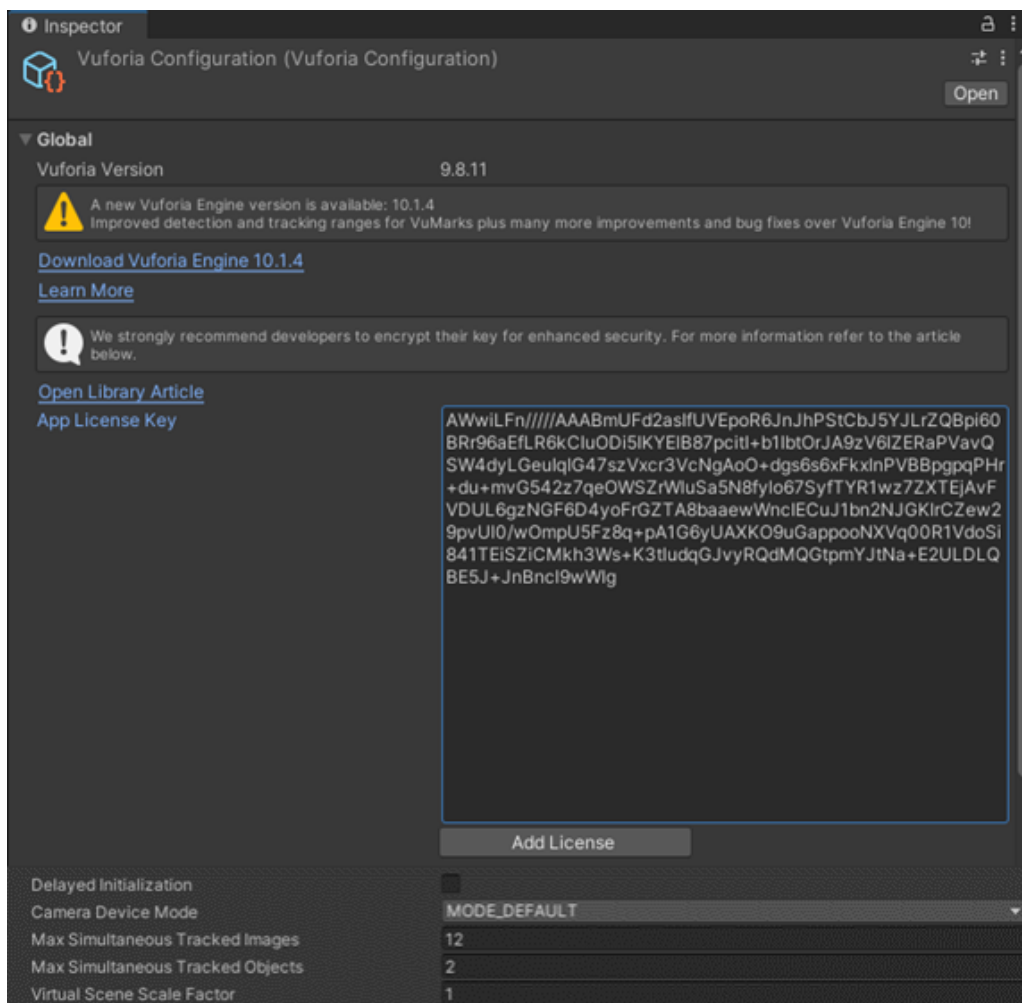


Figure 3. 44 Vuforia Engine configuration panel.

Finally, after connecting PC to the same Wi-Fi network, through Internet Protocol Version 4 (IPv4) of the Microsoft HoloLens V2 device, the HMD portal can be opened and following the path 'Views → Hologram Stability → Settings' the 'Override Application Re-Projection Method' option have been set to 'Depth Reprojection'.

### 3.5.3.3 Scene Creation

The following step is the scene creation.

As first passage, the directional light is converted to 'Point Light' in the 'Type' section of its inspector.

Then, targets (M1 and M2) must be inserted in the scene and virtual contents (osteotomy lines, drilled holes, Reference Frame, and 3D-arrows) must be introduced and configured in the correct place and level of the Hierarchy.

Moreover, when placing virtual contents also their alignment with respect to correspondent target must be ensured. However, since Unity is not the easiest software in which perform that procedure, the marker-hologram alignment has been already ensured in the Rhinoceros 6 software.

Furthermore, it must be pointed out that by assigning holograms as child of a target they will be automatically displayed whenever and wherever the parent target is tracked by the HMD. For this reason, using multi-targets, such as the cuboid markers, a stable visualization of the hologram is guaranteed since the HMD is capable of tracking multiple faces of the target and to position and orient holograms based on the type of face that it is tracking at each frame.

The first objects to be introduced in the scene are the targets. To introduce them the 'Game Object → Vuforia Engine → Multi Target' path must be followed twice (Figure 3. 45), and the created multi-target object must be created within the 'Mixed Reality Playspace' object of the Hierarchy.

The created multi-targets can be named as 'M1' and 'M2' respectively. Then, opening the inspector of both M1 and M2, under the 'Multi Target Behaviour (Script)' field, the database from which the multi-targets will be taken can be specified and the selected target can be imposed within that database. We can specify the imported marker database and impose first to the game object M1 the correspondent M1 target of imported database (Figure 3. 46) and then to the game object M2 the correspondent M2 of imported database (Figure 3. 47). Moreover, in the 'Default Trackable Event Handler (Script)' component, the 'Tracked' option has been selected to consider the target as visible only if its status is the tracked status (Figure 3. 46 and Figure 3. 47).

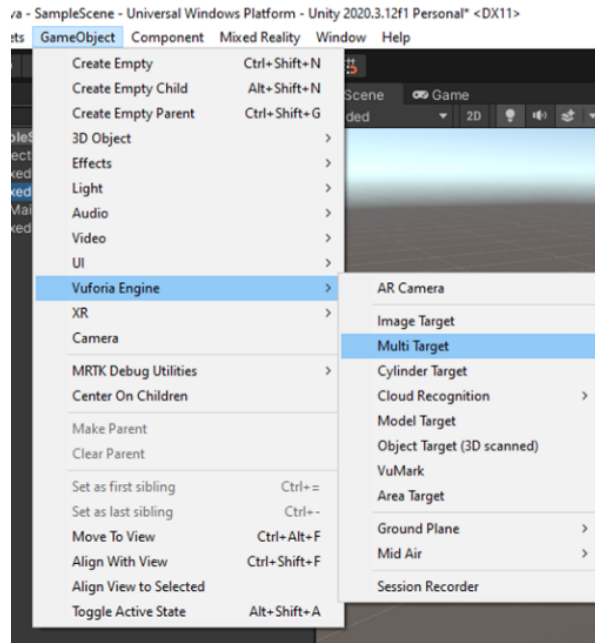


Figure 3. 45 Multi-target creation path.

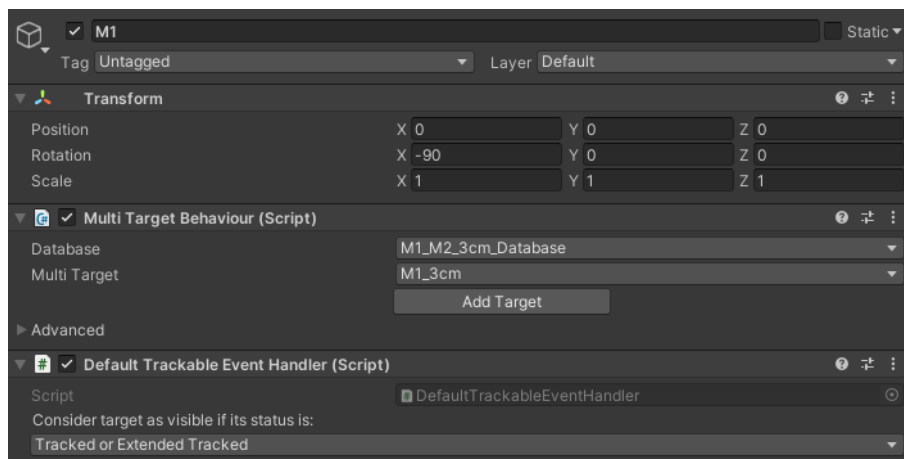


Figure 3. 46 Inspector of the multi-target M1.

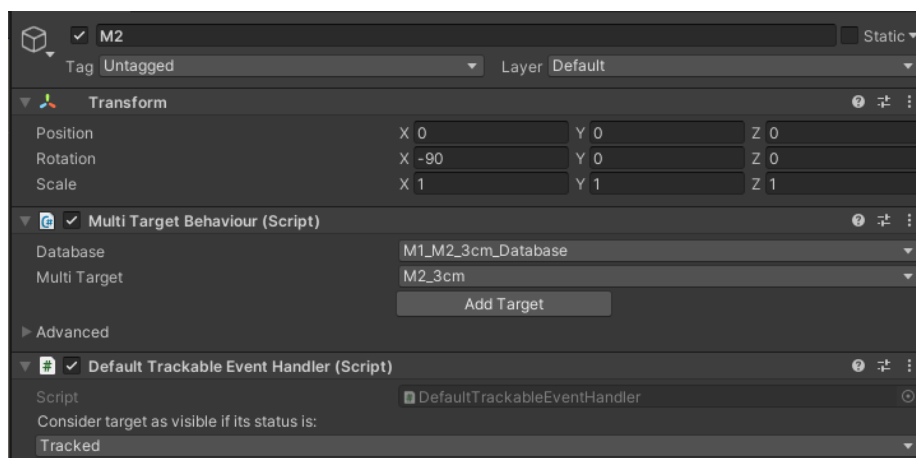


Figure 3. 47 Inspector of the multi-target M2.

Then the \*.OBJ file of virtual contents (osteotomy lines, drilled holes, 3D-arrows and the 3 axes of the Reference Frame) have been dragged and dropped in the 'Assets'.

Object model, rig, animation, and material can be modified from the inspector of imported files. The following procedure will be performed for any of the imported \*.OBJ files (osteotomy lines, drilled holes, any of the arrows of the set of the 3D-arrows and any of the axes of the Reference Frame).

After these modifications have been applied, any of the 3D-arrows have been assigned as a child of an empty object named as '3DArrows'. Figure 3. 48 shows the outlook of this object. Moreover, any of the 3 axes of the Reference Frame have been assigned as child of an empty object named as 'OrientationAxes'. Figure 3. 49 shows the outlook of this object.

Modifications of the uploaded \*-OBJ files expects multiple fields to be tuned.

'Model' field has been modified by setting the 'Scale Factor' to 0.001 (since Unity works with meter units while the models were developed in millimeters), by unchecking the 'Convert Units' option, by enabling the 'Bake Axis Conversion' option (since Unity uses a left reference frame and this option converts it to the system of the object) and by setting the 'Normal Mode' to 'Unweighted (Legacy)'.

'Rig' field has been modified by setting the 'Avatar Definition' to 'Create from This Model', to create an avatar for the object display in the device.

At this point the material must be created to be then assigned to the specific object (Figure 3. 50). In all the cases, a material with null smoothness has been created, dark blue color has been assigned in 'Albedo' field for the osteotomy lines (Figure 3. 51), dark violet color has been assigned in 'Albedo' field of the drilled holes (Figure 3. 52), orange color has been assigned in 'Albedo' field for the 3D arrows (Figure 3. 53) and dark blue, green, and red color have been assigned in 'Albedo' field of the 3 axes of the Reference Frame (mediolateral, up-down, antero-posterior axes in that order) as shown in Figure 3. 54, Figure 3. 55, and Figure 3. 56.

Finally, 'Material' field of the object has been modified setting 'Default Mat' option to specific material of the object configured. At each step, modifications are applied with 'Apply' button. Figure 3. 57, Figure 3. 58 and Figure 3. 59 show all these settings.

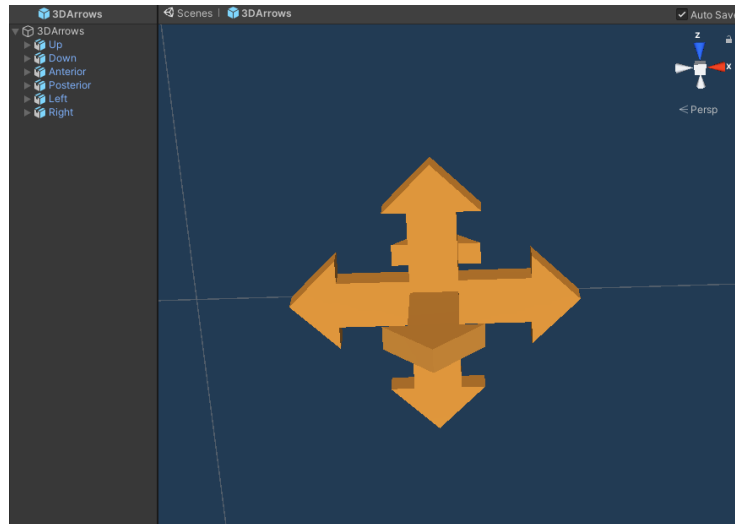


Figure 3. 48 Set of 3D-Arrows object.

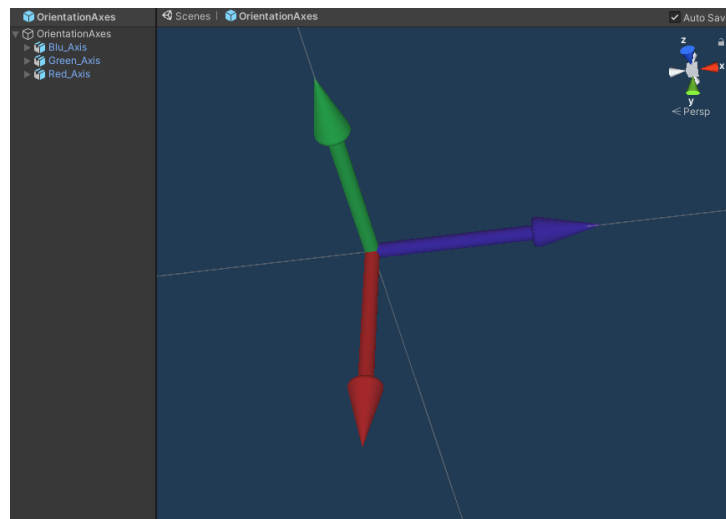


Figure 3. 49 Reference Frame object.

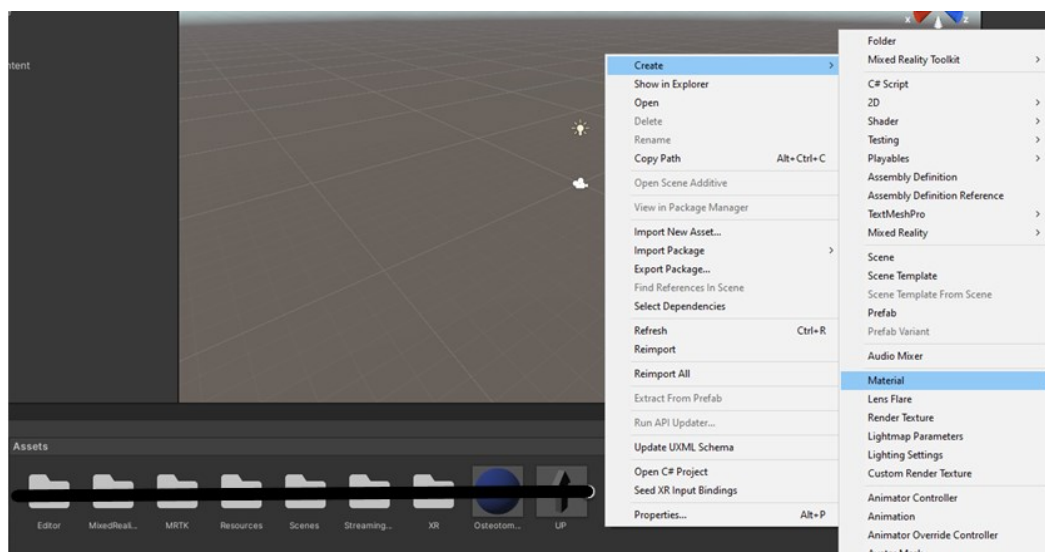


Figure 3. 50 Procedure for the creation of a new material.

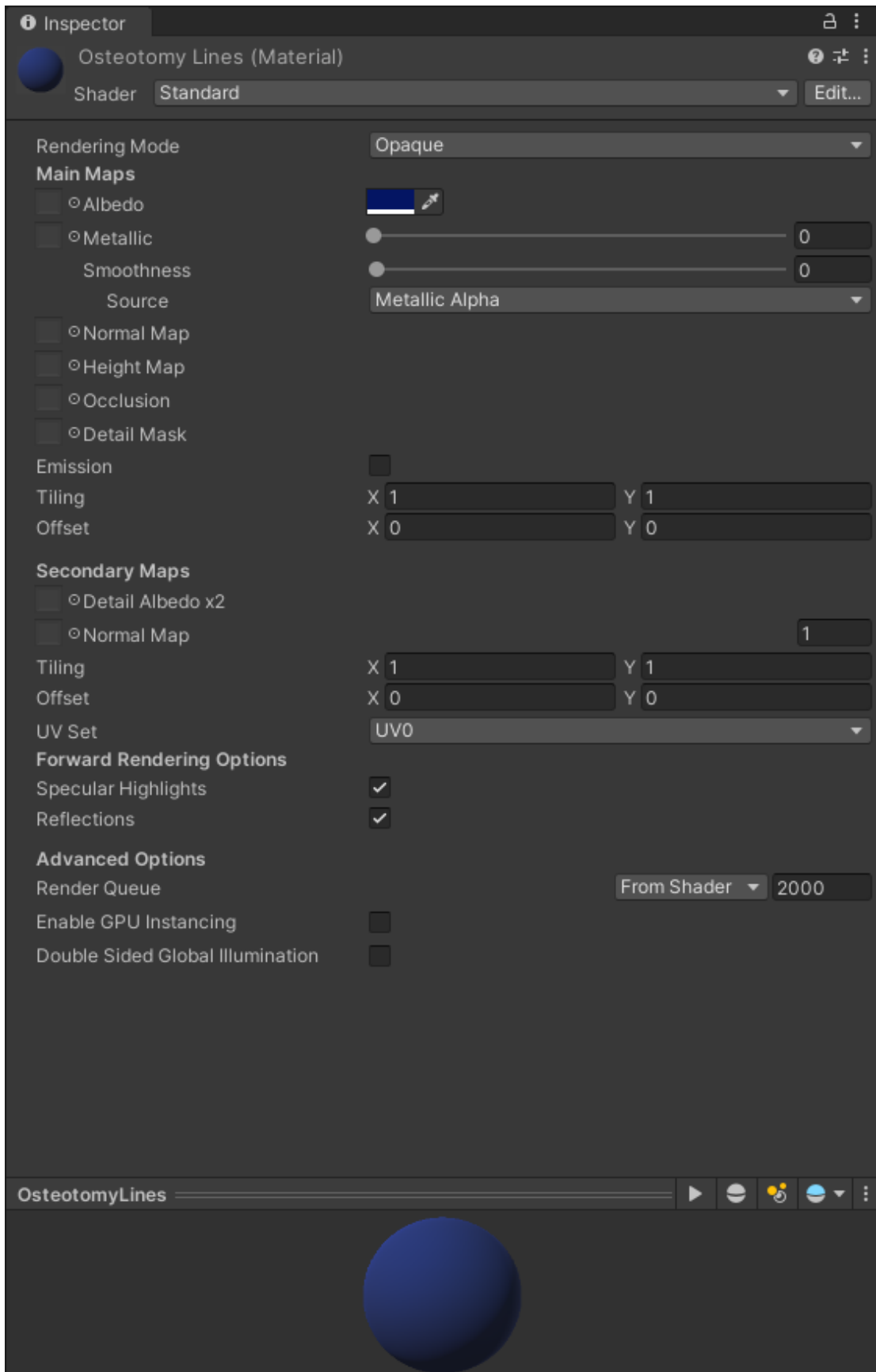


Figure 3. 51 Material to be assigned to osteotomy lines.

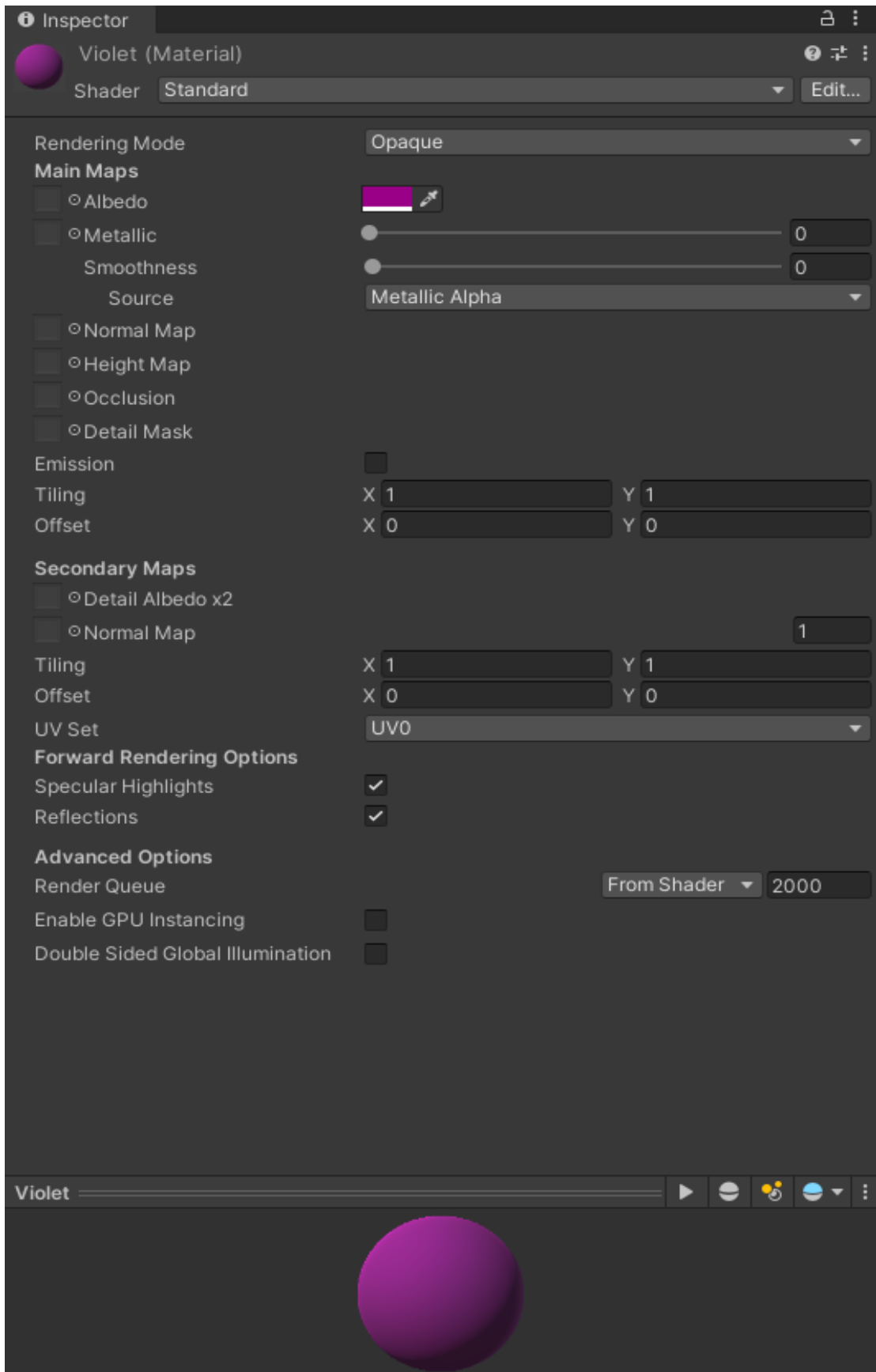


Figure 3. 52 Material to be assigned to drilled holes.



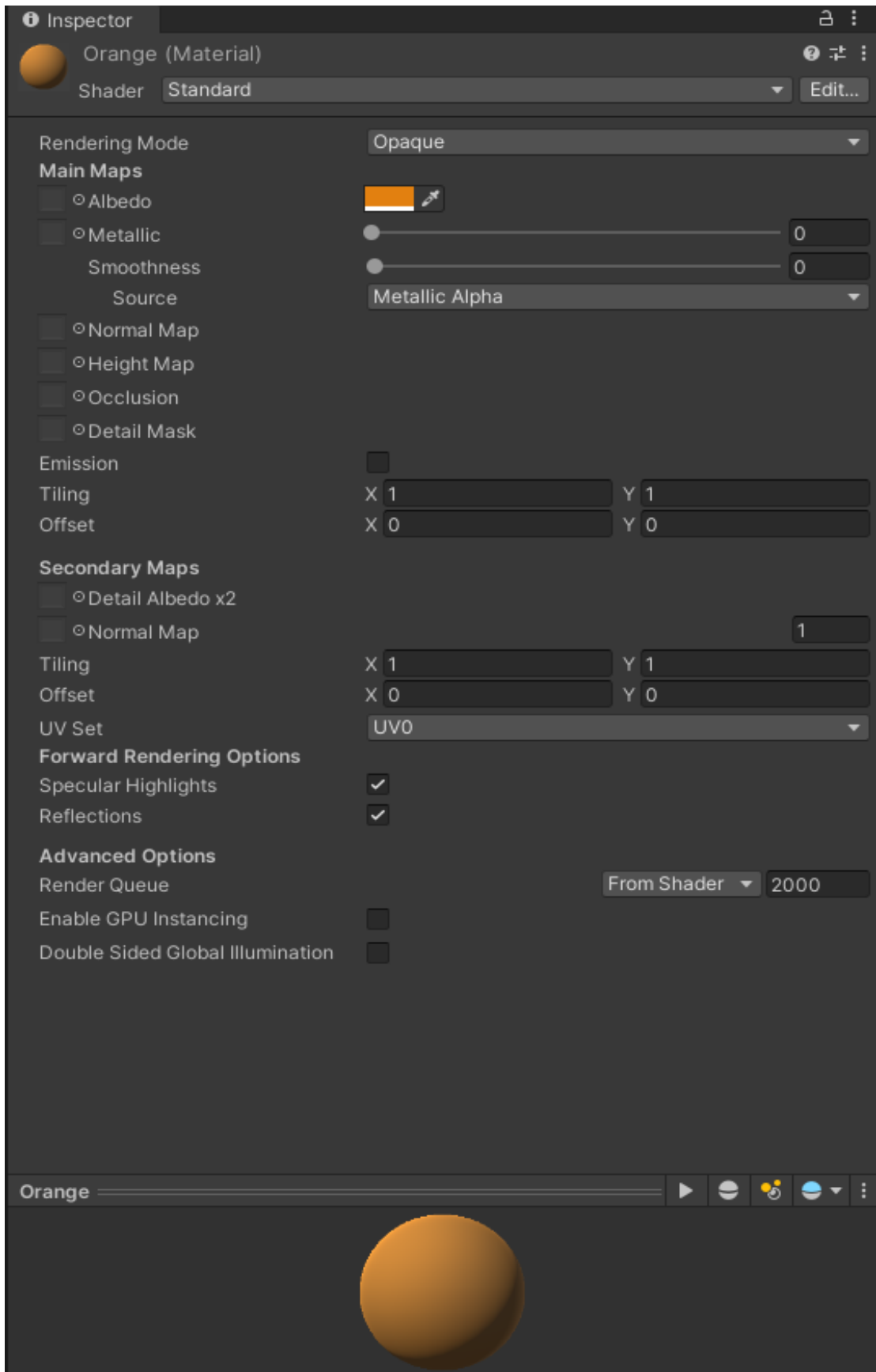


Figure 3. 53 Material to be assigned to 3D-arrows.

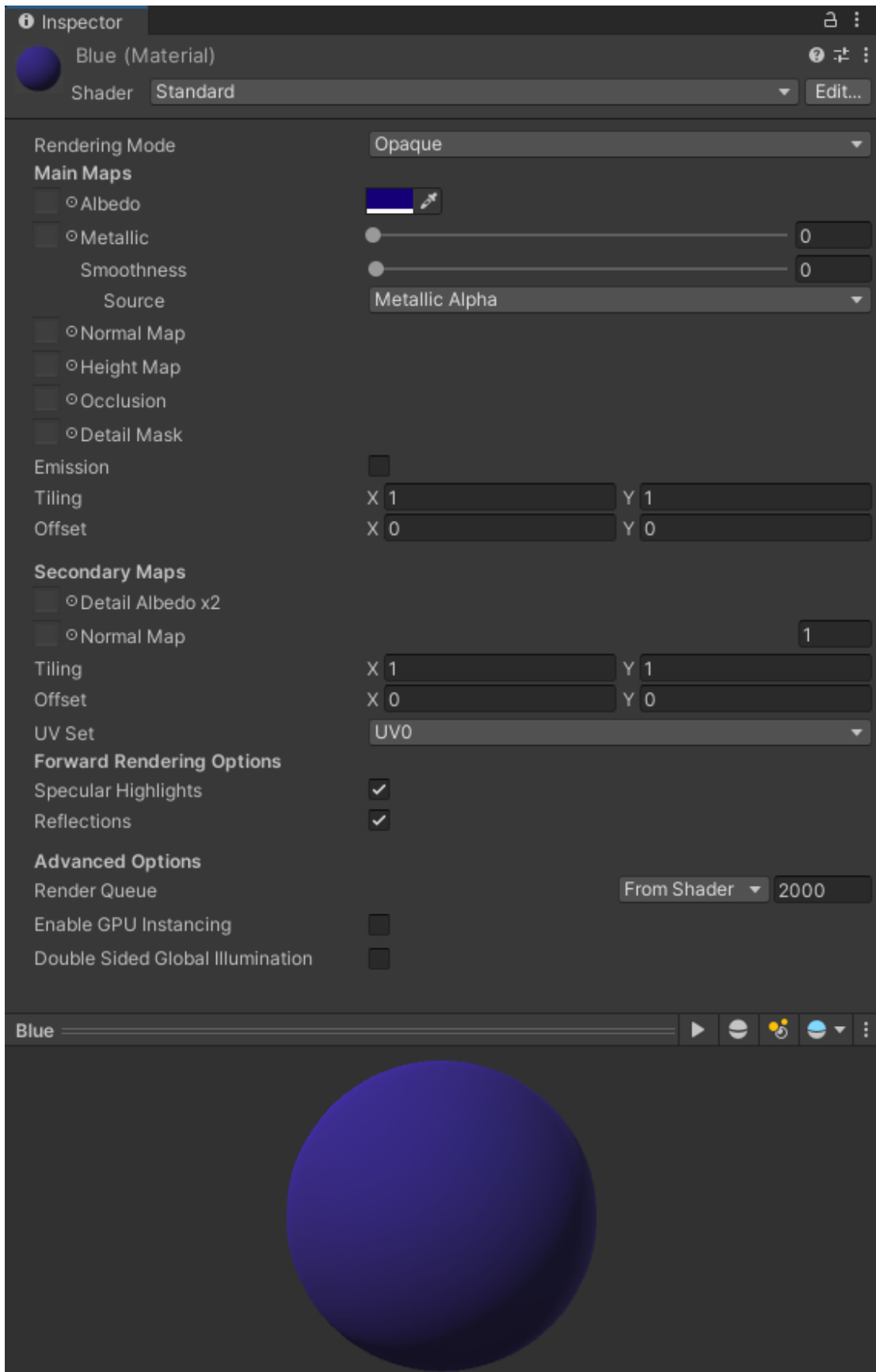


Figure 3. 54 Material to be assigned to mediolateral axis of the Reference Frame.



Figure 3. 55 Material to be assigned to up-down axis of the Reference Frame.

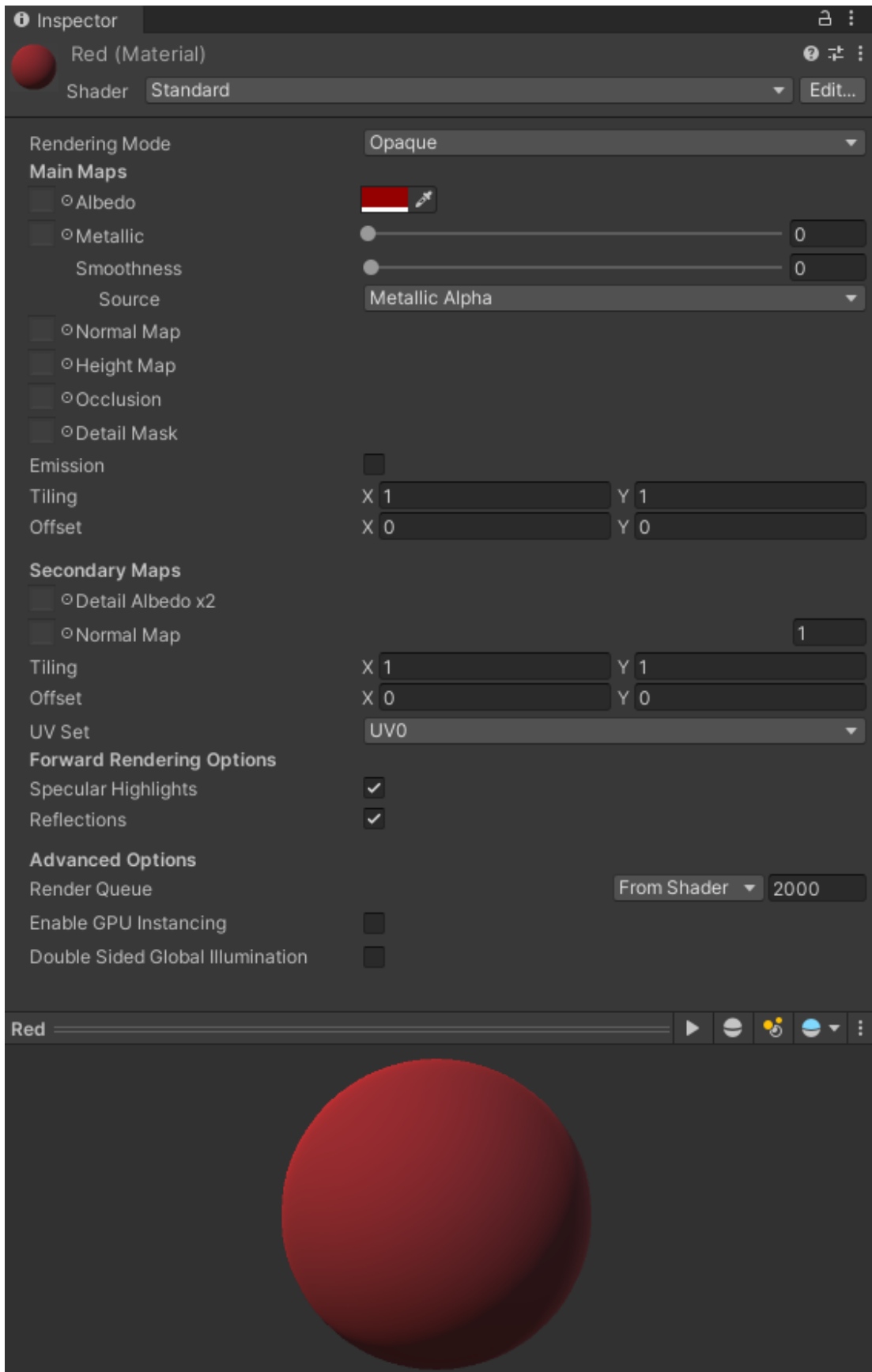


Figure 3. 56 Material to be assigned to anteroposterior axis of the Reference Frame.

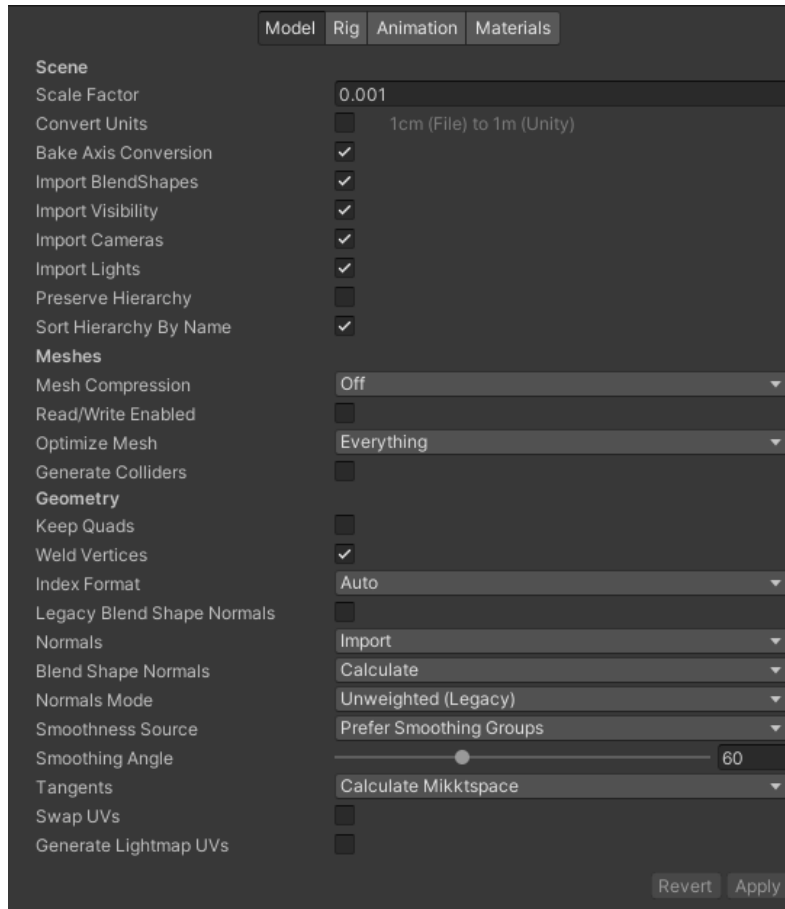


Figure 3. 57 Model settings of the imported \*.OBJ file.

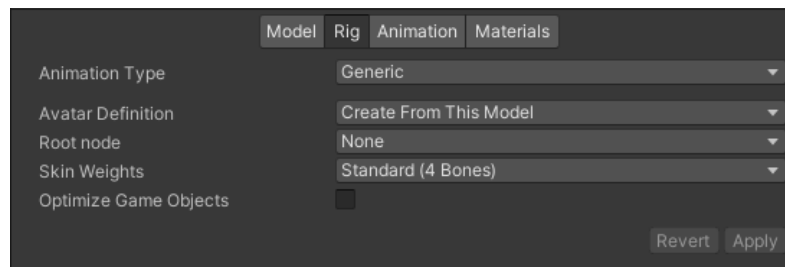


Figure 3. 58 Rig settings of the imported \*.OBJ file.

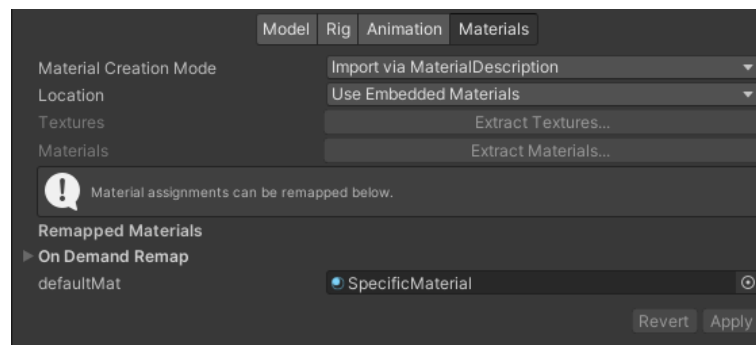


Figure 3. 59 Materials settings of the imported \*.OBJ file.

The cube hologram is a cube exactly dimensioned as M2 that must be oriented according to the pre-operative plan and be placed at the target position to be reached at the end of the repositioning of the osteotomized fragment. The cube is generated as a game object by following the path 'Game Object → 3D Object → Cube' (Figure 3. 60). The cube is assigned as a child of M2, and then its inspector is managed to exactly dimension the cube as the multi-target M2 (3 x 3 x 3 cm). Figure 3. 61 shows the inspector 'Transform' component of the cube.

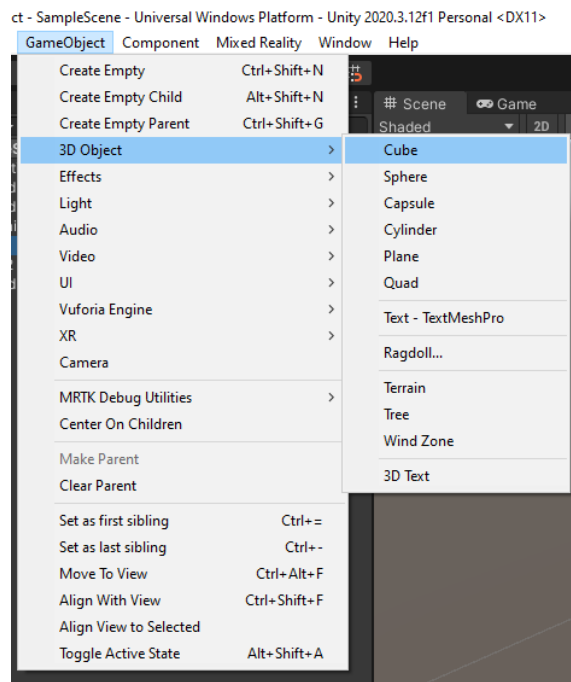


Figure 3. 60 Procedure for the cube creation.

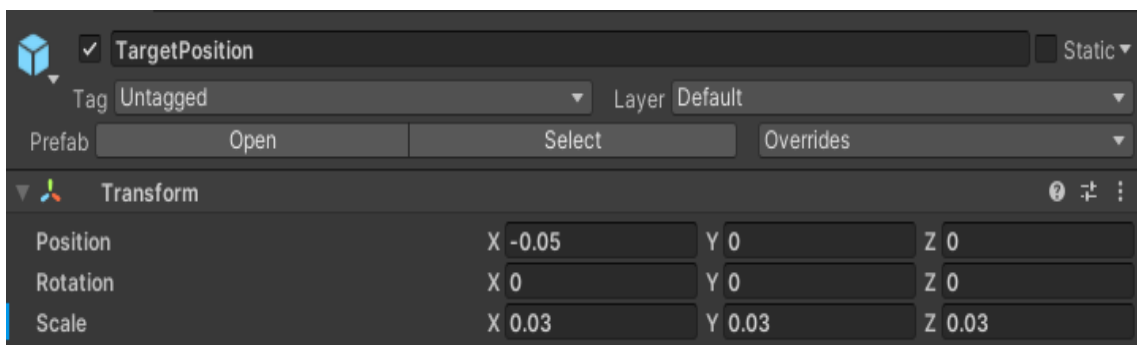


Figure 3. 61 Transform component of the cube hologram.

The cube hologram is the object whose color will be tuned to implement the alarm system that will be, together with 3D-arrows, Reference Frame and deltas

visualization, the feedback received by the user. Hence, cube hologram material is changing through the script that will be later deeply described, in detail, the cube hologram material will change based on deltas value (differences in position of the actual marker M2 position and the target position of the cube hologram) passing from red, wrong position, to green, correct position. In this section are described the 2 materials that can be assigned to the cube hologram. All these materials are created as null-smoothness materials as shown in Figure 3. 62 and Figure 3. 63.

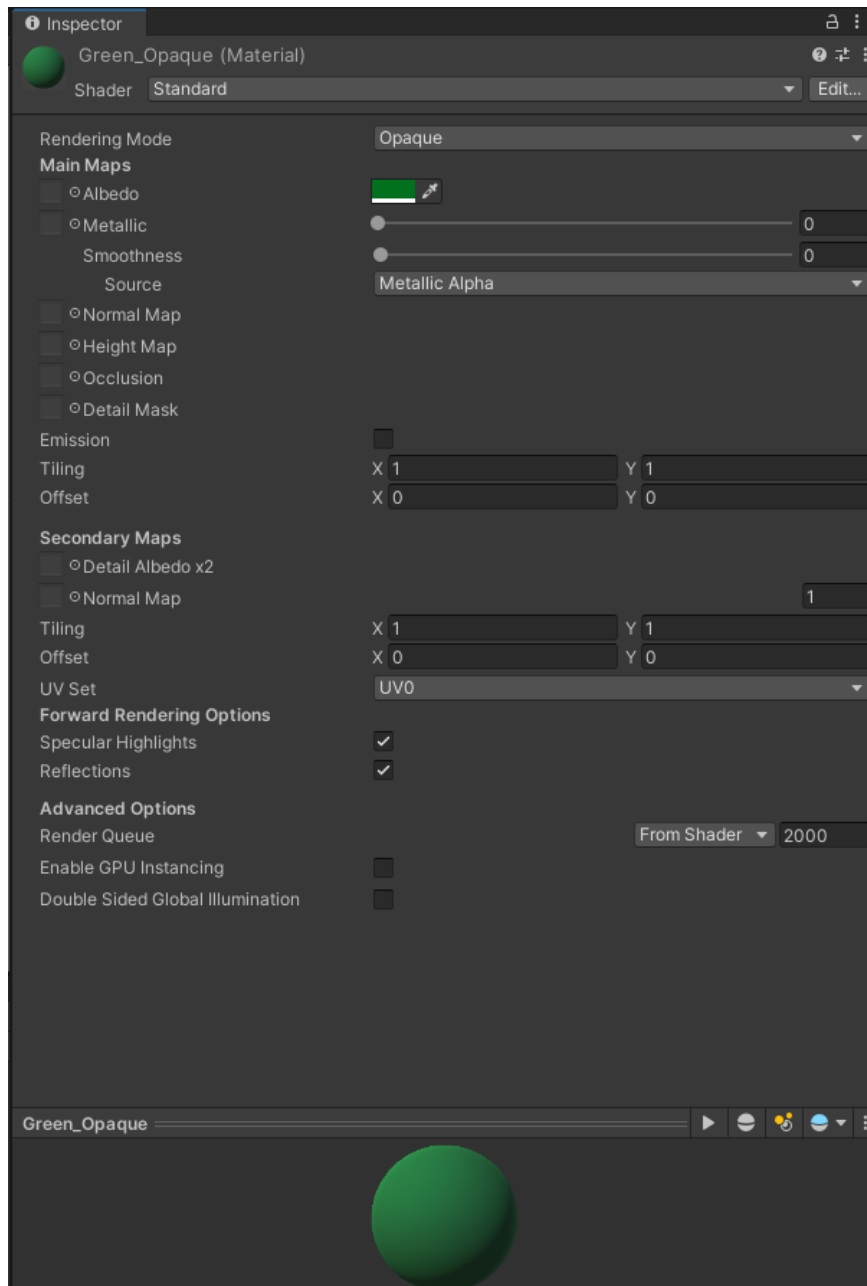


Figure 3. 62 Green material to be assigned to the cube hologram.

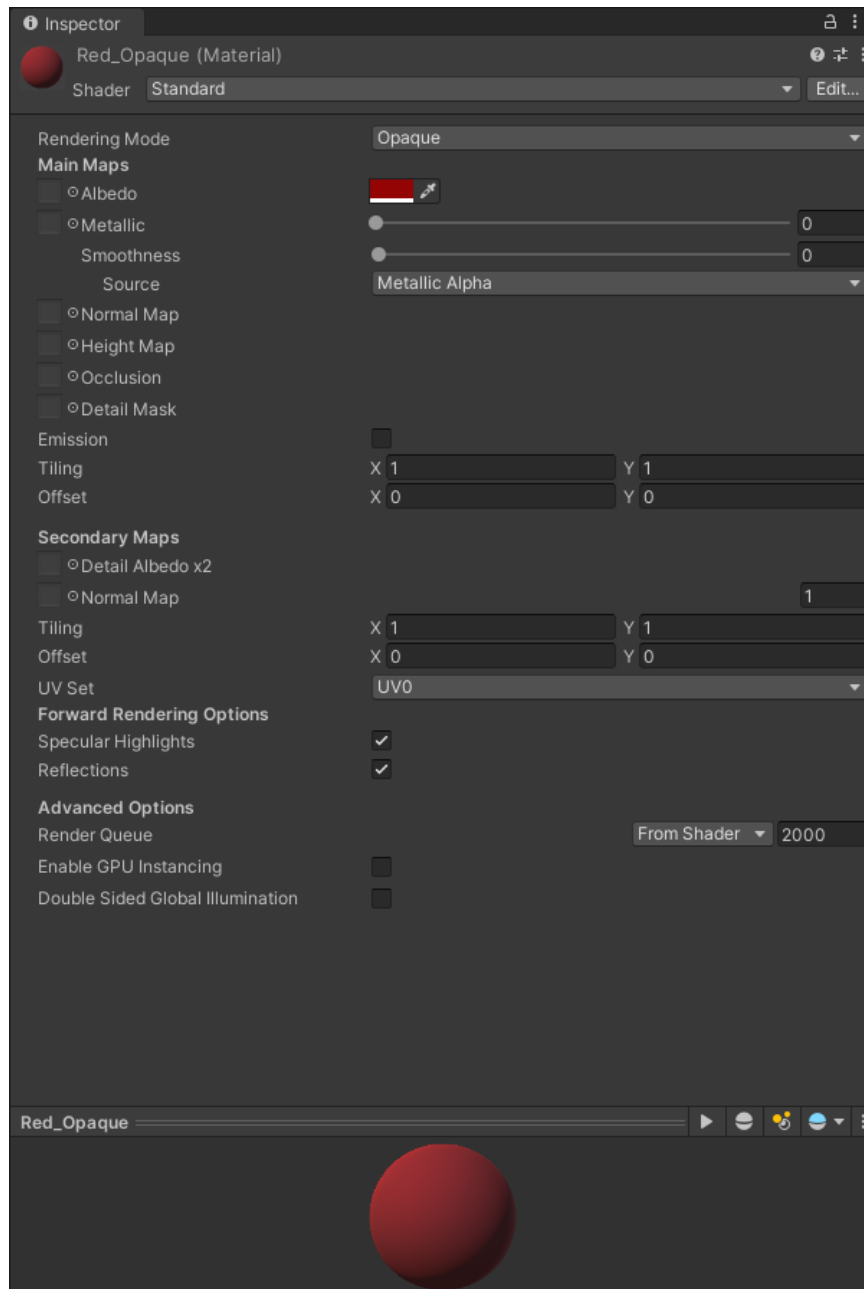


Figure 3. 63 Red material to be assigned to cube hologram.

At the end, 2 elements must be added. The first is a dialog panel that will permit to user to have the visual access to the deltas value. The second is a menu will permit first the correct positioning of the cube hologram, by activating the specific script that will be described in the following section, the activation and the deactivation of specific holograms allowing to distinguish an Osteotomy Mode, in which only the osteotomy lines and the drilled holes are displayed, and a Repositioning Mode, in which instead



only the cube hologram is displayed together with the 3D-arrows, the Reference Frame and the dialog panel on which deltas values are visualized and in which the script dedicated to the management of these elements is activated.

To create the dialog window 2 quads have been added. Figure 3. 64 and Figure 3. 65 show the 'Transform' component of the bigger and smaller quad respectively. The smaller panel is set as the child of the bigger one and then 3 TMP objects has been added as child of it. A dark blue null-smoothness material has been assigned to smaller panel (Figure 3. 66) and white null-smoothness material has been assigned to the bigger one (Figure 3. 67) to create a sort of white outer frame. Figure 3. 68 shows the path to create a TMP objects. Figure 3. 69, Figure 3. 70, and Figure 3. 71 show 'Transform' and 'Text' component of the 3 TMP objects. Any of these 3 elements then hold a correspondent child TMP object. Figure 3. 72, Figure 3. 73 and Figure 3. 74 show the 'Transform' component of these child objects. Figure 3. 75 shows the 'Text' component that is equal in all of them. Finally, the title has been added as an ulterior TMP object whose 'Text' and 'Transform' component are shown in Figure 3. 76. Figure 3. 77 show the final outlook of the panel.

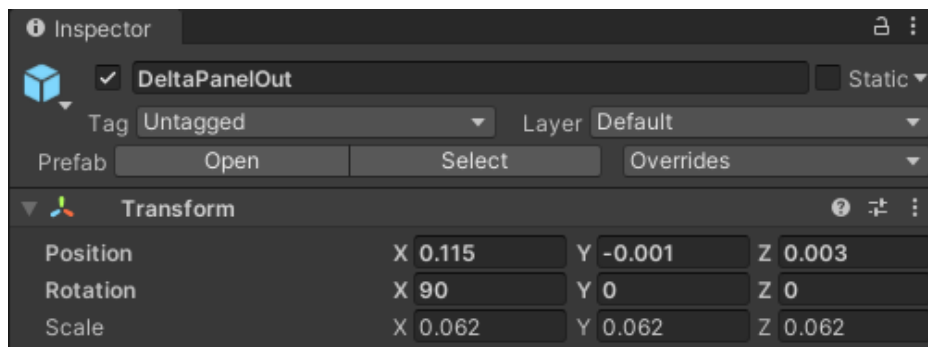


Figure 3. 64 Transform component of the bigger quad of the delta dialog panel.

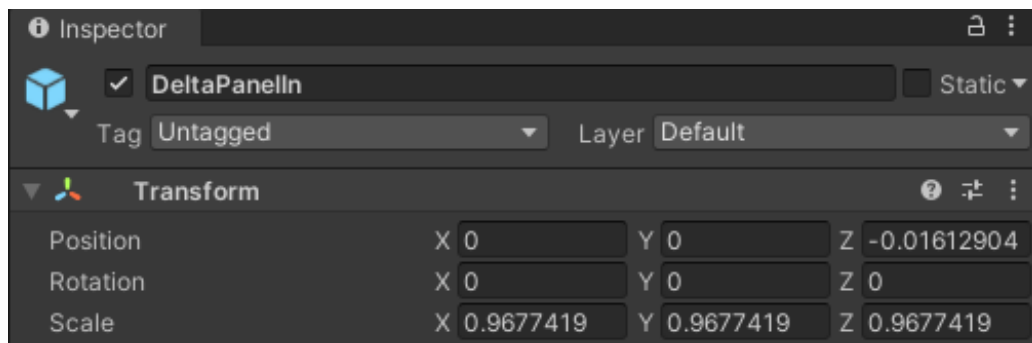


Figure 3. 65 Transform component of the smaller quad of the delta dialog panel.

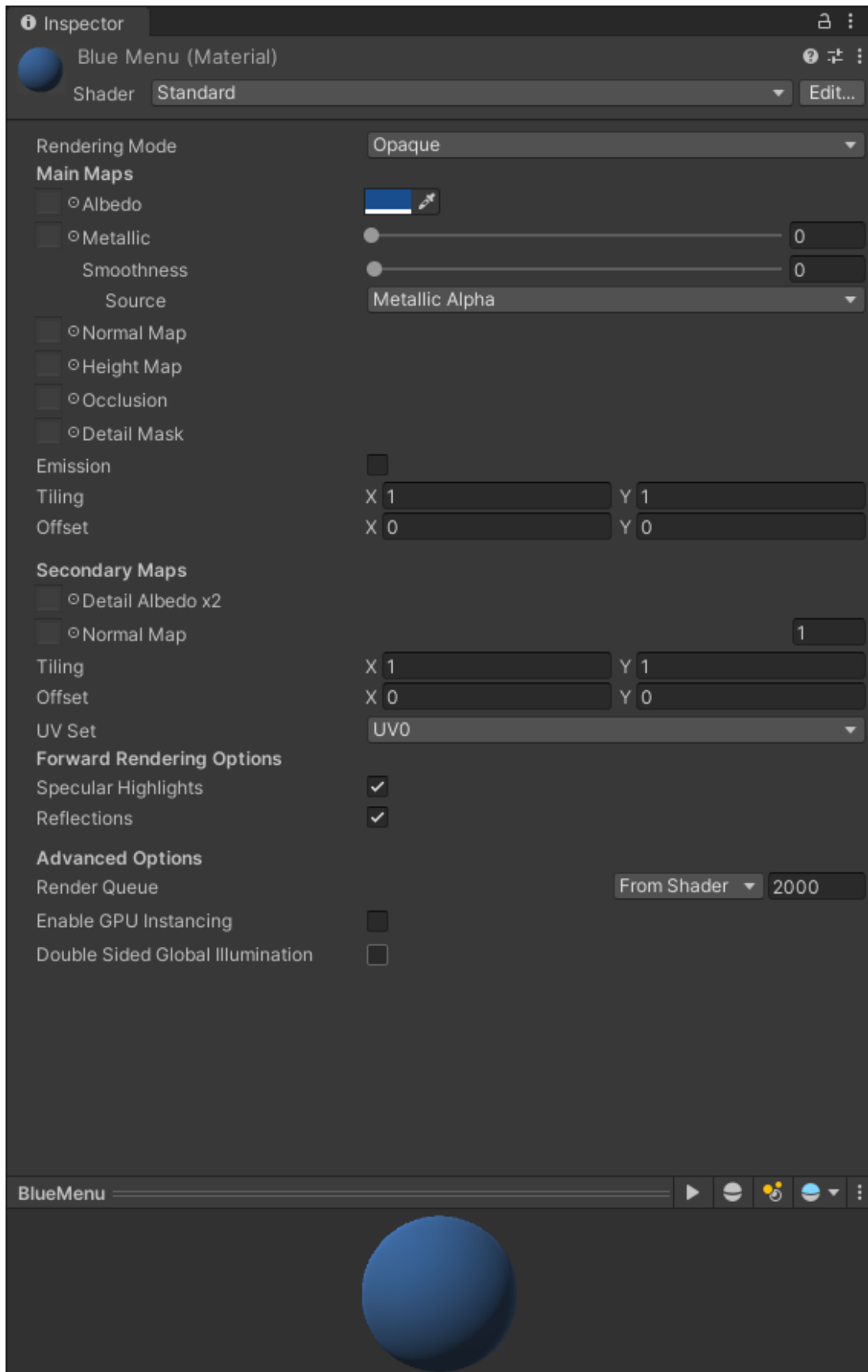


Figure 3. 66 Material to be assigned to the smaller quad of the delta dialog panel.

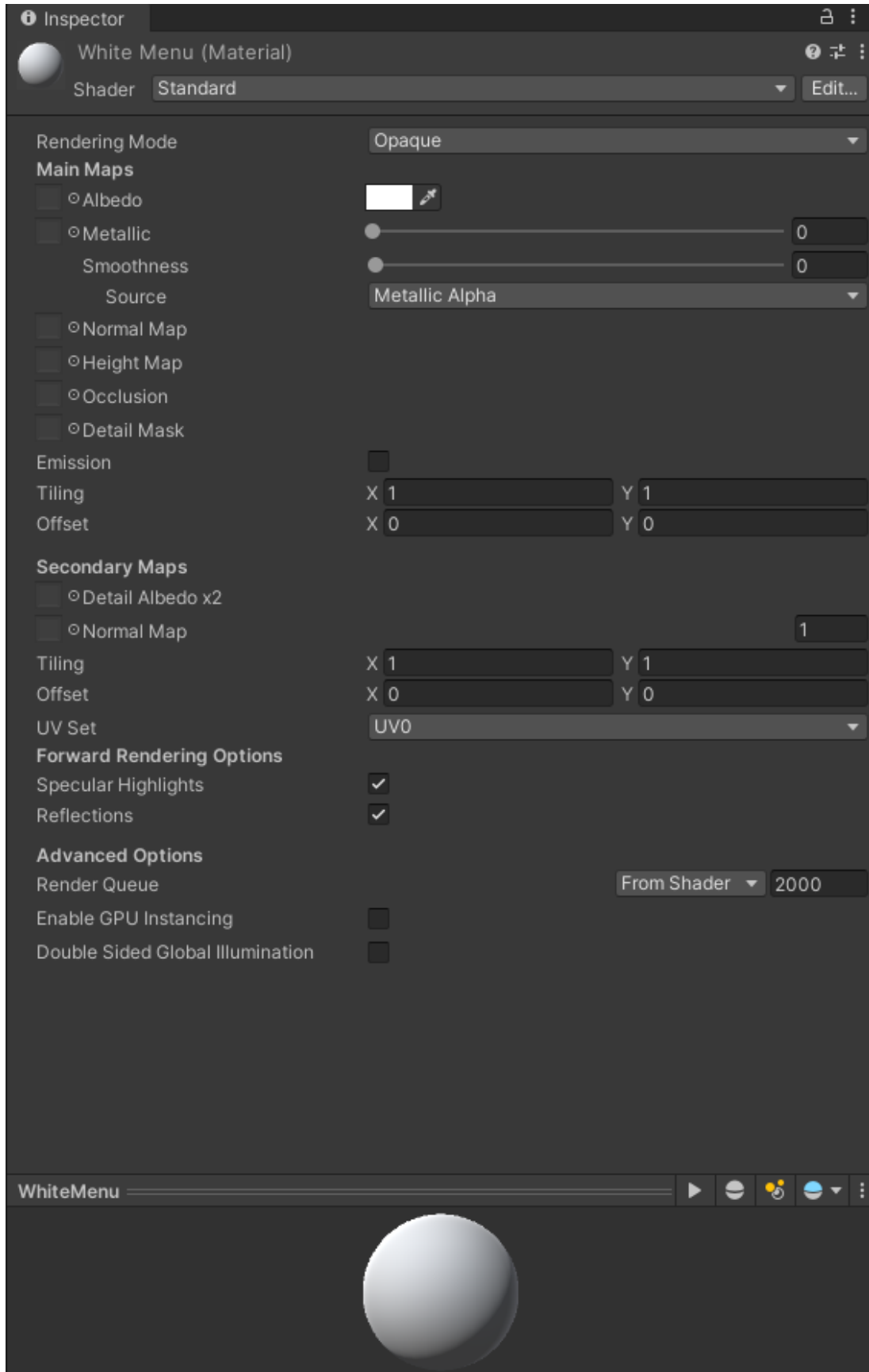


Figure 3. 67 Material to be assigned to the bigger quad of the delta dialog panel.

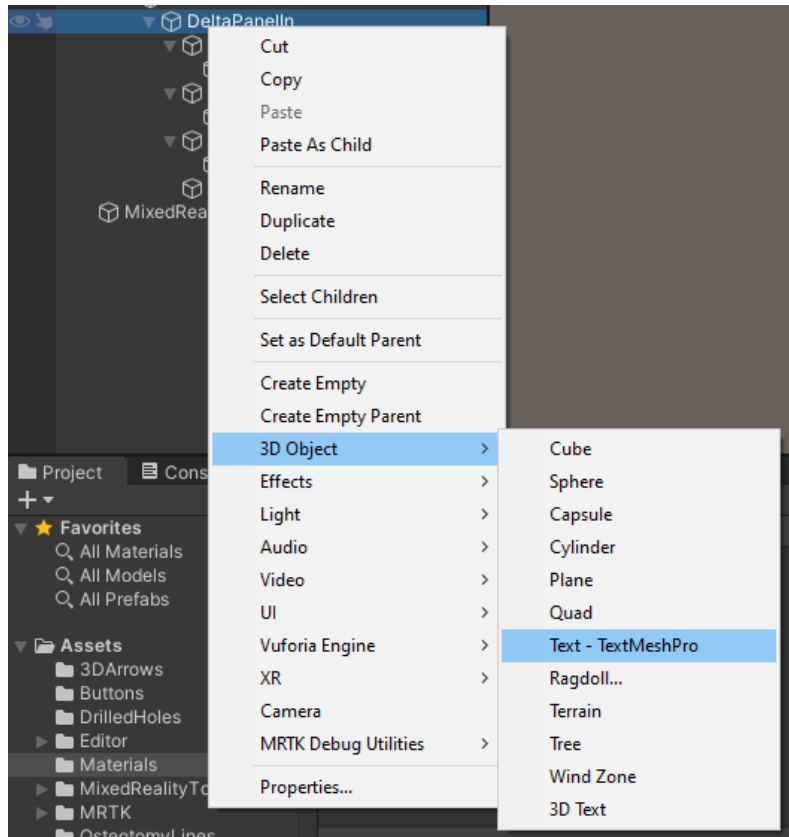


Figure 3. 68 Path for the creation of a Text Mesh Pro object.

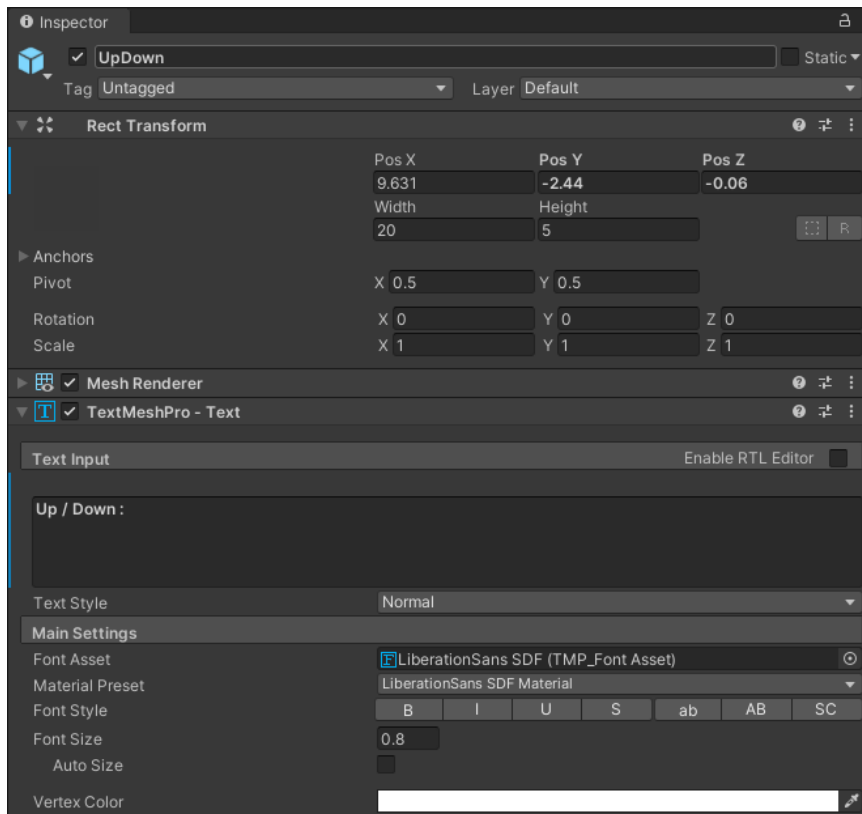


Figure 3. 69 Transform and Text component of the Up/Down label.

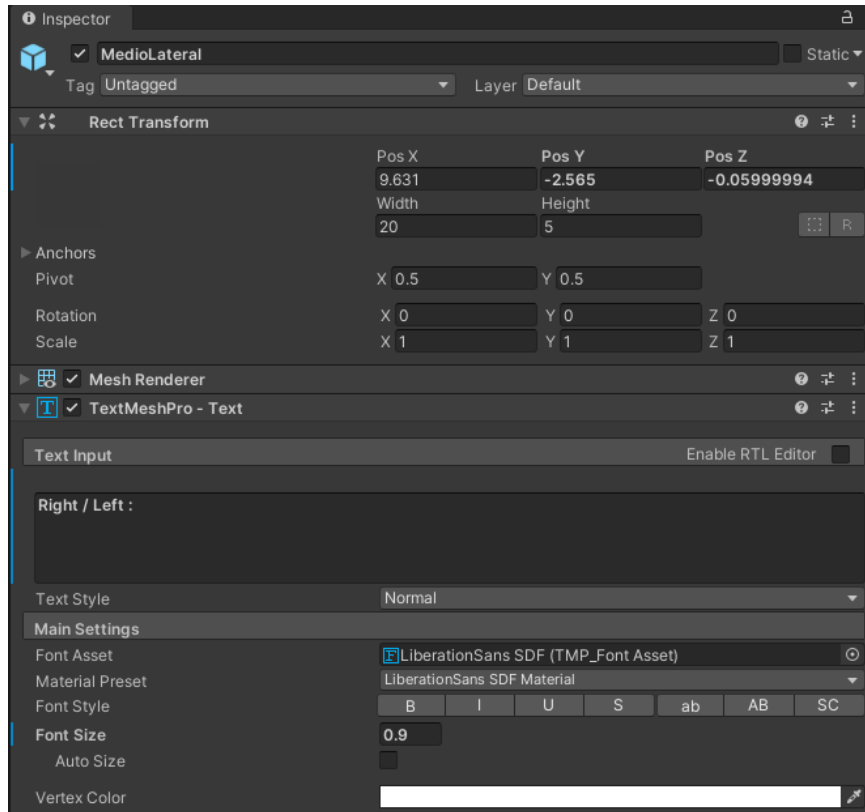


Figure 3. 70 Transform and Text component of the Right/Left label.

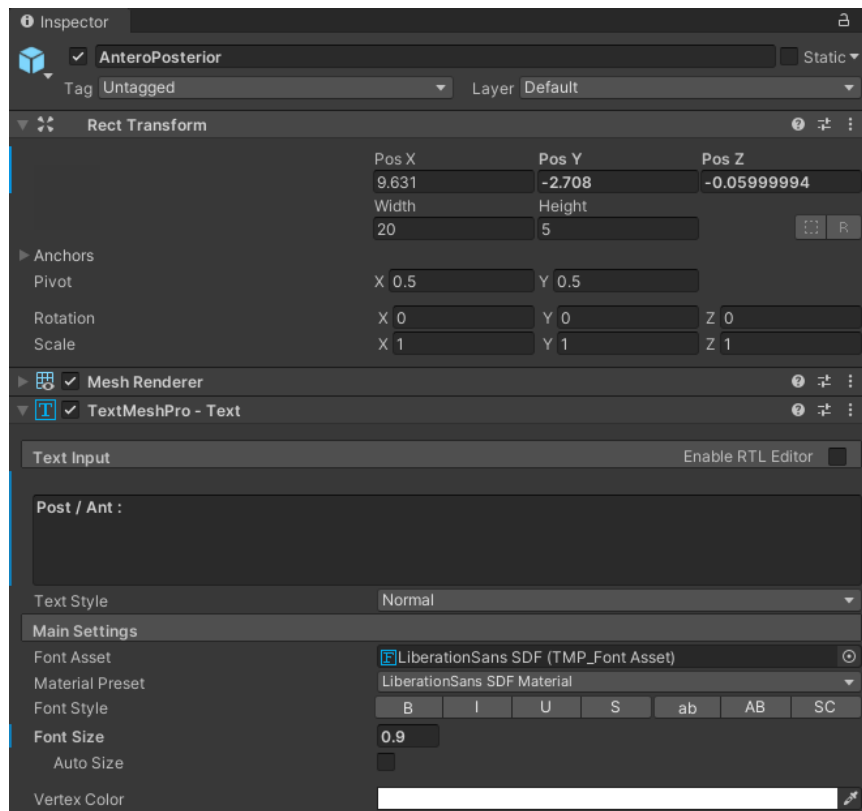


Figure 3. 71 Transform and Text component of the Posterior/Anterior label.

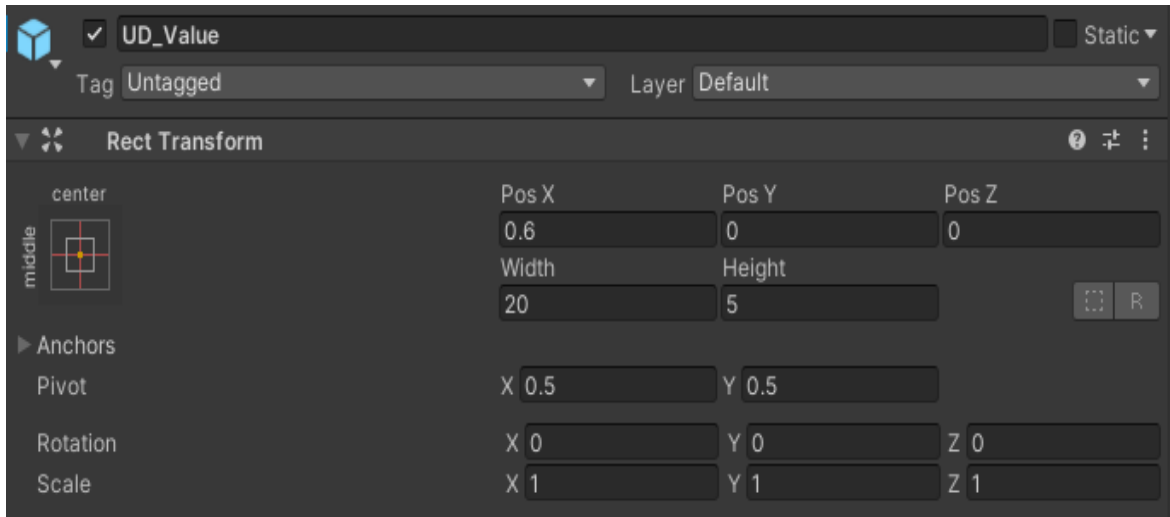


Figure 3. 72 Transform component of the Text Mesh pro elements for current y-delta display.

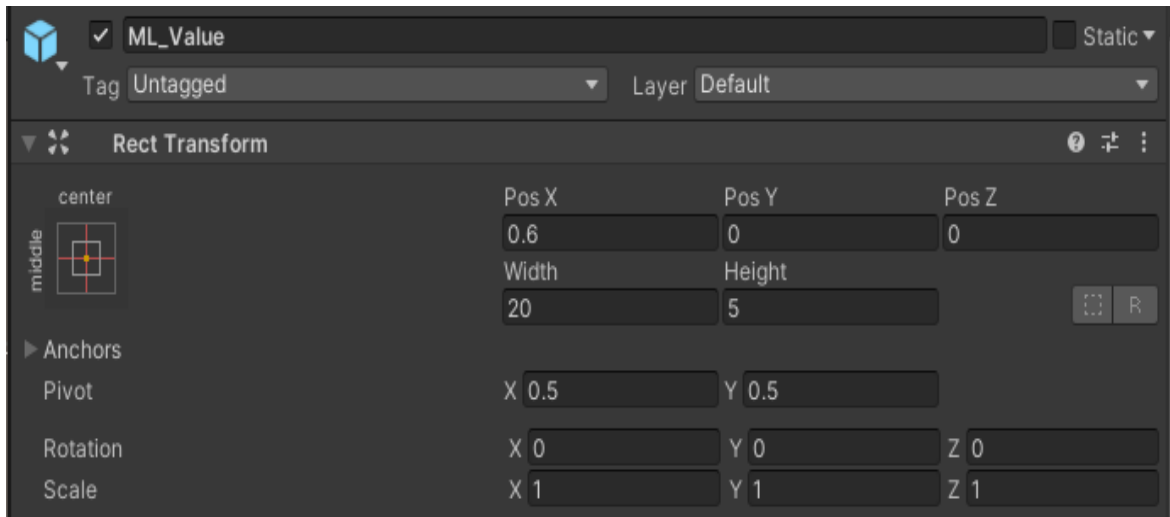


Figure 3. 73 Transform component of the Text Mesh pro elements for current x-delta display.

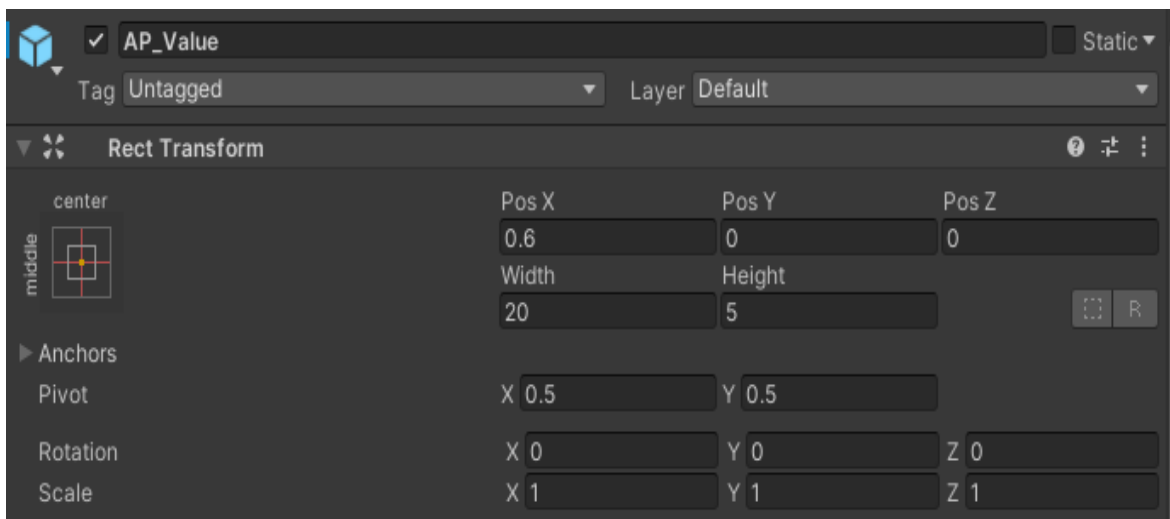


Figure 3. 74 Transform component of the Text Mesh pro elements for current z-delta display.

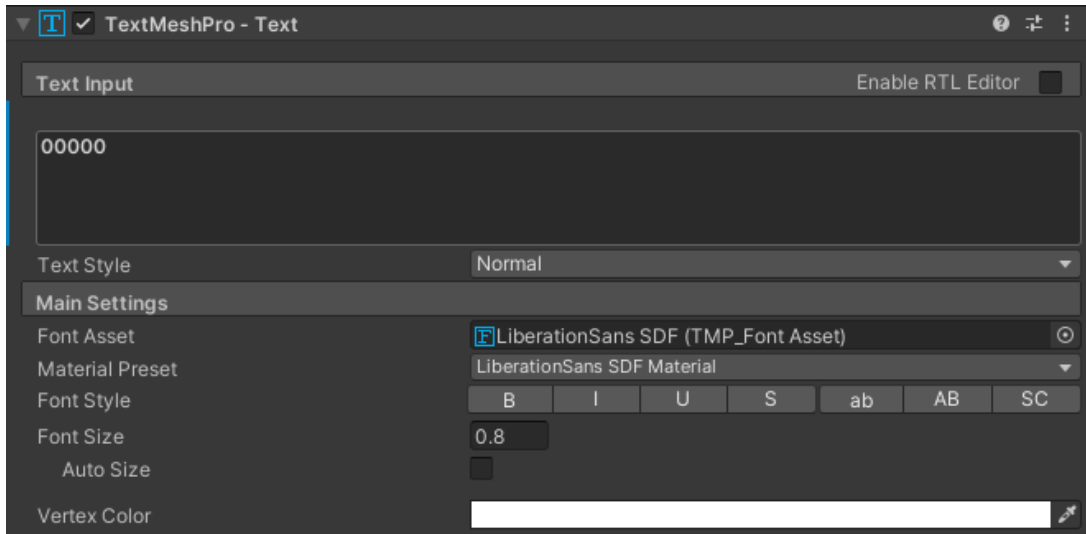


Figure 3. 75 Text component of the Text Mesh pro elements for the current delta display.

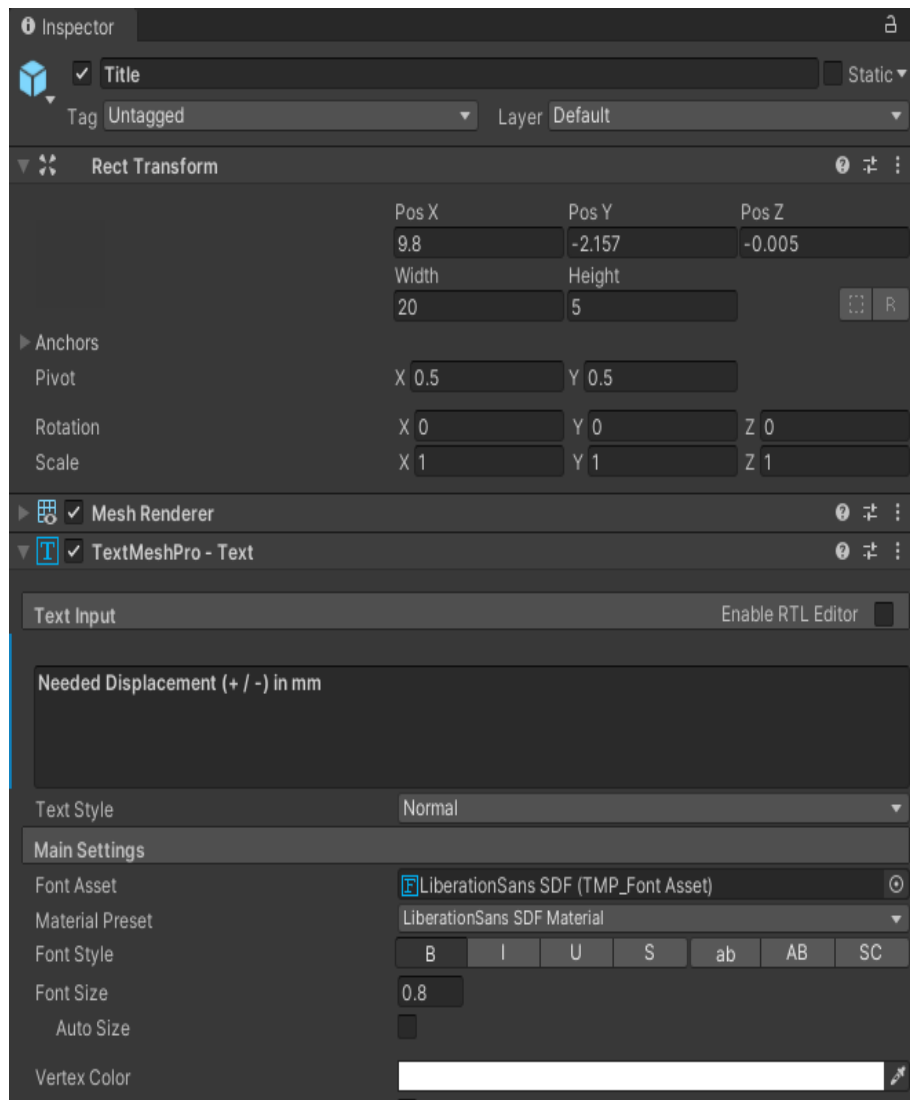


Figure 3. 76 Transform and Text component of the panel title.

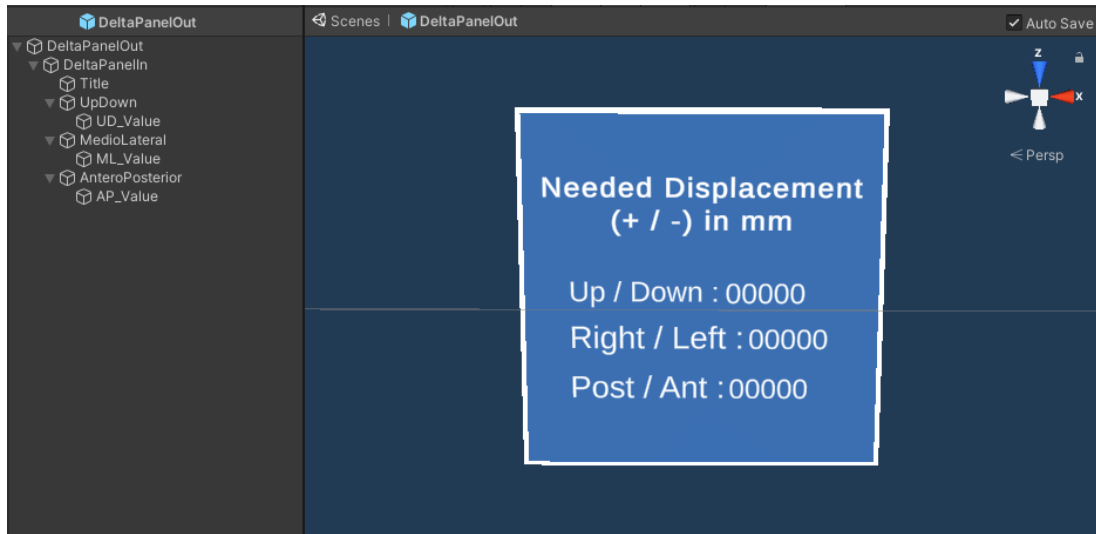


Figure 3. 77 Final outlook of the delta dialog panel.

Osteotomy lines, drilled holes, '3DArrows' object and delta panel are assigned as child of M2. 'Orientation Axes' object has been assigned as child respectively of M2 and the cube hologram.

Figure 3. 78 and Figure 3. 79 shows 'Transform' component of 'Orientation Axes' empty object in the scene as child of M2 and cube hologram respectively.

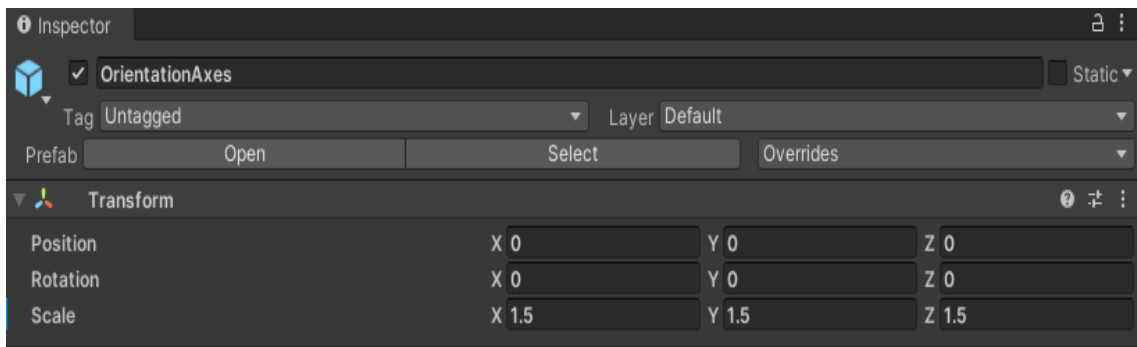


Figure 3. 78 'Transform' component of the 'OrientationAxes' object child of M2.

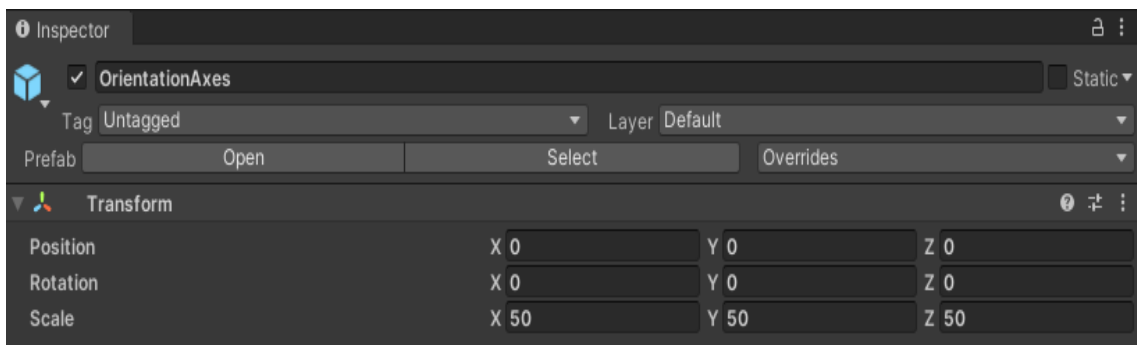


Figure 3. 79 'Transform' component of the 'OrientationAxes' object child of cube hologram.



By following the path 'Packages → Mixed Reality Toolkit Foundation → SDK → Features → UX → Prefabs' the 'NearMenu3x1' prefab has been added in the scene as a child of M1. This menu contains a pin button that then allow the user to arbitrarily position and fix it in the scene during the AR experience. Then the menu is composed by 3 buttons with their correspondent icon component and text element. 'Icon' components have been changed by opening the button inspector and looking for the most appropriate icon between the default ones proposed in the icon component (Figure 3. 80). Text elements has been changed by modifying the 'Text' component as shown in Figure 3. 81, Figure 3. 82, and Figure 3. 83. Moreover, for each button 'On Click' function is available. This component permits to rapidly implement events based on the interaction of user with buttons by finger clicks during the AR experience. In detail, the 'On Click' component of the first button or 'App Start' button, has been managed to obtain the activation of a script, that will be described in the following section and that is appositely created to implement the positioning and orientation of the cube hologram at the target pose to be reached during repositioning phase. The script to be activated is assigned to M1, hence in the 'On Click' component we need to get access to M1 properties. Figure 3. 84 shows 'On Click' component of this first button. The other 2 buttons have been managed in the 'On Click' component to implement the switch among the Osteotomy and the Repositioning Mode by activating or deactivating specific game objects and scripts. Figure 3. 85 shows the 'On Click' component of the first button or 'Osteotomy Mode' button, it activates the osteotomy lines and the drilled holes and turns off all the elements of repositioning feedback and deactivate the dedicated script for cube hologram positioning. Figure 3. 86 shows the 'On Click' component of the second button or 'Repositioning Mode' button, it activates all the elements of the repositioning feedback, it turns off the osteotomy lines and the drilled holes and finally it activates the script, that will be described in the next section and that will manage the feedback elements just activated. The script is assigned to M1 hence in the 'On Click' component we need to get access to M1 properties. Figure 3. 87 shows the 'Transform' component of the Near Menu. Final outlook of the menu is shown in Figure 3. 88.

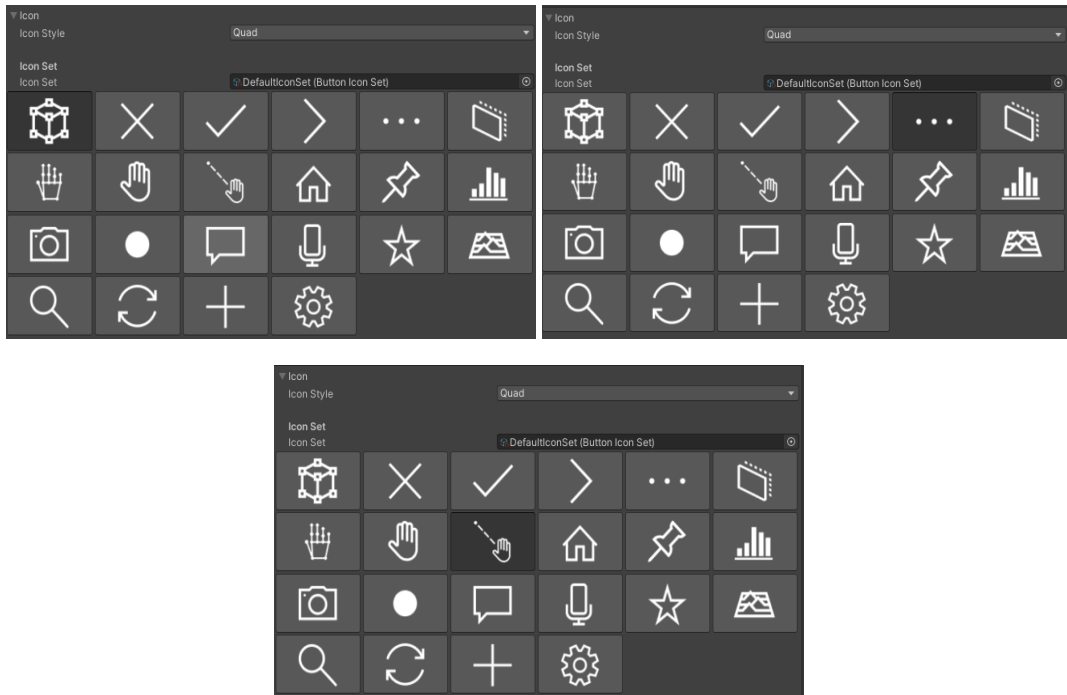


Figure 3. 80 Icon component for the first, second and third button.

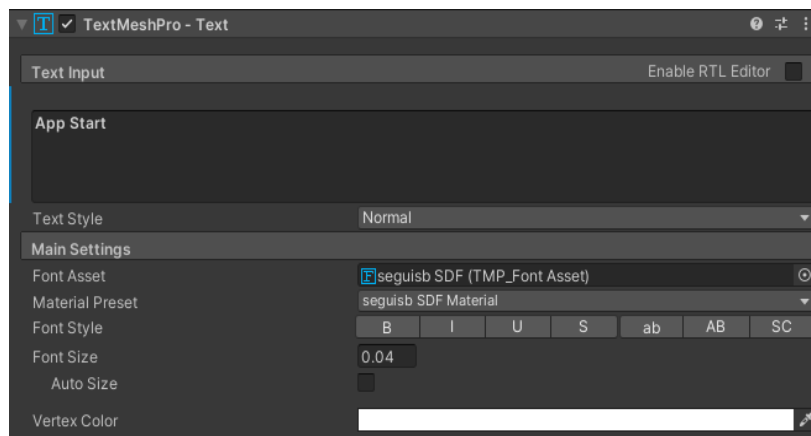


Figure 3. 81 Text Mesh Pro component for the text of the first button.

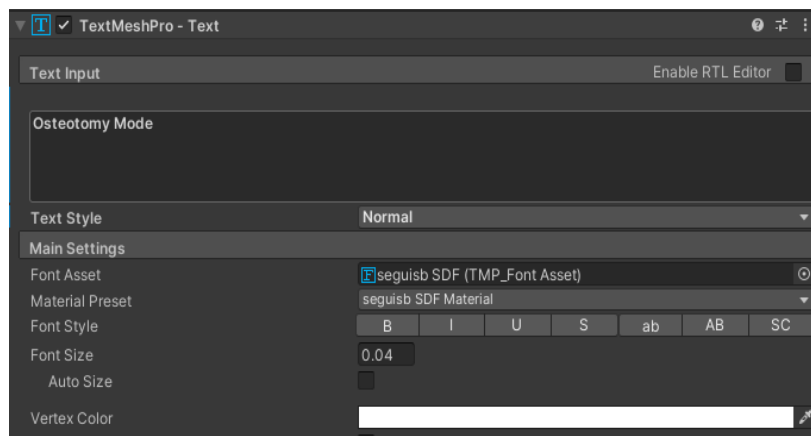


Figure 3. 82 Text Mesh Pro component for the text of the second button.

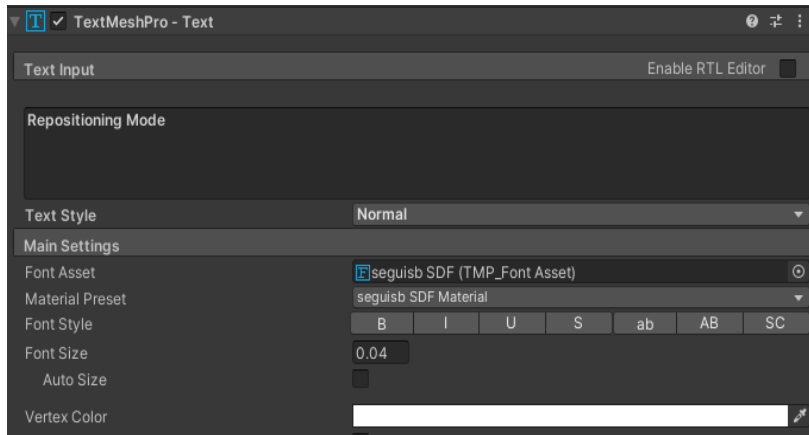


Figure 3. 83 Text Mesh Pro component for the text of the third button.

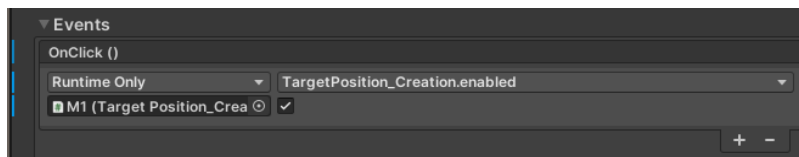


Figure 3. 84 On Click component of the first button.

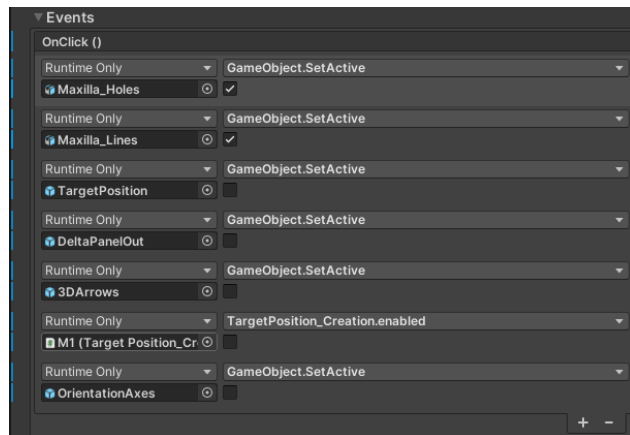


Figure 3. 85 On Click component of the second button.

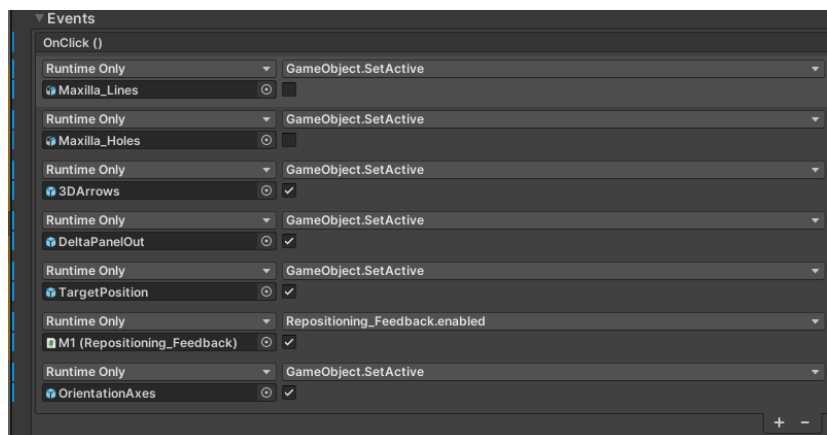


Figure 3. 86 On Click component of the third button.

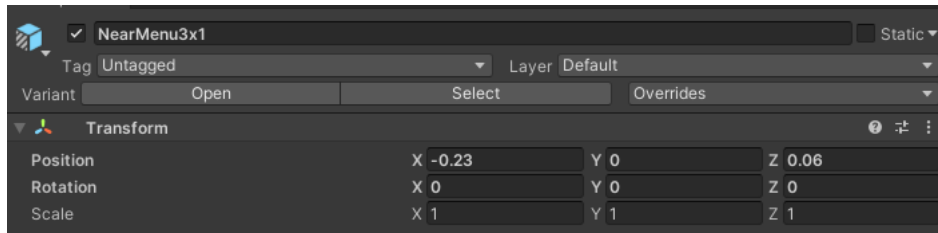


Figure 3. 87 'Transform' component of the Near Menu.

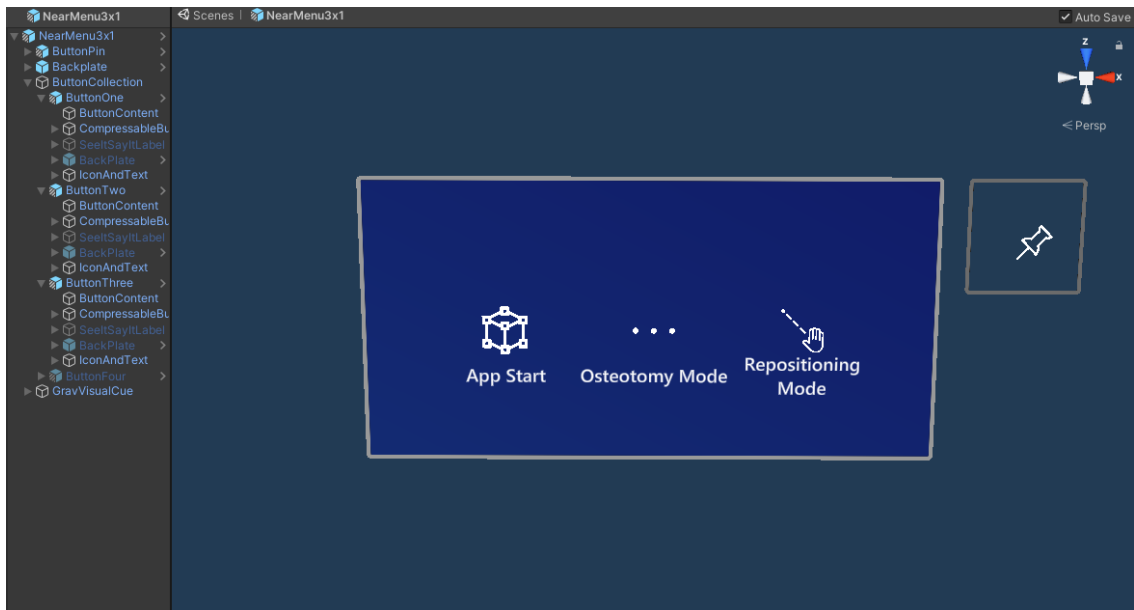


Figure 3. 88 Final outlook of the Near Menu.

Figure 3. 89 shows the final outlook of the hierarchy.

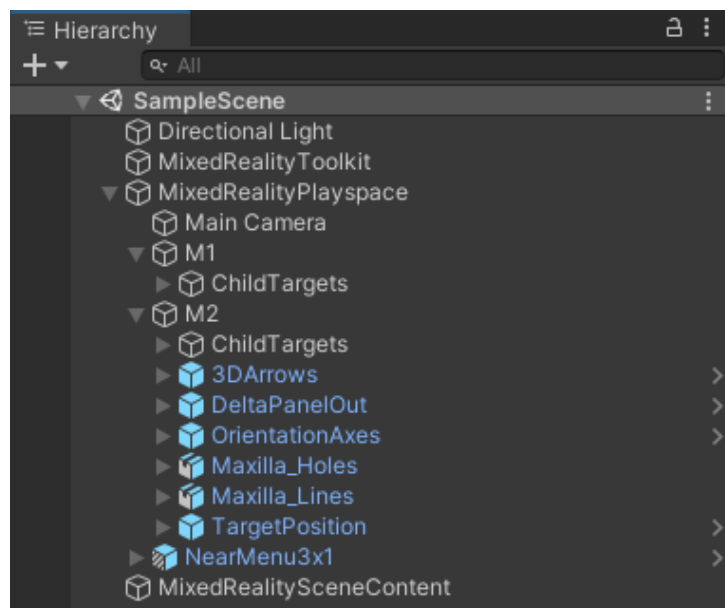


Figure 3. 89 Final outlook of the Unity scene.

### 3.5.3.4 Script

To mediate the main functionalities expected by the developed AR application, 2 C# scripts have been implemented in Visual Studio.

The first script, named as 'TargetPosition\_Creation', implements based on surgical plan the positioning of cube hologram at target pose to reach during the repositioning phase. Before going on with the description of the script it must be remarked that this script will be launched at any frame after the first or 'App Start' button has been clicked by the user. To implement the cube hologram positioning 4 inputs are necessary:

- M1 game object
- Cube hologram game object
- Pre-operatory plan vectors of 3 translations and 3 rotations (ordered Z-X-Y).

Cube hologram positioning must be performed once at first frame and it must be prevented the iterative creation after the script is launched. To achieve this purpose, a private Boolean variable ('firstframe') has been introduced and by default set to 'true'. Then in the Update block an if structure has been added that establishes that, if 'firstframe' variable is true, a private method for hologram creation will be performed and the same variable will be set to false. In this manner, the if statement will run only once at first frame after 'App Start' button has been clicked on the scene. At this point it must be described how the cube hologram is positioned. 'Hologram\_Generator' private method, called in the if statement, receives as input M1 game object, cube hologram and 2 preoperatory plan vectors. With these inputs, private method imposes cube hologram 'Transform' component in 'localPosition' and 'localEulerAngles' fields, component by component (X-Y-Z), respectively as equal to translational and rotational vectors of pre-operatory plan. Pre-operatory plan translations are expressed in millimeters while Unity works with meters, thus, the millimeters-to-meters conversion is implemented in this assignment. Finally, it assigns cube hologram as a child of M1. It must be noticed that local X-axis means mediolateral axis pointing leftward, Y-axis means anteroposterior axis pointing forward and the Z-axis is up-down axis pointing upward. Figure 3. 90 shows the line of codes of 'TargetPosition\_Creation' script.

```

using System.Collections;
using System.Collections.Generic;
using UnityEngine;

public class TargetPosition_Creation : MonoBehaviour
{
    public Vector3 displ_preop_plan;

    public Vector3 rot_preop_plan;

    public GameObject TargetPosition;

    public Transform M1;

    private bool primoframe = true;

    // Start is called before the first frame update
    void Start()
    {

    }

    // Update is called once per frame
    void Update()
    {
        if (primoframe)
        {
            Hologram_Generator(M1, TargetPosition, displ_preop_plan, rot_preop_plan);
            primoframe = false;
        }
    }

    // PRIVATE METHODS:
    // (1) Target Position Hologram Creation

    private void Hologram_Generator(Transform Marker1, GameObject Hologram, Vector3 Displacement, Vector3
Rotation)
    {
        Hologram.transform.localPosition = new Vector3(Displacement.x / 1000, Displacement.y / 1000,
Displacement.z / 1000);
        Hologram.transform.localEulerAngles = new Vector3(Rotation.x, Rotation.y, Rotation.z);
        Hologram.transform.parent = Marker1;
    }
}

```

*Figure 3. 90 Line of codes of the 'TargetPosition\_Creation' script.*

The second script, named as 'Repositioning\_Feedback', implements the management of all the feedback elements for the repositioning. Before going on with the description of the script it must be remarked that this script will be launched at any frame after the third or 'Repositioning Mode' button has been clicked by the user. Moreover, it must be marked also that the in the global coordinate system X-axis of stands for mediolateral axis pointing leftward, the Y-axis means the up-down axis pointing upward and the Z-axis is the anteroposterior axis pointing backward. The main functions to be executed through the script are:

- Delta calculation between cube hologram position and current M2 position.
- Management of the cube hologram color based on delta values.
- Management of 3D-arrows based on delta values.
- Display of delta values in the dedicated dialog panel.

Within the Update block, to implement deltas calculation, the difference between 'position.x'/'position.y'/'position.z' field of 'Transform' of cube hologram and, respectively, 'position.x'/'position.y'/'position.z' field of 'Transform' component of M2 are assigned to 3 private float variables ('deltaX', 'deltaY' and deltaZ'). Then, these deltas will be employed to manage the various feedback elements. To implement the function that manages 3D-arrows based on delta values some inputs are necessary:

- Up 3D-arrow game object
- Down 3D-arrow game object
- Left 3D-arrow game object
- Right 3D-arrow game object
- Anterior 3D-arrow game object
- Posterior 3D-arrow game object

The basic concept of this function is to activate, based on the displacement delta values, those arrows that correspond to the directions to be followed by moving M2 to reach the target position of the cube hologram. To achieve this purpose the private method 'Arrows\_Manager' is performed 3 times within the update at any frame after the 'Hologram Creation' button has been clicked. The private method receives as inputs alternatively one of the delta values and the correspondent two 3D arrows (couples: 'deltaX' - 'Right', 'Left'; 'deltaY' - 'Posterior', 'Anterior'; 'deltaZ' - 'Up', 'Down'). The method, through multiple if-then statements on the delta with respect to the displacement threshold and by mean of the 'SetActive' function, imposes as active the positive arrow when the delta is higher than the threshold or imposes as active the negative arrow when the delta is lower than minus the threshold or finally imposes as inactive both negative and positive arrows when delta is within the tolerance range. It must be noticed even here that Unity works with meters while the threshold is

expressed in millimeters, thus, conversion from meter to millimeters is implemented within the if statements. Figure 3. 91 shows 'Arrows\_Manager' private method.

```
private void Arrow_Manager(GameObject Positive, GameObject Negative, float delta, float
threshold)
{
    if (delta > threshold / 1000)
    {
        Positive.SetActive(true);
        Negative.SetActive(false);
    }
    else
    {
        if (delta < -threshold / 1000)
        {
            Positive.SetActive(false);
            Negative.SetActive(true);
        }
        else
        {
            Positive.SetActive(false);
            Negative.SetActive(false);
        }
    }
}
```

Figure 3. 91 Lines of codes of the 'Arrows\_Manager' private method.

Then, to implement the function to display delta values on the specific text box, 3 game objects, correspondent to the 3 TMP box where values are displayed, must be given. Moreover, to get access and modify their TMP component, 3 private variables of the type 'TextMeshPro' are initialized and used in the Start block to get access through the 'GetComponent' function to the 'TextMeshPro' component of the 3 input objects. Then, in the Update block, the 'Txt\_Manager' private method is called 3 times at any frame after the 'Repositioning Mode' button has been clicked. The private method receives as inputs alternatively one of the delta values and the private 'TextMeshPro' variable with the access to the 'TextMeshPro' component of the correspondent box. Finally, within the private method, the 'Text' component of the input 'TextMeshPro' private variable is assigned as the delta value, converted from meters to millimetres and approximated at the first non-decimal value. Figure 3. 92 shows the 'Txt\_Manager' private method.

```
private void Txt_Manager(TextMeshPro Value, float delta)
{
    Value.text = (delta * 1000).ToString("0");
}
```

Figure 3. 92 Lines of code of the 'Txt\_Manager' private method.



To achieve this purpose, some new inputs are needed:

- List of materials, they correspond to the 3 levels of the alarm system (red - yellow - green)
- Displacement threshold, a float variable that corresponds to the maximum distance from target position to be tolerated.

The private method 'Color\_Manager' is performed within the update at any frame after the third button or 'Repositioning Mode' button has been clicked. It receives as input the list of materials (red material Figure 3. 63 at the first position and green material Figure 3. 62 at the second position), the 3 just calculated deltas, the displacement threshold, and a private variable of the 'Renderer' type that by the 'GetComponent' function in the Start block allow to get access to the 'Material' component of the cube hologram game object. The private method then with an if-else statements allows to assign top the 'Material' component of the cube hologram game object different materials based on the actual values of deltas with respect to the imposed thresholds. Essentially, the cube hologram material will be assigned to the first element of the material list (red) when all the deltas are outside the tolerance range, or to the second element of the material list (green) when all the deltas are within the tolerance range. Even here it must be noticed that deltas are extracted by Unity in meters while the threshold is expressed in millimeters, thus, the delta conversion from meters to millimeters is implemented within the if statements. Figure 3. 93 shows the 'Color\_Manager' private method.

```
private void Color_Manager(Material[] levels, float delta1, float delta2, float delta3,
float threshold, Renderer rend_access)
{
    if (delta1 <= threshold / 1000 && delta1 >= -threshold / 1000 && delta2 <= threshold
/ 1000 && delta2 >= -threshold / 1000 && delta3 <= threshold / 1000 && delta3 >= -threshold
/ 1000)
    {
        rend_access.material = levels[1];
    }
    else
    {
        rend_access.material = levels[0];
    }
}
```

Figure 3. 93 Lines of code of the 'Color\_Manager' private method.

Figure 3. 94 illustrates the line of codes of the 'Repositioning\_Feedback' script.

```
using System.Collections;
using System.Collections.Generic;
using UnityEngine;
using UnityEngine.UI;
using System;
using TMPro;

public class Repositioning_Feedback : MonoBehaviour
{
    public GameObject TargetPosition;
    public GameObject M2;

    private float deltaX;
    private float deltaY;
    private float deltaZ;

    public GameObject ValueML;
    private TextMeshPro textX;
    public GameObject ValueUD;
    private TextMeshPro textY;
    public GameObject ValueAP;
    private TextMeshPro textZ;

    public float displ_threshold;

    public GameObject Posterior;
    public GameObject Anterior;
    public GameObject Left;
    public GameObject Right;
    public GameObject Up;
    public GameObject Down;

    private Renderer meshRend_access;
    public Material[] alarm_levels;

    // Start is called before the first frame update
    void Start()
    {
        textX = ValueML.GetComponent<TextMeshPro>();
        textY = ValueUD.GetComponent<TextMeshPro>();
        textZ = ValueAP.GetComponent<TextMeshPro>();

        meshRend_access = TargetPosition.GetComponent<MeshRenderer>();
    }

    // Update is called once per frame
    void Update()
    {
        deltaX = TargetPosition.transform.position.x - M2.transform.position.x;
        Txt_Manager(textX, deltaX);
        Arrow_Manager(Right, Left, deltaX, displ_threshold);

        deltaY = TargetPosition.transform.position.y - M2.transform.position.y;
        Txt_Manager(textY, deltaY);
        Arrow_Manager(Up, Down, deltaY, displ_threshold);

        deltaZ = TargetPosition.transform.position.z - M2.transform.position.z;
        Txt_Manager(textZ, deltaZ);
        Arrow_Manager(Posterior, Anterior, deltaZ, displ_threshold);

        Color_Manager(alarm_levels, deltaX, deltaY, deltaZ, displ_threshold, meshRend_access);
    }
}
```

Figure 3. 94 Lines of code of the 'Repositioning\_Feedback' script.

Both scripts are assigned to the game object M1 and then the input assignment can be performed directly in Unity and, from Unity interface, user can adjust preoperatory plan. Figure 3. 95 shows input assignment for 'TargetPosition\_Creation' script. Figure 3. 96 the input assignment for the 'Repositioning\_Feedback' script.

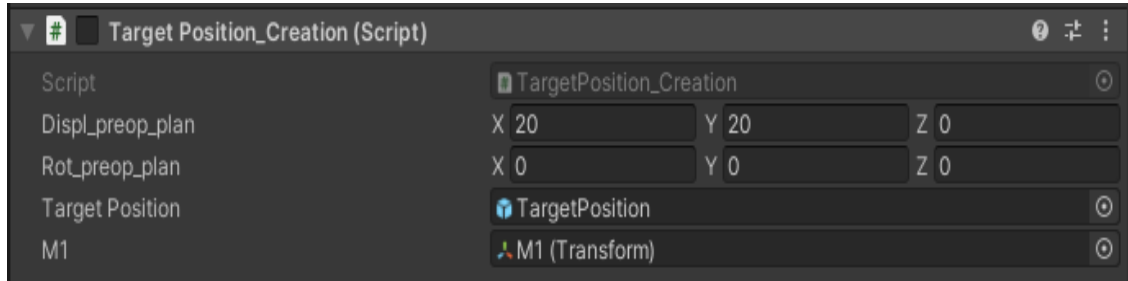


Figure 3. 95 Input assignment in the 'TargetPosition\_Creation' script.

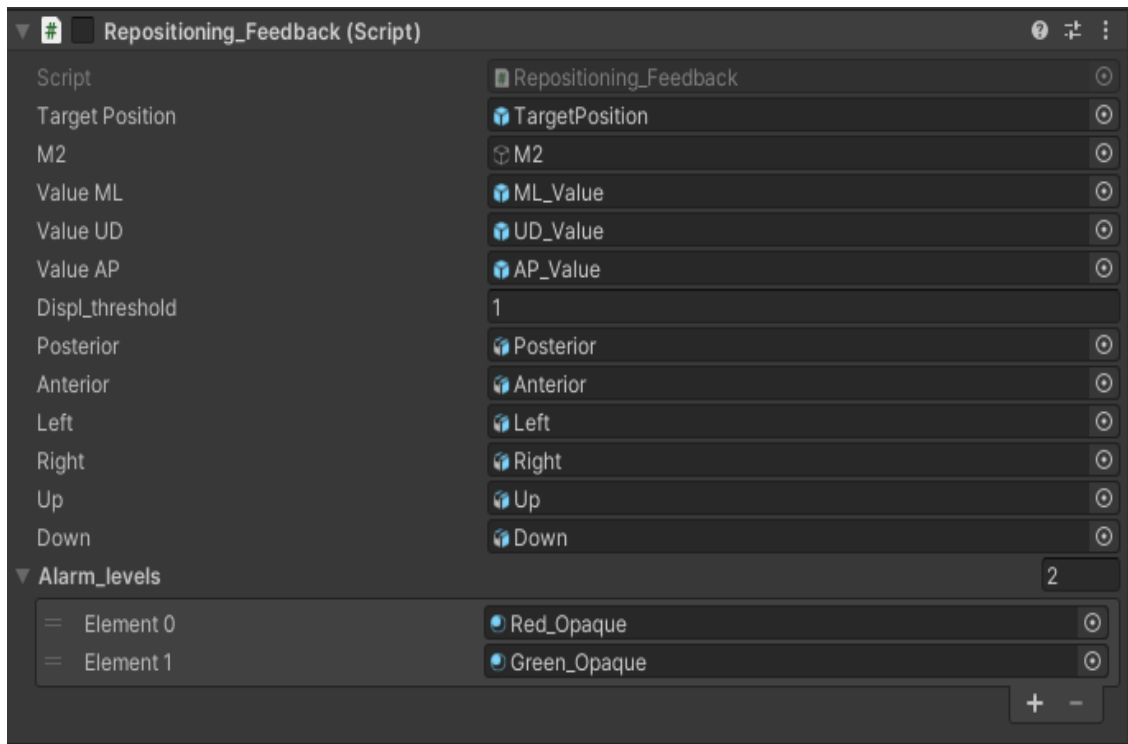


Figure 3. 96 Input assignment in the 'Repositioning\_Feedback' script.

### 3.5.3.5 Build, Compilation and Distribution

Last step to be performed in Unity is the fifth one or build creation. A build is the process of converting source code files into standalone software artifact that can be run on the specific device. The building process expects 3 main steps that are saving of the scene, addition of the scene to the project and build generation of the project. As first,

the scene ('File → Save') and the whole project ('File → Save Project') have been saved, then the scene has been added ('File → Build Settings → Add Open Scene', as shown in Figure 3. 97), and finally the build is created ('File → Build Settings → Build'). At this point Unity asks to select the folder in which the build files will be created. For this purpose, a specific folder, named as 'App\_OR\_Build', has been created. At the end of the building process, the folder just created contains the solutions to be opened in Visual Studio and that will be then compiled and distributed to deploy and finally use the developed application in the target device.

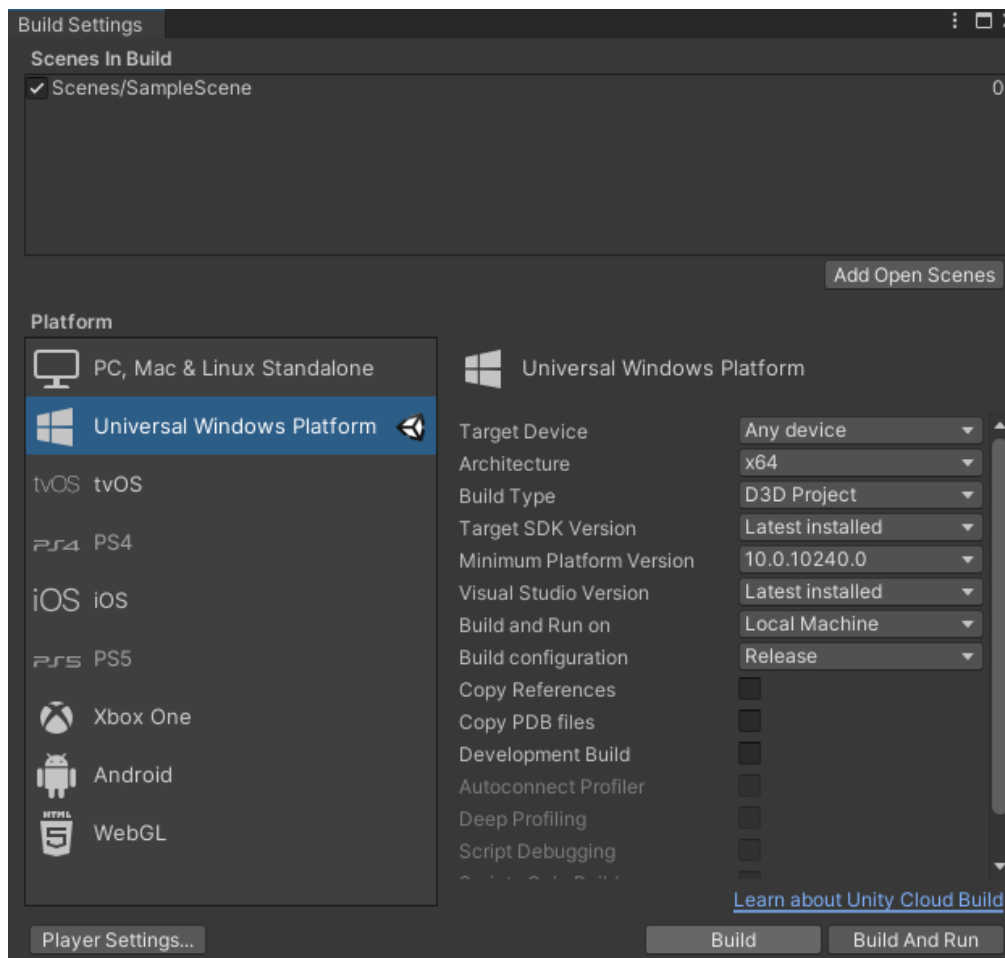


Figure 3. 97 Build creation window.

At the end, compilation, and distribution, have been performed in Visual Studio. The solution (.sln file), just created, has been opened. The 'Solution Configuration' option has been set to 'Release', the 'Solution Platform' option has been set to 'ARM64' and the 'Target Device' option has been set to 'Dispositivo' (Figure 3. 98).

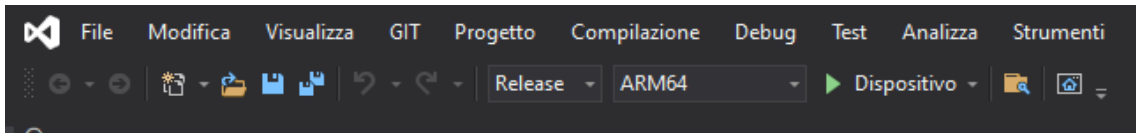


Figure 3. 98 Visual Studio settings to perform compilation and distribution.

After adjusting these settings and connecting the target device (Microsoft HoloLens V2) to the PC, the solution is compiled and distributed by following the path 'Debug → Avvia senza eseguire debug' (Figure 3. 99). At the end of this procedure the application will be available on the HMD and can be launched.

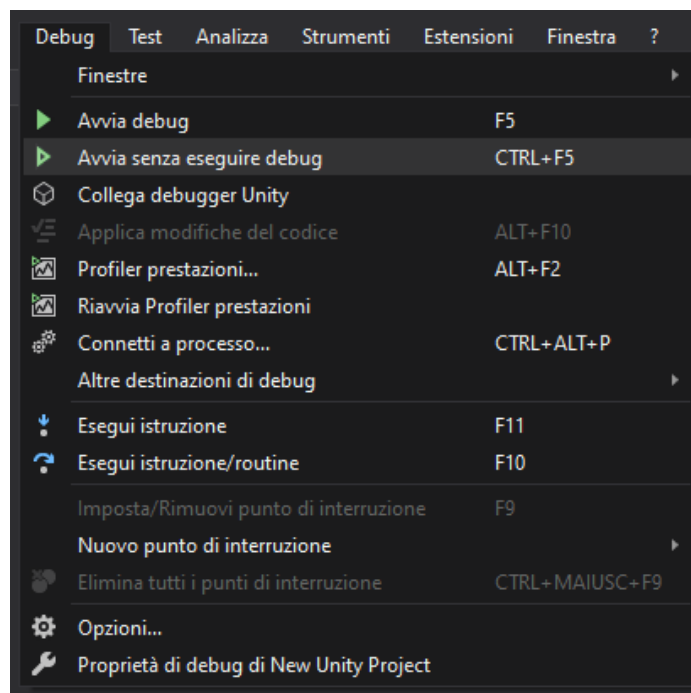


Figure 3. 99 Path for the launch of the compilation and distribution of the solution.

### 3.5.4 Proposals for Marker M1 Placement

In this section, 5 proposals (Design A – Design B – Design C – Design D – Design E) for the placement of the marker M1 are analyzed focusing on their advantages and disadvantages in a hypothetical clinical practice.

Moreover, these designs will be illustrated through technical drawings developed in Rhinoceros 6. However, it should be noticed that these are theoretical concepts whose effectiveness needs to be approved and practically tested.

Design A (Figure 3. 100) expects the realization of a box or marker box deprived of the top face and with a holed bottom face. The hole in the bottom face has a shorter diameter respect to the diameter of the head of the screw. The screw can be easily fastened through the missing upper face of the marker box and its fastening ensures the marker box on the skull. The main disadvantage of this solution is the absence of upper face of the marker.

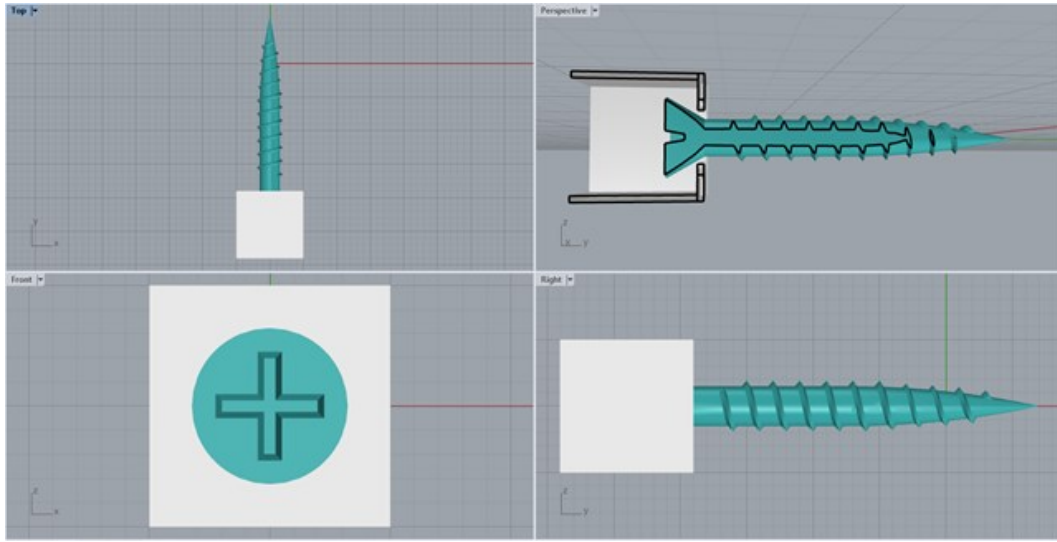


Figure 3. 100 Cranial marker Design A.

Design B (Figure 3. 101) and Design C (Figure 3. 102) expects the realization of a metallic ring support with a shorter diameter than the diameter of the head of the screw and equipped with 1 or 2, respectively, L-shaped inserts (with cylindrical or prismatic section). In the Design B, the L-shaped insert is custom-made for the insertion in a cylindrical or prismatic channel that is part of the hollowed marker box deprived of bottom face. In the Design C instead, the 2 L-shaped inserts are custom-made for the insertion in 2 dug channels that are created in a completely solid marker box, on its bottom face. In both cases, the screw fastening is free, and it ensures the ring support to the skull. In turn, by assembling of the cube on the L-shaped inserts, also the marker box is ensured. The main advantage of this solution is the possibility of realizing marker and support in different materials, allowing to achieve small thicknesses. However, the main disadvantage of these solutions is the poor structural rigidity and stability.

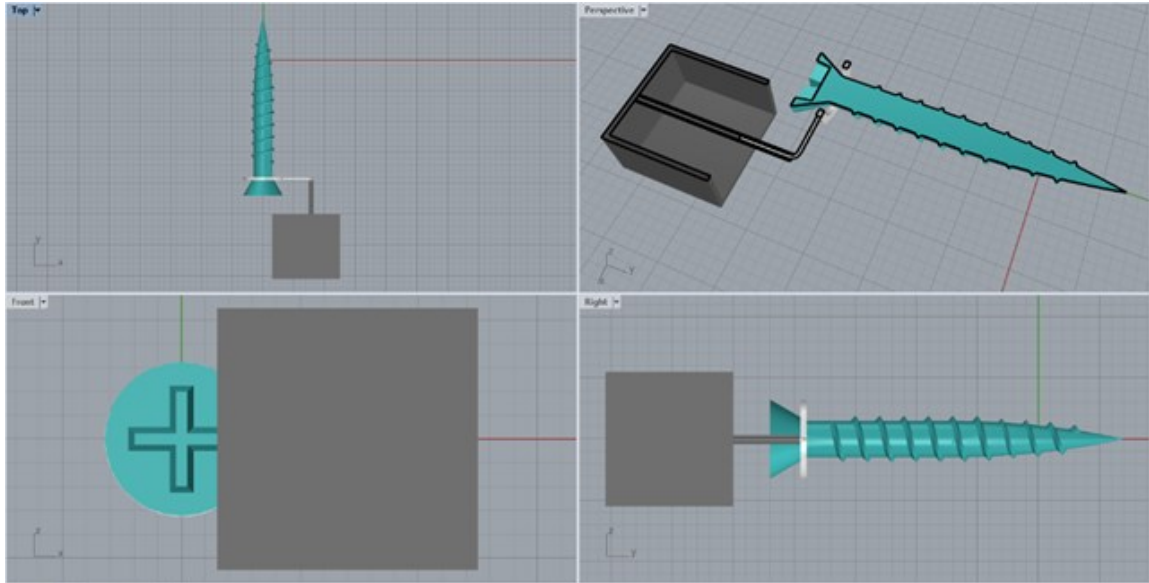


Figure 3. 101 Cranial marker Design B.

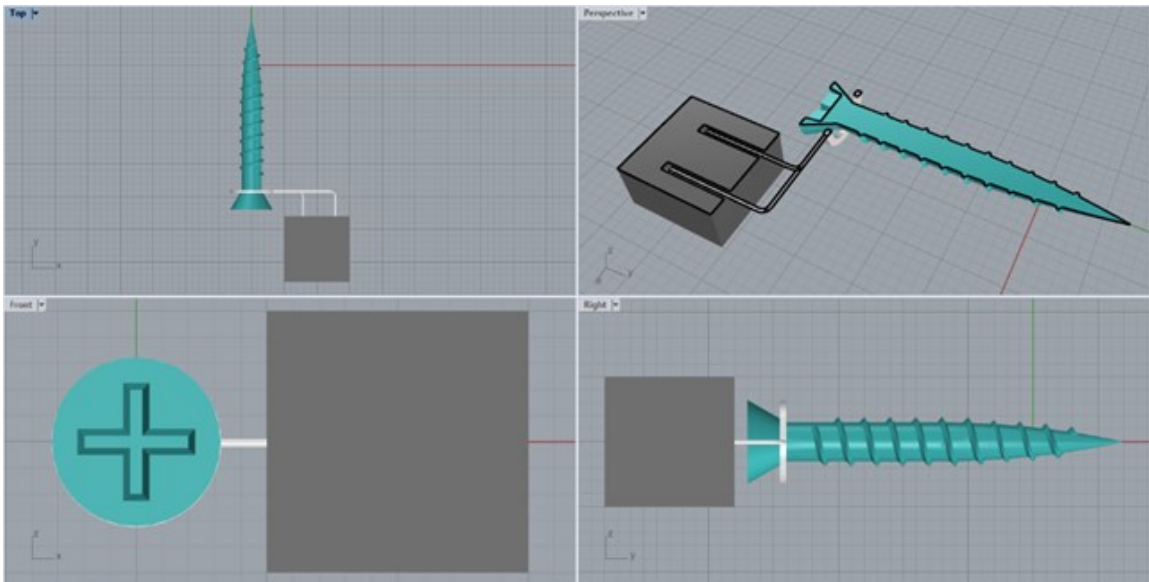


Figure 3. 102 Cranial marker Design C.

Design D (Figure 3. 103) expects the realization of a metallic squared support exactly dimensioned as a marker box face. Metallic support is holed, and its hole has a shorter diameter than the head of the screw. Moreover, the metallic support is equipped with 4 cylinders that are custom-made for the insertion in 4 channels that are dug in the almost completely solid marker box, on its bottom face. In this alternative, the screw fastening is free, and it ensures the metallic support to the skull. In turn, by assembling the cube through the 4 cylindrical inserts, also the marker box

is ensured on the patient anatomy. The main advantage of this design is the possibility of manufacturing marker and support in different materials that permits to reach small thicknesses for the support realization. However, this solution does not guarantee high rigidity and structural stability.

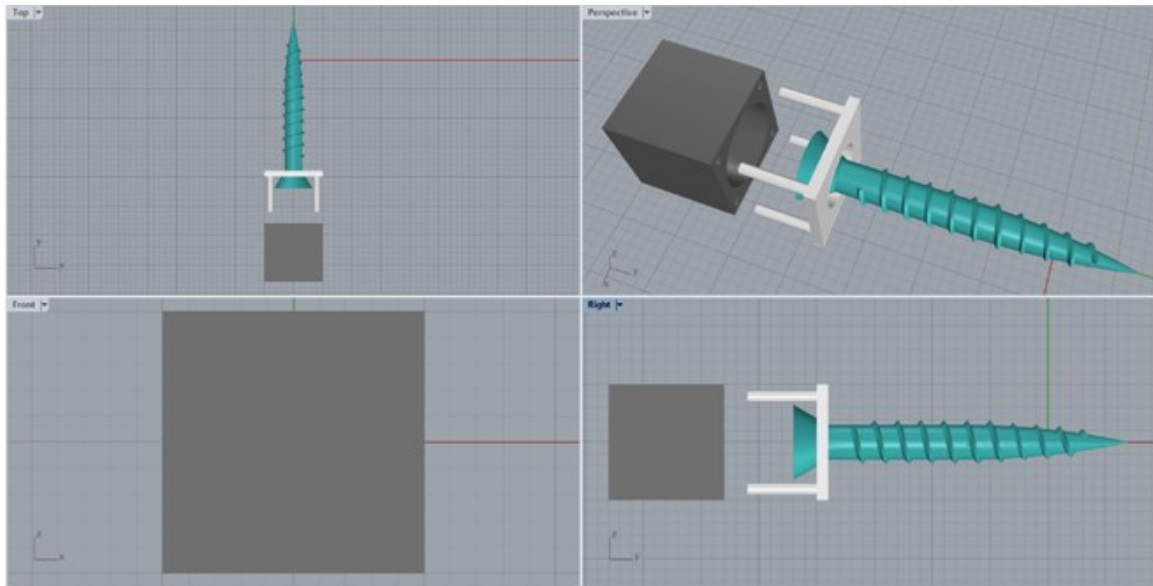


Figure 3. 103 Cranial marker Design D.

Design E (Figure 3. 104) is the most likely to be employed in the clinical practice. It expects the realization of a metallic squared support exactly dimensioned as the marker box face. The realization of this element with metallic materials allows to reach small thicknesses that do not hamper the screw fastening. The metallic support is equipped with 4 laminar semi-elastic metallic wings that mediate the assembly of the support component with the marker box. Marker box is a hollowed cube deprived of the bottom face and whose faces are internally dug to host the profile of the 4 wings. The coupling of the elastic wings of the metallic support with these internal custom-made slots of the marker box is a fast and stable assembly mechanism. Hence, the fastening of the screw is free to be performed and it ensures the support on the skull. In turn, after the rapid assembly of support wings on marker box slots, also the marker box is ensured on the patient anatomy. This is a plausible solution to be employed in the clinical practice, since the marker placement is stable, easy, and fast to be achieved, it guarantees a high level of stability and permits an easy and efficient screw fastening.



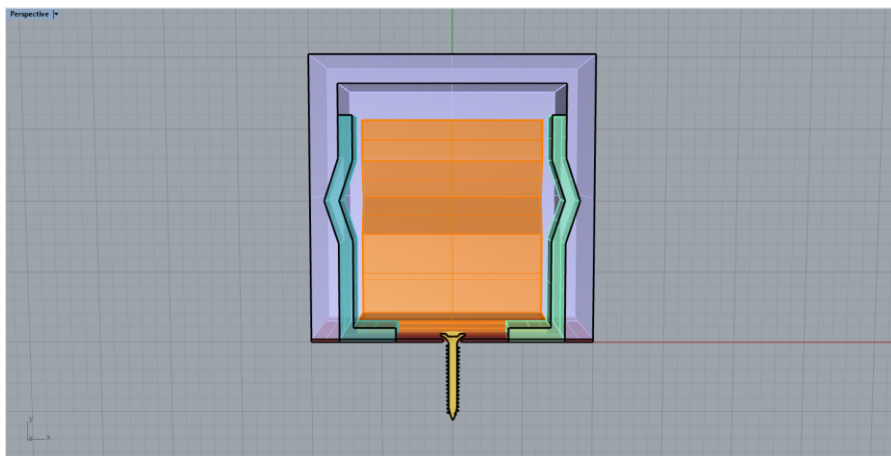
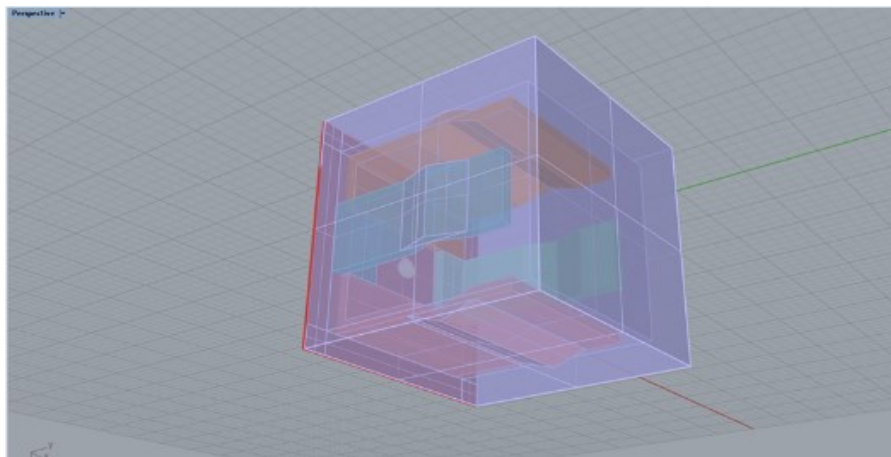
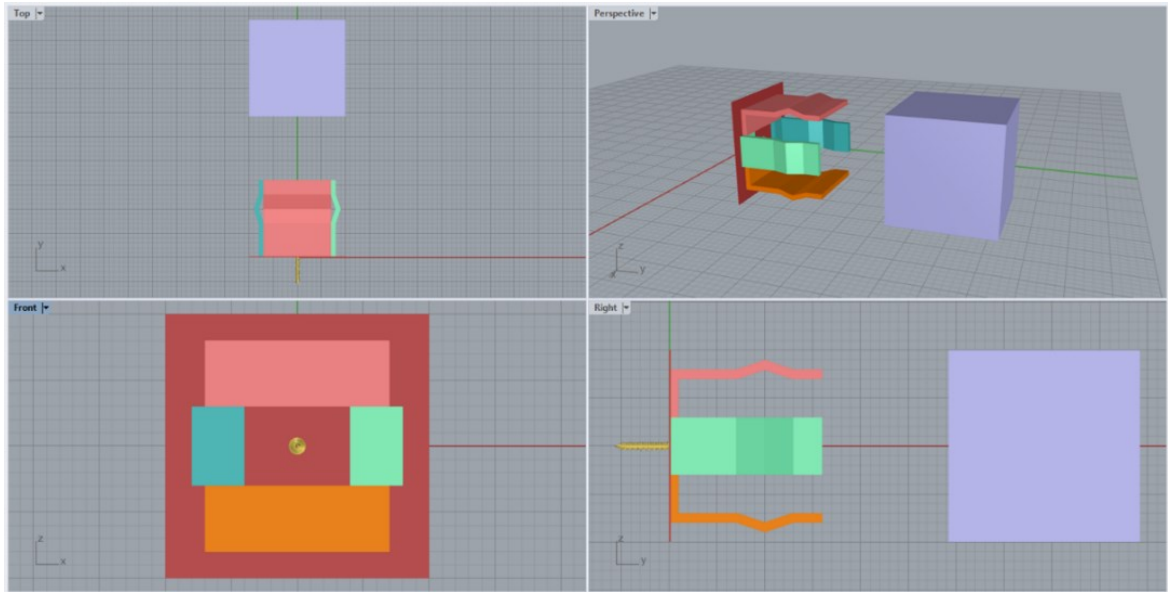


Figure 3. 104 Cranial marker Design E.

## 4 Case Study

The developed AR application, just described, can be used to assist both osteotomy and repositioning operations. In detail, in this thesis, it has been conducted a study over a virtual patient to test the effectiveness of the developed AR application on the maxillary osteotomy and maxillary fragment repositioning.

To test the AR application a custom-made physical phantom is required. Hence, in this thesis it has been modelled a skull three-dimensional CAD model. The unique requirement that phantom must respect is the multifunctionality. As first, this means that phantom must allow to test both maxillary and mandibular operations and user must be easily able to select the treated anatomy. Hence, the modelled skull phantom will expect both the maxillary and mandibular components and user has the possibility to easily select the treated anatomy by assembling M2 to correspondent bite (i.e., upper bite to treat the maxilla and lower bite to treat the mandible). As second, multifunctionality means that phantom must allow to test both osteotomies and repositioning tasks. Hence, the phantom must expect a fast assembling and disassembling mechanism that permits, when the whole assembly is attached to test osteotomies and then when the single osteotomized fragment is detached to test repositioning tasks. However, the case study involved on this thesis will uniquely regards the maxillary operations.

At this point it can be useful to define the workflow of this project. As first the marker images must be generated in the online website, Piffero QR Generator. The QR codes are the same uploaded in the Vuforia SDK to create the marker database that is then employed in Unity for the development of the AR application described in previous section. Then, modelling phase is initiated in Rhinoceros 6. Modelling expects first the global shaping of the model (scaling, reduction of the overall volume), then the addition of the cranial marker (M1) and the dental marker (M2) that, in turn, expects the design of the bite structures. Moreover, the surgical guides are developed (osteotomy cutting lines and drilled holes), these guides are both exported, after a fine

alignment with respect to marker has been performed, as \*.OBJ files that will compose the virtual content of the AR application. Osteotomy lines have been designed as cylinders of 0.7mm diameter, that are customized on the three-dimensional model of the skull and that user can easily visualize and follow to perform maxillary cuts. For what concern drilled holes, they have been developed as cylinders of 1.7mm diameter that highlight a circular area over the osteotomized maxillary fragment in which user can perform the drilling. Furthermore, osteotomy lines have been used to split the model in the various assembly components. Finally, the assembly mechanisms among the various component are embedded and the assembly components are exported as \*.STL or \*.VRML files to be 3D-printed. 3D-Printing has been performed using the CJP technology of ZPrinter 450 and it returns the phantom over which the developed AR application will be tested, after applying paper-printed QR codes with bi-adhesive tape on specific marker faces. To complete the scene of the AR application, virtual surgical guides, exported from in the \*.OBJ format, are inserted in the Unity scene of the developed AR application as described in the previous section. For what concern the repositioning a 20 mm translation on the x-axis (medio-lateral, positive left and negative right), a 20 mm translation on the y-axis (antero-posterior, positive forward and negative backward) and a 0 mm translation on the z-axis (up-down, positive upward and negative downward) compose the pre-operative plan that is completed by 3 null rotations and that must be inserted in the dedicated script. All the script inputs can be assigned, the build of the AR application is generated, the solution is compiled and distributed on the Microsoft HoloLens V2 HDM.

At the end, the application is available on the HMD and ready to be launched. At this point, the AR application has been tested over the 3D-printed phantom multiple times asking users to first perform maxillary osteotomies by following with a pencil the cutting lines projected over the phantom, then to mark with the pencil the maxillary drilled holes as indicated by the correspondent virtual surgical guide and finally to proceed with its repositioning guided by the feedback elements. The tested phantom has been scanned twice using Go!Scan3D device. First scanning session immediately follows the osteotomy lines and drilled holes performance. Second

scanning sessions immediately follows the repositioning of the osteotomized fragment. At the end scans are processed in the dedicated software, CloudCompare, to extract results in terms of absolute deviations for all the performed tasks (osteotomy lines, drilled holes, repositioned fragment). Figure 4. 1 illustrates the phases workflow above described.

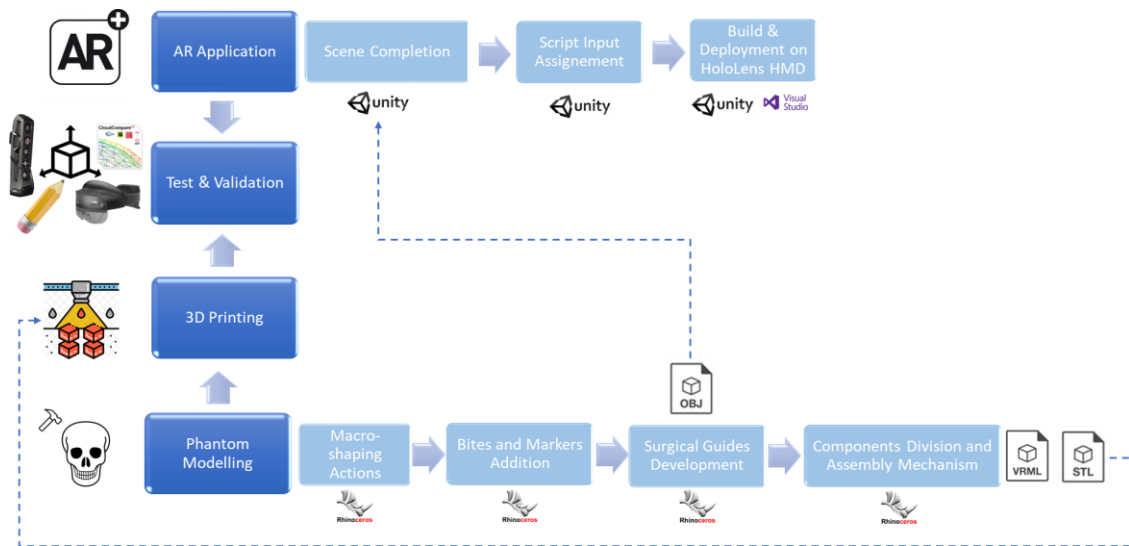


Figure 4. 1 Steps of the various phases of the thesis workflow.

## 4.1 Modelling

### 4.1.1 Skull CAD Model

Models of the patient anatomy permits to obtain the three-dimensional model to be 3D-printed and over which design the virtual surgical guides. Rhinoceros 6 has been employed to perform this phase. The skull three-dimensional model, shown in Figure 4. 2, Figure 4. 3, and Figure 4. 4 in multiple viewports, has been exported from the online Sketchfab CAD model library.

It is made of 4 mesh components:

- 1) Upper skull
- 2) Upper teeth
- 3) Lower teeth
- 4) Mandible

The skull CAD model has been scaled, with 'Scale 3D' command, to obtain a model with suitable dimensions for a practical usage.



*Figure 4. 2 Skull CAD model from the top viewport.*

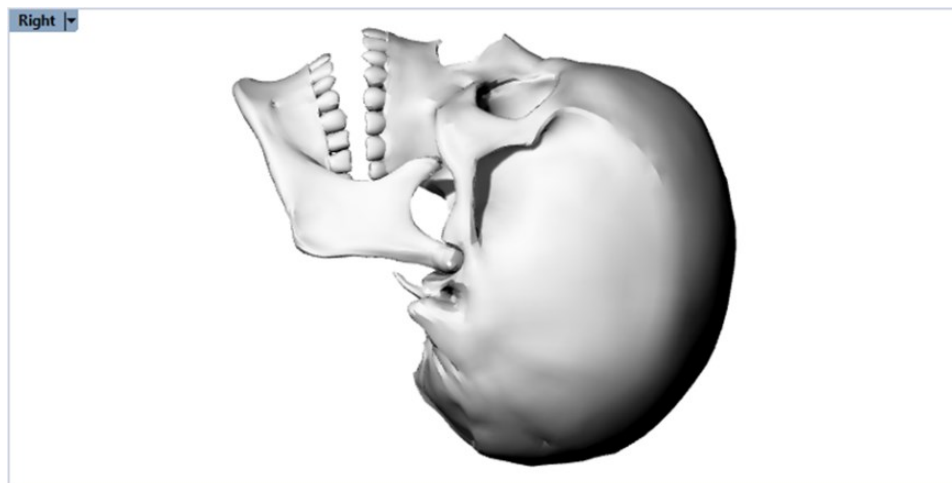


*Figure 4. 3 Skull CAD model from the right viewport.*



*Figure 4. 4 Skull CAD model from the perspective viewport.*

Moreover, to reduce the overall weight of the skull phantom, the upper skull component has been cut beyond the condyles and shelled by removing the internal volume. To cut the upper skull a plane has been created with the 'Rectangular Plane: Corner to Corner' command and then meshed with the 'Mesh' command. This plane has been then used in the 'Mesh Boolean Split' command to split the upper skull just beyond the condyles. Moreover, the exceeding bony structures have been removed. Then, the split upper skull has been shelled with the internal volume of the skull, through the 'Mesh Boolean Difference' command. Figure 4. 5 and Figure 4. 6 show the result of this procedure from multiple views. This procedure makes the upper skull a shelled structure with a 5 mm thickness that is suitable to be 3D-printed.

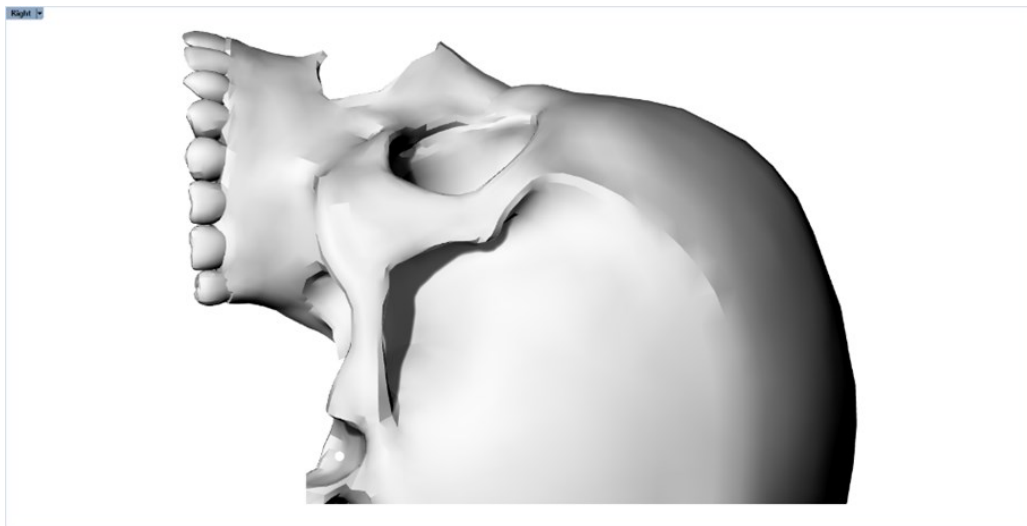


*Figure 4. 5 Split and shelled upper skull from the right viewport.*



*Figure 4. 6 Split and shelled upper skull from perspective viewport.*

## 4.1.2 Bites, Marker M2 and Marker M1

Custom-made mandibular and maxillary splints or bites have been developed in the Rhinoceros 6 software for lower and upper teeth. These 2 bites are necessary to permit and support the placement of specific marker (M2) in the lower part of the skull that will be then employed for the registration of the virtual contents that compose the augmentation of the real-world expected by the developed AR application.

First step of bites creation is the generation of a curve passing through some reference points of the specific dental arch, with the 'Curve: Interpolate Points' command. This curve is then employed as rail for the creation of a pipe of radius 6 mm, with the 'Pipe' command, that is then meshed with 'Mesh' command. Then a bridge support has been added in which it has been customized the assembly mechanism that will permit the attachment of marker for hologram registration. This element is constructed with 'Box' and 'Mesh' commands and then 'Mesh Boolean Union' command is used to attach bridge element on pipe constructed at previous step. Then, a 3 x 3 x 3 cm cube (marker M2), has been created with 'Box' and 'Mesh' commands. Finally, 'Mesh Boolean Difference' command has been applied to bridge support element and cube to create assembly channels by digging elements with 2 cylinders (2mm diameter - 10mm length). Figure 4. 7 shows this assembly mechanism.

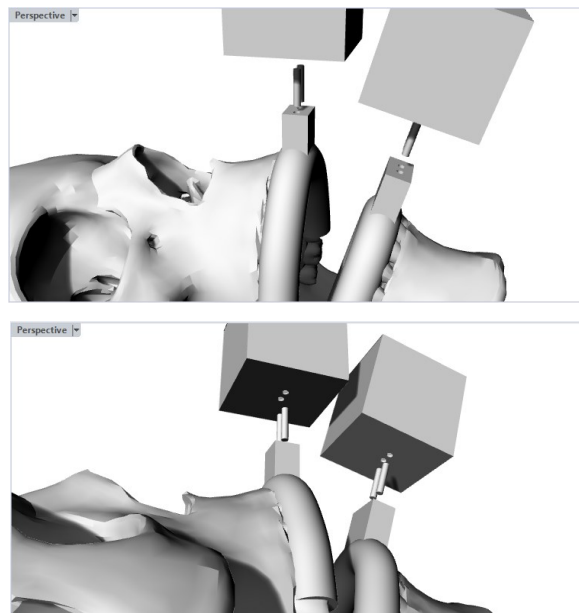
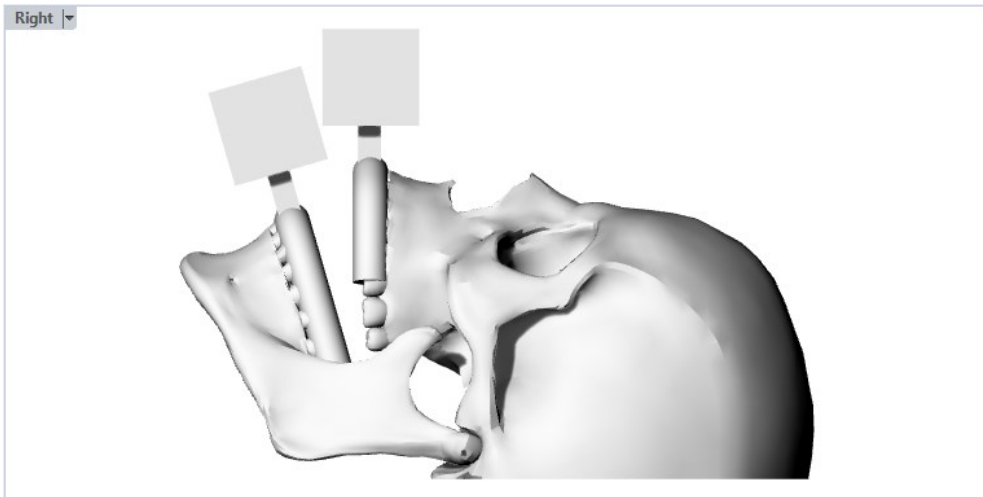


Figure 4. 7 Assembly mechanism of bridge support and marker M2 from different views.

Figure 4. 8, Figure 4. 9, and Figure 4. 10 show final outlook of the model.



*Figure 4. 8 Skull and bites from the top viewport.*



*Figure 4. 9 Skull and bites from the right viewport.*

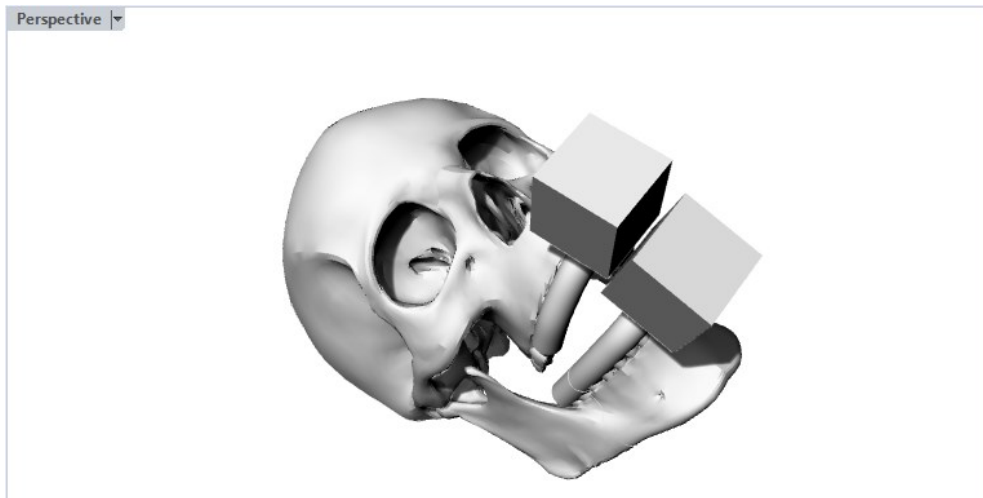


*Figure 4. 10 Skull and bites from the perspective viewport.*



As described in the previous section, the AR application expects the placement of a second marker (M1) outside the osteotomized fragment. It is hypothesized to be placed on the patient upper skull on frontal bone. For the practical usage of this thesis, the placement of the cranial marker on the phantom of the patient skull is non-exactly reproduced according to most suitable design proposal for a practical usage (Design D) described but the marker is directly embedded in the upper skull as a 3 x 3 x 3 cm cube through a sort of bridge structure. Both elements have been realized with 'Box' command and then, after meshing with 'Mesh' command, the bridge element has been blended to upper skull with 'Mesh Boolean Union' command. Finally, 'Mesh Boolean Difference' command has been applied to bridge element and marker cube (M1) to create assembly channels by digging these elements with 2 cylinders (2mm diameter - 10mm length) appositely positioned. Figure 4. 11 shows the assembly mechanism. Figure 4. 12, Figure 4. 13, and Figure 4. 14 show the outlook of the model at this step.

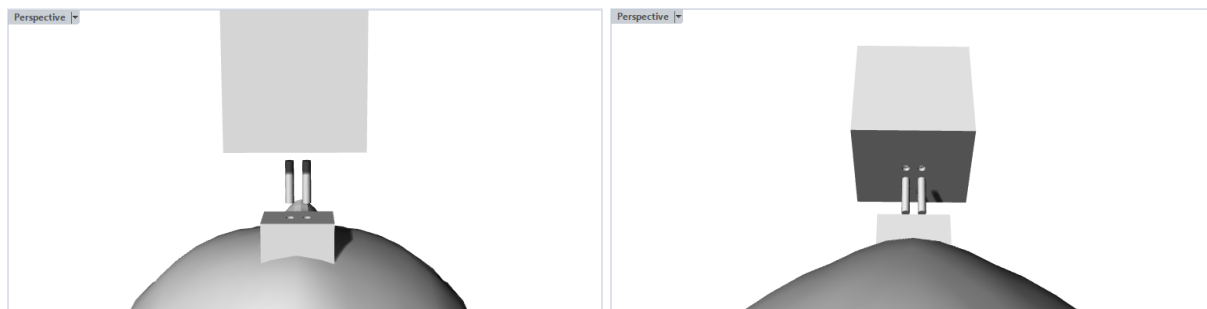


Figure 4. 11 Assembly mechanism of bridge support and marker M1 from different views.



Figure 4. 12 Skull, bites, and cranial marker from the top viewport.

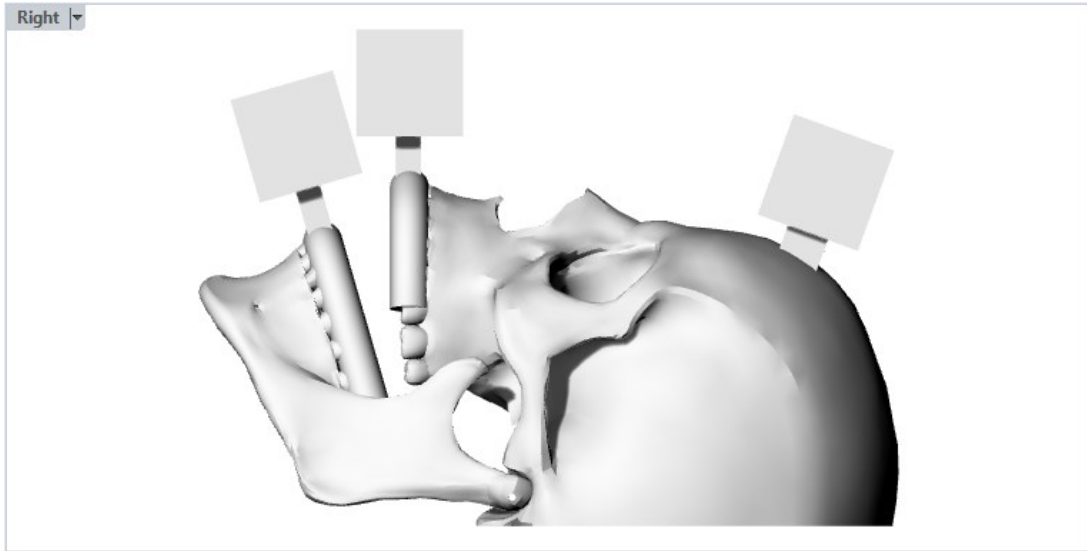


Figure 4. 13 Skull, bites, and cranial marker from the right viewport.

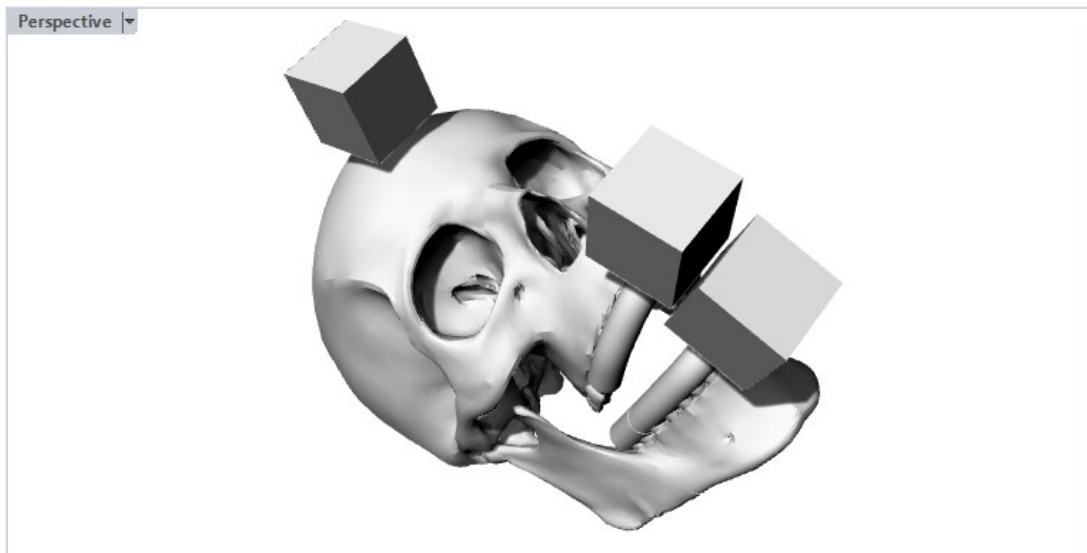


Figure 4. 14 Skull, bites, and cranial marker from the perspective viewport.

At the end some operations are needed to facilitate the marker recognition and correct assembling on the correspondent components. To be able to understand the right orientation of the marker cubes, the bottom face of any of the three marker cubes has been colored by setting the red color on the 'Print Color' of the properties. To be able to distinguish marker cubes, the left face of any of the three marker cubes has been colored by setting a specific color (blue for M1, green for M2 on the upper skull and magenta for M2 on the lower bite) on the 'Print Color' of the properties. Figure 4. 15 and Figure 4. 16 show the final outlook of marker cubes.

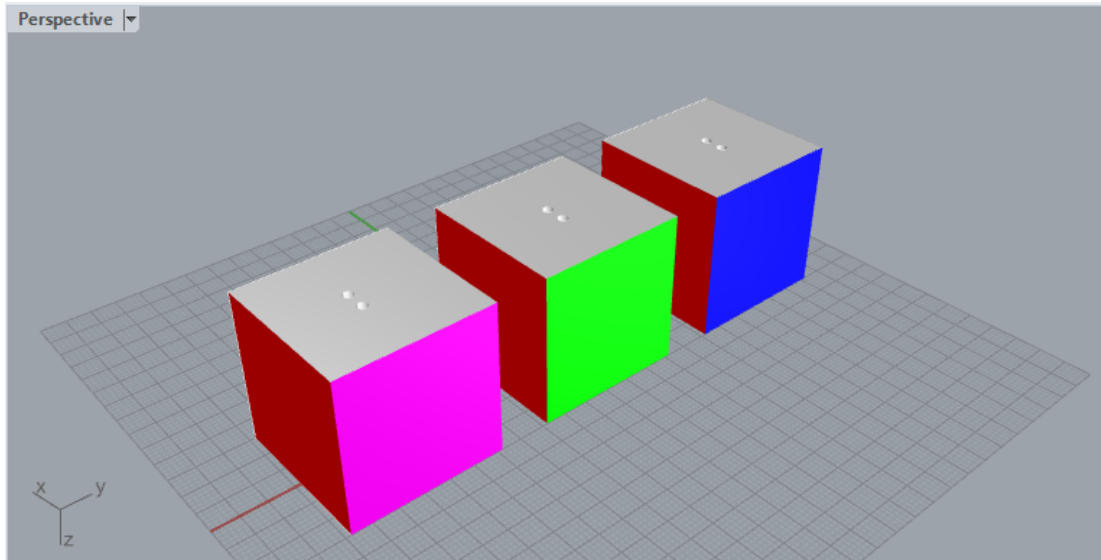


Figure 4. 15 Colored markers (M1, M2 for upper and lower bite) from the perspective viewport.

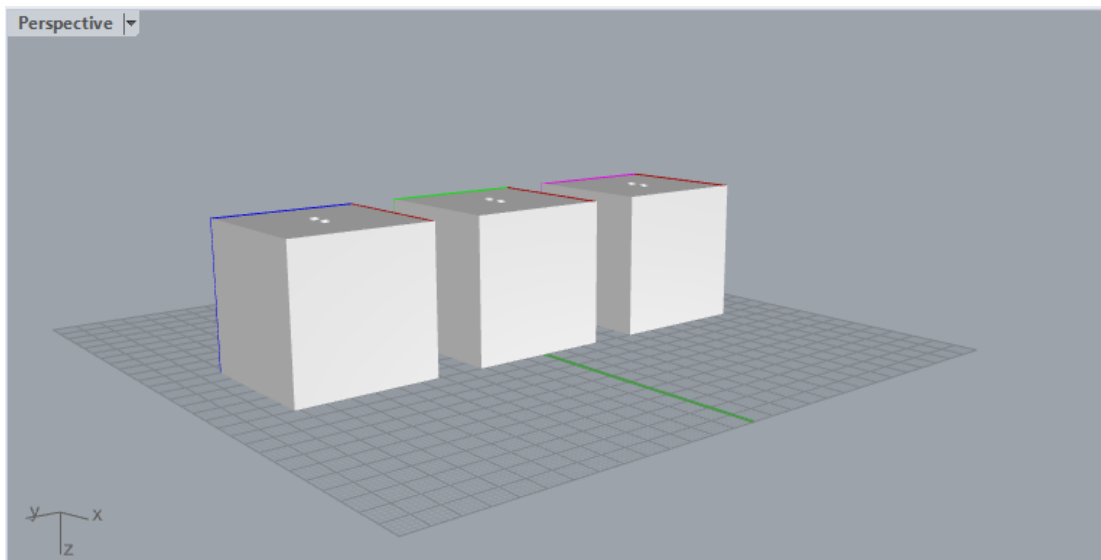


Figure 4. 16 Colored markers (M1, M2 for upper and lower bite) from the perspective viewport.

### 4.1.3 Osteotomy Lines and Drilled Holes

Osteotomy lines are the surgical guides visualized to guide user in osteotomy performance. Getting inspired from maxillofacial surgeries instructions and online videos of open surgeries [1], the cutting lines to guide multiple osteotomies (maxillary osteotomy, SSO, MASO and genioplasty) have been developed. The first step for any of the osteotomy plan is the creation of the cutting planes. Cutting planes have been created using the 'Rectangular Plane from 3 Points' command or by extruding lines,

combining the 'Polyline' or 'Single Line' or 'Curve: Interpolate Points' commands with the 'Extrude Closed Planar Curves' command. The result of this operation is meshed (Figure 4. 17), with the 'Mesh' command, and it is used to obtain the intersection curves between cutting planes and the anatomical structure to be cut, through the 'Mesh Intersect' command. The intersection curves have been reconstructed, using the 'Rebuild Curve Non-Uniform' command with a tolerance of 0.1, and the reconstructed intersection curves have been used to generate pipes with a diameter of 0.75 mm, with 'Pipe' command. The following step is the creation of the relimitation planes for any of the created pipes. Relimitation planes have been created using the 'Rectangular Plane from 3 Points' command or by extruding lines, combining the 'Polyline' or 'Single Line' or 'Curve: Interpolate Points' commands with the 'Extrude Closed Planar Curves' command. Figure 4. 18 shows the created relimitation planes.

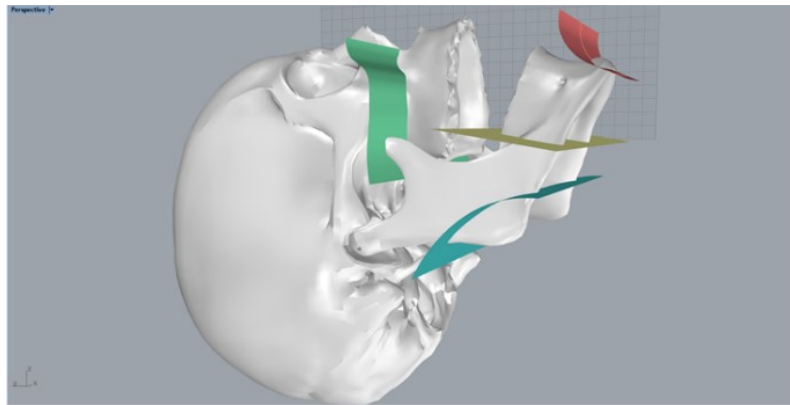


Figure 4. 17 Osteotomy cutting planes.

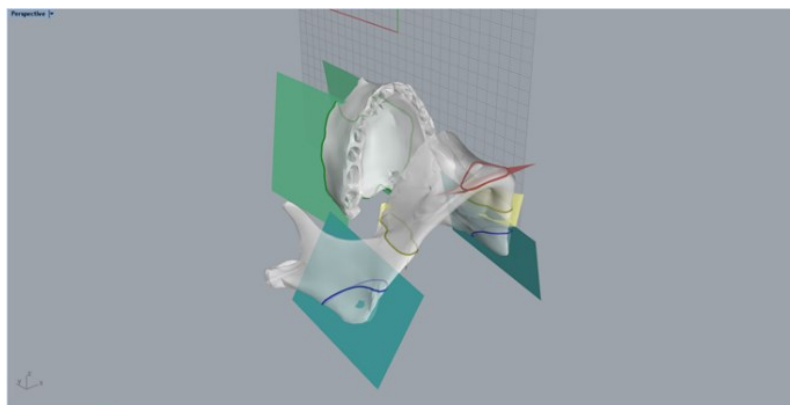
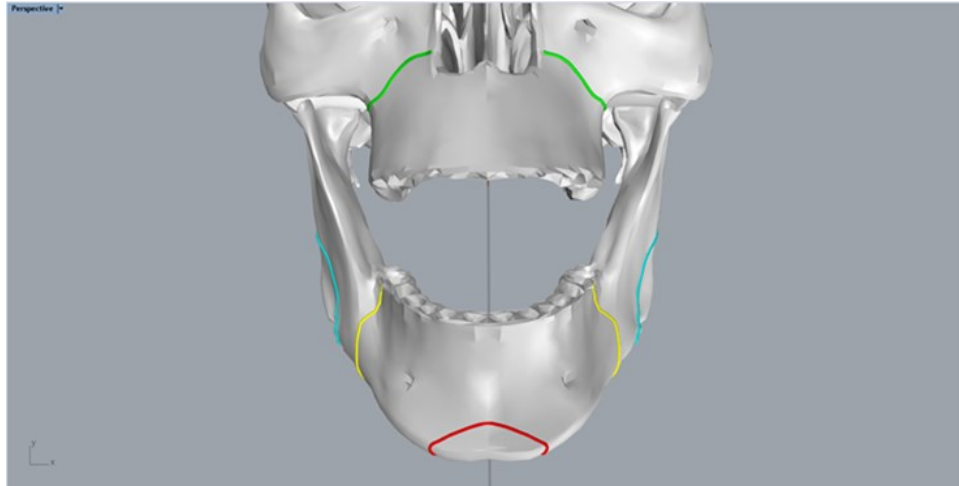


Figure 4. 18 Relimitation Planes.

Pipes generated at the previous step are then split with the relimitation planes, using the 'Split' command. Then the internal split parts of any of the pipes are removed

and the external ones are preserved. Figure 4. 19 shows the final outlook of the relimited osteotomy cutting lines. At the end, all the relimited osteotomy cutting lines are meshed with the 'Mesh' command.



*Figure 4. 19 Relimited osteotomy cutting lines.*

Drilled holes are created as cylinders with a 1.7 mm diameter, correspondent to the diameter of the screws in the Stryker manual [9], and 5 mm length (upper left/right holes) and 7 mm length (lower left/right holes) using 'Cylinder' command. Getting inspired from maxillofacial surgeries instructions and online videos of open surgeries [1] [9], cylinders are positioned below maxillary osteotomy lines. Finally, cylinders are meshed with 'Mesh' command. Figure 4. 20 shows developed drilled holes.

The virtual surgical guides are finally exported in the \*.OBJ format.

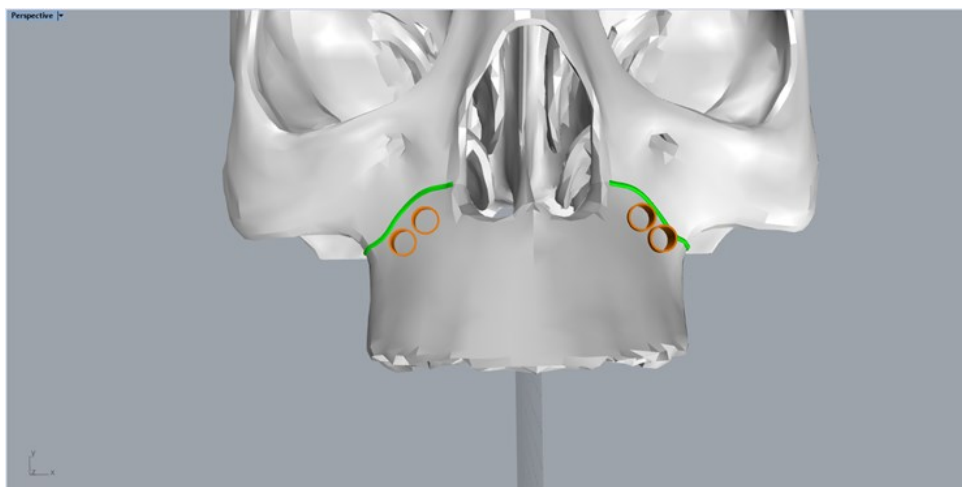


*Figure 4. 20 Drilled holes.*

#### 4.1.4 Skull Components Assembly

Mandible and upper skull must be divided in multiple components to permit the detachment of osteotomized maxillary or mandibular fragments during test and validation of the developed AR application. However, to have a multifunctional phantom that allows to work on maxilla and mandible separately or simultaneously and that suits the requirements to test the osteotomy and/or the repositioning modality of the developed AR application, a fast assembly and disassembly mechanism must be created among the components.

The basic idea is to generate assembly channels between the various components, then metallic exactly dimensioned cylinders will be placed throughout these channels allowing to easily and fast attach and detach the various components. To achieve this purpose, all the components of the phantom (osteotomized mandible fragment, rest of the mandible, osteotomized maxillary fragment and rest of the upper skull) have been split with the cutting planes generated in the development of the osteotomy cutting lines, through the 'Mesh Boolean Split' command. Possibly, split components can be open meshes, hence, to close them the 'Fill Mesh Holes' has been performed. Then, the split and close components have been dug with cylinders (2 mm diameter, 10 mm length), appropriately placed over the correspondent cutting line, through the 'Mesh Boolean Difference' command. Maxillary and mandibular osteotomized fragments have been joined, through the 'Mesh Boolean Union' command, with correspondent teeth and upper and lower bite, respectively. All the markers (M1 and the two M2s), instead, have been left as separated component to be printed. Finally, the remaining teeth of the lower dental arch have been joined to the rest of the mandible with the 'Mesh Boolean Union' command.

Moreover, to permit the assembly of mandible and upper skull, 2 cylinders (2 mm diameter, 30 mm length), placed at the condyles, have been used to dig both the mandible and the upper skull, through the 'Mesh Boolean Difference' command (Figure 4. 21). However, in this manner the mandible is still able to rotate around the condyles, hence, 2 small hooks (Figure 4. 22) have been internally added to both bites.

An elastic, clamped on these 2 structures, permit to block, and stabilize the mandible. Hooks have been generated using a curve ('Curve: Interpolate Points' command), that is piped ('Pipe: Round Caps' command) and finally meshed ('Mesh' command). Hooks are blended to the correspondent bite-osteotomized fragment complex using 'Mesh Boolean Union' command. Figure 4. 23 shows the results of this procedure.

All the components of the phantom and markers have been exported in the \*.STL and \*.VRML format, respectively, to suit the compatibility requirements for the 3D-printing machinery.

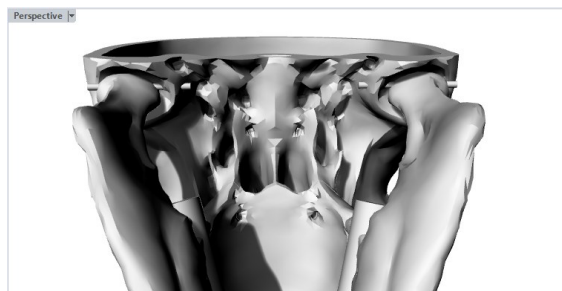


Figure 4. 21 Mandible-upper skull assembly mechanism.

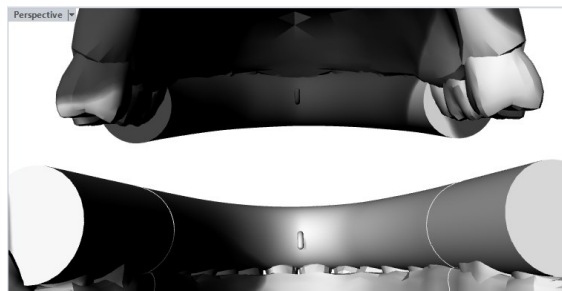


Figure 4. 22 Internal hooks of the bites for the mandible stabilization.

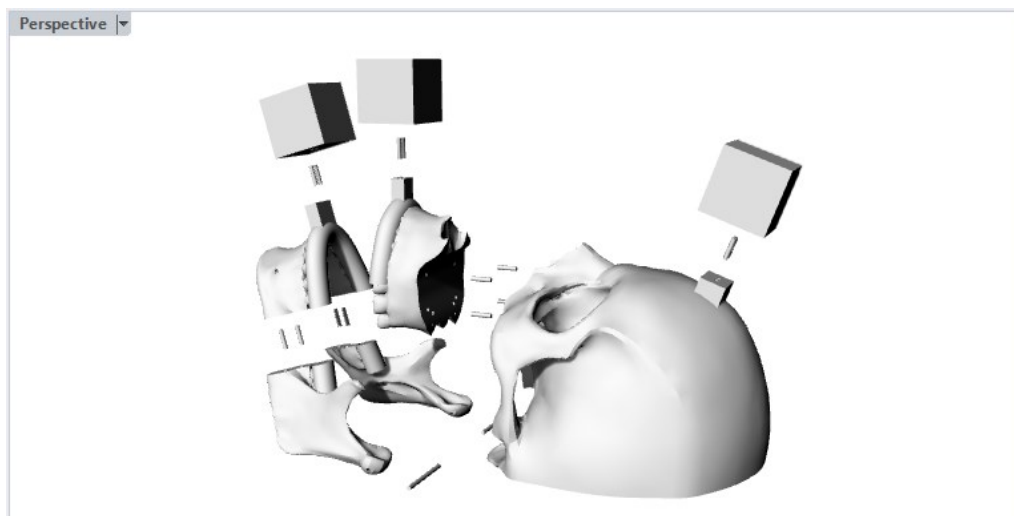


Figure 4. 23 Exploded view of the phantom from perspective viewport.

## 4.1.5 AR Application Settings

### 4.1.5.1 Scene Completion

The \*.OBJ file of the virtual contents (maxillary osteotomy lines and drilled holes) have been dragged and dropped in the 'Assets'. Object model, rig, animation and material can be now modified from the inspector of the files imported in the 'Assets' panel as described in the previous section. Virtual surgical guides can be assigned to as child of marker M2, as described in the previous section.

Figure 4. 25 shows the final outlook of the scene without the Near Menu and when the multi-target M2 has been hidden. Hence, Figure 4. 24 shows the outlook of M1-related scene. Figure 4. 25, vice versa, the final outlook of the scene without the Near Menu and when the multi-target M1 has been hidden. Hence, Figure 4. 25 shows the outlook of M2-related scene. Finally, Figure 4. 26 shows the Near Menu, already presented in the previous section.

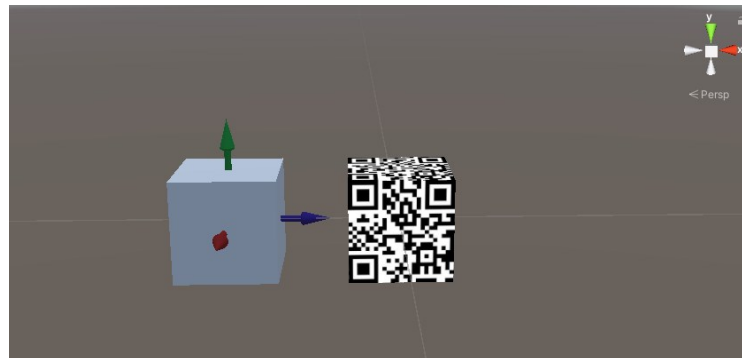


Figure 4. 24 Final outlook of the M1-related Unity scene.

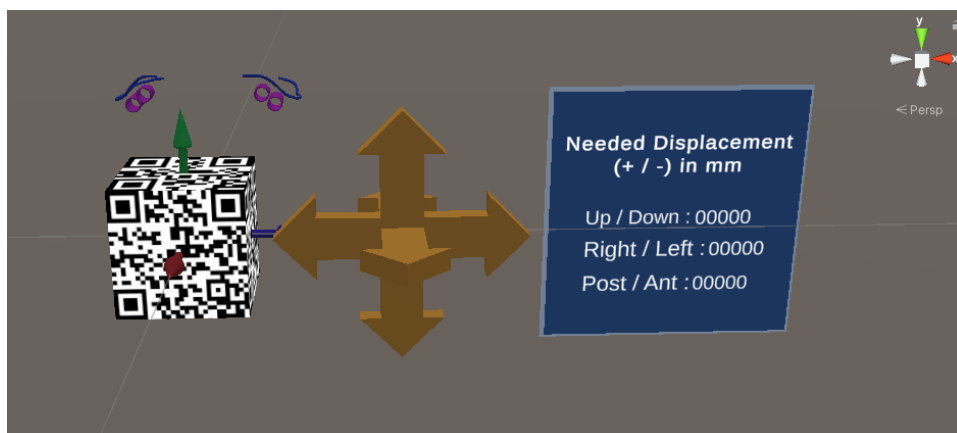


Figure 4. 25 Final outlook of the M2-related Unity scene.



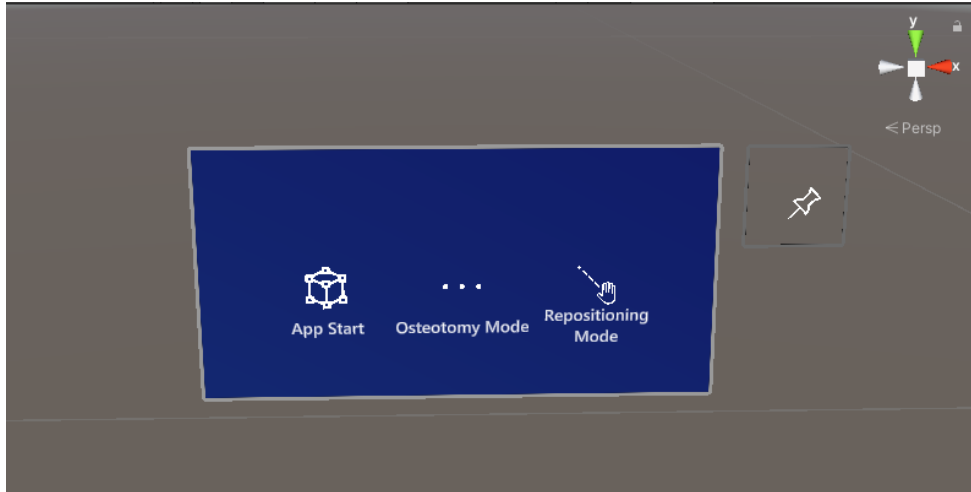


Figure 4. 26 Outlook of the NearMenu.

Finally, 'On Click' component of the Near Menu has been completed by inserting the game objects of osteotomy lines and drilled holes as described in previous section.

#### 4.1.5.2 Script Inputs Assignment

From the Unity interface the user can adjust the preoperative plan as expected by the case study employed in this thesis. Figure 4. 27 shows the input assignment for the 'TargetPosition\_Creation' script.

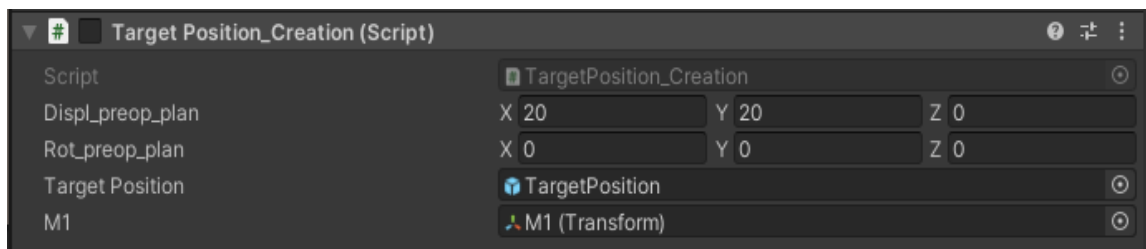


Figure 4. 27 Input assignment in the 'TargetPosition\_Creation' script.

#### 4.1.5.3 Build, Compilation and Distribution

At the end, scene and whole project are saved, the build is created and the solution (.sln file), has been opened. After adjusting these settings as described in the previous section and connecting the target device (Microsoft HoloLens V2) to the PC, the solution is compiled and distributed. At the end of this procedure the application will be available on the HMD and can be launched.

## 4.2 3D-Printing of Skull Phantom

As already anticipated in previous sections, ZPrinter 450 has been employed for 3D-printing of skull phantom. Moreover, material used for the 3D-printing process of any of the components is a high-performance mixture powder containing calcium sulfate hemihydrate combined with a binder, a solution dispensed through the print head and applied to the powder. After printing is finished, a drying cycle occurs to add strength to the parts and it is followed by a cleaning process, that removes the un-sintered powder, and the post-processing phase performed using an infiltrant, which soaks into the part and bonds the printed powder together to give more durability.

The process is guided by imported CAD model that has been appositely exported with the \*.STL format (skull assembly components) and \*.VRML format (marker cubes) from Rhinoceros 6 and the object disposition on the printing plate has been optimized to minimize powder wastes and reduce failure probability. The whole printing process lasts 9 hours and 20 minutes for the skull assembly components and 1 hour and 20 minutes for the colored markers. Figure 4. 28, Figure 4. 29 and Figure 4. 30 show the final outlook of the 3D-printed phantom in the dis-assembled and assembled configuration respectively.

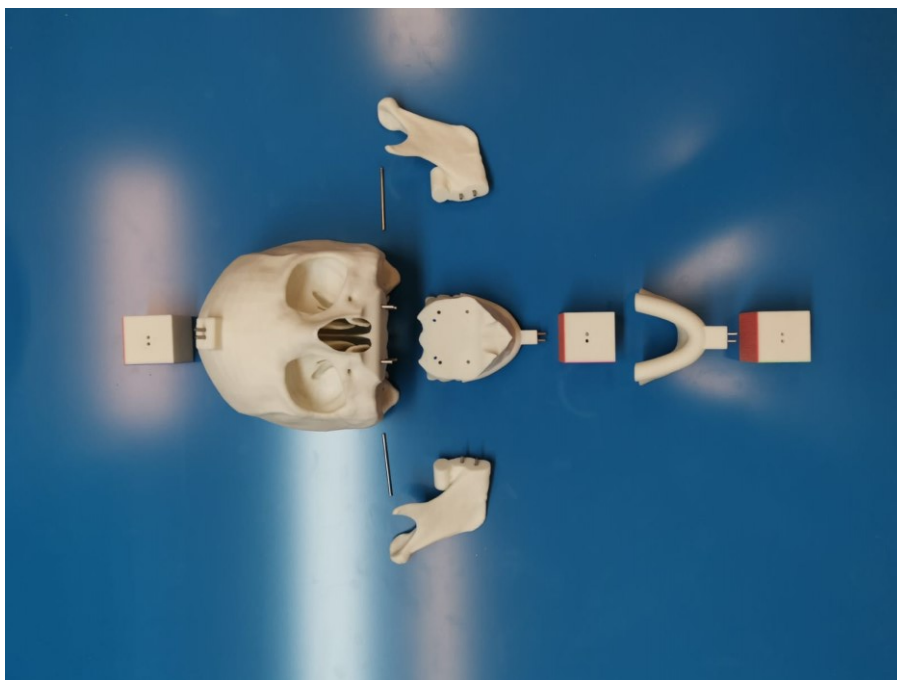


*Figure 4. 28 Dis-assembled 3D-printed skull phantom.*

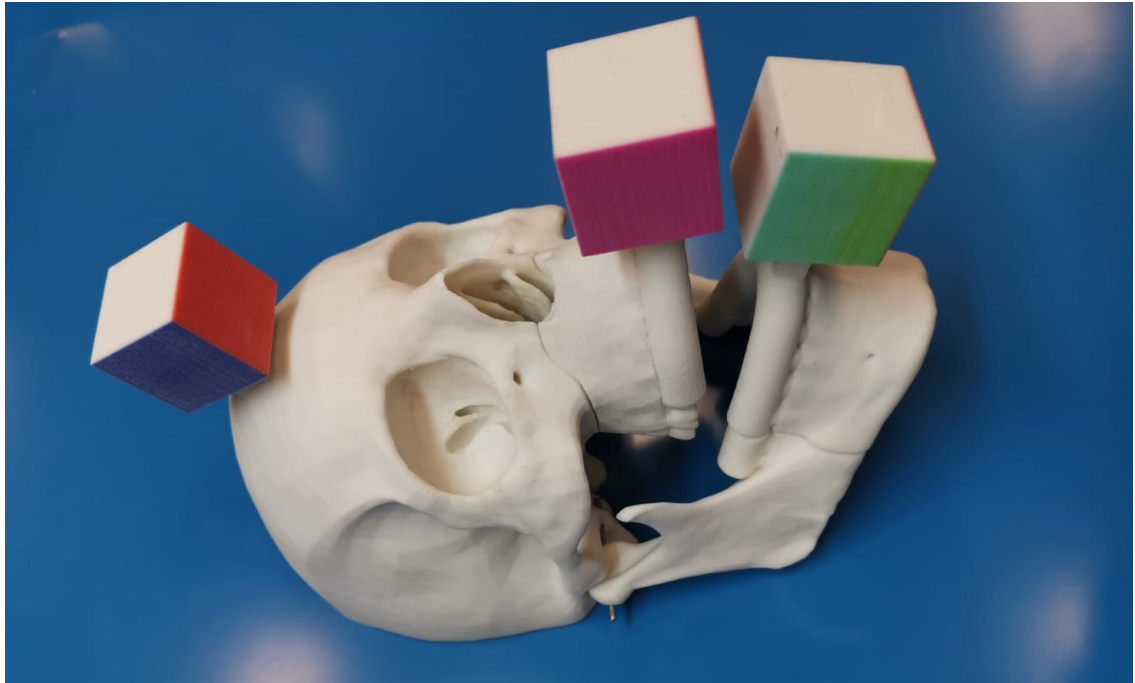


*Figure 4. 29 Assembled 3D-printed skull phantom.*

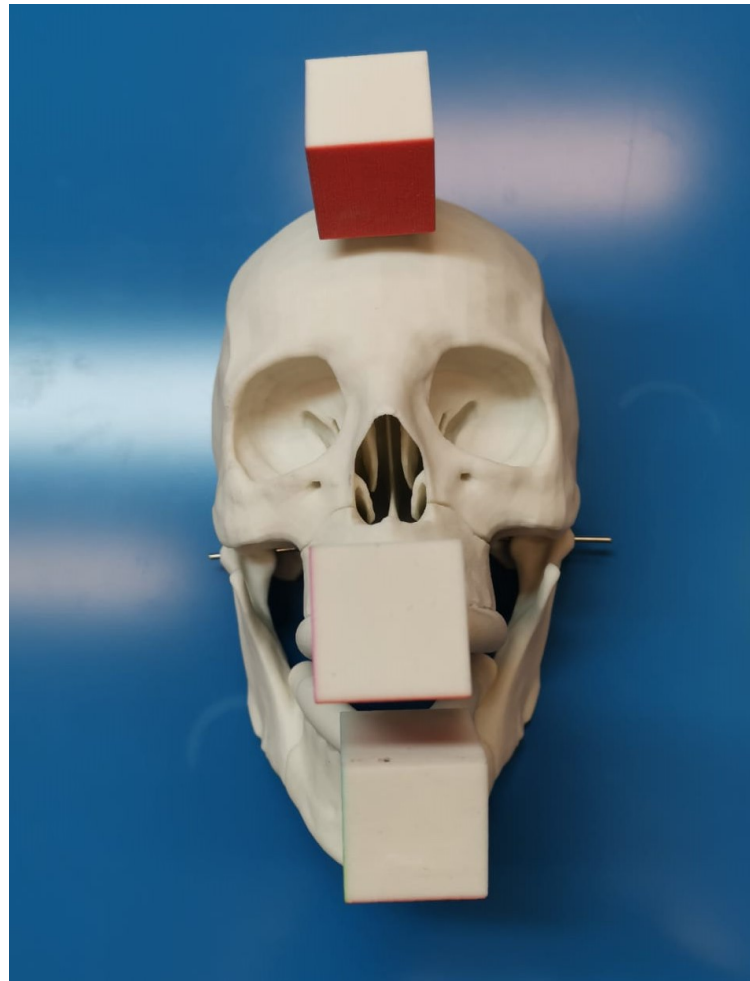


*Figure 4. 30 Assembled 3D-printed skull phantom.*

Markers have been 3D-printed as colored components. However, it must be noticed that accuracy of 3D-printing textures over marker with CJP does not guarantee an appropriate accuracy. Hence, QR codes cannot be directly applied on the marker surfaces reaching an optimal texture quality to fulfill the AR application requirements. Thus, to solve this problem, QR codes have been applied on 3D-printed markers using bi-adhesive tape. Figure 4. 31 show the final outlook of the assembled skull phantom with attached QR codes on M1 and M2. It must be marked that Multi Jet Fusion technology, on the contrary, can be the perspective technology to be employed directly embedding QR codes textures on marker surfaces.



*Figure 4. 31 3D-printed phantom with QR codes attached on markers.*

Finally, for the purposes of this thesis, uniquely maxilla and upper skull will be employed. Figure 4.32 and Figure 4.33 respectively show the outlook of dis-assembled and assembled model employed during test and validation, with QR codes applied.

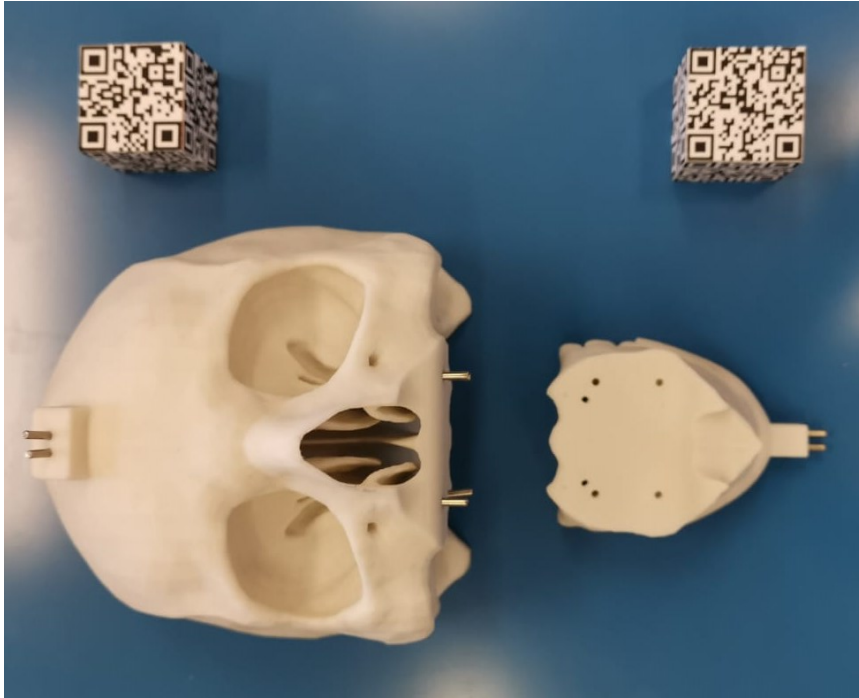


*Figure 4. 32 Dis-assembled model employed during tests and validation.*



*Figure 4. 33 Assembled model employed during tests and validation.*

## 4.3 AR Application Outlook

In this section, some frames are reported regarding an experimental session performed at the end of the AR application development.

These frames allow to understand the global functioning and outlook of the developed AR application launched on Microsoft HoloLens V2 and tested on 3D-printed phantom that has been described in previous section.

Figure 4. 34 shows the real scene augmented with virtual contents associated to both markers M1 and M2. Figure 4. 35 illustrates the outlook of the Near Menu in the real scene where it is positioned with hand-gesture by the user. In fact, the Near Menu basically follows user in its motion, but it can be moved and scaled by user through pinching gesture and then fixed with the pin button. Figure 4. 36 shows the augmented scene after user clicked the 'App Start' button and thus, where the cube hologram has been positioned and oriented according to pre-operative plan and associated as child of M1. Figure 4. 37 illustrates the outlook of Osteotomy Mode, in which the application is switched after user clicked the 'Osteotomy Mode' button. Last two figures of this section show the outlook of Repositioning Mode, in which the application is switched after user clicked the 'Repositioning Mode' button. Figure 4. 38 illustrates the situation in which M2 has not already reached target pose, Figure 4. 39, vice versa, reports the situation in which M2 has reached target pose.

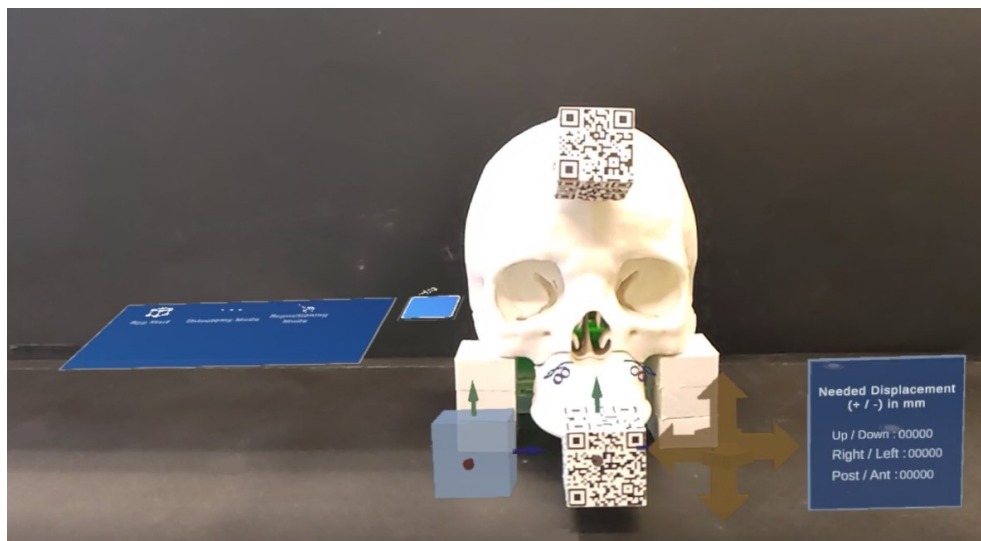


Figure 4. 34 Initial outlook of augmented scene.



Figure 4. 35 Outlook of the Near Menu in the augmented scene.

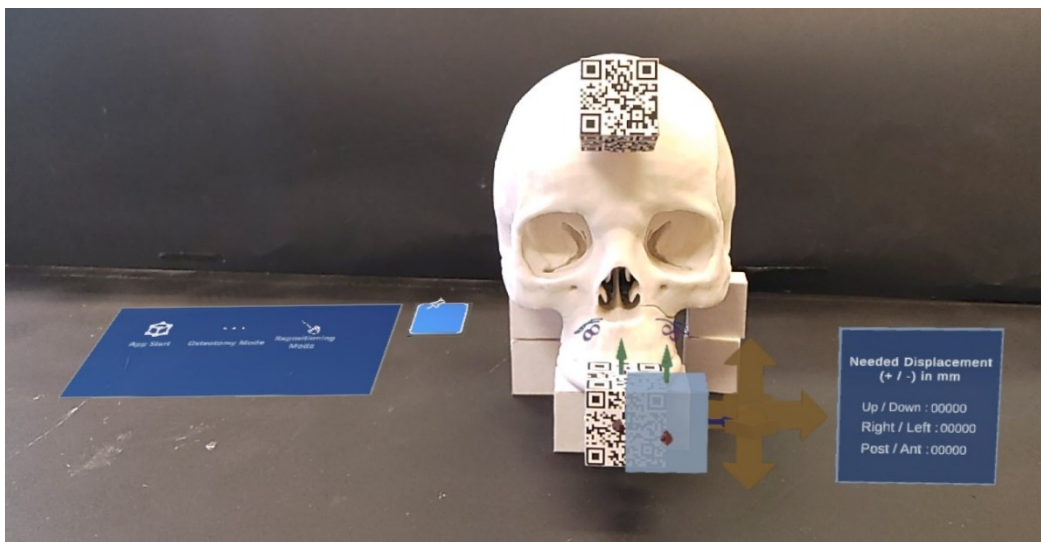


Figure 4. 36 Outlook of augmented scene after clicking 'App Start' button.

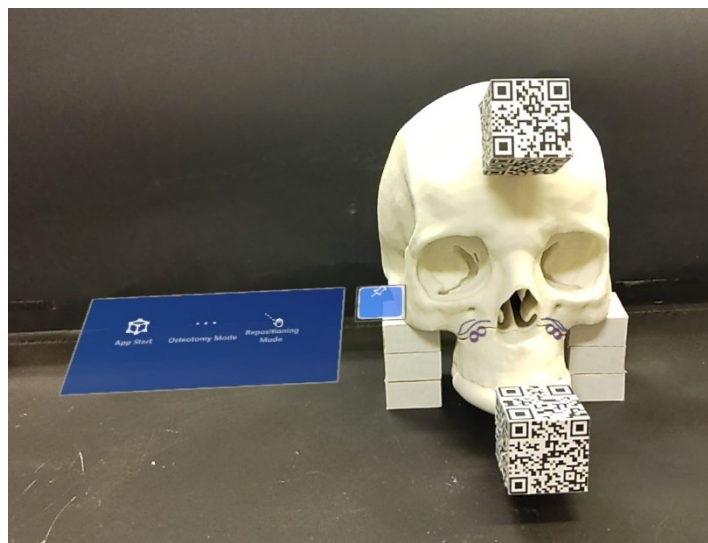


Figure 4. 37 Outlook of augmented scene after clicking 'Osteotomy Mode' button.

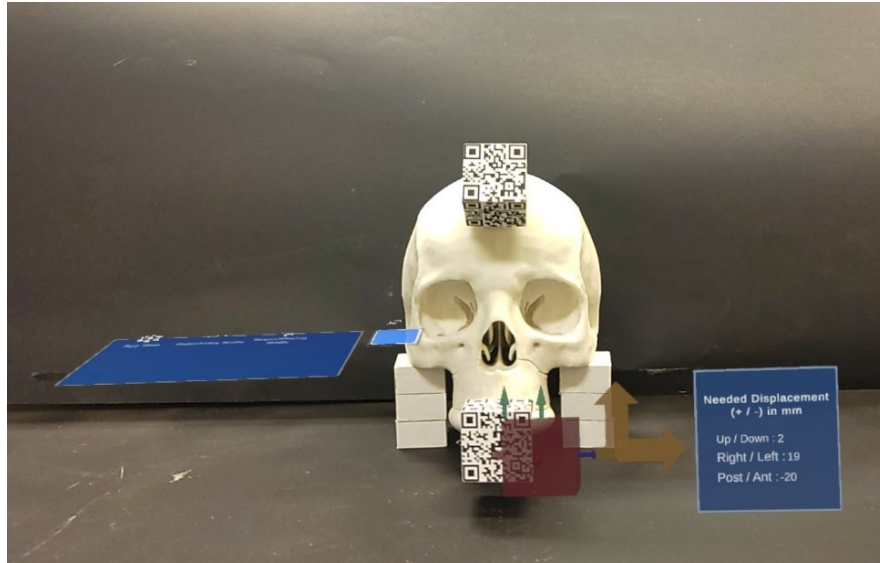


Figure 4. 38 Outlook of augmented scene after clicking 'Repositioning Mode' button.

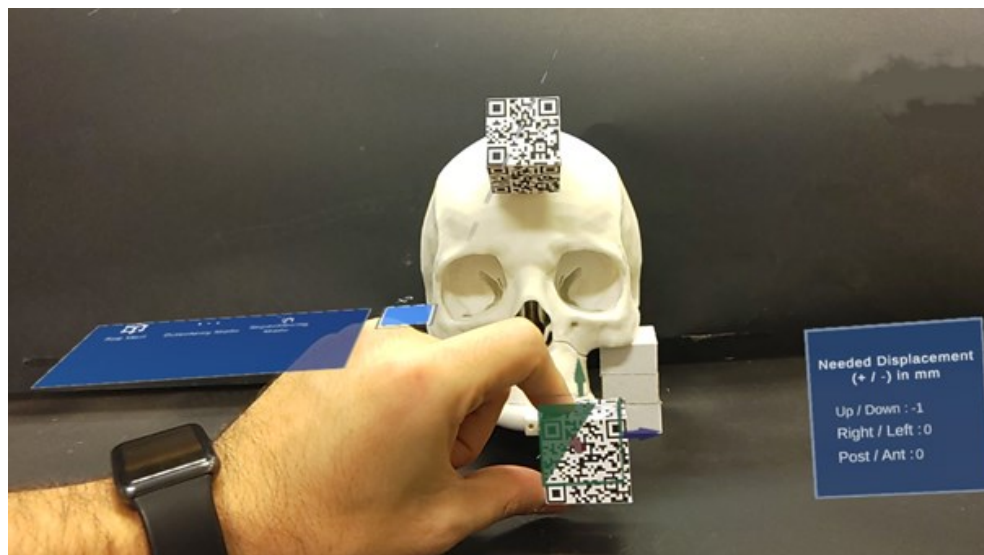


Figure 4. 39 Outlook of augmented scene after M2 has been repositioned.

## 4.4 Test

Once the application has been deployed on the Microsoft HoloLens V2 HMD and the skull phantom has been 3D-printed, the test phase starts.

To test the developed AR application 3 people have been selected. First user (U01) was a PhD researcher with familiarity with AR technology, second user (U02) was a university professor with a lower familiarity with AR technology, and third user (U03) was a student just introduced on the AR technology.



Both Osteotomy Mode and Repositioning Mode need to be tested. Hence users were asked to fulfil two different tasks. Before tasks has been performed each user is asked to perform ocular calibration by following the path 'Menu → Impostazioni → Sistema → Calibrazione → Esegui Calibrazione Oculare' directly on the HoloLens device.

First task aims to test Osteotomy Mode. Before the task the skull phantom has been assembled and the assembling interfaces has been covered with gummed paper tape. Then, user is asked to wear HoloLens device, to look at the dental multi-target (M2) to understand that the app was correctly launched, to select through the apposite menu the Osteotomy Mode and then by mean of a pencil and guided by the visualized surgical guides (osteotomy lines and drilled holes) to trace first the cutting lines over the phantom and then 4 points that stand for the drilled holes for the final fixation of the osteotomized fragment. A unique trial for each of the users have been performed. Since none of the participants had experience in the medical field also time has been recorded. Figure 4. 40, Figure 4. 41 and Figure 4. 42 show this task.



*Figure 4. 40 Osteotomy task, cutting lines performance.*



*Figure 4. 41 Osteotomy task, drilled holes performance.*



*Figure 4. 42 Osteotomy task.*

Second task aims to test Repositioning Mode. To perform this task the graph paper has been used. Moreover, uniquely the dental marker (M2) has been moved over it to reach target position, this choice is coherent since M2 then will be solidly attached on the osteotomized fragment and prevent from the management of a cumbersome structure such as the marker-osteotomized fragment complex. Furthermore, the second or cranial marker (M1) has been assembled on the skull and it has been arbitrarily positioned to give user the possibility to simultaneously visualize both markers. Even though, this solution limits translations on mediolateral and anteroposterior axes and orientation on the vertical axis, this remains a valid alternative to preliminary test and evaluate the developed AR application. As first, M2 and M1 are positioned over the graph paper, then M2 position is marked and its centroid on the paper sheet is extracted, marked, and used to define and mark, at the end of the test, the target position that M2 centroid is aimed to reach. Then, user is asked to wear HoloLens device, to look at both multi-targets (M1 and M2) to understand that the app was correctly launched, to start the app by clicking the 'App Start' button, to select the 'Repositioning Mode' by clicking the appropriate button on the menu and then to manually position M2 guided by the elements of the repositioning feedback. At the end of the task, the final M2 position is marked, and its centroid is extracted and marked. Since none of the participants had experience in the medical field also time has been recorded. Figure 4. 43 and Figure 4. 44 shows this task.

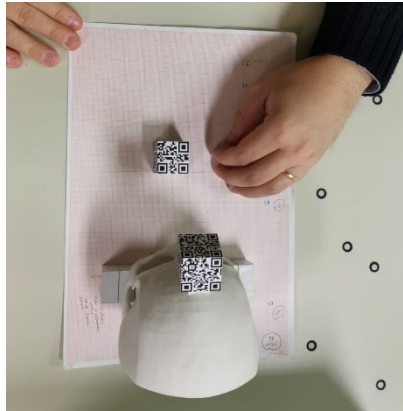


*Figure 4. 43 Repositioning task.*



*Figure 4. 44 Repositioning task.*

## **4.5 Validation**

To assess app precision in both tasks a validation method must be employed.

For osteotomy task validation, the aim is to compare the experimental cutting lines and drilled holes drawn by users over the skull phantom with the nominal cutting lines and drilled holes, to extract at the end the deviations. To fulfil the validation, the tested phantom must be scanned and then the scans must be processed to obtain a textured CAD file over which the drawn cutting lines and drilled holes are visible and can be reconstructed. Experimental and nominal geometries (cutting lines and drilled holes) have been reconstructed on Rhinoceros 6 while CloudCompare has been used to perform the comparison and extract deviations in terms of millimeters.

First step of the Osteotomy task validation consists of scanning phase. As first the Go!Scan3D is handled by user and it is employed to perform calibration and establish the reference plane. Reference plane is a white table that has been appositely prepared by attaching multiple small circular adhesive markers. The tested skull phantom has been positioned on the reference plane. Before starting the scanning session, the parameter 'Metodo di Posizionamento' must be set to 'Target/Geometria' and the 'Resolution' parameter must be set to '0.50 mm' on the scanner dedicated software. Then, the Go!Scan3D device is handled and moved around the phantom to acquire the geometry from multiple views. The scanner gives a green light feedback if the distance between it and the object is right otherwise it gives a red-light feedback. Simultaneously on the pc, using the scanner dedicated software, appears the scanned object with its texture. The acquired scan is then processed to remove noise and unnecessary points and finally it is exported in the \*.VRML format to keep texture information. Figure 4. 45 shows the outlook of a scanned geometry.

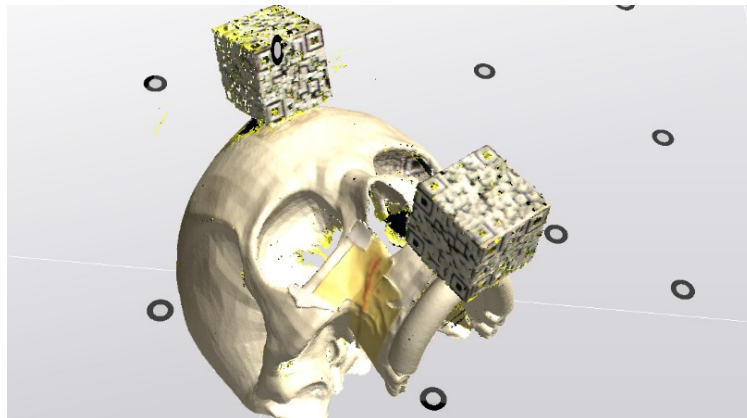


Figure 4. 45 Scanned geometry visualized in the dedicated software of Go!Scan3D.

Then, the second phase consists of the reconstruction of the experimental cutting lines and drilled holes starting from the \*.VRML file just exported. Figure 4. 46 shows the outlook of the \*.VRML file imported in Rhinoceros 6. Then, to reconstruct cutting lines a cloud of points is created through the 'Multiple Points' command and using the 'Vertex' snap the mesh vertexes within the visible experimental cutting line are selected, an interpolating line is created through the 'Polyline Through Points' command and it is rebuilt with the 'Rebuild Curve Non-Uniform', setting the tolerance

to 0.1. Rebuilt lines are piped with the 'Pipe' command by setting the radius to 0.375 mm and finally meshed with the 'Mesh' command. Figure 4. 47 shows the final outlook of reconstructed experimental cutting lines. To reconstruct drilled holes, points are created through the 'Multiple Points' command, using the 'Vertex' snap and selecting mesh vertexes within the visible marked points. Then, spheres centered on these points and with a radius of 0.25 mm are generated with the 'Sphere: Center Radius' command and finally meshed with the 'Mesh' command. Figure 4. 47 shows the final outlook of reconstructed experimental drilled holes. Finally, experimental cutting lines, experimental drilled holes and the scanned skull are separately exported as \*.STL files to be then imported and managed in the CloudCompare software.

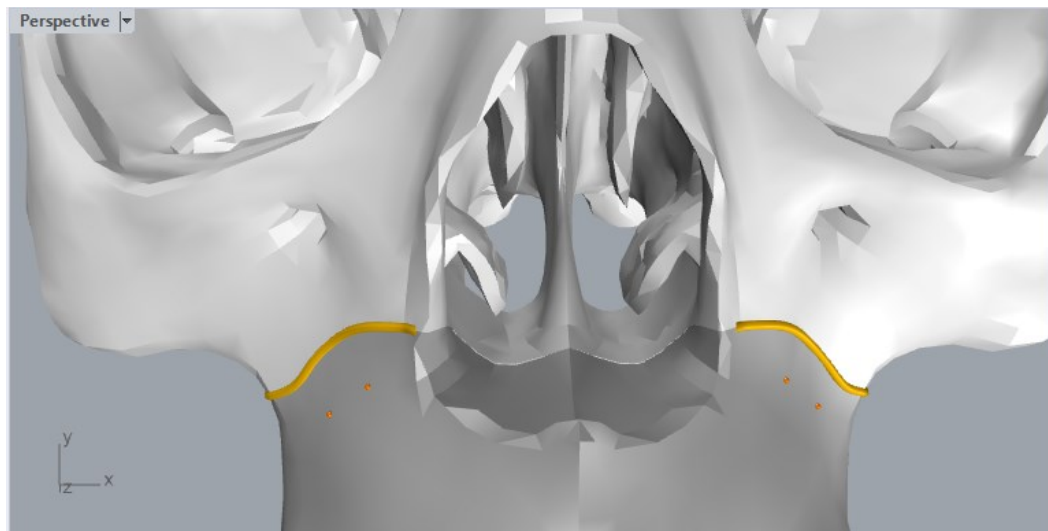


Figure 4. 46 Scanned geometry opened in Rhinoceros 6.



Figure 4. 47 Reconstructed experimental cutting lines and drilled holes.

To be able to perform the comparison also nominal curves must be imported in CloudCompare. Before exporting them, drilled holes must be created in a suitable manner to be compared then with experimental ones. Hence, as first the frontal and back circumferences of the designed cylinders are constructed using the 'Circle: 3 Points' command and the center of both has been marked with a point using the 'Center' snap and 'Multiple Points' commands. These two centers have been used to reconstruct the cylinder axis through the 'Single Line' command. Then, the 'MeshToNURBS' command has been used to convert the maxilla fragment from mesh to NURBS and then to use the converted element with the cylinder axis in the 'Intersect' command to determine the intersection point. Finally, the 'Sphere: Center Radius' has been used to create on the intersection point a sphere with a radius of 0.25 mm that is finally meshed with the 'Mesh' command. Figure 4. 48 shows the final outlook of the nominal cutting lines and drilled holes. Finally, nominal cutting lines, experimental drilled holes and the skull model are separately exported as \*.STL files to be then imported in CloudCompare.



*Figure 4. 48 Nominal cutting lines and drilled holes.*

All the \*.STL files of the nominal and experimental geometries have been imported in CloudCompare by drag and drop of them from folders to CloudCompare main window. To make clear the geometries management, by following the path 'Edit → Colors → Set Unique' the visualization color can be set to yellow for nominal

geometries and to red for the experimental ones. Figure 4. 49 shows imported nominal and experimental geometries.

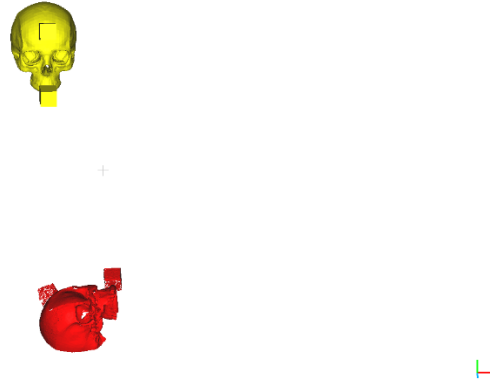


Figure 4. 49 Imported nominal (yellow) and experimental (yellow) geometries).

Before starting the comparison nominal and experimental geometries must be aligned. To perform the alignment some reference points of the nominal geometry can be sampled and used as reference within an automatic algorithm of the software that allows the match or alignment of the same points sampled on experimental geometry with these reference samples. To perform this operation, experimental cutting lines, drilled holes and scanned skull must be selected together with nominal skull and by using the command 'Align Two Clouds by Picking Equivalent Points' the sampling process can be initiated. Before initiating the sampling process, it must be stated which are the geometries to be aligned and which are the one to be set as reference. Experimental geometries must be highlighted (experimental cutting lines, drilled holes and the scanned skull) to be selected as geometries to be aligned and then the remaining geometry will be accounted as reference (nominal skull model). Then, the sampling process starts. First, points must be manually sampled on the geometry to be aligned (red one or experimental geometry), as shown in Figure 4. 50, and then the same points must be manually sampled on reference geometry (yellow one or nominal geometry), as shown in Figure 4. 51. The 'Align' button then can be clicked and it starts the algorithm for the alignment of the two sets of geometries. Figure 4. 52 shows the result of the alignment procedure. Figure 4. 53 shows the detail of cutting lines and drilled holes after alignment has been performed.

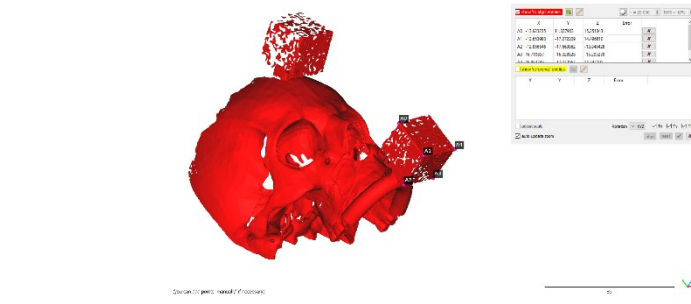


Figure 4. 50 Sampled points on experimental geometry for the alignment.

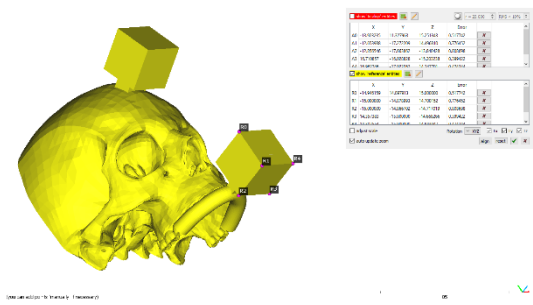


Figure 4. 51 Sampled points on nominal geometry for the alignment.

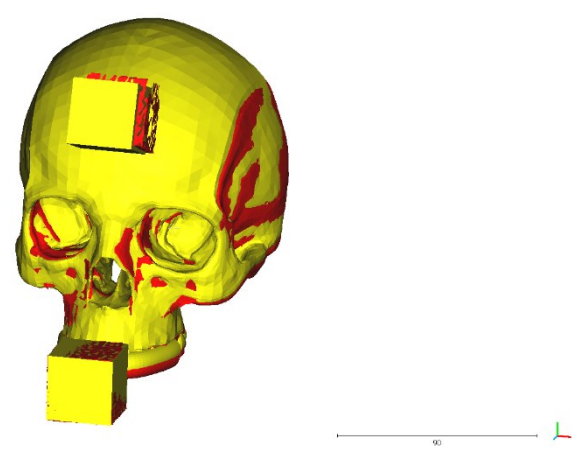


Figure 4. 52 Aligned experimental and nominal geometries.

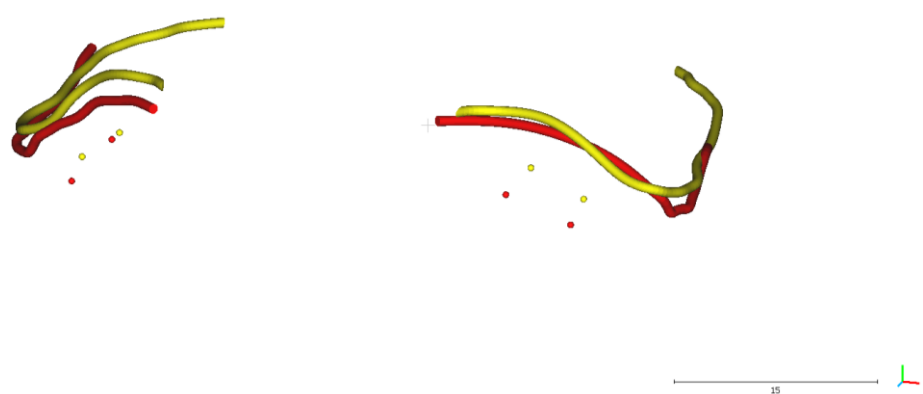


Figure 4. 53 Cutting lines and drilled holes after alignment.



Finally, the comparison can be performed by selecting the experimental geometries (i.e., cutting lines of User01 or drilled holes of User02) and the nominal geometries (i.e., nominal cutting lines or nominal drilled holes) in that order and using the 'Compute Cloud/Mesh Distance'. The 'Max Distance' has been set to 10 mm, the 'Signed Distance' has been unchecked and the 'Compute' button is clicked to start the comparison. At this point, all the results that will be described in the following section are available by selecting the compared experimental geometry and can be easily exported as images or files to be used and processed in specific environments such as Microsoft Excel.

For repositioning task validation, the aim is to compare the M2 centroid position reached with the aid of the AR application with the target one, both measured on graph paper, and extract the linear absolute deviations on anteroposterior and mediolateral axes and angular absolute deviations around the vertical axes. The deviations have been calculated directly on paper graph using rulers and goniometers.

## 5 Results

Results must be extracted and analyzed to complete the test and validation phase of the developed AR application in both the osteotomy and repositioning tasks.

For the osteotomy tasks results have been extracted from CloudCompare. Here, we can easily and fast extract absolute or non-signed deviations and approximated distances through the procedure that has been illustrated in the previous section. In detail, both drilled holes and cutting lines deviations needs to be reported. For the analysis of the drilled holes the average approximated distance with its standard deviation, the maximum and minimum approximated distances are reported for the unique trial performed by any of the selected users. In detail, the ‘Compute Cloud/mesh Distance’ command has been used by selecting experimental drilled holes first and nominal ones then to extract these results. U01-OST1\_DH indicates the trial performed by first user and in detail drilled holes drawing task, U02-OST1\_DH indicates the trial performed by second user and in detail drilled holes drawing task and U03-OST1\_DH indicates the trial performed by third user and in detail drilled holes drawing task. Table 5. 1 reports all the selected results for these three sessions. The mean approximated distance of the 3 trials was 1.17111 mm.

*Table 5. 1 Approximated distances of the drilled holes in the three osteotomy tasks.*

<b>Trial</b>	<b>Average Approximated Distance ± Standard Deviation (mm)</b>	<b>Maximum Approximated Distance (mm)</b>	<b>Minimum Approximated Distance (mm)</b>
<b>U01-OST1_DH</b>	1.47882 ± 1.03058	2.89438	0
<b>U02-OST1_DH</b>	1.43862 ± 0.72431	2.74959	0.298235
<b>U03-OST1_DH</b>	0.59590 ± 0.32966	1.32428	0

For the analysis of the osteotomy cutting lines the parameters relative to approximated distances have been computed, the cloud-to-mesh absolute distances have been extracted together with the Weibull function and the data regarding

samples distribution with respect to deviation values have been used to generate cumulative distribution function and calculate 75% percentile for the unique trial performed by any of selected users. In detail, the ‘Compute Cloud/mesh Distance’ command has been used by selecting experimental cutting lines first and nominal ones then to extract these results. Then parameters such as average approximated distance, standard deviation, maximum and minimum distances are directly available after the computation of this command has been performed. Weibull graph can be obtained, superimposed to the histogram of the cloud-to-mesh absolute distance, by using the ‘Fits A Statistical Model on The Active Scalar Field’ command and from the opened window the \*.CSV file containing all the data regarding samples distribution with respect to deviations can be exported. These data can be then used in Microsoft Excel to generate the cumulative distribution function and extract the 75% percentile. U01-OST1\_CL indicates the trial performed by first user and in detail cutting lines drawing task, U02-OST1\_CL indicates the trial performed by second user and in detail cutting lines drawing task and U03-OST1\_CL indicates the trial performed by third user and in detail cutting lines drawing task. Table 5. 2 reports average approximated distance with its standard deviation, maximum and minimum distances for any of 3 sessions. The mean approximated distance of the 3 trials is 0.93763 mm.

*Table 5. 2 Approximated distances of the cutting lines in the three osteotomy tasks.*

<b>Trial</b>	<b>Average Approximated Distance ± Standard Deviation (mm)</b>	<b>Maximum Approximated Distance (mm)</b>	<b>Minimum Approximated Distance (mm)</b>
<b>U01-OST1_CL</b>	0.80984 ± 0.48505	2.23420	0
<b>U02-OST1_CL</b>	1.08007 ± 0.50814	2.63215	0
<b>U03-OST1_CL</b>	0.92297 ± 0.61294	2.99419	0

Below, then, are reported images regarding cloud-to-mesh absolute distance with a color scale appositely created within CloudCompare. It is composed by 3 levels, first level is green that correspond to the lowest value, third level is red that correspond to

the highest value and finally middle value is associated to the yellow color. In detail, following pictures reports cloud-to-mesh absolute distance mapping over drawn cutting lines, cloud-to-mesh absolute distance histogram with superimposed the Weibull distribution function, the cumulative distribution function for any of the three sessions. It must be remarked the theoretical background of these results to better understand the. Cloud-to-mesh absolute distance means the absolute distance between a selected cloud of points and a selected mesh, its histogram reports the number of samples with respect to deviation values, Weibull distribution function is a continuous probability distribution that can fit an extensive range of distribution shapes and the 75% percentile is a value such that 75% of sorted data is lower or equal to itself. Figure 5. 1, Figure 5. 2, Figure 5. 3, Figure 5. 4, and Figure 5. 5 show results of U01-OST\_CL session. Figure 5. 6, Figure 5. 7, Figure 5. 8, Figure 5. 9, and Figure 5. 10 show results of U02-OST\_CL session. Figure 5. 11, Figure 5. 12, Figure 5. 13, Figure 5. 14, and Figure 5. 15 show results of U03-OST\_CL session. Table 5. 3 reports 75% percentile for any of 3 sessions. The mean 75% percentile of the 3 trials is 1.24342 mm.

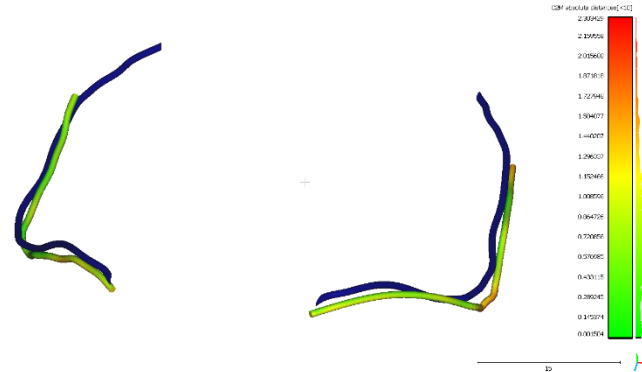


Figure 5. 1 User 01 mapping of cloud-to-mesh absolute distance and nominal (blue) lines.

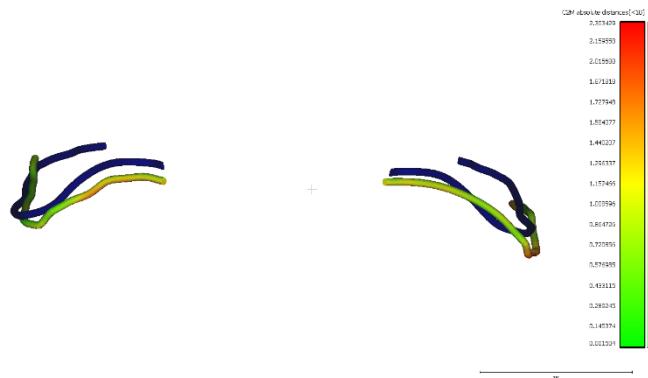


Figure 5. 2 User 01 mapping of cloud-to-mesh absolute distance and nominal (blue) lines.

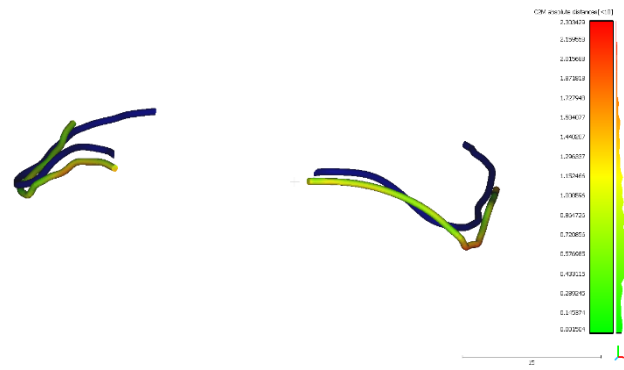


Figure 5.3 User 01 mapping of cloud-to-mesh absolute distance and nominal (blue) lines.

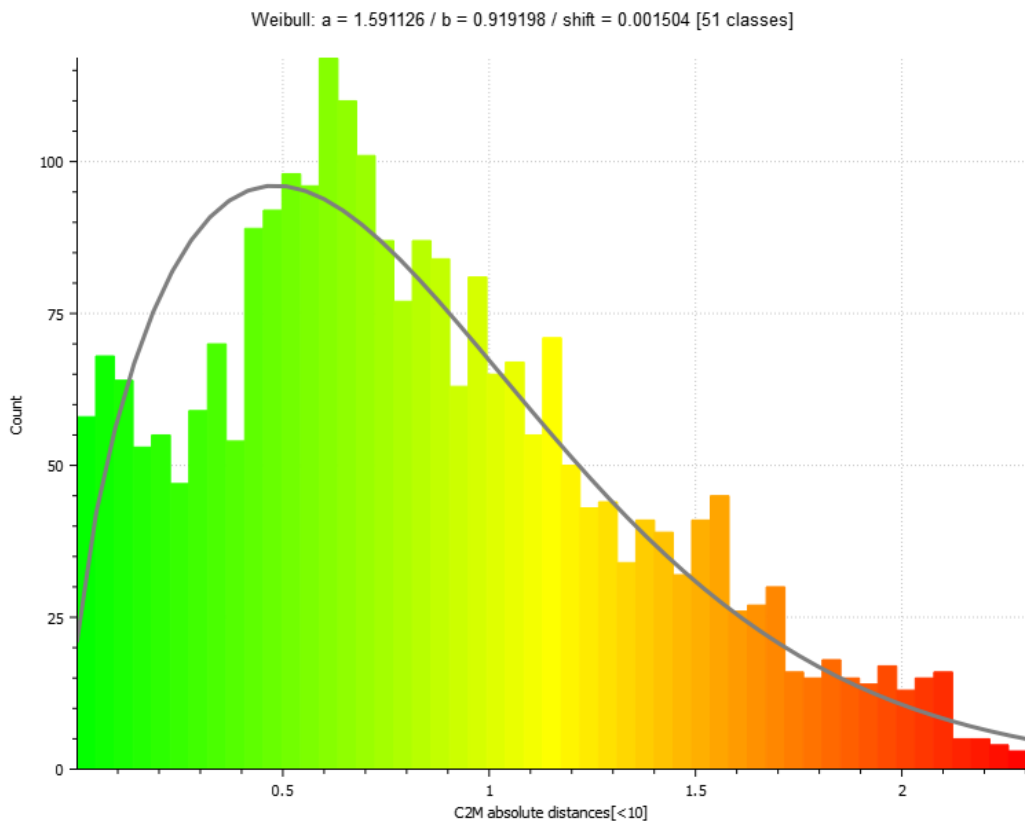


Figure 5.4 User 01 cloud-to-mesh absolute distance histogram and Weibull function.

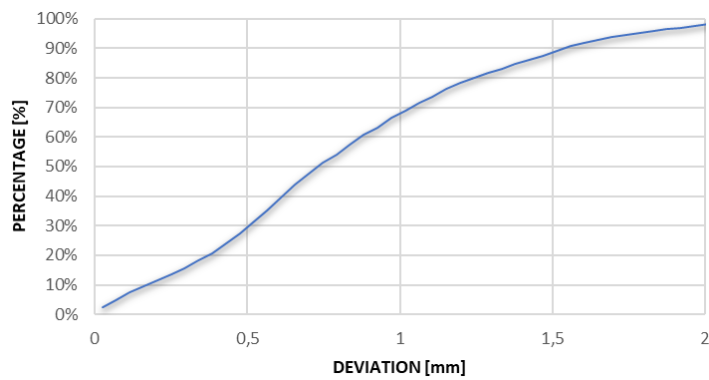


Figure 5.5 User 01 cumulative distribution function.

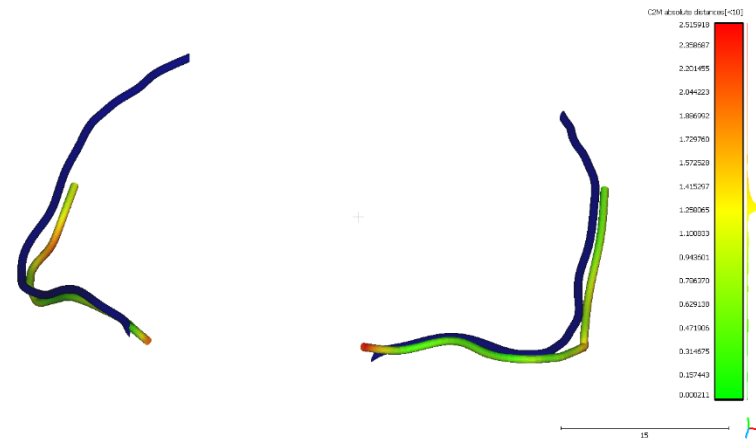


Figure 5. 6 User 02 mapping of cloud-to-mesh absolute distance and nominal (blue) lines.

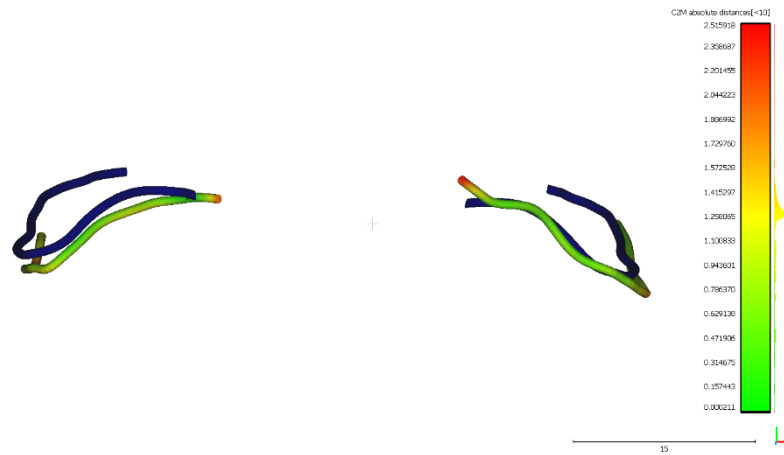


Figure 5. 7 User 02 mapping of cloud-to-mesh absolute distance and nominal (blue) lines.

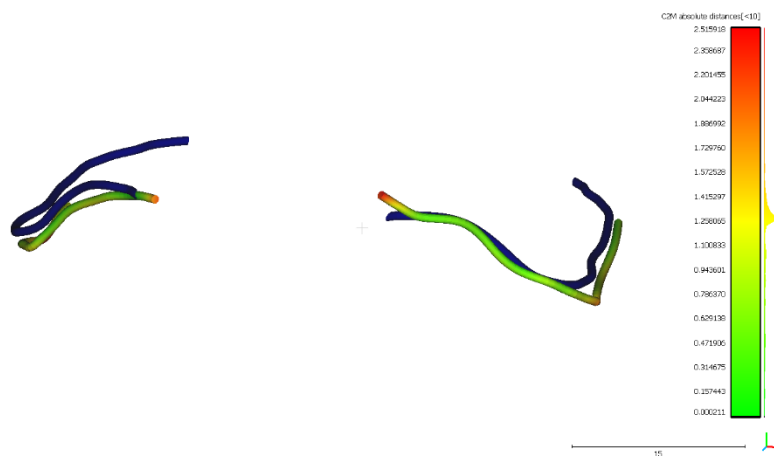


Figure 5. 8 User 02 mapping of cloud-to-mesh absolute distance and nominal (blue) lines.

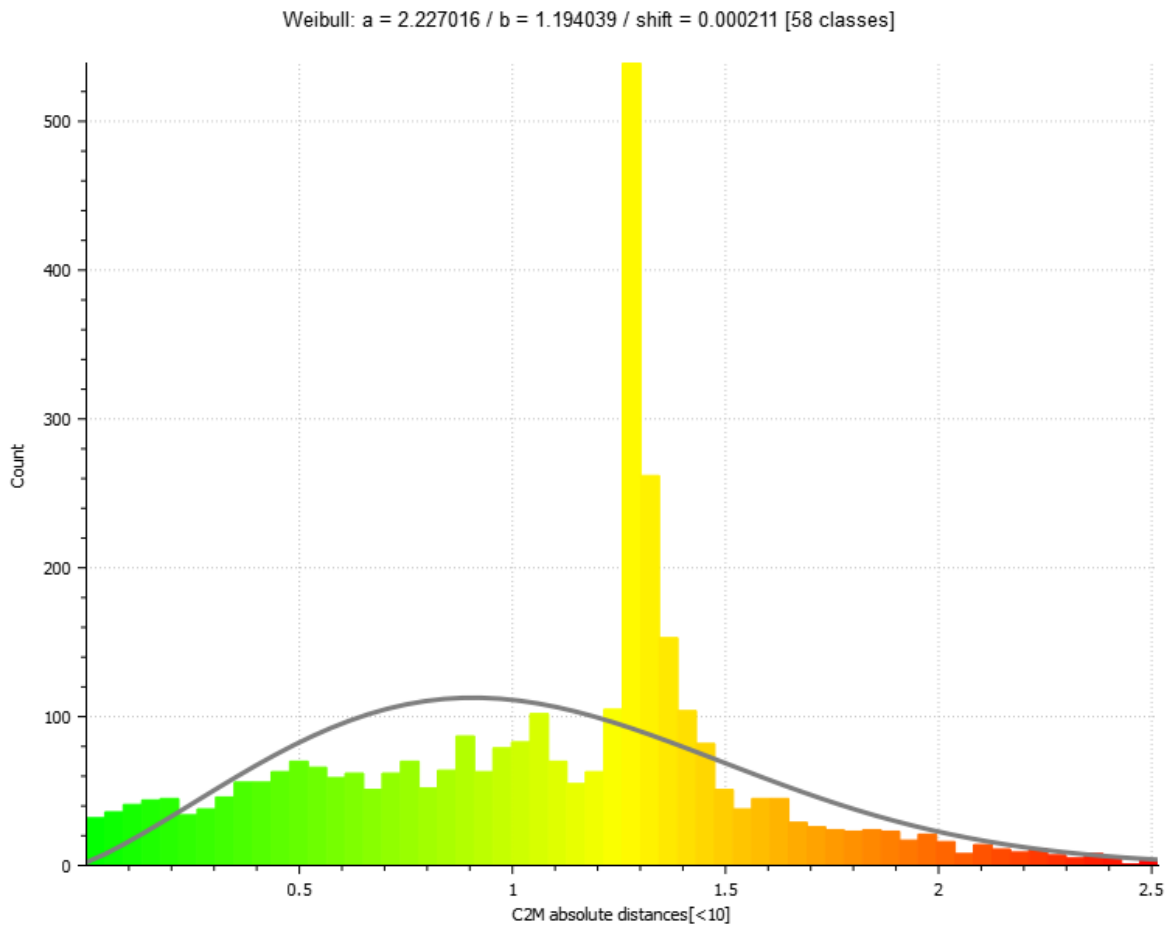


Figure 5. 9 User 02 cloud-to-mesh absolute distance histogram and Weibull function.

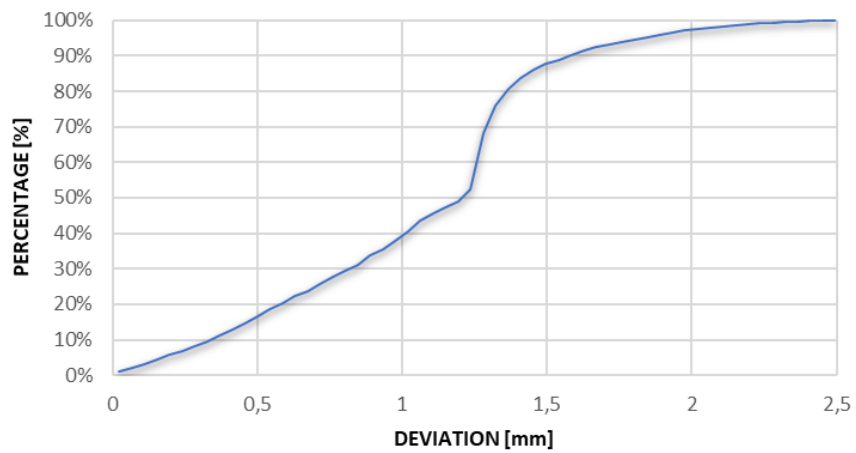


Figure 5. 10 User 02 cumulative distribution function.

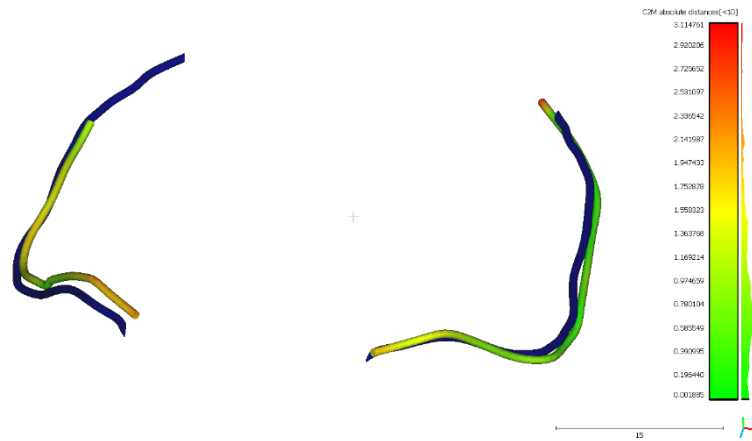


Figure 5.11 User 03 mapping of cloud-to-mesh absolute distance and nominal (blue) lines.

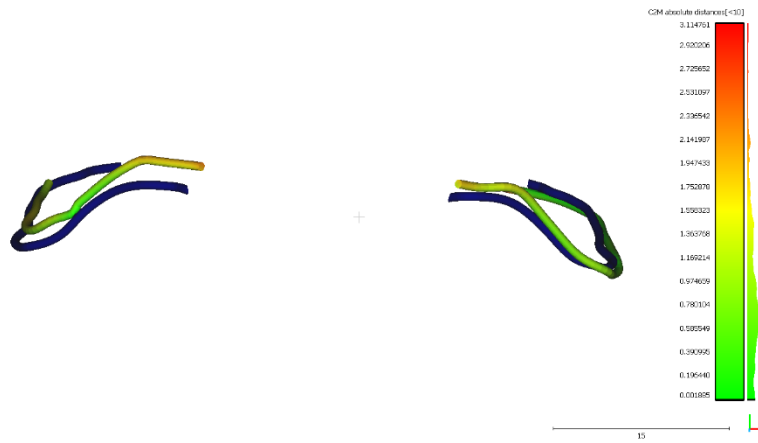


Figure 5.12 User 03 mapping of cloud-to-mesh absolute distance and nominal (blue) lines.

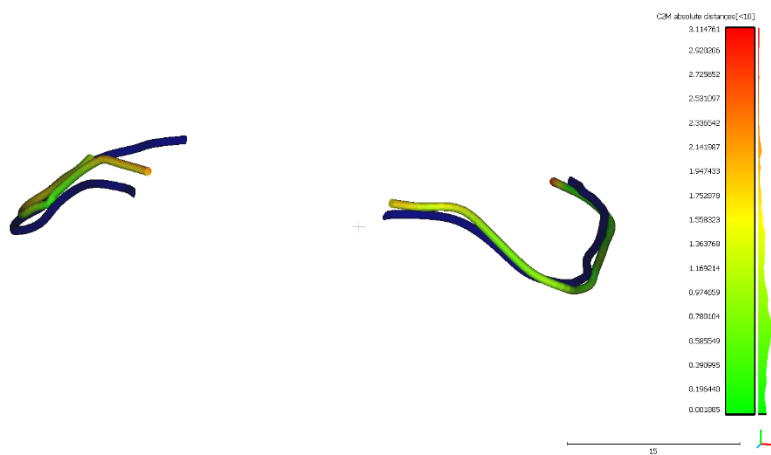


Figure 5.13 User 03 mapping of cloud-to-mesh absolute distance and nominal (blue) lines.



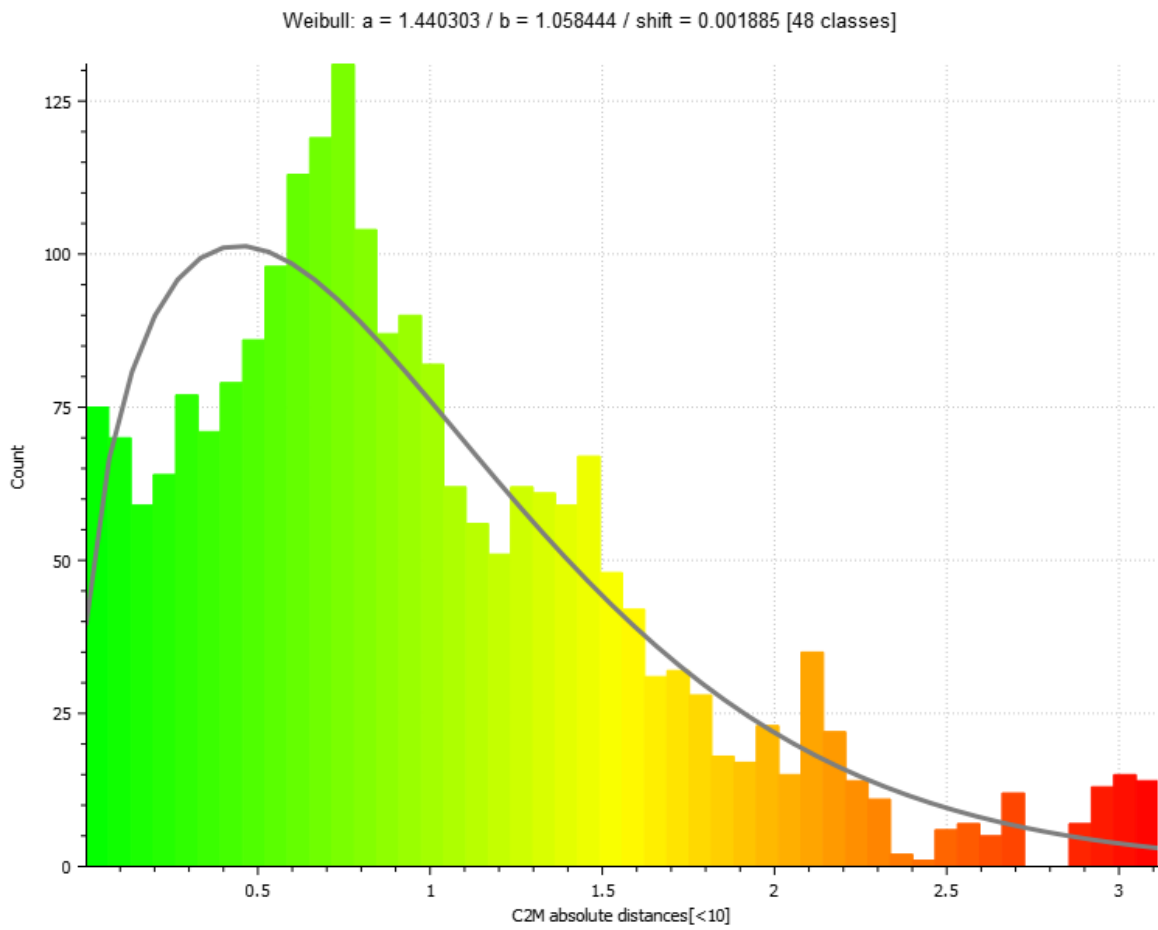


Figure 5. 14 User 03 cloud-to-mesh absolute distance histogram and Weibull function.

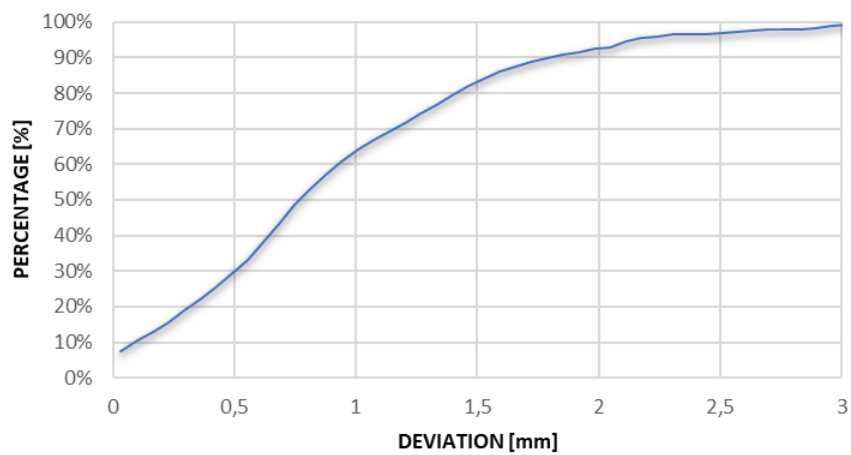


Figure 5. 15 User 03 cumulative distribution function.

Table 5. 3 Values of 75% Percentile for cutting lines in the three osteotomy tasks.

Trial	75% Percentile (mm)
U01-OST1_CL	1.12990
U02-OST1_CL	1.30144
U03-OST1_CL	1.29892

Finally, operational time have been recorded using a stopwatch. User 01 employed 1 min and 24 s for the osteotomy task, operational time for user 02 was 2 min and 59 s and osteotomy task of user 03 lasted 2 min and 21 s. The overall mean operational time was 2 min and 15 s.

For the repositioning tasks results have been extracted directly from the graph paper. In detail linear deviations on the anteroposterior and mediolateral axes are accounted together with the angular deviation from the vertical axis. Linear deviations are calculated by marking the target position that the centroid of marker M2 must reach and the one that M2 assume when user ended the repositioning task and measuring with rulers the distances between these 2 points on the anteroposterior and mediolateral axes without accounting for their sings. Angular deviation instead has been calculated with goniometers by measuring the angle between the anteroposterior and mediolateral axes and the current inclination of M2 after user ended the repositioning task. U01-REP\_1/2/3 indicates the respectively first, second and third trial performed by first user, U02-REP\_1/2/3 indicates respectively the first, second and third trial performed by second user and U03-REP\_1/2/3 indicates respectively the first, second and third trial performed by third user. Table 5. 4 reports linear deviations, both anteroposterior and mediolateral, and angular deviation for any of 3 trials of first user. Table 5. 5 reports linear deviations, both anteroposterior and mediolateral, and angular deviation for any of 3 trials of second user. Table 5. 6 reports linear deviations, both anteroposterior and mediolateral, and angular deviation for any of 3 trials of third user. Mean anteroposterior linear deviation of the 9 trials is 2.31 mm. Mean mediolateral linear deviation of the 9 trials is 0.53 mm. Mean angular

deviation on vertical axes of the 9 trials is  $0.5^\circ$ . Mean operational time of the 9 trials is 57 s. However, it must be noticed that only 22% of samples analyzed exceeded 4.5 mm range and can be accounted as outliers (U03-REP\_2 and U03-REP\_3). Without them, mean anteroposterior linear deviation of the 7 trials is 0.97 mm, mean mediolateral linear deviation is 0,54 mm, mean angular deviation on vertical axes is  $0.42^\circ$  and the mean operational time is 52 s.

*Table 5. 4 User 01 performances in the three trials of the repositioning task.*

<b>Trial</b>	<b>Antero-Posterior Deviation (mm)</b>	<b>Mediolateral Deviation (mm)</b>	<b>Angular Deviation (<math>^\circ</math>)</b>	<b>Operational Time (min: s)</b>
U01-REP_1	4	1	0	0: 23
U01-REP_2	0.8	0.5	0	0: 22
U01-REP_3	0.5	0.5	0	0: 35

*Table 5. 5 User 02 performances in the three trials of the repositioning task.*

<b>Trial</b>	<b>Antero-Posterior Deviation (mm)</b>	<b>Mediolateral Deviation (mm)</b>	<b>Angular Deviation (<math>^\circ</math>)</b>	<b>Operational Time (min: s)</b>
U02-REP_1	0	0	0	2: 0
U02-REP_2	0	0	0	0: 21
U02-REP_3	1.5	1.8	2	1: 50

*Table 5. 6 User 03 performances in the three trials of the repositioning task.*

<b>Trial</b>	<b>Antero-Posterior Deviation (mm)</b>	<b>Mediolateral Deviation (mm)</b>	<b>Angular Deviation (<math>^\circ</math>)</b>	<b>Operational Time (min: s)</b>
U03-REP_1	0	0	1	1: 29
U03-REP_2	8	0	1.5	1: 0
U03-REP_3	6	1	0	0: 35

## 6 Discussions

In this section all the reported results obtained for drilled holes performances, cutting lines drawing and repositioning tasks will be discussed and compared with previous literature findings.

As first we can discuss results regarding drilled holes. Drilled holes were performed by sampling a unique point within the circular area with a diameter of 1.7 mm that projected cylinders highlight over the osteotomized fragment. Drilled holes results are presented in the form of absolute approximated distances in millimeters from the target center of that highlighted area. Mean approximated distance for the 3 trials is 1.17111 mm. This result appears elevated. However, it must be noticed that the modality in which drilled holes has been designed and the way in which they guide user sampling point process makes this an acceptable and promising result. Drilled holes appears to be effectively traced within the projected circular area with a diameter of 1.7 mm. Literature does not provide AR studies that precisely involved these types of structures even though we can easily find studies that treat similar operations such as spinal screw insertions [44] [82] [83], K-wire placements [54], percutaneous needle insertions [72], external ventricular drain operations [38] [73] and osteotomies performed by drilling a certain number of navigational points [42] [43] [63]. Findings of these AR applications can be compared with the ones obtained with the aid of the AR application developed in this study during the drilled holes performance. Many studies [38] [44] [54] [72] [73] [82] [83] reported a significantly higher positional error than the deviation obtained in the developed AR application. Xu et al. [42] study reported a mean positional error of 0.95 mm for the experimental group and 1.64 mm for the control group in the robot-assisted performance of navigational points in the MASO operation. Jiang et al. [43] study reported a mean positional error of 1.29 mm for the entry points and of 2.47 mm at the end points of the drilling paths for the performance of navigational points in the MASO operation on beagle dogs. Zhou et al. [63] study reported a mean position error of 1.04 mm at the entry points and a 1.22 mm

error at the target points of the drilling path for the performance of MASO operations on dogs with the assistance of a force feedback control unit. These results are close to the findings of the developed AR application suggesting that the conceptual idea behind the drilled holes is appropriate. Furthermore, the perspective of the proposed guidance for the performance of drilled holes is strengthened by the fact that comparable results have been obtained without the assistance of external units (robotic structures or sensor units). However, a millimeter-order cannot be acceptable in the medical field and must be improved.

Now, we can discuss results regarding osteotomy cutting lines. Cutting lines were performed by drawing a line on the skull phantom by following the projected pipes with a diameter of 0.75 mm. Cutting lines results are presented in the form of mean approximated distance, cloud-to-mesh absolute distance mapping on drawn lines and histogram (samples against deviation values) with Weibull function, cumulative distribution function (samples percentage against maximum deviation value) and 75% percentile value. Mean approximated distance for the 3 trials is 0.93763 mm and the mean 75% percentile is 1.24342 mm. Cloud-to-mesh absolute distance histogram and associated Weibull function confirm the concentration of samples distribution around these values of deviation. However, it must be remarked the higher significance of the 75% percentile. It indicates the maximum deviation value that characterize the 75% of the total samples collected. Hence, 75% percentile can be a strong factor to evaluate the precision of the developed AR application. Results of 75% percentile are in line with other studies [57] found in literature that treat with different approaches the same type of osteotomy. Zhu et al. [57] study reported a mean discrepancy of 1.18 mm between pre-pre-operative plan and post-operative evaluation in the drilling of navigational points in the MASO operation guided by the visualization of cutting planes. However, cutting planes has been also used as virtual surgical guides in the Ackermann et al. [39] study, where it has been obtained a mean error of 10.8 mm for the starting point of periacetabular osteotomies, demonstrating that the usage of cutting planes more than cutting lines can be debated. Then, among the reviewed study also the Garcia-Mato et al. [37] study must be cited. Here, a mean linear error of 0.62 mm has been

reported for the supraorbital and frontal cranial osteotomies. This is the lowest result achieved in literature, but it must be noticed that simplicity and smoothness of cranial anatomical bony structures can be a factor. At the end, we can better analyze the mapping of the cloud-to-mesh absolute distance over the experimental cutting lines. It can be noticed the constant appearance of areas with high deviation (red zones) in correspondence of the switching point from the frontal to the lateral view that can be justified by the passage from the hologram projection through the frontal face of marker M2 to the hologram projection through the lateral face of marker M2. High deviation zones (red zones) can be found also at the start point of the drawn cutting lines and this can be justified by an unclear visualization of the cylinder due to light conditions or to its empty nature that make user visualizing a pipe that is prolonged by itself back internal surface. However, in general, cloud-to-mesh mapping appears to be characterized by low deviation zones (green zones) that means a good performance in the cutting lines drawing. Finally, almost all the sessions show shorter experimental drawn cutting lines than the nominal ones, except for the left maxillary cutting line drawn in the U03-REP\_1 session. This is justified by the cumbersomeness of the scanner employed for the tested skull acquisition that makes hard a perfect scanning of the whole geometry and easy the loss of deep tracts of the scanned anatomy such as the deepest part of the maxilla where cutting lines end and that is partially hidden by the orbital regions of the upper skull. Hence, the proposed guidance concept for the performance of cutting lines is an appropriate proposal to be further refined to reduce deviations below the millimeter order.

Furthermore, the whole osteotomy task, including both drilled holes and cutting lines performances, has been recorded with a stopwatch. In fact, operational time can be a strong factor to evaluate the effectiveness of the developed AR application. The operational time always remains lower than 3 minutes in the 3 sessions and the mean overall time for the performance of drilled holes and cutting lines is 2 min and 15 s. This is a perspective result since users selected for the 3 trials do not exhibit any direct or indirect experience of these surgical operations.

At the end we can discuss results regarding the repositioning task. Repositioning task were performed by moving the marker M2 over a graph paper sheet guided by the feedback elements (3D arrows, delta values between current position of M2 and target position of cube hologram visualized over the dedicated panel, cube hologram positioned at target position and an alarm system to tune its color based on deltas). In detail, repositioning task expect to reach a position that correspond to the position of tracked M2 plus a 20 mm translation on anteroposterior axis and a 20mm translation on the mediolateral axis. Orientation vector was set to null rotations about all the 3 axes. In this manner, we are limiting the repositioning to the anteroposterior-mediolateral plane and this resembles the type of motion that the surgeon perform after the fragment has been detached or osteotomized. However, even though this can be a valid preliminary study to fast estimate the precision of the developed AR application, a complete pre-operative plan with non-null rotations and translations about all the 3 axes needs to be tested. Results have been extracted with rulers and goniometers after marking the initial position of the centroid of M2, estimating its target position to be reached and marking the final position reached by the centroid of M2 when user ended the repositioning. Results that have been extracted are the linear deviation on anteroposterior and mediolateral axes and the angular deviation about the vertical axis. Any of the user performed 3 trials of the same repositioning task and is asked to annotate any technical event that occurred during current session. Among all the trials 2 were considered as outliers (U03-REP\_2 and U03-REP\_3) and thus they have been removed from the mean computations. Mean linear deviation for the 7 trials is 0.97 mm on the anteroposterior axis and 0.54 mm on the mediolateral axis. Mean angular deviation is 0.42°. Technical notes have been taken throughout 5 of the 9 trials. During U01-REP\_2 session user annotated a temporary crash of cube hologram positioning. During U01-REP\_3 user ended the repositioning without the green color of the cube hologram being confident about that positioning and when, on the contrary, the vertical delta values on the dedicated panel was 4 mm. During U02-REP\_2 user positioned M2 uniquely based on cube hologram visualization being unconfident of displayed delta values. During U03-REP\_3 user annotated a crash of

the cube hologram and the need of re-launching the application. During U03-REP\_3 user repeated the task being unconfident of the hologram stability during the first attempt. Moreover, time of the whole repositioning task has been recorded with a stopwatch. The operational time always remain lower than 2 minutes and the mean duration of the repositioning task is 52 s. These results can be compared with literature studies where medical instrumentation positioning or anatomical structure repositioning have been treated. The developed AR application shows significantly higher results than other studies found in literature [39] [40]. However, it must be noticed how the Ackermann et al. [39] study treated the repositioning of pelvic structures directly on cadavers while our AR application were tested on a phantom in comfortable conditions and that the Gao et al. [40] study provided errors regarding the orientation of the surgical instrument employed for MASO operation. Moreover, other studies find in literature [37] [80] exhibit results that are in line with the ones of the developed application. Garcia-Mato et al. [37] study reported a 0.7 mm mean translational deviation and a  $0.43^\circ$  angular deviation for supraorbital advancement operations, a 0.67 mm translational deviation and a  $0.39^\circ$  angular deviation for frontal advancement operations. Koyachi et al. [80] study reported a 0.38 mm absolute deviation for the maxillary/mandibular repositioning. However, it must be noticed that in this study the repositioning was simultaneously aided by AR virtual surgical guides and the custom-made repositioning instrument that instead is not employed in the Garcia-Mato et al. [37] study and in the AR application that has been developed in this thesis. At the end, mean operational time combined with the fact that selected users lack medical experience regarding these types of operations proves the effectiveness of the developed conceptual idea for the assistance of the repositioning task. Hence, results are promising, and looking at both mean deviations and technical user annotations it can be stated that the proposed guidance feedback for the repositioning task is efficient even though the overall application can be improved in its stability to prevent crashes and guarantee the optimal combination of all the feedback elements.



## 7 Conclusions and Future Research

In this final section it will be reported all the innovativeness embedded in the developed AR application and its qualitative and quantitative analysis.

The aim of the present study was to develop an AR application applicable in maxillofacial surgery using Microsoft HoloLens V2 HMD. In detail, the developed AR application aims to aid mandibular and maxillary osteotomies and repositioning.

For the assistance of maxillofacial osteotomies, the virtual assistance is composed by cutting lines as pipes of a diameter of 0.75 mm and the augmented scene is completed by the drilled holes visualized as cylinders that highlight a circular area over the osteotomized fragment with a diameter of 1.7 mm. Drilled holes represents a completely new virtual content that none of the literature studies exhibit. For what concern cutting lines, instead the innovative aspect is represented by the direct visualization of lines over the target anatomy while on the contrary commonly literature studies proposed the visualization of cutting planes that intersect the treated anatomy. This solution is aimed to reduce surgeon mental load, to speed up the procedure and it attempts to improve accuracy of the performances by reducing interpretation errors. For the assistance of maxillofacial repositioning operations, the developed AR application aims to aid user by the visualization of 3D-arrows that indicates the direction to be followed, the visualization of a cube hologram exactly positioned and oriented according to pre-operative plan and whose color is tuned by an alarm system based on the calculation of deltas between the current position of the osteotomized fragment and the target one (it will be red when deltas are outside the acceptance range and green when they are within this range) and finally the visualization of delta values in millimeters on the dedicated panel. Commonly, developed AR application in a static manner by uniquely displaying treated structures at the target positions, thus, the innovative aspect of this solution lies in the dynamicity of the interactive feedback that attempts to prevent under/over-shooting in the repositioning making user more confident from the start to the end of the procedure.

Furthermore, the conceptual idea of the integration of both Osteotomy and Repositioning modes is rarely found in literature and is a completely novel methodology in the maxillofacial surgery field making the developed AR application a potentially attractive package to be employed by surgeons in the treatment of complex and simple clinical cases.

The first advantage introduced by this application is the reduction of the duration of surgical operations, that is also proved by recorded time for both repositioning and osteotomy tasks. Then, it allows to simplify the clinical data consultation for the surgeon reducing time wasting and distraction problems due to the continuous shift of the view outside of the surgical field to consult patient data. Moreover, it facilitates the pre-operative plan and improves the patient-to-surgeon communication. The developed AR application has the whole potential to reduce risk of errors and improve the safety of the performed surgical operation. Furthermore, it homogenizes the efficiency of the performed surgical operation with respect to the user experience, allowing also to non-expertise or novice surgeons to receive an appropriate assistance and to be confident of their current operation. Both operations are assisted through a clear and easily handled feedback that can be managed by user simply by hand interactions in the appositely designed 3-buttons menu. The user interface is simple, intuitive, and non-chaotic. Finally, it aims to completely substitute custom-made and 3D-printed surgical cutting guides and dental splints removing all the related drawbacks concerning costs and construction times. From a more practical point of view, the developed AR application guarantees a minimal invasiveness, since the fixation of the 2-marker system is respectively mediated by non-invasive dental bites (M2) or through small resorbable screws (M1). Furthermore, marker dimensions (3 x 3 x 3 cm) match both the trackability requirements of the Microsoft HoloLens V2 HMD and the practical constraints imposed to prevent the hampering of the surgical procedure caused by the reduction of the line-of-sight caused by marker cumbersomeness. Moreover, the design choice of the multi-targets, in detail cubic markers, guarantees the stable hologram registration even when the user moves 360°- around the phantom or patient. Finally, the usage of passive feature rich markers, in

detail QR codes, prevent from any of the possible dangerous interaction that an active marker can induce in the operating room. At the end of the qualitative analysis of the developed AR application we must mark the importance of the selected AR system methodology. The usage of the HMD and thus a video see-through AR system gives to the AR experience a more immersive appearance that at the mean time does not compromise the real-world perception. It makes more challenging the AR experience to be applied in the pre-operative training, it makes more efficient the AR experience in the pre-operative planning and it can be more suitable for a future integration in the clinical routine.

Now it can be presented a quantitative analysis of the precision of the developed AR application for both osteotomy and repositioning tasks. Results obtained are in line with literature proving that the innovativeness embedded in the developed applications exhibits a concrete potential to be applied in the maxillofacial surgery field as well as in many other similar medical spheres. However, it must be noticed that error entities are not sufficient to immediately proceed with a clinical test of the developed AR application and further improvement are needed mainly from the technological point of view, as widely sustained in literature. From a general point of view, in the developed AR application several of the faced problems are still open issues in the AR technology field and they need to be solved to significantly improve their precision and definitively introduce the AR systems and applications also in the medical clinical routing. As first the hologram drift needs to be reduced reducing the offset with which holograms are displayed by user in the augmented scene. Then, Microsoft HoloLens V2 device, such as many other commercialized HMDs, has a long optimal distance to obtain the best comfort and the highest performance of the augmentation (i.e., for the Microsoft HoloLens V2 device the optimal distance is 2 m) and this can decrease the hologram stability. These problems can be solved by the advancement of newly developed technologies and HMD generations or through a deeper analysis and tuning of the application settings to ensure the highest possible holograms stability. More in the detail of the proposed work, some prompts for future development can be the realization of the 3D-printed multi-functional skull phantom

with a more performing and accurate 3D-printing technology such as Multi Jet Fusion to ensure a better fitting in the assembly mechanisms embedded in the geometry and to further embed QR codes as textures to be directly 3D-printed on the marker cubes with the optimal accuracy to be trackable by HMD. Then, to strengthen the validation of the developed AR application, it can be improved the number of trials for the osteotomy task, and it can be enlarged the testing dataset for both osteotomy and repositioning task also involving surgeons and medical expertise. Moreover, to improve the testing phase for the repositioning task, it can be tested a more complex pre-operative plan based on 3 non-null translations and 3 non-null rotations by employing a more advanced method of validation based on scanner usage. From the AR application development point of view, it can be interesting to improve the orientation feedback returned during repositioning task by passing from a pure visual aid (simultaneous visualization of reference frames superimposed on both M2 and cube hologram) to something more interactive, finding a way to return user also angular deltas to be visualized and to be used in the alarm system to implement a new intermediate level (yellow color) in which only the angular deltas or the linear deltas are within the acceptance range. Moreover, the assistance in the drilling holes performance task can be improved by reducing the diameter of the cylinders employed as visual aids and the osteotomy cutting lines performance can be improved by sectioning the developed pipes to leave uniquely their external surface and reduce the enlarged appearance at the extremities caused by their empty nature.

In conclusion this study has confirmed the potentiality of the AR application in the maxillofacial surgeries field, and it has proposed an attractive and efficient complete package for the assistance of clinical cases that needs to undergo maxillofacial osteotomies and/or repositioning that can be currently employed in the pre-operative phases and training and that needs further improvements to be introduced in the real operating rooms.

## 8 Bibliography

- [1] H. Kashani and L. Rasmusson, "Osteotomies in Orthognathic Surgery", *A Textb. Adv. Oral Maxillofac. Surg. Vol. 3*, 2016, doi: 10.5772/63345.
- [2] A. Cortese, "Le Fort I Osteotomy for Maxillary Repositioning and Distraction Techniques", *Role Osteotomy Correct. Congenit. Acquir. Disord. Skelet.*, no. June, 2012, doi: 10.5772/37211.
- [3] S. H. Kang, H. J. Kim, H. W. Park, and S. H. Lee, "Maxillary cutting guide for executing a simulated osteotomy and removing the bony interference during orthognathic surgery", *J. Med. Devices, Trans. ASME*, vol. 9, no. 4, pp. 1-4, 2015, doi: 10.1115/1.4031162.
- [4] P. Pietruski *et al.*, "Supporting mandibular resection with intraoperative navigation utilizing augmented reality technology - A proof of concept study", *J. Cranio-Maxillofacial Surg.*, vol. 47, no. 6, pp. 854-859, 2019, doi: 10.1016/j.jcms.2019.03.004.
- [5] S. Mathew, P. G. Antony, N. Nandagopal, and A. Sebastian, "New, easier, effective, and stable splinting technique for maxillofacial osteotomy", *Br. J. Oral Maxillofac. Surg.*, vol. 57, no. 9, pp. 948-949, 2019, doi: 10.1016/j.bjoms.2019.07.025.
- [6] T. Shirota *et al.*, "CAD/CAM splint and surgical navigation allows accurate maxillary segment positioning in Le Fort I osteotomy", *Heliyon*, vol. 5, no. 7, p. e02123, 2019, doi: 10.1016/j.heliyon.2019.e02123.
- [7] E. W. Steinäuser, "Bone screws and plates in orthognathic surgery", *Int. J. Oral Surg.*, vol. 11, no. 4, pp. 209-216, 1982, doi: 10.1016/S0300-9785(82)80069-0.
- [8] Y.-W. Park, "Bioabsorbable osteofixation for orthognathic surgery", *Maxillofac. Plast. Reconstr. Surg.*, vol. 37, no. 1, pp. 1-9, 2015, doi: 10.1186/s40902-015-0003-7.
- [9] Stryker Company, "Stryker Craniomaxillofacial, Universal 2 Reference Guide".
- [10] H. Jung, "Basic Physical Principles and Clinical Applications of Computed

- Tomography”, *Prog. Med. Phys.*, vol. 32, no. 1, pp. 1–17, 2021, doi: 10.14316/pmp.2021.32.1.1.
- [11] Y. Watanabe, “Derivation of linear attenuation coefficients from CT numbers for low- energy photons”, *Phys. Med. Biol.*, vol. 44, no. 9, pp. 2201–2211, 1999, doi: 10.1088/0031-9155/44/9/308.
- [12] L. W. Goldman, “Principles of CT and CT technology”, *J. Nucl. Med. Technol.*, vol. 35, no. 3, pp. 115–128, 2007, doi: 10.2967/jnmt.107.042978.
- [13] S. Aukstakalnis, *Practical Augmented Reality*. 2016.
- [14] S. Zlatanova, *Augmented Reality Technology Dr . Dipl . Ing . S . Zlatanova*, no. January. 2015.
- [15] M. A. Callahan, “A 3-D Display Head-set for personalized computing”, Miami University of Oxford, 1983.
- [16] I. E. Sutherland, “A head-mounted three dimensional display”, University of Utah, Fall Joint Computer Conference, 1968.
- [17] B. Arora and N. Parkar, “Augmented Reality: Tracking Methods”, vol. 5, no. 01, pp. 1–4, 2017, [Online]. Available: [www.ijert.org](http://www.ijert.org).
- [18] P. Yang, W. Wu, M. Moniri, and C. C. Chibelushi, “A sensor-based SLAM algorithm for camera tracking in virtual studio”, *Int. J. Autom. Comput.*, vol. 5, no. 2, pp. 152–162, 2008, doi: 10.1007/s11633-008-0152-6.
- [19] F. N. Afif, A. H. Basori, and N. Saari, “Vision-based Tracking Technology for Augmented Reality : A Survey”, *Int. J. Interact. Digit. Media*, vol. 1, no. 1, pp. 46–49, 2013.
- [20] L. Chen, F. Zhang, W. Zhan, M. Gan, and L. Sun, “Optimization of virtual and real registration technology based on augmented reality in a surgical navigation system”, *Biomed. Eng. Online*, vol. 19, no. 1, pp. 1–28, 2020, doi: 10.1186/s12938-019-0745-z.
- [21] R. T. Azuma, “A survey of augmented reality”, *Teleoperators and Virtual Environments* 6, 997.
- [22] Q. Wang, W.-C. Cheng, N. Suresh, and H. Hua, “Development of the local magnification method for quantitative evaluation of endoscope geometric

- distortion”, *J. Biomed. Opt.*, vol. 21, no. 5, p. 056003, 2016, doi: 10.1117/1.jbo.21.5.056003.
- [23] D. Schmalstieg and T. Höllerer, *AR Textbook Tobias*. 2016.
- [24] J. Y. C. Chen and G. Fragomeni, *Virtual Augmented and Mixed Reality*.
- [25] R. T. Azuma, “Predictive Tracking for Augmented Reality”, no. February, p. 262, 1995, [Online]. Available: <http://www.cs.unc.edu/techreports/95-007.pdf>.
- [26] P. Vávra *et al.*, “Desarrollo reciente de la realidad aumentada en cirugía: una revisión”, vol. 2017, 2017, [Online]. Available: <https://www.hindawi.com/journals/jhe/2017/4574172/>.
- [27] M. Farronato *et al.*, “Current state of the art in the use of augmented reality in dentistry: A systematic review of the literature”, *BMC Oral Health*, vol. 19, no. 1, 2019, doi: 10.1186/s12903-019-0808-3.
- [28] J. Jiang, Z. Huang, W. Qian, Y. Zhang, and Y. Liu, “Registration technology of augmented reality in oral medicine: a review”, *IEEE Access*, vol. 7, pp. 53566–53584, 2019, doi: 10.1109/ACCESS.2019.2912949.
- [29] C. M. Andrews, A. B. Henry, I. M. Soriano, M. K. Southworth, and J. R. Silva, “Registration Techniques for Clinical Applications of Three-Dimensional Augmented Reality Devices”, *IEEE J. Transl. Eng. Heal. Med.*, vol. 9, no. December 2020, 2021, doi: 10.1109/JTEHM.2020.3045642.
- [30] G. Badiali *et al.*, “Review on Augmented Reality in Oral and Cranio-Maxillofacial Surgery: Toward ‘Surgery-Specific’ Head-Up Displays”, *IEEE Access*, vol. 8, pp. 59015–59028, 2020, doi: 10.1109/ACCESS.2020.2973298.
- [31] M. Benmahdjoub, T. van Walsum, P. van Twisk, and E. B. Wolvius, “Augmented reality in craniomaxillofacial surgery: added value and proposed recommendations through a systematic review of the literature”, *Int. J. Oral Maxillofac. Surg.*, vol. 50, no. 7, pp. 969–978, 2021, doi: 10.1016/j.ijom.2020.11.015.
- [32] V. Mago, “Augmented Reality in Plastic Surgery Education”, *Egypt. J. Plast. Reconstr. Surg.*, vol. 45, no. 1, pp. 19–25, 2021, doi: 10.21608/ejprs.2021.165782.
- [33] D. Mehrotra and A. F. Markus, “Emerging simulation technologies in global craniofacial surgical training”, *J. Oral Biol. Craniofacial Res.*, vol. 11, no. 4, pp. 486–

- 499, 2021, doi: 10.1016/j.jobcr.2021.06.002.
- [34] S. Park, S. Bokijonov, and Y. Choi, "Review of microsoft hololens applications over the past five years", *Appl. Sci.*, vol. 11, no. 16, 2021, doi: 10.3390/app11167259.
- [35] W. Jiang *et al.*, "Evaluation of the 3D Augmented Reality-Guided Intraoperative Positioning of Dental Implants in Edentulous Mandibular Models", *Int. J. Oral Maxillofac. Implants*, vol. 33, no. 6, pp. 1219-1228, 2018, doi: 10.11607/jomi.6638.
- [36] S. Tsukada, H. Ogawa, M. Nishino, K. Kurosaka, and N. Hirasawa, "Augmented reality-based navigation system applied to tibial bone resection in total knee arthroplasty", *J. Exp. Orthop.*, vol. 6, no. 1, pp. 0-6, 2019, doi: 10.1186/s40634-019-0212-6.
- [37] D. García-Mato *et al.*, "Augmented reality visualization for craniostyosis surgery", *Comput. Methods Biomech. Biomed. Eng. Imaging Vis.*, vol. 9, no. 4, pp. 392-399, 2021, doi: 10.1080/21681163.2020.1834876.
- [38] M. Kramers, R. Armstrong, S. M. Bakhshmand, A. Fenster, S. De Ribaupierre, and R. Eagleson, "Evaluation of a mobile augmented reality application for image guidance of neurosurgical interventions", *Stud. Health Technol. Inform.*, vol. 196, no. April, pp. 204-208, 2014, doi: 10.3233/978-1-61499-375-9-204.
- [39] J. Ackermann *et al.*, "Augmented reality based surgical navigation of complex pelvic osteotomies – a feasibility study on cadavers", *Appl. Sci.*, vol. 11, no. 3, pp. 1-19, 2021, doi: 10.3390/app11031228.
- [40] Y. Gao, L. Lin, G. Chai, and L. Xie, "A feasibility study of a new method to enhance the augmented reality navigation effect in mandibular angle split osteotomy", *J. Cranio-Maxillofacial Surg.*, vol. 47, no. 8, pp. 1242-1248, 2019, doi: 10.1016/j.jcms.2019.04.005.
- [41] Y. K. Lin, H. T. Yau, I. C. Wang, C. Zheng, and K. H. Chung, "A Novel Dental Implant Guided Surgery Based on Integration of Surgical Template and Augmented Reality", *Clin. Implant Dent. Relat. Res.*, vol. 17, no. 3, pp. 543-553, 2015, doi: 10.1111/cid.12119.
- [42] L. Lin *et al.*, "Mandibular angle split osteotomy based on a novel augmented



- reality navigation using specialized robot-assisted arms - A feasibility study”, *J. Cranio-Maxillofacial Surg.*, vol. 44, no. 2, pp. 215–223, 2016, doi: 10.1016/j.jcms.2015.10.024.
- [43] T. Jiang, M. Zhu, G. Chai, and Q. Li, “Precision of a Novel Craniofacial Surgical Navigation System Based on Augmented Reality Using an Occlusal Splint as a Registration Strategy”, *Sci. Rep.*, vol. 9, no. 1, pp. 1–8, 2019, doi: 10.1038/s41598-018-36457-2.
- [44] J. T. Gibby, S. A. Swenson, S. Cvetko, R. Rao, and R. Javan, “Head-mounted display augmented reality to guide pedicle screw placement utilizing computed tomography”, *Int. J. Comput. Assist. Radiol. Surg.*, vol. 14, no. 3, pp. 525–535, 2019, doi: 10.1007/s11548-018-1814-7.
- [45] C. A. Agten, C. Dennler, A. B. Roskopf, L. Jaberg, C. W. A. Pfirrmann, and M. Farshad, “Augmented Reality-Guided Lumbar Facet Joint Injections”, *Invest. Radiol.*, vol. 53, no. 8, pp. 495–498, 2018, doi: 10.1097/RLI.0000000000000478.
- [46] T. Itamiya, T. Iwai, and T. Kaneko, “The Holographic Human for Surgical Navigation using Microsoft HoloLens”, vol. 1, pp. 26–20, 2018, doi: 10.29007/wjjx.
- [47] D. Mitsuno, K. Ueda, Y. Hirota, and M. Ogino, “Effective Application of Mixed Reality Device HoloLens: Simple Manual Alignment of Surgical Field and Holograms”, *Plast. Reconstr. Surg.*, vol. 143, no. 2, pp. 647–651, 2019, doi: 10.1097/PRS.00000000000005215.
- [48] J. Wang, H. Suenaga, L. Yang, E. Kobayashi and I. Sakuma, “Video see-through augmented reality for oral and maxillofacial surgery:”, *Int. J. Med Robotics Comput Assist Surg*, 2017.
- [49] Y. Zuo *et al.*, “A Novel Evaluation Model for a Mixed-Reality Surgical Navigation System: Where Microsoft HoloLens Meets the Operating Room”, *Surg. Innov.*, vol. 27, no. 2, pp. 193–202, 2020, doi: 10.1177/1553350619893236.
- [50] T. Frantz, B. Jansen, J. Duerinck, and J. Vandemeulebroucke, “Augmenting microsoft’s HoloLens with vuforia tracking for neuronavigation”, *Healthc. Technol. Lett.*, vol. 5, no. 5, pp. 221–225, 2018, doi: 10.1049/htl.2018.5079.

- [51] J. W. Meulstee *et al.*, "Toward Holographic-Guided Surgery", *Surg. Innov.*, vol. 26, no. 1, pp. 86–94, 2019, doi: 10.1177/1553350618799552.
- [52] M. Zhu, G. Chai, Y. Zhang, X. Ma, and J. Gan, "Registration strategy using occlusal splint based on augmented reality for mandibular angle oblique split osteotomy", *J. Craniofac. Surg.*, vol. 22, no. 5, pp. 1806–1809, 2011, doi: 10.1097/SCS.0b013e31822e8064.
- [53] L. Cercenelli *et al.*, "The wearable vostars system for augmented reality-guided surgery: Preclinical phantom evaluation for high-precision maxillofacial tasks", *J. Clin. Med.*, vol. 9, no. 11, pp. 1–13, 2020, doi: 10.3390/jcm9113562.
- [54] K. Schlueter-Brust *et al.*, "Augmented-reality-assisted K-wire placement for glenoid component positioning in reversed shoulder arthroplasty: A proof-of-concept study", *J. Pers. Med.*, vol. 11, no. 8, 2021, doi: 10.3390/jpm11080777.
- [55] M. Qu *et al.*, "Precise positioning of an intraoral distractor using augmented reality in patients with hemifacial microsomia", *J. Cranio-Maxillofacial Surg.*, vol. 43, no. 1, pp. 106–112, 2015, doi: 10.1016/j.jcms.2014.10.019.
- [56] G. Yavas, K. E. Caliskan, and M. S. Cagli, "Three-dimensional-printed marker-based augmented reality neuronavigation: a new neuronavigation technique", *Neurosurg. Focus*, vol. 51, no. 2, pp. 1–10, 2021, doi: 10.3171/2021.5.FOCUS21206.
- [57] M. Zhu *et al.*, "Does intraoperative navigation improve the accuracy of mandibular angle osteotomy: Comparison between augmented reality navigation, individualised templates and free-hand techniques", *J. Plast. Reconstr. Aesthetic Surg.*, vol. 71, no. 8, pp. 1188–1195, 2018, doi: 10.1016/j.bjps.2018.03.018.
- [58] G. Chen, W. Zeng, H. Yin, Y. Yu, R. Ju, and W. Tang, "The Preliminary Application of Augmented Reality in Unilateral Orbitozygomatic Maxillary Complex Fractures Treatment", *J. Craniofac. Surg.*, vol. 31, no. 2, pp. 542–548, 2020, doi: 10.1097/SCS.0000000000006238.
- [59] F. Cofano *et al.*, "Augmented Reality in Medical Practice: From Spine Surgery to Remote Assistance", *Front. Surg.*, vol. 8, no. March, pp. 1–10, 2021, doi: 10.3389/fsurg.2021.657901.

- [60] M. F. Hossain, S. Barman, N. Biswas, and A. K. M. Bahalul Haque, "Augmented reality in medical education: AR bones", *Proc. - IEEE 2021 Int. Conf. Comput. Commun. Intell. Syst. ICCIS 2021*, pp. 348–353, 2021, doi: 10.1109/ICCIS51004.2021.9397108.
- [61] W. Han *et al.*, "A new method for cranial vault reconstruction: Augmented reality in synostotic plagiocephaly surgery", *J. Cranio-Maxillofacial Surg.*, vol. 47, no. 8, pp. 1280–1284, 2019, doi: 10.1016/j.jcms.2019.04.008.
- [62] M. Zhu *et al.*, "Effectiveness of a novel augmented reality-based navigation system in treatment of orbital hypertelorism", *Ann. Plast. Surg.*, vol. 77, no. 6, pp. 662–668, 2016, doi: 10.1097/SAP.0000000000000644.
- [63] C. Zhou *et al.*, "Robot-Assisted Surgery for Mandibular Angle Split Osteotomy Using Augmented Reality: Preliminary Results on Clinical Animal Experiment", *Aesthetic Plast. Surg.*, vol. 41, no. 5, pp. 1228–1236, 2017, doi: 10.1007/s00266-017-0900-5.
- [64] M. Zhu *et al.*, "A novel augmented reality system for displaying inferior alveolar nerve bundles in maxillofacial surgery", *Sci. Rep.*, vol. 7, no. February, pp. 1–11, 2017, doi: 10.1038/srep42365.
- [65] R. Moreta-Martinez, A. Pose-Díez-De-la-lastra, J. A. Calvo-Haro, L. Mediavilla-Santos, R. Pérez-Mañanes, and J. Pascau, "Combining augmented reality and 3d printing to improve surgical workflows in orthopedic oncology: Smartphone application and clinical evaluation", *Sensors (Switzerland)*, vol. 21, no. 4, pp. 1–17, 2021, doi: 10.3390/s21041370.
- [66] M. Schneider, C. Kunz, A. Pal'a, C. R. Wirtz, F. Mathis-Ullrich, and M. Hlaváč, "Augmented reality-assisted ventriculostomy", *Neurosurg. Focus*, vol. 50, no. 1, pp. 1–7, 2021, doi: 10.3171/2020.10.FOCUS20779.
- [67] B. J. Park, S. J. Hunt, G. J. Nadolski, and T. P. Gade, "Augmented reality improves procedural efficiency and reduces radiation dose for CT-guided lesion targeting: a phantom study using HoloLens 2", *Sci. Rep.*, vol. 10, no. 1, pp. 1–8, 2020, doi: 10.1038/s41598-020-75676-4.
- [68] S. Ćuković, M. Gattullo, F. Pankratz, G. Devedžić, E. Carrabba, and K. Baizid,

- “Marker based vs. natural feature tracking augmented reality visualization of the 3D foot phantom”, 2015.
- [69] M. C. Rassweiler-Seyfried *et al.*, “iPad-assisted percutaneous nephrolithotomy (PCNL): a matched pair analysis compared to standard PCNL”, *World J. Urol.*, vol. 38, no. 2, pp. 447–453, 2020, doi: 10.1007/s00345-019-02801-y.
- [70] H. J. Kim, S. H. Jeong, J. H. Seo, I. S. Park, H. Ko, and S. Y. Moon, “Augmented reality for botulinum toxin injection”, *Concurr. Comput. Pract. Exp.*, vol. 32, no. 18, pp. 1–7, 2020, doi: 10.1002/cpe.5526.
- [71] F. Ferraguti *et al.*, “Augmented Reality and Robotic-Assistance for Percutaneous Nephrolithotomy”, *IEEE Robot. Autom. Lett.*, vol. 5, no. 3, pp. 4556–4563, 2020, doi: 10.1109/LRA.2020.3002216.
- [72] D. J. Long *et al.*, “Comparison of Smartphone Augmented Reality, Smartglasses Augmented Reality, and 3D CBCT-guided Fluoroscopy Navigation for Percutaneous Needle Insertion: A Phantom Study”, *Cardiovasc. Intervent. Radiol.*, vol. 44, no. 5, pp. 774–781, 2021, doi: 10.1007/s00270-020-02760-7.
- [73] F. Van Gestel *et al.*, “The effect of augmented reality on the accuracy and learning curve of external ventricular drain placement”, *Neurosurg. Focus*, vol. 51, no. 2, pp. 1–9, 2021, doi: 10.3171/2021.5.FOCUS21215.
- [74] P. K. Kanithi, J. Chatterjee, and D. Sheet, “Immersive augmented reality system for assisting needle positioning during ultrasound guided intervention”, *ACM Int. Conf. Proceeding Ser.*, 2016, doi: 10.1145/3009977.3010023.
- [75] J. Gibby, S. Cvetko, R. Javan, R. Parr, and W. Gibby, “Use of augmented reality for image-guided spine procedures”, *Eur. Spine J.*, vol. 29, no. 8, pp. 1823–1832, 2020, doi: 10.1007/s00586-020-06495-4.
- [76] T. P. C. Van Doormaal, J. A. M. Van Doormaal, and T. Mensink, “Clinical accuracy of holographic navigation using point-based registration on augmented-reality glasses”, *Oper. Neurosurg.*, vol. 17, no. 6, pp. 588–593, 2019, doi: 10.1093/ons/opz094.
- [77] H. Liu, E. Auvinet, J. Giles, and F. Rodriguez y Baena, “Augmented Reality Based Navigation for Computer Assisted Hip Resurfacing: A Proof of Concept

- Study", *Ann. Biomed. Eng.*, vol. 46, no. 10, pp. 1595–1605, 2018, doi: 10.1007/s10439-018-2055-1.
- [78] H. Choi, Y. Park, H. Cho, and J. Hong, "An augmented reality based simple navigation system for pelvic tumor resection", *Proc. 11th Asian Conf. Comput. Aided Surg. (ACCAS 2015)*, no. Accas, pp. 9–11, 2015.
- [79] G. Badiali *et al.*, "Augmented reality as an aid in maxillofacial surgery: Validation of a wearable system allowing maxillary repositioning", *J. Cranio-Maxillofacial Surg.*, vol. 42, no. 8, pp. 1970–1976, 2014, doi: 10.1016/j.jcms.2014.09.001.
- [80] M. Koyachi *et al.*, "Accuracy of Le Fort I osteotomy with combined computer-aided design/computer-aided manufacturing technology and mixed reality", *Int. J. Oral Maxillofac. Surg.*, vol. 50, no. 6, pp. 782–790, 2021, doi: 10.1016/j.ijom.2020.09.026.
- [81] P. Pietruski *et al.*, "Supporting fibula free flap harvest with augmented reality: A proof-of-concept study", *Laryngoscope*, vol. 130, no. 5, pp. 1173–1179, 2020, doi: 10.1002/lary.28090.
- [82] F. Liebmann *et al.*, "Pedicle screw navigation using surface digitization on the Microsoft HoloLens", *Int. J. Comput. Assist. Radiol. Surg.*, vol. 14, no. 7, pp. 1157–1165, 2019, doi: 10.1007/s11548-019-01973-7.
- [83] J. M. Spirig, S. Roner, F. Liebmann, P. Fürnstahl, and M. Farshad, "Augmented reality-navigated pedicle screw placement: a cadaveric pilot study", *Eur. Spine J.*, no. 0123456789, 2021, doi: 10.1007/s00586-021-06950-w.
- [84] P. Scolozzi and Z. Catherine, "Applications of maxillo-facial computer assisted surgery | Applications de la chirurgie maxillo-faciale assistée par ordinateur", *Rev. Med. Suisse*, vol. 15, no. 655, pp. 1226–1230, 2019.
- [85] R. Carey, G. Bell, and C. Marrin, "Virtual Reality Modeling Language (VRML97)", 1997.
- [86] M. Szilvási-Nagy and G. Mátyási, "Analysis of STL Files", *Math. Comput. Model.*, vol. 38, no. 7–9, pp. 945–960, 2003, doi: 10.1016/s0895-7177(03)90079-3.
- [87] "Alias / WaveFront Object (. obj ) File Format".

- [88] R. McNeel, "Rhinoceros User Guide", 2020, [Online]. Available: <http://docs.mcneel.com/rhino/6/usersguide/en-us/index.htm>.
- [89] R. Mac, "Rhinoceros Guida all'uso", 2019.
- [90] D. Amin and S. Govilkar, "Comparative Study of Augmented Reality Sdk's", *Int. J. Comput. Sci. Appl.*, vol. 5, no. 1, pp. 11-26, 2015, doi: 10.5121/ijcsa.2015.5102.
- [91] T. A. Vakaliuk and S. I. Pochtoviuk, "Analysis of tools for the development of augmented reality technologies", *CEUR Workshop Proc.*, vol. 2898, pp. 119-130, 2021.
- [92] F. Winkler, "Scripting in Unity3D (vers. 4.2)", no. 1, pp. 1-10, 2013.
- [93] T. Norton, "Learning C # by Developing Games with Unity 3D Beginner's Guide", 2013.
- [94] B. Pablo and F. Navarro, "Learn Unity by Creating a 3D Multi-Level Platformer Game", 2018.
- [95] A. G. Taylor, "Develop Microsoft HoloLens Apps Now", *Dev. Microsoft HoloLens Apps Now*, pp. 91-100, 2016, doi: 10.1007/978-1-4842-2202-7.
- [96] H. P. Halvorsen, "Introduction to Visual Studio", 2017.
- [97] C. W. Hull, "Apparatus for Production of Three-Dimensional Objects By Stereo Photography", *Patent*, no. 19, p. 16, 1984, [Online]. Available: <https://patents.google.com/patent/US4575330>.
- [98] A. M. Kalla and G. Thomas, "Food Marketing & Technology An overview on 3D printing of foods", no. December, pp. 0-2, 2018.
- [99] "CloudCompare User's Manual for version 2.1", 2018, Available: [www.cloudcompare.net](http://www.cloudcompare.net).
- [100] "CloudCompare version 2.6.1. user manual", 2015, Available: <http://www.danielgm.net/cc/>.

